



HAL
open science

Identification of antagonistic functions of GCN2 on ribosome biogenesis depending on nutrients availability

Marie Piecyk

► **To cite this version:**

Marie Piecyk. Identification of antagonistic functions of GCN2 on ribosome biogenesis depending on nutrients availability. Cellular Biology. Université Claude Bernard - Lyon I, 2023. English. NNT : 2023LYO10020 . tel-04460315

HAL Id: tel-04460315

<https://theses.hal.science/tel-04460315v1>

Submitted on 15 Feb 2024

HAL is a multi-disciplinary open access archive for the deposit and dissemination of scientific research documents, whether they are published or not. The documents may come from teaching and research institutions in France or abroad, or from public or private research centers.

L'archive ouverte pluridisciplinaire **HAL**, est destinée au dépôt et à la diffusion de documents scientifiques de niveau recherche, publiés ou non, émanant des établissements d'enseignement et de recherche français ou étrangers, des laboratoires publics ou privés.



**THESE de DOCTORAT DE L'UNIVERSITE
CLAUDE BERNARD LYON 1**

**Ecole Doctorale N° 340
Biologie Moléculaire Intégrative et Cellulaire**

Spécialité de doctorat : Cancérologie
Discipline : Biologie cellulaire et intégrative

Soutenue publiquement le 28/02/2023, par :
Marie Piecyk

**Identification de fonctions antagonistes de
GCN2 sur la biogenèse des ribosomes
selon la disponibilité en nutriments**

Devant le jury composé de :

MOYRET-LALLE, Caroline, Professeure, UCBL1

COLLURA Ada, CR, INSERM
FAFOURNOUX Pierre, DR, CNRS
LE CAM Laurent, DR, INSERM
MARCEL Virginie, DR, INSERM

FERRARO-PEYRET Carole, MCU-PH, UCBL1
CHAVEROUX Cédric, CR, CNRS

Présidente

Rapporteuse
Rapporteur
Examineur
Examinatrice

Directrice de thèse
Co-directeur de these

LIST OF CONTENTS

REMERCIEMENTS	3
ABBREVIATIONS LIST	9
DEFINITIONS OF THE DIFFERENT STRESSES	11
LIST OF FIGURES & TABLE	13
RESUME	14
SUMMARY	15
INTRODUCTION	17
I. INTRATUMORAL HETEROGENEITY IN NUTRIENT ACCESSIBILITY AND THE ASSOCIATED PHENOTYPIC MODIFICATIONS OF CANCER CELLS.....	17
1) <i>Altered vascularization within tumors and consequences on the intratumor metabolic microenvironment</i>	<i>17</i>
a. Heterogeneity of tumor perfusion rate	17
b. The altered metabolic microenvironment in tumors	19
2) <i>Phenotypic consequences of the nutritional stress on tumor cells</i>	<i>23</i>
a. Cell cycle arrest and apoptosis	23
b. Cell plasticity and acquisition of aggressive features	25
3) <i>Impact of the nutritional stress on patients' outcome and therapeutic resistances.....</i>	<i>27</i>
SUPPLEMENTARY BOX 1: GENERALITIES ON COLORECTAL CANCER.....	30
II. ADJUSTMENT OF RIBOSOME BIOGENESIS AND TRANSLATIONAL FUNCTION UNDERLY CELLULAR PLASTICITY AND OUTCOME.....	33
1) <i>Description of the ribosome biogenesis and translational function.....</i>	<i>34</i>
a. 47S pre-rRNA transcription by RNA polymerase I & processing.....	36
b. Transcription of 5S rRNA by RNA polymerase III and maturation	41
c. Ribosomes assembly, maturation and role in translation	41
2) <i>Consequences of the impairment of ribosome biogenesis and activity</i>	<i>43</i>
a. The nucleolar stress.....	43
i. Consequences of the nucleolar stress.....	44
ii. Impact of the nutritional stress on the nucleolar homeostasis.....	48
b. Impairment of ribosome function: ribosome stalling and collision.....	50
III. NUCLEOLAR AND RIBOSOMAL STRESSES AND RELATED SIGNALING PATHWAYS	51
1) <i>Modulation of RNA polymerases activity by mTORC1</i>	<i>51</i>
2) <i>The ribosomal-stress surveillance pathways.....</i>	<i>54</i>
a. The ribosome quality control	54
b. Ribotoxic stress response (RSR).....	56
c. The GCN2 pathway	57
i. Modalities of activation of GCN2 signaling	58
ii. Activation of the ISR and consequences	61
iii. Other substrates of GCN2	65
iv. Towards a non-canonical GCN2 pathway and new functions in unstressed cell?.....	65
OBJECTIVES & RESULTS OF THE STUDY	67
I. CONTEXT OF THE STUDY.....	67
II. RESULTS.....	69
ARTICLE.....	70
DISCUSSION & PERPESCTIVES.....	123
ANNEXES.....	139
BIBLIOGRAPHY	167

REMERCIEMENTS

Je remercie mes deux directeurs de thèse qui m'ont soutenue tout au long de ce parcours de doctorante, proche d'une course contre la montre sur les dernières semaines.

À **Mr Cédric Chaveroux**, pour l'investissement dont tu as fait preuve dans ma formation scientifique et pour m'avoir transmis ton intérêt pour ce projet GCN2 qui m'aura tant torturé l'esprit ces dernières années. Merci pour tout le temps passé à rédiger les articles et à corriger les manuscrits de thèse (ça y est, c'est le dernier). Je te remercie d'avoir cru en mes compétences et de m'avoir toujours poussée à aller plus loin. Bien que certaines aient été plus agréables que d'autres, merci aussi pour les longues discussions que nous avons pu avoir et qui ont participé à me faire avancer.

À **Mme Carole Ferraro-Peyret**, sans qui je n'aurais pu rejoindre ce groupe de recherche au début de mon internat de pharmacie et vivre cette aventure qu'est le doctorat. Je vous suis sincèrement reconnaissante pour le temps que vous avez pris pour m'accompagner, me former, et me guider dans ce parcours d'interne puis de doctorante. Merci de m'avoir encouragée pendant toutes ces années et de m'avoir apporté vos conseils, aussi bien d'ordre professionnel que plus personnel. Je vous remercie pour votre écoute, pour votre aide et pour votre bienveillance.

Je souhaite aussi adresser mes remerciements à **Mesdames Ada Collura, Virginie Marcel et Caroline Moyret-Lalle**, ainsi qu'à **Messieurs Pierre Fafournoux et Laurent Le Cam** pour m'avoir fait l'honneur d'être membres de mon jury de thèse. Je remercie particulièrement mes rapporteurs, Mme Collura et Mr Fafournoux, pour le délai supplémentaire accordé pour leur rendre ce mémoire et pour le temps qu'ils ont passé à le relire. Merci sincèrement pour vos remarques et vos conseils constructifs qui m'ont permis d'améliorer ce manuscrit.

Merci aux membres de mon comité de suivi de thèse, **Mme Sophie Vasseur et Messieurs Jean-Jacques Diaz et Klaus-Peter Janssen**. Je vous suis très reconnaissante de m'avoir accordé du temps pour vous présenter l'évolution de mes travaux au cours de ce doctorat et pour vos conseils avisés pour faire avancer ce projet.

Merci tout particulièrement à toi, Klaus, de m'avoir donné la chance de vivre cette belle expérience à Munich et de m'avoir accueillie aussi chaleureusement au sein de ton équipe.

Merci à mes co-équipiers du **groupe Chaveroux**, Joëlle, Cédric, Pierre-Alexandre et Paul, qui m'ont apporté soutien technique et moral pour venir à bout de ce marathon doctoral.

Merci à l'irremplaçable duo **Jojo et Cédric** (alias Junior) de m'avoir transmis vos connaissances quand ma formation technique était encore à construire entièrement. Merci de m'avoir épaulée personnellement et merci pour votre aide inestimable à bien des égards dans tout ce travail d'équipe. Un immense merci aussi à **PA et Paul** pour l'appui technique, particulièrement précieux durant les dernières semaines de préparation de cette soutenance.

Surtout, merci à l'ensemble du groupe pour cet environnement de travail presque familial, merci de m'avoir autant fait rire et d'avoir rendu agréables ces longues journées au labo. Contrairement à ce que diraient certains, c'est pas le syndrome de Stockholm mais de vraies rencontres dans un petit groupe de recherche que l'on pourrait qualifier de singulier... Merci à tous d'avoir rendu cette expérience professionnelle aussi enrichissante, j'ai autant adoré travailler avec vous que d'apprendre à vous connaître.

Merci à tous les amis et collègues rencontrés au labo, membres des **équipes Renno et Petrilli**, d'hier et d'aujourd'hui, sans qui l'ambiance au 6^{ème} étage du Cheney D ne serait pas ce qu'elle est ! Merci pour vos encouragements, pour le soutien, et pour votre bonne humeur. C'était un plaisir de vous retrouver chaque matin et de travailler en votre compagnie.

Un merci tout particulier à **Hélène** et **Jojo** encore, pour l'inestimable soutien moral. Merci d'avoir été là, aussi bien pour partager mes fous rires que pour sécher mes larmes. Plus que des collègues, merci d'avoir été des alliés infailibles tout au long de ce parcours.

Merci à **Sabine** et à **Stéphane** pour votre soutien et votre bienveillance. Merci Sabine de m'avoir transmis ton savoir et ta passion pour le noyau et les ribosomes, et merci de m'avoir toujours généreusement proposé ton aide. Merci Stéphane d'avoir partagé tes connaissances scientifiques et d'avoir pris du temps pour relire mon travail. Merci aussi pour ton optimisme et tes blagues au quotidien.

Merci à **Mélissa** pour ton amitié, ton énergie, ton écoute attentive et tes conseils sincères. Merci aussi pour les pauses thé et chocolat qui soulagent les cœurs et les esprits. Merci aussi à nos formidables pâtissières, **Delphine** et **Léa**, c'est toujours plus motivant de travailler quand on a la chance de pouvoir déguster régulièrement de merveilleux gâteaux. Surtout merci à vous d'avoir autant contribué à faire vivre le 6^{ème} et à rendre l'atmosphère si chaleureuse. Pour la décoration évolutive du labo au fil des saisons, le concours du meilleur « labtissier », ou encore pour l'organisation impeccable du Secret Santa (entre autres), un grand merci les filles.

À **tous les doctorants du 6^{ème}** mais pas seulement, je souhaite un parcours stimulant, riche humainement et en nouvelles découvertes !

Je remercie tous ceux qui ont participé au projet présenté dans ce mémoire qui est le fruit de tout un travail d'équipe.

Un merci tout particulier à l'**équipe Diaz** pour l'accueil et l'aide technique et scientifique. Merci à Seb et Fleur de m'avoir initiée aux joies du Northern Blot, une expérience qui n'est pas donnée à tout le monde aujourd'hui, et merci à Frédéric pour les conseils méthodologiques.

Un immense merci aussi à **Laura**, **Mouna** et **Mélanie** pour votre contribution dans la réalisation des expériences présentés dans cet article.

À **ma famille**, et à **mes grands-parents**, pour leur confiance en moi et leur soutien.

À **mes parents** avant tout. Je vous suis infiniment reconnaissante de m'avoir épaulée tout au long de ce cursus universitaire qui paraissait interminable. Merci d'avoir cru en moi en toutes circonstances, pour vos mots réconfortants, et pour votre amour sans faille.

Merci aussi à **mes frères et sœurs**, Romain, Clara et Lucas pour leurs encouragements.

Merci à toi Lucas, pour le soutien infailible au quotidien et pour les séances d'ostéopathie qui apaisent. À toi, mon petit frère pour qui les études ne font que (re)commencer... même si le chemin est long et parfois difficile, j'espère qu'elles seront aussi enrichissantes qu'elles l'ont été pour moi. Je crois fort en toi !

À **mes amis**, à Lyon et ailleurs...

Merci à toute la bande, aux corréziens expatriés et à ce groupe d'amis soudés au fil des années. Une pensée très spéciale pour **Audrey** et **Émilie**, à mes côtés avant même mon entrée à l'université. Je vous suis extrêmement reconnaissante d'être les amies et piliers que vous êtes pour moi depuis plus de 10 ans maintenant.

Sachez que tout ce long chemin était plus facile à parcourir à vos côtés. À vous, à tous ces moments passés ensemble et à tous ceux que l'avenir nous réserve encore !

À toi **Mathieu**, pour ton amour et ton soutien inconditionnel. Merci pour ton optimisme, pour ta confiance en mes capacités et pour l'aide précieuse que tu m'apportes au quotidien. Merci de m'avoir supportée, dans tous les sens du terme. J'ai beaucoup de chance d'être accompagnée et soutenue par un tel coéquipier. Merci pour tout.

Merci aussi à tous ceux que je n'ai pas cités. À tous les professeurs qui ont marqué mes années d'études et qui m'ont transmis cette envie d'apprendre, aux professionnels avec qui j'ai appris à travailler et qui m'ont donné foi en mes compétences, et à toutes les personnes qui m'ont accompagnée pour un bout de chemin au cours de ce long parcours d'étudiante.

Identification of antagonistic functions of GCN2 on
ribosome biogenesis depending on nutrient availability

ABBREVIATIONS LIST

47S pre-rRNA: 47S precursor rRNA	eEF1A: eukaryotic elongation factor 1-alpha 1
5-FU: 5-fluorouracil	eEF2: eukaryotic elongation factor 2
5'UTR: 5'-untranslated regions	eIF2a: eukaryotic translation initiation factor 2 alpha subunit
5S RNP: 5S ribonucleoprotein particle	eIF2B: eukaryotic Initiation Factor 2B
aa-tRNA: aminoacyl-tRNA	EMT: epithelial-mesenchymal transition
ABCE1: ATP-binding cassette sub-family E member 1	ETS: external transcribed spacers
Act. D: actinomycin D	FAP: familial adenomatous polyposis
AIMP3: ARS-interacting multifunctional proteins 3	FDG-PET: fluorodeoxyglucose (FDG)-positron emission tomography
ALDH1: aldehyde dehydrogenase	FOLFOX: folinic acid, 5-fluorouracil, oxaliplatin
ANKZF1: ankyrin repeat and zinc finger peptidyl tRNA hydrolase 1	G4: G-quadruplex
APC: adenomatous polyposis coli	GCN2: general amino acid control non-derepressible 2
ASCC1/2/3: activating signal cointegrator 1 complex subunit 1/2/3	GMP: guanosine monophosphate
ATF4: activating transcription factor 4	GTP: guanosine-5'-triphosphate
ATM: ataxia-telangiectasia mutated kinase	H3K27: histone 3 lysine 27
ATR: ataxia telangiectasia and Rad3-related protein	H3K4: histone 3 lysine 4
BRCA1/2: breast cancer 1/2	H3K9: histone 3 lysine 9
CAT tails: carboxy-terminal alanine and threonine residues	HisRS-like: histidyl tRNA-synthetase like
CD31: cluster of differentiation 31	HMG: high mobility group
CD44: cluster of differentiation 44	HNPCC: hereditary non polyposis colorectal cancer
CD45: cluster of differentiation 45	HRI: heme-regulated inhibitor
CDK2: cyclin-dependent kinase 2	IBD: inflammatory bowel disease
CIMP: CpG island methylator phenotype	IMPDH: inosine monophosphate dehydrogenase
CIN: chromosome instability	IPRES: innate anti-PD-1 resistance
CK2: casein kinase 2	ISR: integrated stress response
CMS: consensus molecular subtypes	ITS: internal transcribed spacers
COAD: colon adenocarcinoma	JNK: c-Jun N-terminal kinase
CRC: colorectal cancer	KLF4: Krüppel-like factor 4
CTC: circulating tumor cells	KRAS: Kirsten rat sarcoma viral oncogene homolog
CTD: C-terminal domain	LUAD: lung adenocarcinoma
DDR: DNA damages response	MAPK: mitogen-activated protein kinases
DEPTOR: DEP domain containing mTOR interacting protein	MDM2: murine double minute 2
DNA: deoxyribonucleic acids	MEF: mouse embryonic fibroblast
DNA-PKcs: DNA-depend protein kinases	Met-tRNAi: methionyl-tRNA initiator
DRP1: dynamin-related protein 1	MetRS: methionyl tRNA-synthetase
DSS: dextran sulfate sodium	MLH1: MutL protein homolog 1
E2F1: E2F transcription factor 1	

mLST8: mammalian lethal with Sec13 protein 8
MMR: mismatch repair
mRNA: messenger RNA
MSH2: MutS homolog 2
MSH6: MutS homolog 6
MSI: microsatellite instability
MSS: microsatellite stable
mTOR: mechanistic target of rapamycin
mTORC1: mechanistic target of rapamycin complex 1
mTORC2: mechanistic target of rapamycin complex 2
NNMT: nicotinamide N-methyltransferase
NANOG: homeobox transcription factor Nanog
NODAL: Nodal growth differentiation factor
NOR: nucleolar organizers regions
NPM1: nucleophosmin
NTD: N-terminal domain
OCT4: octamer-binding transcription factor 4
PARP: poly (ADP-ribose) polymerase
PD-1: programmed cell death protein 1
PD-L1: programmed cell death ligand 1
PDAC: pancreatic ductal adenocarcinoma
PERK: PKR-like endoplasmic reticulum kinase
PKR: double-stranded RNA-dependent protein kinase
PMS2: PMS1 homolog 2, mismatch repair system component
PP2A: Protein phosphatase 2
PRAS40: proline-rich Akt substrate of 40 kDa
PVOD: pulmonary veno-occlusive disease
Raptor: regulatory protein associated with mTOR
rDNA: ribosomal DNA
Rictor: rapamycin insensitive companion of mTOR
RNA: ribonucleic acid
RNA Pol: RNA polymerase
RP: ribosomal protein
RPL11: ribosomal protein 11
RPL5: ribosomal protein 5

RPS3: ribosomal protein S3
RPS10: ribosomal protein S10
RPS20: ribosomal protein S20
RQC: ribosome quality control
rRNA: ribosomal RNA
RSR: ribotoxic stress response
S6K1: 40S ribosomal S6 protein kinase
SNAIL: Zinc finger protein SNAI1
snoRNAs: small nucleolar RNA
SOX2: sex determining region Y-box 2TCGA
TFIIIA: transcription factor IIIA
TFIIIBb: transcription factor IIIB beta
TFIIIC1: transcription factor IIIC1
TFIIIC2: transcription factor IIIC1
TGFβ: transforming growth factor β
TIF-IA: transcription initiation factor 1A
TIF-IB: transcription initiation factor 1B
TMA: tissue micro-array
TP53: tumor protein 53
TRIP4: thyroid hormone receptor interactor 4
tRNA: transfer RNA
TTF-1: transcription termination factor 1
TWIST1: Twist-related protein 1
UBF: upstream binding factor
uORF: upstream open reading frame
UV: ultraviolet
Wnt: Wingless-related integration site
ZEB1: zinc finger E-box-binding homeobox1
ZNF598: RING E3 ubiquitin ligase zinc finger 598

DEFINITIONS OF THE DIFFERENT STRESSES

Nutritional/metabolic stress: limitations in nutrient availability leading to metabolic homeostasis impairment. The metabolic stress covers starvation in nutrients and hypoxia.

Nucleolar stress: disruption of nucleolar homeostasis, highlighted by the modification of normal nucleolar structure and function.

Ribosome biogenesis stress: impairment of at least one process involved in ribosomes biogenesis (rRNA transcription, processing, and/or ribosomes assembly) leading to a compromised production of mature ribosomes.

Ribosomal stress: impairment of ribosome translational function during the elongation phase of protein synthesis. Ribosomal stresses lead to stalling (= pausing) eventually collision of translating ribosomes.

Ribotoxic stress response: signaling pathway triggered by ZAKα in response to a ribosomal stress and leading to the induction of the stress-activated kinases: p38 and JNK.

LIST OF FIGURES & TABLE

FIGURE 1: THE ABNORMAL VASCULARIZATION IN TUMORS FAVORS A SPATIAL HETEROGENEOUS ACCESS TO NUTRIENTS.	18
FIGURE 2: THE VARIABILITY OF BLOOD FLOW IN DIFFERENT HUMAN CANCERS.	19
FIGURE 3: ANAEROBIC GLYCOLYSIS AND OXIDATIVE METABOLISM IN CANCER CELLS.	20
FIGURE 4: PANCREATIC DUCTAL ADENOCARCINOMAS DISPLAY LOWER CONCENTRATIONS OF SEVERAL NUTRIENTS COMPARED TO THE ADJACENT TISSUE.....	21
FIGURE 5: AMINO ACIDS CONCENTRATIONS ACCORDING TO SPATIAL LOCALIZATION WITHIN THE TUMOR.	22
FIGURE 6: THE METABOLIC CRISIS FACED BY TUMOR CELLS DRIVES TUMORIGENESIS.	24
TABLE 1: THE CONSENSUS MOLECULAR SUBTYPES CLASSIFICATION OF COLORECTAL CANCER.	31
FIGURE 7: RIBOSOME BIOGENESIS AT A GLANCE.	35
FIGURE 8: THE DIFFERENT NUCLEOLAR COMPARTMENTS VISUALIZED THROUGH ELECTRON MICROSCOPY.....	36
FIGURE 9: rDNA TRANSCRIPTION.	37
FIGURE 10: PROCESSING OF THE 47S PRE-rRNA IN HUMAN.	40
FIGURE 11: THE ELONGATION STEP OF TRANSLATION.	42
TABLE 2: CANONICAL AND NON-CANONICAL INDUCERS OF NUCLEOLAR STRESS.	43
FIGURE 12: DELOCALIZATION OF NUCLEOLAR MARKERS UPON NUCLEOLAR STRESS.	45
FIGURE 13: THE SIGNALING PATHWAYS OF mTORC1 AND mTORC1 COMPLEXES.	52
FIGURE 14: OVERVIEW OF THE RIBOSOME QUALITY CONTROL PATHWAY.....	55
FIGURE 15: SCHEMATIC REPRESENTATION OF THE RIBOTOXIC STRESS RESPONSE.	56
FIGURE 16: STRUCTURE OF THE HUMAN GCN2 PROTEIN KINASE.....	57
FIGURE 17: THE P-STALK PROTRUSION OF RIBOSOME.	58
FIGURE 18: PROPOSED MODEL FOR P-STALK MEDIATED ACTIVATION OF GCN2 BY HARDING ET AL.	59
FIGURE 19: GCN2 TRIGGERS THE ISR IN RESPONSE TO RIBOSOME STALLING.	61
FIGURE 20: THE PRE-INITIATION COMPLEX FORMATION.....	62
FIGURE 21: REGULATION OF PRE-INITIATION COMPLEX FORMATION BY EIF2B AND PHOSPHORYLATION OF EIF2A.	62
FIGURE 22: THE ROLE OF EIF2A IN THE CONTROL OF SELECTIVE TRANSLATION.	64
FIGURE 23: THE PYRIMIDINE AND PURINE SYNTHESIS PATHWAYS.	125
FIGURE 24: HYPOTHESIS SCHEME FOR THE PIVOTAL ROLE OF THE GCN2-METRS AXIS IN CANCER CELLS.....	127
FIGURE 25: DISCREPANCIES BETWEEN DIFFERENT GCN2 INHIBITORS.	128
FIGURE 26: ACTIVATION OF THE DDR UPON RNA POL I INHIBITOR ACCORDING GCN2 STATUS.	129
FIGURE 27: ASSOCIATION BETWEEN AMINO ACID DEPRIVATION SIGNATURE AND MSI STATUS IN COLORECTAL CANCER.	132
FIGURE 28: GENETIC LOSS OF GCN2 AND GENOMIC INSTABILITY.	134

RESUME

La vascularisation anormale des tumeurs conduit à une hétérogénéité spatiale d'accès aux nutriments pour les cellules cancéreuses. Leur adaptation au stress métabolique local implique à la fois des mécanismes de survie et de changement d'identité associés aux résistances thérapeutiques et donc favorisant la progression tumorale. Cette réponse adaptative nécessite la répression de processus anaboliques afin de préserver les ressources énergétiques et prévenir la mort induite par privation en énergie. Ceci passe notamment par la limitation concomitante de la biogenèse des ribosomes (RiBi) et la synthèse protéique, deux voies métaboliques hautement consommatrices en métabolites dérivés des nutriments. Toutefois, les mécanismes moléculaires à l'origine de ces ajustements restent partiellement élucidés. Ce travail de thèse s'inscrit donc dans la compréhension des mécanismes associés à la survie des cellules tumorales en réponse au manque en nutriments. Plus spécifiquement, cette étude a été focalisée sur l'identification de nouvelles voies de signalisation régulant la voie de biogenèse des ribosomes en fonction du contexte nutritionnel.

Des études récentes suggéraient qu'une kinase impliquée dans le « sensing » des nutriments, GCN2, était nécessaire au maintien de l'intégrité nucléolaire, site de la RiBi, bien que les conditions nutritionnelles associées n'étaient pas clairement définies. Ainsi, dans une première partie de mon projet de recherche, j'ai démontré que, sous stress nutritionnel, la kinase GCN2 contribue à la répression de l'activité de l'ARN polymérase I, enzyme responsable de la transcription du précurseur 47S essentiel à la RiBi. La perte de GCN2 dans ces conditions de déprivation aboutit à un stress nucléolaire et la mort par apoptose. Dans une seconde partie du projet, j'ai également mis en évidence que GCN2 soutient de manière inattendue la prolifération des cellules tumorales en condition riche en nutriments. Le mécanisme sous-jacent implique que GCN2 stimule la transcription de ce même précurseur 47S et, par extension, l'activation de la voie mTORC1 dans les cellules tumorales coliques en prolifération. L'inhibition de GCN2 dans ce contexte aboutit à une forte diminution de l'activité de l'ARN polymérase I, provoquant un stress nucléolaire. Cette vulnérabilité potentialise les effets cytotoxiques des agents chimiothérapeutiques perturbant la RiBi, conduisant alors à une mort importante des cellules.

Collectivement, mes résultats démontrent que la kinase GCN2 contrôle différenciellement l'activité de l'ARN polymérase I en fonction de la disponibilité en nutriments dans l'environnement. L'inhibition de GCN2 aboutit à : i) un stress nucléolaire indépendamment du contexte nutritionnel, ii) la mort des cellules lorsqu'elle est combinée à un second stress impactant la RiBi. Ces travaux ouvrent de nouvelles perspectives pour l'amélioration des traitements déjà utilisés en clinique, notamment dans le cadre des cancers colorectaux.

SUMMARY

Abnormal tumor vascularization leads to spatial heterogeneity of nutrient access for cancer cells. Their adaptation to local metabolic stress involves both survival and identity modifications mechanisms associated with therapeutic resistance and thus, favoring tumor progression. This adaptive response requires the repression of anabolic processes in order to preserve energy resources and prevent cell death induced by energy exhaustion. This is achieved through the concomitant limitation of ribosome biogenesis (RiBi) and protein synthesis, two metabolic pathways that are highly consuming in nutrient-derived metabolites. However, the molecular mechanisms underlying these adjustments remain partially elucidated. This thesis work is therefore part of the understanding of the mechanisms associated with tumor cells survival in response to nutrient deficiency. More specifically, this study focused on the identification of novel signaling pathways regulating the ribosome biogenesis pathway in response to the nutritional context. Recent studies suggested that a kinase involved in nutrient sensing, GCN2, was required for the maintenance of nucleolar integrity, the site of RiBi, although the associated nutritional conditions were not clearly defined. Thus, in a first part of my research project, I demonstrated that, under nutritional stress, GCN2 kinase contributes to the repression of RNA polymerase I activity, enzyme responsible for the transcription of the 47S precursor essential for RiBi. The loss of GCN2 under these conditions of deprivation leads to a nucleolar stress and cell death through apoptosis. In a second part of the project, I also demonstrated that GCN2 unexpectedly supports tumor cell proliferation in nutrient-rich conditions. The underlying mechanism involves that GCN2 stimulates the transcription of the same 47S precursor and, by extension, the activation of the mTORC1 pathway in proliferating colon cancer cells. Inhibition of GCN2 in this context results in a strong decrease in RNA polymerase I activity, causing nucleolar stress. This vulnerability potentiates the cytotoxic effects of RiBi-disrupting chemotherapeutic agents, leading to significant cell death. Collectively, my results demonstrate that GCN2 kinase differentially controls RNA polymerase I activity depending on the availability of nutrients in the environment. Inhibition of GCN2 results in: i) nucleolar stress independently of the nutritional context, ii) cell death when combined with a second stress impacting RiBi. This work opens new perspectives for the improvement of treatments already used in the clinic, in particular for colorectal cancers.

INTRODUCTION

I. INTRATUMORAL HETEROGENEITY IN NUTRIENT ACCESSIBILITY AND THE ASSOCIATED PHENOTYPIC MODIFICATIONS OF CANCER CELLS

1) Altered vascularization within tumors and consequences on the intratumor metabolic microenvironment

a. Heterogeneity of tumor perfusion rate

Along their development, most tumors cells are characterized by dysregulation of growth-associated pathways and cell cycle checkpoints, enabling an unrestrained growth and proliferation. The acquisition of mutations in coding genes of protein involved in the control of proliferation pathways, rendering cancer cells insensitive to the regulation of growth factor signaling (1).

Consequently, the high proliferation rate of tumor cells requires sustained anabolic processes that involve high demands of nutrients, supplied by blood vessels. Yet, vascularization in solid tumors is known to be abnormal and dysfunctional (for review see (2),(3)). The organization and structure of blood vessels within tumors appear to be different, resulting in a sinuous network and a chaotic blood flow (2) (Figure 1A). To illustrate this tight relationship between the perfusion and division rates, tumor cells close to blood vessels, and thus having a facilitated access to nutrients and oxygen (Figure 1B), display enhanced proliferative capacities (4). Conversely, cancer cells confined in poorly vascularized and exposed to a metabolic stress evidenced by hypoxic and necrotic areas (Figure 1C), do not divide (4).

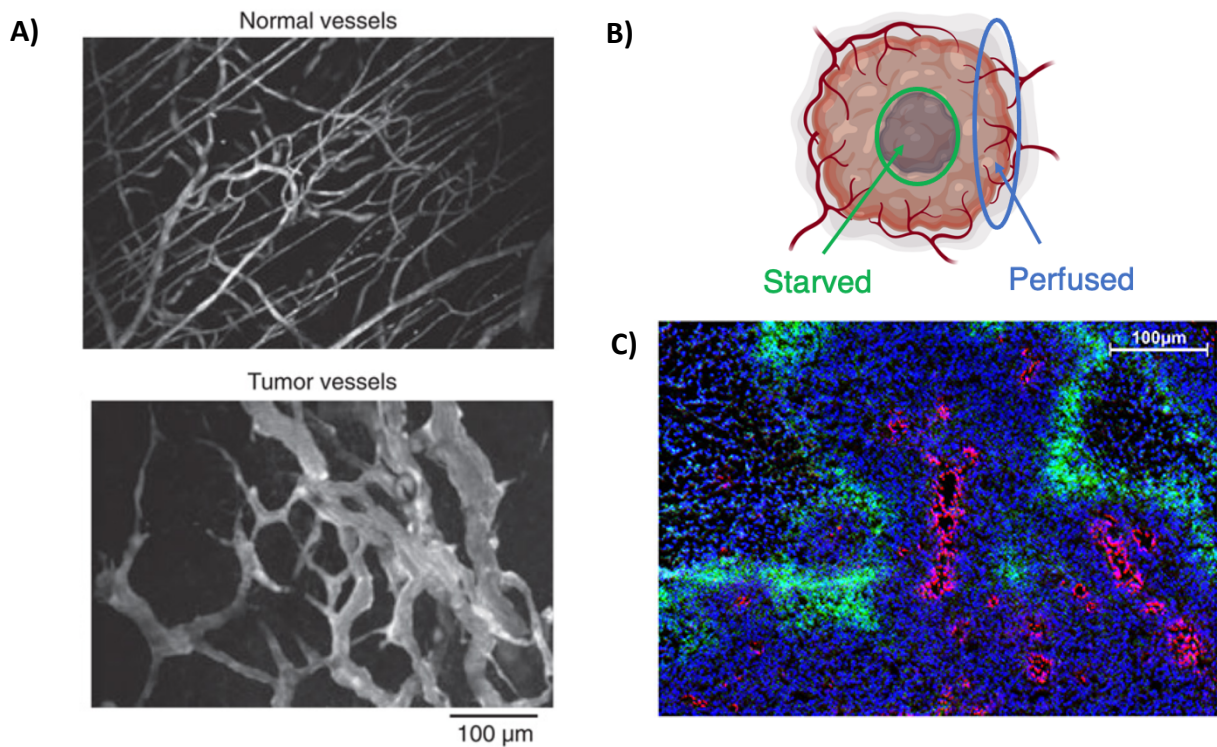


Figure 1: The abnormal vascularization in tumors favors a spatial heterogeneous access to nutrients.

A) Images of normal blood vessels (left) and vessels of a human colon cancer xenograft (right) in mice using FITC-dextran and multiphoton laser-scanning microscopy (3). **B)** Schematic representation of the intratumor heterogeneity of nutrients accessibility. Cells close to blood vessels have a facilitated access to nutrients in comparison with cells in poorly vascularized regions exposed to nutritional stress. **C)** Immunofluorescent staining of DNA (DAPI in blue), blood vessels (CD31 in red), and hypoxia (EF5 chemical marker in green) in xenografted tumors derived from pancreatic cell line. Hypoxic areas are heterogeneous and localized far away from blood vessels, illustrating the unequal supply of nutrients within the tumor (extracted from (4)).

Moreover, the matrix stiffening observed along tumor progression also participate to the impairment of the vascular system. As revealed notably in pancreatic ductal adenocarcinomas, the fibrotic extracellular matrix intensifies the interstitial pressure, leading to tumor blood vessels collapsing and in lower nutrients and oxygen supply (5,6).

Vascular density decreases as tumors grow and, accordingly, dense and bigger tumors are subjected to significantly lower bloodstream (2,7,8). Since each tumor has a particular vascularization pattern, blood perfusion is heterogenous between tumors within a same histopathological group (Figure 2)(7). Interestingly, these alteration of perfusion rates generate local variations in nutrient availability that will then contribute to the tumor cell heterogeneity and clonal expansion.

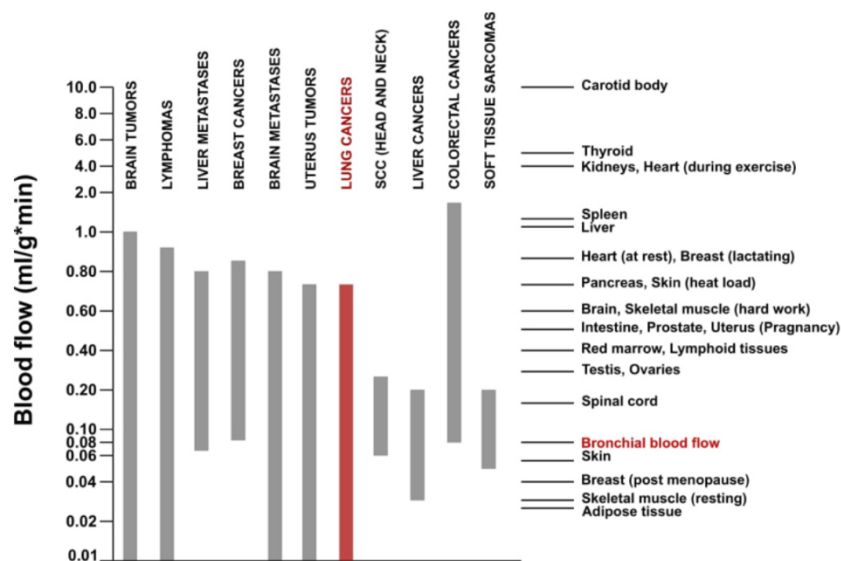


Figure 2: The variability of blood flow in different human cancers.

Mean of blood flow values in normal tissues are indicated on the right. Modified by Dr. Helena Dragic, from Vaupel P et al (7)

b. The altered metabolic microenvironment in tumors

This heterogenous blood flow thus leads to an altered metabolic microenvironment consisting in drastic changes in the availability of various metabolites. Furthermore, as the viability and division capacities of tumor cells are highly dependent on nutrients and oxygen supplies, these variations imply profound metabolic and phenotypic modifications of the cells that have been extensively investigated in the literature.

One widely-accepted characteristic of tumors cells is that they are notably addicted to glucose because of oncogenic mutations sustaining high proliferation rate that requires increased building blocks levels for cellular anabolic processes (1,9). This enhanced avidity for glucose is even exploited for cancer diagnosis by clinicians using FDG-PET scan imaging (9). High demand for glucose is a hallmark of tumor cells, highlighted by the work of Dr Warburg in the 1920s. He demonstrated that cancer cells have a dysregulated glucose metabolism favoring the glycolytic pathway, independently of the levels of oxygen, to produce energy (1,9). At the moment of his discovery, Warburg proposed that this aerobic glycolysis is caused by mitochondrial defect in tumor cells (9). However, this dogma of an “on/off” switch from oxidative phosphorylation to glycolysis in tumors such as proposed by the so-called Warburg effect is currently reconsidered

as some tumors are able to increase both anaerobic and aerobic glycolysis capacities (Figure 3) (9,10).

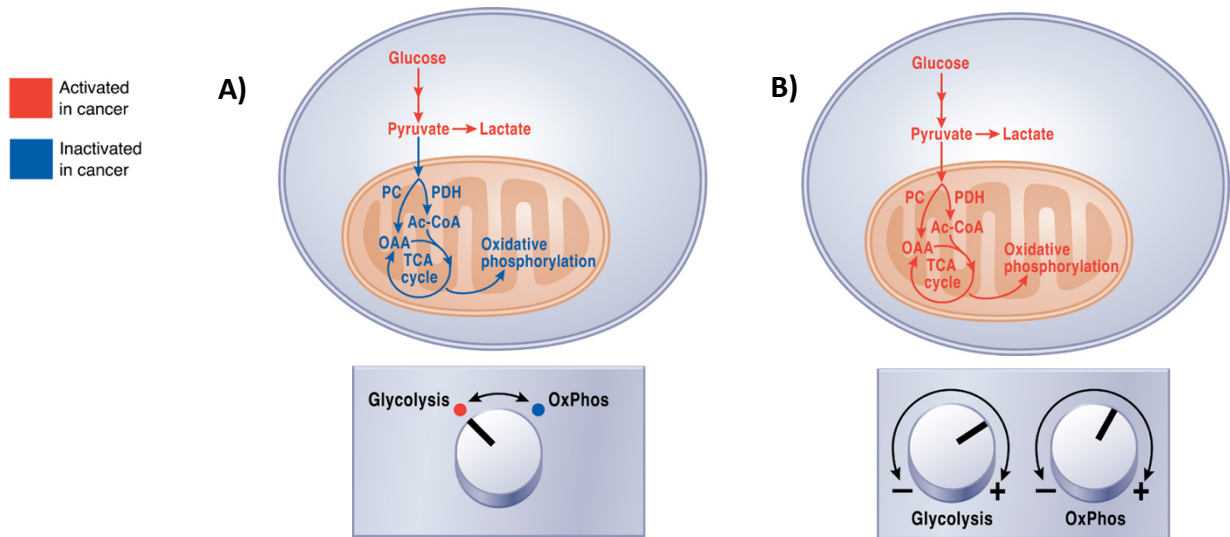


Figure 3: Anaerobic glycolysis and oxidative metabolism in cancer cells.

A) Representation of the Warburg effect describing, in the 1920s, an enhanced glycolysis and a repressed oxidative phosphorylation in cancer cells. **B)** Metabolomic analysis in 2016 revealing that tumor cells increase both glycolysis and glucose oxidation. Adapted from (9).

Consistent with these observations, due to a high conversion of glucose, several studies measured lower glucose amounts in the tumor compared to the adjacent normal tissue (10,11). For instance, the metabolomic study of Hirayama and colleagues, performed in paired-tissue samples of colon tumors, revealed a 10-fold decrease in glucose concentrations in tumors compared to the normal counterpart (10). This was associated to enhanced levels of metabolic intermediates of several pathway involving glucose: the glycolysis, the pentose phosphate and Krebs cycle pathways (10). In pancreatic tumors as well, characterized by a massive stroma, glucose concentrations were decreased in the tumors compared to normal tissue, associated to an enhanced aerobic glycolysis (Figure 4) (11).

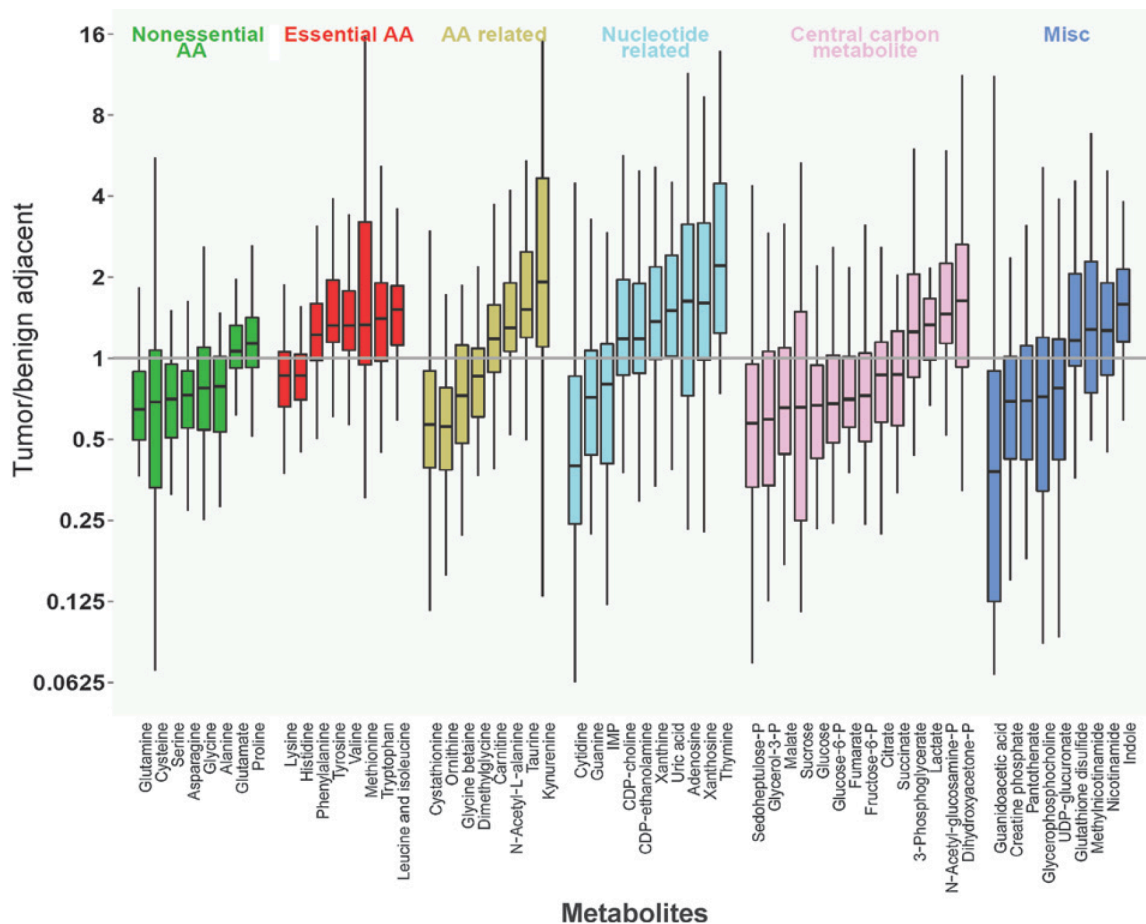


Figure 4: Pancreatic ductal adenocarcinomas display lower concentrations of several nutrients compared to the adjacent tissue.

Concentrations of several metabolites in PDAC tumors compared to benign adjacent counterpart. Of note, glucose and several amino acids such as glutamine, serine or asparagine are decreased in tumors. Extracted from (11).

However, tumor cells not only rely on glucose consumption but use also other nutrients to sustain an excessive growth rate. Indeed, in the same study, Kamphorst and coworkers measured decreased concentrations of several amino acids in pancreatic tumors in comparison with the normal tissue (Figure 4) (11). Consistent results have been reported by Dr Muir's lab showing lower amounts of glucose and amino acids (arginine, tryptophan) in pancreatic tumoral interstitial fluid than in plasma (12). However, several amino acids amounts were higher in colon tumors compared to adjacent tissue. Particularly glutamate was found accumulated in colon tumor cells although glutamine amount is unchanged. This suggests an active conversion of glutamine into glutamate through the glutaminolysis pathway and, by extension, that glutamine is limiting in the microenvironment of colon tumors (10).

In addition to a bulk nutrient scarcity in tumors, the oxygen and nutrients availability within the tumor is spatially heterogeneous as previously shown in Figure 1B-C. As expected, lower concentrations of several amino acids are observed in poorly-perfused regions of the melanoma tumors compared to those at the periphery of vessels (Figure 5) (13). Of note, the arginine, asparagine and glutamine are the amino acids whose concentrations drop the most in tumor area with high vascularization defects.

Table 1 Amino acid concentrations in tumour periphery and core regions.

Amino acid	Mean (μM)		Ratio (Core/periphery)	P
	Periphery	Core		
Arg	133.87	27.73	0.20	0.00030
Asn	121.41	28.99	0.29	0.022
Gln	487.66	229.15	0.46	0.0033
Ser	575.73	277.54	0.47	0.0060
Asp	666.86	387.92	0.55	0.0058
Hyp	18.46	14.40	0.69	0.040
Trp	22.11	20.21	0.71	0.24
Phe	82.47	65.75	0.72	0.047
Tyr	194.13	152.47	0.76	0.064
Ala	978.48	807.27	0.82	0.00045
Gly	1077.70	898.67	0.83	0.18
Taurine	378.89	350.62	0.85	0.25
Met	148.07	126.03	0.87	0.034
Ile	140.70	126.12	0.88	0.050
Leu	260.55	226.25	0.90	0.034
Glu	1870.06	1675.91	0.90	0.031
Citrulline	99.02	110.02	0.91	0.69
Thr	527.11	476.26	0.91	0.10
Lys	174.50	165.59	0.92	0.19
His	167.78	153.61	0.93	0.28
Orn	44.67	53.27	0.96	0.89
Val	284.05	271.62	0.97	0.48
Pro	301.11	330.89	1.16	0.048
Cys-Cys	12.15	8.69	50.82	0.23

Figure 5: Amino acids concentrations according to spatial localization within the tumor.

Concentrations of amino acids measured in melanoma tumors at the periphery compared to the core. Table from (13).

2) Phenotypic consequences of the nutritional stress on tumor cells

The perfusion rate and accessibility to blood supplies define the fate of the tumor cell as well as its phenotypical features. Notably, cell survival in conditions of restricted access to nutrients rely on profound changes driving modifications of cell phenotype and acquisition of pro-tumoral abilities.

a. Cell cycle arrest and apoptosis

The degree of starvation defines the balance between proliferation arrest and cell death. Hence, the intensity, the nature and duration of the metabolic stress is critical for cell outcome (14). If the cell is exposed to a severe and unsalvageable stress, a pro-apoptotic signaling will be triggered, leading ultimately to cell death (15–20). Therefore, cell adaptation towards the evolution of the nutritional microenvironment is determinant in the process of tumorigenesis.

The initiation step of tumorigenesis represents a relevant model of cell death caused by the metabolic stress.

In response to oncogenic mutations, malignant cells increase their demand of nutrients to support the dysregulated proliferation. This exacerbated uptake and conversion of nutrients can result in nutrient exhaustion within the microenvironment and potential lethal metabolic stress. Firstly, limitation of biosynthetic processes will prevent intracellular exhaustion of ATP and amino acid and is accompanied with cell cycle arrest (21,22). DNA replication and progression along the different phases of cell cycle are under control of cell-cycle checkpoints. These checkpoints are surveillance mechanisms ensuring notably that microenvironmental conditions are suitable for genomic replication and integrity during mitosis. If not, the cyclin-dependent kinases (CDKs) and cyclin inhibitors hinder cell cycle progression by regulating the transitions between each phase of the cell cycle (G1, S, G2, M). Delays in cell cycle progression have been observed in condition of nutritional depletion such as glucose or glutamine deprivation, but the checkpoints dysregulated are unclear and appears to be context/model-dependent (23–29). For instance, controversial data are observed for glutamine, since deprivation for this amino acid can lead to cell cycle arrests in G1, S or G2/M (23,24,27,29). These discrepancies might be explained by the type of i) applied starvation (complete or partial) and ii) stress submitted to the cell. Indeed, glutamine starvation can induce both growth

impairment and DNA damages. The stress severity can thus determine whether the cell will be arrested in G1/S phase (cell growth impairment) or G2/M (DNA damage response pathways). The phase in which the cell is originally positioned before the stress is also determinant. In asynchronous cells, glutamine deprivation triggers a G1/S arrest whereas, in synchronous cells, the same stress slows down also the G2/M phase (24). Finally, the intrinsic capacity of the tumor cells to cope with the nutritional stress is another determinant for the type of cell cycle arrest. Overall, these data illustrate the complexity to mimick a relevant starvation state *in vitro*. Nevertheless, based on *in vivo* or 3D models, tumor cells located in poorly-perfused areas are majorly blocked in G1/S indicating that a complex metabolic stress is rather associated to growth impairment (30). Overall, modulating the cell-cycle checkpoints activity remains an efficient mechanism to survive to transient stressful conditions as it allows tumor cells to “rest” until conditions favorable for their progression are met again.

However, if the stress is prolonged at an intolerable degree, most of the transforming cells will die by apoptosis; this event constituting a first “antitumoral barrier” (15–20). Therefore, only tumor cells that are able to adapt and undergo profound modifications, mostly related to differentiation state and plasticity, will survive and promote the tumor onset (Figure 6).

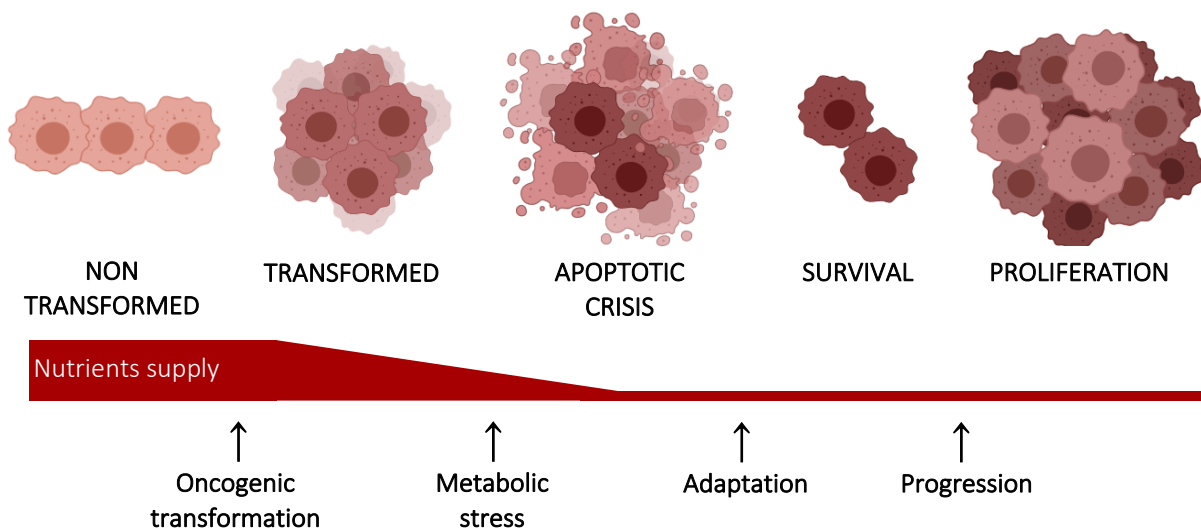


Figure 6: The metabolic crisis faced by tumor cells drives tumorigenesis.

Adaptation to metabolic stress is determinant for tumor cell survival at early stages of tumorigenesis. Transformed cells have excessive demands in nutrients, higher than what is supplied by blood vessels, leading to a metabolic stress. Most of the cells undergo apoptosis, whereas cells able to adapt will survive and foster tumor progression. Adapted from (16) and designed with BioRender.

b. Cell plasticity and acquisition of aggressive features

As a matter of fact, the intratumor nutritional stress acts as a selective pressure on malignant cells. Indeed, apoptosis escape and survival implicate the establishment of a complex plasticity program supporting dedifferentiation and invasive features (13,31,32). These phenotypic modifications are accompanied by the acquisition of novel characteristics supporting tumor cell resistance to conventional treatments.

- **Loss of differentiation**

Cell adaption to prolonged metabolic stress particularly involves a plasticity program related to cell identify modification and driving loss of cell differentiation. Functionally, cancer stem cells isolated from pancreatic adenocarcinomas are insensitive to glycolysis inhibition induced by galactose treatment and artificially mimicking glucose deprivation, demonstrating that these cells, naturally evolving in starved-niches, remain resistant to metabolic stress (33). Indeed, low levels of oxygen and nutrients induce stress pathways that promote the expression of markers related to stemness in tumor cells. For instance, in several types of cancer, the metabolic stress leads to an augmentation of the stemness-like markers, such as OCT-4 (34,35). Consistently, OCT-4 expression is localized in poorly-perfused areas of hepatocarcinomas (36). This observation is in line with the work of Jewer and colleagues on breast cancer cells, highlighting that elevation of stemness-related markers upon stress, SNAIL, NODAL and NANOG, relies on a specific translational rewiring rather than a transcriptomic program (31).

Beyond the shortage of glucose, glutamine restriction also contributes to the upregulation of stemness-related markers (NANOG, OCT4, SOX2, KLF4) in various tumor cell lines and *in vivo* in and patients (13,36). The underlying mechanisms involves epigenetics remodeling including the elevation of histones trimethylation (H3K4, H3K9 and H3K27) that promotes their expression of these genes. In a similar manner, glutamine deprivation decreases the availability of alpha-ketoglutarate, required to maintain hypomethylation of DNA and the transcription of genes involved in the differentiation process of colon cancer cells. Accordingly, low levels of glutamine activate the Wnt signaling pathway, a well-known pathway involved in dedifferentiation of colon cancer cells (37). Lastly, glutamine scarcity leads to the generation of ROS that, rather than forcing cells to undergo apoptosis, favors the phosphorylation of the mitochondrial fission

regulator GTPase DRP1 protein, resulting in mitochondrial fragmentation and higher proportions of stem cells expressing the CD44 and CD45 dedifferentiation markers (38).

Altogether, these studies highlight that reduced glutamine amounts within the tumor cells microenvironment is particularly determinant for the loss of differentiation. Though glutamine is necessary to sustain high proliferation rates, it is not essential for their survival. Hence, it supports the idea that glutamine is a critical nutrient for cancer cells as it strongly participates in the tumor cell identity modifications in response to stress, allowing the acquisition of aggressive features that condition tumor cells sensitivity to treatments and patients' prognosis.

- **Invasiveness**

Tumor cells exposed to low concentrations of oxygen and nutrients also develop migration and dissemination capacities. Notably, a well-known phenomenon called epithelial-mesenchymal transition (EMT) allow tumor cells to repress epithelial characteristics to gain mesenchymal features. As a consequence of exposure to nutritional stress, the activation of EMT: i) participates to an increased proportion of cancer stem cells, characterized by quiescence, a state of reversible cell cycle arrest associated to low proliferation rate and decreased anabolic processes (see next paragraph) and ii) promotes tumor cells mobility and ability to disseminate (39).

Cell lines adapted to low oxygen conditions have enhanced tumorigenic properties and invasive capacities as demonstrated by their facilitated ability to form tumors once injected in mice tails, independently of their histological subtype origin (35). In accordance, cells subjected to nutrient starvation such as glucose deprivation induce the expression of matrix metalloproteinases, enzymes involved in matrix remodeling that permit to degrade the extracellular matrix and to escape (40). In hepatocarcinoma models, EMT can be triggered by combining glucose starvation and hypoxia (41). Glutamine starvation contributes also to metastasis induction as it enables the expression of specific proteins related to an enhanced invasiveness, including the EMT marker Snail2 in pancreatic breast and skin cancers (31,42) (13). Collectively, these data underline that: i) contrarily to most *in vitro* studies, the acquisition of dissemination properties relies on the exposition to plural nutrients deprivation as observed in the complex intratumor metabolic microenvironment, ii) an impairment of the mitochondria metabolism (hypoxia, glutamine starvation) is critical for EMT induction. Moreover, in colon cancer, the nutritional stress experienced by cancer cells, such as hypoxia, augments the

synthesis of cytokines that trigger signals to normoxic cells and promotes their metastatic properties (43). This demonstrates that the heterogeneity of the nutritional environment in the tumor actually has a global impact on tumor progression.

3) Impact of the nutritional stress on patients' outcome and therapeutic resistances

Although exposure to nutritional stress triggers plasticity programs in tumor cells, whether these observations, mostly in preclinical models, can be extended to clinical outcome remain a critical point to address. Observations reported in patients confirm that the exposition of cancer cells to scarcity is associated to increased resistance to therapeutics and high risk of relapses for patients in a wide panel of cancer. The activation of stress responses induced by the nutritional starvation, majorly highlighted through proteomics approaches, have been reported and associated to poorer prognosis in several tumors such as melanomas, gastric, ovarian cancers, or lung and pancreatic adenocarcinomas (44–48).

My thesis project focused on colon adenocarcinoma (COAD) (see the associated supplementary box 1 for extended information on the pathology) and several evidences suggest that the nutritional stress participates in COAD aggressiveness and resistance to conventional therapies. For instance, the consensus molecular subtype (CMS) classification showed that the CMS4 subgroup is associated to a high stromal signature and an increased expression of genes involved in dedifferentiation and EMT (Table 1 in supplementary box 1) (49,50). Cancers classified in this particular subgroup display a high enrichment for gene signatures related to hypoxia and low DNA repair (51), consistent with the known defects in DNA repair pathway in cells exposed to hypoxic conditions (52,53). Patients diagnosed with a colon cancer of the CMS4 subgroup have the worse overall and progression-free survival compared to the other subgroups (49,50), supporting that the metabolic stress in COAD contributes to tumor progression and poor response to treatment.

In a similar manner, in clinics, the number of circulating tumor cells (CTC), that already have acquire the ability to migrate, is correlated to patients' outcome in metastatic colon cancer

disease (54). However, the pool of CTC is constituted of different subpopulations expressing singular genetic and phenotypic features. Consequently, even if every CTC is able to disseminate, not all of them will be able to raise secondary tumors. Only cancer cells that have acquired dedifferentiated and invasive characteristics are equipped to create niches auspicious for the development of metastasis. Accordingly, an elevated proportion of CTC expressing stem-related and mesenchymal markers such as CD44, ALDH1 and TWIST1 are predictive of bad prognosis and recurrence in digestive and breast cancers (55–57). Consequently, the tumoral microenvironment might also contribute to cancer cells behavior *in vivo* as well and the subsequent patients' outcome.

Resistance to chemotherapies

The poor prognosis for patients bearing tumors chronically exposed to metabolic stress is also related to the decrease sensibility of tumor cells adapted to nutrient scarcity when exposed to therapeutic agents. For instance, the CMS4 group of colon cancers is resistant to commonly used therapeutics such as 5-FU and Oxaliplatin in the FOLFOX regimen or to anti-EGFR treatment (49). Studies *in vitro* indeed demonstrated that colon cancer cells developing resistance to conventional chemotherapies Oxaliplatin or 5-FU share common features with cancer stem cells. This supports that the deprived nutritional environment not only delays cell cycle progression to promote the entry in a quiescent state, naturally resistant to chemotherapeutic agents exclusively targeting proliferative cells, but also drives the acquisition of dedifferentiated markers also promoting therapeutic resistance (58)(59,60).

Immunotherapy resistance

Correlative data show that alteration of the metabolic microenvironment is also contributing to immunotherapy resistance. Notably, the strong expression of metabolic stress-related biomarkers in microsatellite stable tumors is associated with cancer relapse (61). Interestingly, these tumors are naturally poorly sensitive to immunotherapy and majorly classified into the CMS2 or the CMS4 subgroups, the latter being particularly characterized by an enrichment in genes induced by metabolic stress exposure (62). Conversely, in microsatellite instable colon tumors, mostly gathered in the CMS1 subgroup and originally responsive to immune checkpoints inhibitors, a metabolic reprogramming promoting glycolysis such as observed upon metabolic stress is associated with immunotherapy failure (63).

This observation has also been reported in other types of cancer. For instance, squamous head and neck tumor cells evolving in a stressful metabolic environment display a low sensitivity to immunotherapy (61,64). Among the mechanisms modulated in response to nutritional stress, a poor response to immunotherapies such as anti-PD-L1 treatments in melanoma cancer cells is promoted by the translational reprogramming inducing the IPRES (innate anti-PD-1 resistance) gene signature (46).

Moreover, the metabolic rewiring occurring upon nutritional stress not only favors modifications of cancer cells' identity but also impair the capacities of immune cells, all encouraging therapeutic resistance. For instance, as a consequence of the metabolic stress and subsequent alteration of mitochondria function, the production of lactate increases, resulting in an important acidification of the microenvironment, diverted by tumor cells to acquire new pro-survival features such as invasive properties, but is also associated to the repression of T cells or macrophage immune cells activity (65,66). Another example of the crosstalk between cancer cells metabolism and immunosuppression is the enhanced consumption of tryptophan in tumor cells and consequent synthesis of formate that is used to fuel the nucleotide synthesis pathway of tumor and stromal cells (67). Furthermore, tryptophan degradation produces kynurenine, a immunosuppressive metabolite inhibiting immune cells such as T cells (68).

This highlights that the metabolic environment influence patients' response to immunotherapy through the combination of pro-survival phenotypic modifications of cancer cells and the impairment of immune cells abilities.

Altogether, this demonstrates that the metabolic microenvironment conditions the response to both historical and recently developed treatments.

Supplementary box 1: Generalities on Colorectal Cancer

Colorectal cancer (CRC) is the second deadliest cancer and third most frequently diagnosed cancer worldwide with almost 2 million new cases in 2020. Its incidence, favored by western lifestyles, continues to increase nowadays with 3.2 million new cases expected (1.6 million deaths) in 2040 (69).

In clinics, CRC tumors are usually stratified according to: i) the TNM classification in stages I to IV depending on tumors' size and invasiveness, ii) the histological subtype (CRC worldwide >90% adenocarcinomas, 5-20% mucinous, and other rarer subtypes) (70). Depending on the origin of the pathology, CRC can be also either inherited, familial or sporadic: i) inherited CRC (5-10% of CRC) arise in patients with identified genetic alterations such as hereditary non-polyposis colorectal cancer HNPCC (also called Lynch syndrome) linked to mutations in genes of the DNA mismatch repair pathway (MMR); ii) familial CRC (20-25%) is restricted to patients with familial history of CRC and in absence of inherited syndrome; iii) finally, sporadic CRC (70%) gather all the other patients with no hereditary mutations or familial history. A latest group can be defined as colitis-associated CRC that develop from long-standing inflammatory bowel diseases (IBD), exposing to a 3-fold increased risk to develop CRC (71–73).

Concerning the pathogenesis, CRC results from the uncontrolled proliferation of glandular epithelial cells in the colon (72% of CRC) or in the rectum (28% of CRC) (70). CRC frequently results from the clonal expansion of an intestinal cell with stemness features, giving birth to a primary benign lesion that will then eventually transform into an invasive carcinoma (74,75). Development of the disease is majorly related to alterations in pathways regulating stemness, notably altering the crosstalk between Wnt/ β -catenin and Notch pathways, mutually competing with each other to tightly control stem cells differentiation (76).

The progression towards malignancy is enabled by an accumulation of innate or acquired alterations in the genome of colon cancer cells. Notably, CRC tumorigenesis has been linked to mutations in proto-oncogenes (*MYC*, *RAS* or *WNT* for example), in tumor suppressor genes (such as *APC*, *TP53*), and in DNA repair genes (*MSH2*, *MSH6*, *MLH1*, *PMS2* among others) (70,77,78). In sporadic CRC, loss of *APC*, constitutively activating the Wnt pathway, is recognized as the primary event driving adenoma development. This event is usually followed by mutations in the *RAS* pathway and loss of *TP53* tumor suppressor, enabling the shift towards adenocarcinoma (77). In the contrary, in IBD-diverted CRC, an increase in environmental ROS lead primarily to mutations in *TP53* and low-grade dysplasia converting in high-grade dysplasia and finally carcinoma thanks to additional mutations (79). Yet, *APC* mutations occurs lately and is rarely present in the corresponding tumors (79). Additional mechanisms promoting the tumorigenesis are linked to mutations of genes involved in the DNA repair, *WNT*, *RAS* and *TGF β* pathways (80). In a different manner, inherited syndromes covering notably HNPCC and familial adenomatous polyposis (FAP) respectively associated with initial alterations in genes involved in the DNA mismatch repair pathway (81) or *APC* (82). Additional mutations (*KRAS*, *TP53*,...)

will then foster the tumorigenic process (83). Altogether, this illustrates the diversity of genetic alterations participating to the pathogenesis of colon cancer.

All these mutations initiating tumorigenesis can lead to perturbation in cell cycle checkpoints, DNA repair response and accumulation of unrepaired DNA damages, resulting in a pro-tumorigenic instability of the genomic information. Three different pathways underly genomic instability: chromosome instability (CIN), microsatellite instability (MSI), and CpG island methylator phenotype (CIMP) (70). CIN (also known as microsatellite stable MSS status, 85% of CRC) results from errors in chromosomes segregation and leads to alterations in chromosome number and structure. MSI tumors (15% of CRC) represents a subgroup with defects in DNA mismatch repair (MMR) leading to unrepaired hypermutation of microsatellite sequences, in absence of huge chromosomal abnormalities. CIMP is associated to increased methylation of CpG islands driving gene silencing. The majority of sporadic CRC display chromosomal alterations, associated with MSS status. On the other side, tumors with MSI-high status mainly develop in the predisposed context of IBD and in inherited HNPCC. This highlights the complexity to stratify tumors according to their specific features in order to better understand the specificities and vulnerabilities of each pathology. The genetic and proteomic instability of MSI tumors is now clinically considered as a prognostic biomarker for immunotherapy achievement (62).

Beyond the classical CRC classification based on genomic alterations, the Consensus Molecular Subtypes (CMS) of colorectal cancer has emerged has a comprehensive tool for the classification of CRC. These tumors have been separated into different subtypes depending on tumors' genomic background and phenotypical characteristics. The CMS is the result of the analysis of large-scale gene expression studies to define four specific diseases patterns (Table 1) (50).

In this context, MSS tumors are mainly categorized in the CMS2 and CMS4 subgroups whereas MSI tumors represent the majority of the CMS1 and a part of CMS3 subgroup. According to this classification, the CMS4 represents the subgroup with the worse relapse-free and overall survival compared to the other CMS. Intriguingly, the CMS4 is characterized by a strong stromal infiltration, angiogenesis and increase in dedifferentiated markers, common features found in cells exposed to chronic metabolic stress.

CMS1 MSI Immune 14%	CMS2 Canonical 37%	CMS3 Metabolic 13%	CMS4 Mesenchymal 23%
MSI, CIMP high, hypermutation	SCNA high	Mixed MSI status, SCNA low, CIMP low	SCNA high
<i>BRAF</i> mutations		<i>KRAS</i> mutations	
Immune infiltration and activation	WNT and MYC activation	Metabolic deregulation	Stromal infiltration, TGFβ activation, angiogenesis
Worse survival after relapse			Worse relapse-free and overall survival

Table 1: The Consensus Molecular Subtypes classification of colorectal cancer.

Main characteristics of colorectal tumors according the four different CMS subgroups (Extracted from (50))

II. ADJUSTMENT OF RIBOSOME BIOGENESIS AND TRANSLATIONAL FUNCTION UNDERLY CELLULAR PLASTICITY AND OUTCOME

Preamble: adjustment of the global translational machinery in tumor cells' adaptative response

Cancer cell adaptation to this altered intratumoral nutritional environment is a complex process implicating numerous epigenetic, biochemical, molecular and reprogramming pathways. As mentioned above, considering that translation and ribosome biogenesis are high energy consuming processes for the cells (84,85), the regulation of the protein synthesis and the associated translational program are particularly key processes involved in the cellular adaptation upon metabolic stress. Adjustment of the translational program aims at two major outcomes: i) the preservation of energy and nutrients pools to prevent cell death (21,86–88) and, ii) the selective translation of a subset of mRNAs involved in cell plasticity to face the stress (31,89–93). The repression of the initiation phase of translation in cells exposed to nutritional stress is a critical step in the global downregulation of protein synthesis (preservation of metabolites pools), and concomitantly favors the translation of specific mRNAs encoding dedifferentiation and EMT markers for example (13,31).

Yet, the translation is ensured by mature and active ribosomes, ribonucleoprotein complexes in charge of: i) decoding mRNA sequences and ii) the synthesis of the corresponding protein (94). The translational reprogramming and activity require the concomitant adaptation of ribosomes biogenesis. For instance, the downregulation of ribosomes abundance protects the cell from proteotoxic stress induced by misfolded proteins upon arsenic treatment (95). Thus, the production of ribosomes is modulated to tightly match with translation demands and abilities of the cell.

The ribosome biogenesis necessitates nucleotides for ensuring the transcription of rRNAs. However the pool of nucleotides is highly dependent of the available nutrients, mainly glucose and glutamine (96–101). Hence, the control of ribosome biogenesis rates is determinant in conditions of limited access to nutrients (96).

This chapter will be focused on the role of played by the ribosome biogenesis modulation according the nutritional milieu. The first part will be dedicated to the description of the ribosome biogenesis pathway whereas the second part will focus on the consequence of ribosome biogenesis impairment upon stress.

1) Description of the ribosome biogenesis and translational function

The eukaryotic functional ribosome, called the 80S ribosome, is constituted of two subunits: i) the small 40S subunit composed of 18S rRNA and 33 ribosomal proteins, and ii) the large 60S subunit resulting from the association of 28S, 5S and 5.8S rRNAs with 47 ribosomal proteins (97).

The production of ribosomes relies on the synchronization of three RNA polymerases (RNA Pol): i) the RNA Pol I is in charge of the transcription of the precursor rRNA cleaved in 18S, 28S and 5.8S mature rRNA, ii) the RNA Pol III produces the 5S mature rRNA and transfer tRNAs, and iii) the RNA Pol II synthesizes the ribosomal proteins as well as small nucleolar snoRNAs involved in mRNA processing (Figure 7) (102).

Considering its central role in the translational process, the synthesis of ribosomes is tightly regulated and requires the coordination of several processes occurring in different cellular compartments, including the production and maturation of rRNAs, the assembly of ribosomal proteins, and finally the maturation of ribosomes (102).

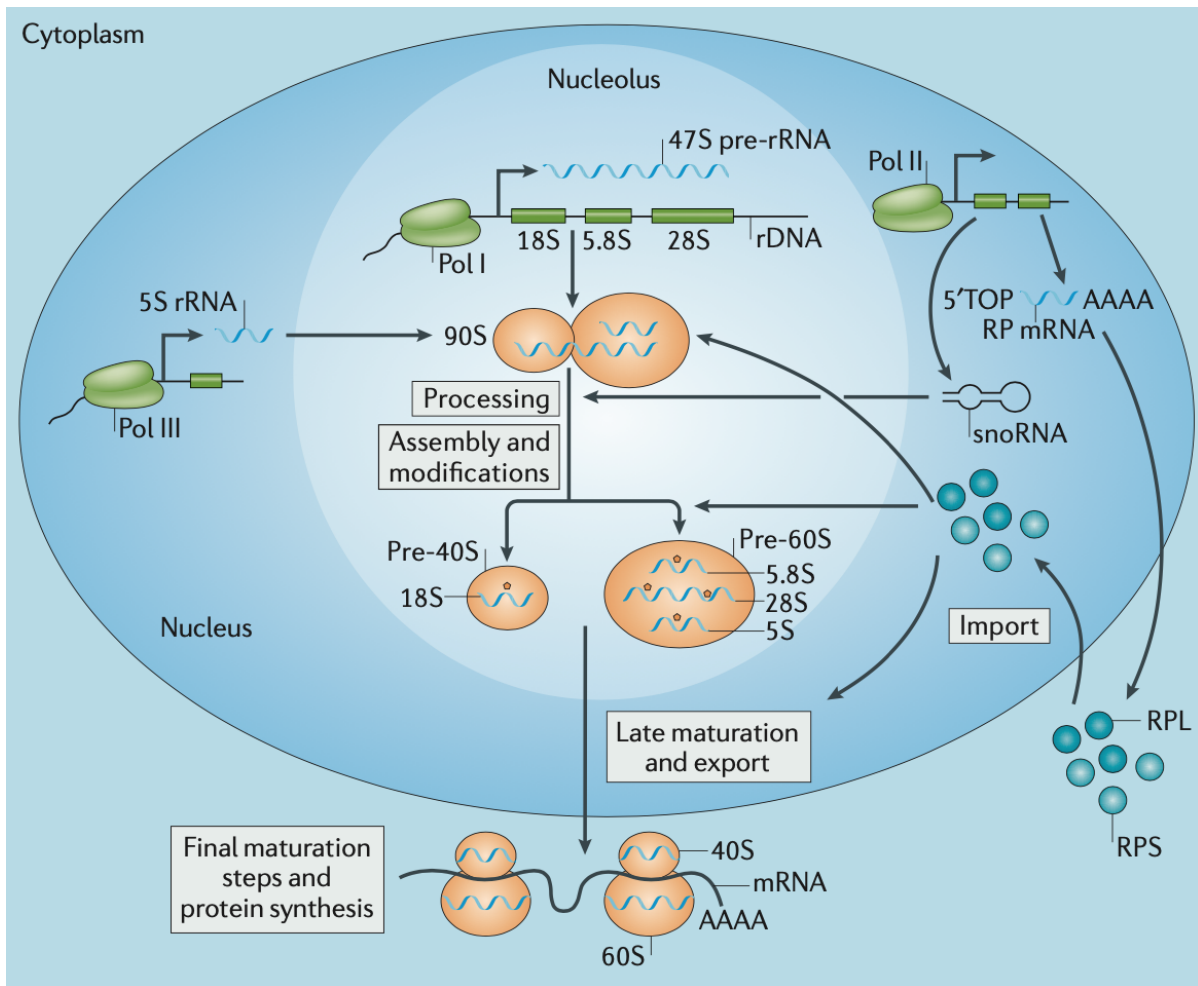


Figure 7: Ribosome biogenesis at a glance.

Ribosome biogenesis mostly occurs in the nucleolus where RNA Pol I transcribes ribosomal DNA (rDNA) to synthesize a 47S precursor-rRNA (47S pre-rRNA) subsequently cleaved in 18S, 28S and 5.8S mature rRNA. In the 90S processome, the 47S pre-rRNA co-transcriptionally binds to: i) 5S rRNA transcribed by RNA Pol III in the nucleoplasm and, ii) ribosomal proteins (RPs) which mRNAs have been transcribed by RNA Pol II in the nucleus, translated and matured in the cytoplasm, and finally re-imported in the nucleolus. Maturation of the 90S processome is required to produce pre-40S and pre-60S ribosomal subunits and rely on the modification and processing of the pre-rRNA by ~200 small nucleolar RNAs (snoRNAs) transcribed by RNA Pol II in the nucleoplasm. Ribosome biogenesis is completed after the export in the cytoplasm and final incorporation of RP in the produced ribosomal subunits, resulting in a mature 80S ribosome ready for protein synthesis. In the figure, orange pentagons represent rRNA modifications; RPL, large subunit ribosomal proteins; RPS, small subunit ribosomal proteins; 5'TOP, 5'-terminal oligopyrimidine tract. Figure extracted from (97).

a. 47S pre-rRNA transcription by RNA polymerase I & processing

Ribosomes biogenesis requires the production of rRNAs by the RNA Pol I that takes place in the nucleolus, a subnuclear membrane-less organelle. The nucleolus is subdivided in three compartments: the granular component, the dense fibrillary component, and the fibrillary center (Figure 8) (103,104).

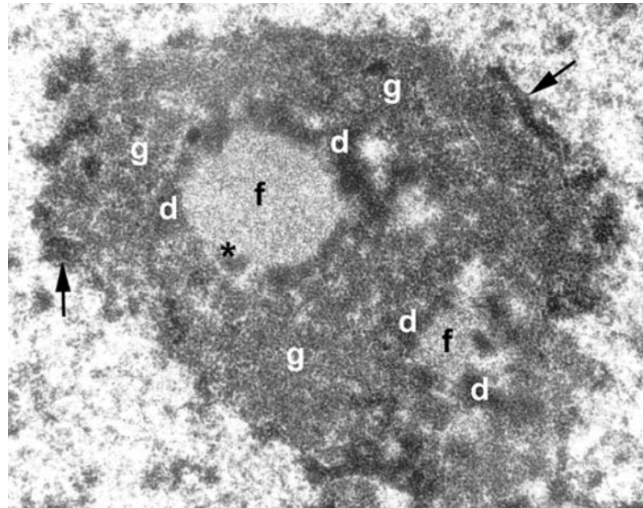


Figure 8: The different nucleolar compartments visualized through electron microscopy.

Nucleolus in a mouse cell. f, d and g respectively correspond to fibrillary centers, dense fibrillar components and granular components. Black arrows point to condensed chromatin in the periphery of nucleolus, the asterisk shows dense fibrillar components clump in the fibrillar center. Figure extracted from (103).

The nucleolus is a dynamic structure organized around nucleolar organizers regions (NORs) that host the ribosomal DNA (rDNA) genes (encoding for rRNAs) and spread over five acrocentric chromosomes (13, 14, 15, 21 and 22) (105).

RNA Pol I-mediated transcription of the rDNA occurs in the fibrillary center of the nucleolus or at its border with the dense fibrillary component, and enables the formation of so-called “Christmas trees” structures with a trunk made of rDNA and branches constituted of the precursor rRNA being synthesized (Figure 9A) (106). In human cells, the nucleolus contains up to 400 repeats of rDNA of approximately 43 kb, consisting in a 30 kb long intergenic transcribed spacer (ITS) and a 13 kb transcribed region corresponding to the 47S precursor rRNA (pre-rRNA) (Figure 9B) (102).

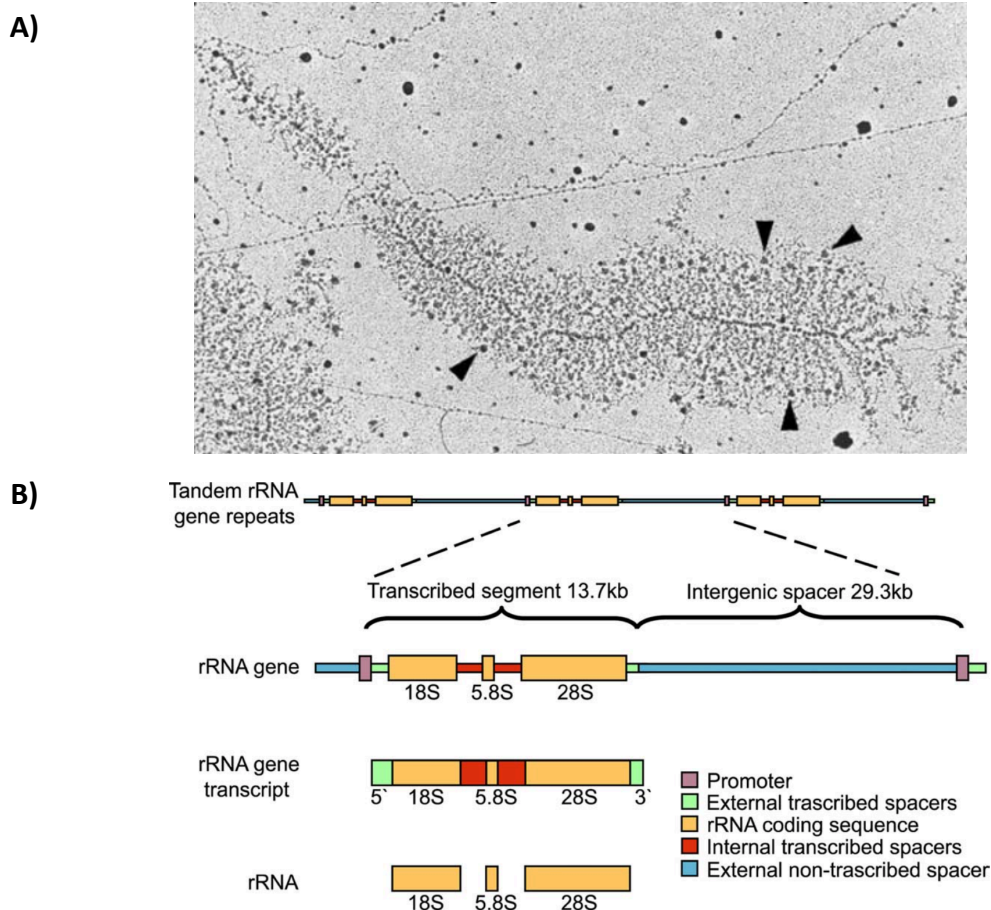


Figure 9: rDNA transcription.

A) Spread Christmas tree structure from a mouse cell is shown. Arrowheads designate terminal balls at the 5' extremity of nascent transcripts. "Christmas tree" structures raised during rDNA transcription in a mouse cell. Arrowheads point towards the 5' extremity of synthesized transcripts (figure extracted from (103) reprinted from Scheer and Benavente, 1990). **B)** Organization of human ribosomal genes in the genome and composition of their transcripts. Figure extracted from (103).

Although several pre-rRNA are synthesized concomitantly, only half of the rDNA repeats can be transcribed at the same moment depending on the chromatin structure (102,107). The transcriptionally inactive rDNAs are characterized by a hypermethylation and inhibitory histone modifications that drive rDNA condensation out of fibrillar component. The transcriptionally active rDNAs, in the contrary, are open thanks to hypomethylation of DNA and acetylated histones.

- **Pre-initiation complex formation**

Transcription mediated by RNA Pol I relies on the open structure of chromatin and the formation of the pre-initiation complex, a complex association of several factors that forms a

platform for molecular interactions. Solely core elements of this complex will be briefly described below.

The recruitment of RNA Pol I to the rDNA necessitates the binding of two factors in the promoter region: i) the upstream binding factor (UBF), a high mobility group (HMG) protein binding to DNA and ii) a multimeric protein called the selectivity factor (SL1), involved in the recruitment of other factors required for the pre-initiation complex formation.

The binding of UBF to rDNA promoter and to the upstream core element UCE induces structural changes leading to the formation of a DNA loop that allows the recruitment of RNA Pol I (83)(84). Moreover, UBF participates in the stabilization of SL1 (known as TIF-IB in mouse) binding to rDNA promoter, required for the enrollment of RNA Pol I (85). Conversely, SL1 stabilizes UBF interaction with the rDNA promoter (86). Altogether, RNA Pol I recruitment and specific binding to rDNA requires the cooperation of UBF and SL1.

In addition, SL1 interacts with the RNA polymerase I-specific transcription initiation factor RRN3 (known as TIF-IA in mouse) mediating the connection between RNA Pol I and promoter binding factors (87). Only RNA Pol I associated to RRN3 are able to initiate transcription (88).

- **Promoter escape & elongation**

Once the pre-initiation complex is formed at the promoter, incorporation of the first ribonucleotides of the RNA during the elongation step, starts as RNA Pol I dissociates from the rDNA, a phenomenon called promoter escape (108) that is the rate limiting step of rRNA transcription (109). This event depends on RRN3 phosphorylation by casein kinase 2 (CK2) associated with the pre-initiation complex (110), and allows RRN3 separation from RNA Pol I that permits transcription elongation (111). UBF stimulates promoter escape and the subsequent elongation, although the exact mechanism remains partially understood (102). For instance, it was shown that UBF is spread over the whole sequence of the rDNA, suggesting a role in the control of the elongation process through modulation of the rDNA chromatin structure (112). Indeed, chromatin remodeling and topological changes in rDNA structure, mediated by histones chaperones or topoisomerases I and II, appear to be critical to promote RNA Pol I activity and the elongation phase of rRNA transcription (102).

- **Termination of pre-rRNA transcription**

Finally, termination of transcription occurs as RNA Pol I faces the transcription termination factor 1 (TTF-1) bound to terminator elements downstream of the rDNA. This event leads to the stalling of RNA Pol I and its removal by the polymerase I and transcript release factor (PTRF) releasing the synthesized 47S pre-rRNA (113). Other factors involved in the cleavage of the nascent pre-rRNA (endonuclease Rnt1 and exonuclease Xrn2 cooperating with RNA helicase Sen1) participate in the termination process (102).

- **Processing of the 47s pre-rRNA**

In the 47S pre-rRNA transcript, the sequences of 28S, 18S and 5.8S rRNAs are separated by two internal transcribed spacers (ITS) and bordered by 5' and 3' external transcribed spacers (ETS) (Figure 10). Hence, to produce these three mature rRNAs required for the constitution of active ribosomes, the 47S pre-rRNA needs to be processed and to undergo several modifications.

This processing begins during the elongation phase and is complex and finely regulated. Hundreds of actors (such as small nucleolar snoRNAs, ribosome assembly factors, nucleolar factors, endo or exonucleases...) are involved in cleavage, folding and chemical modifications (such as pseudouridylation and methylation) of the 47S pre-rRNA to ensure this co-transcriptional maturation of rRNAs and assembly of pre-ribosomal units (114). Only a brief description of the cleavage processes leading to the generation of mature rRNAs will be given here.

Basically, the first step of the processing is to get rid of both 5' and 3'-ETS ending regions of the pre-rRNA by cleavage at sites O1 and O2 leading to 45S pre-rRNA (Figure 10). Then, two co-existing alternative pathways can be pursued:

- i) pathway 1, 45S is processed by cleavage in sites A0 and 1 to become 41S precursor that will then require additional cleavages to result in the 21S and 32S rRNA;
- ii) pathway 2, 45S is first processed at site 2 leading to 32S and 30S precursor, the latter being subsequently cleaved to 26S intermediate or directly to 21S.

Consequently, the two pathways equally lead to the generation of 21S and 32S further processed to 18S, 28S and 5.8S rRNAs. Finally, maturation of 5.8S and 28S is completed in the nucleolus whereas 18S-E associates to ribosomal proteins to be transported out of the nucleus and finish its maturation in the cytoplasm.

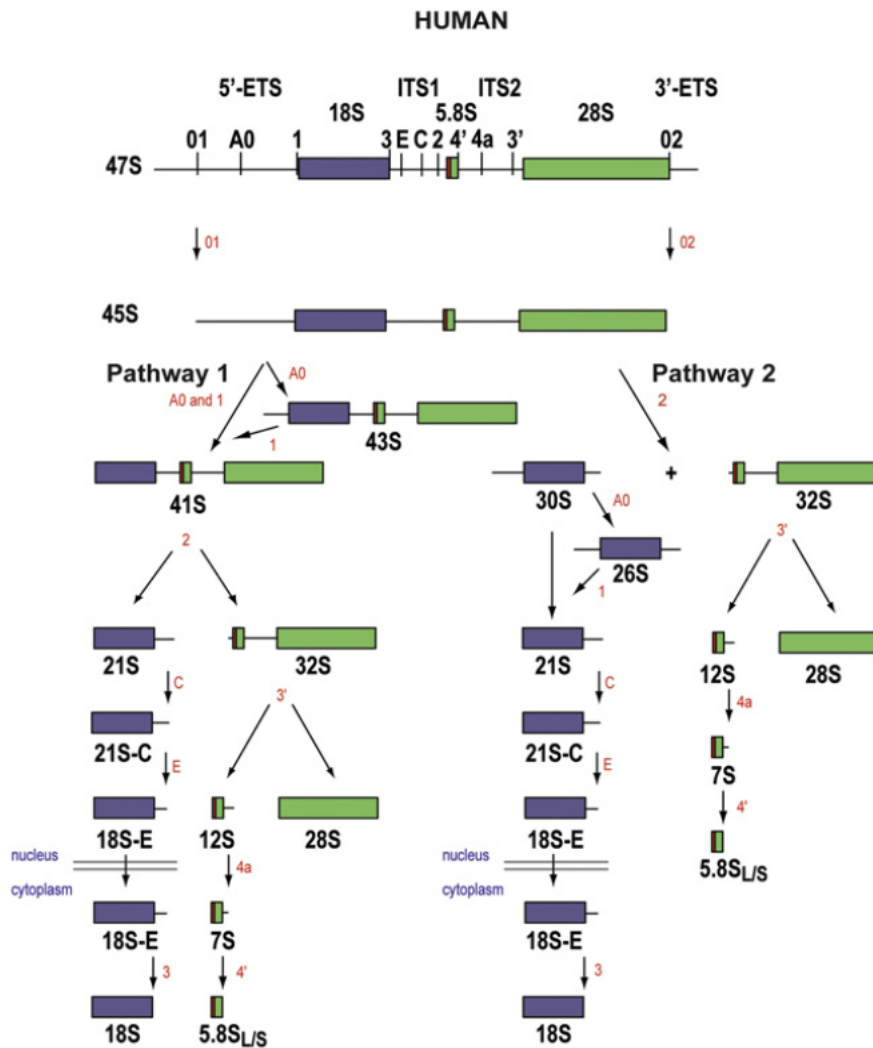


Figure 10: Processing of the 47S pre-rRNA in human.

First, both ends of the 47S pre-rRNA are cleaved at sites O1 and O2, generating the 45S precursor processed by two alternative pathways. In pathway 1, processing starts in the 5'-ETS by concomitant cleavage at sites A0 and 1 to give rise to 41S pre-rRNA; whereas in pathway 2 processing begins in ITS1 at site 2 leading to generation of 30S and 32S pre-rRNAs. Of note, the uncoupling of cleavages at sites A0 and 1 in pathway 1 (represented as a "loop") generate the 43S pre-rRNA. In pathway 1, cleavage at site 2 of the 41S pre-rRNA produces 21S and 32S pre-rRNAs; in pathway 2, 30S is converted in 21S. Of note, in pathway 2, the 30S is either directly matured into 21S by simultaneous cleavages at sites A0 and 1, or through the formation of an intermediate 26S pre-rRNA by subsequent processing in site A0 and site 1 (represented as a "loop"). Then, the 21S is cropped to site C and then to site E, only 24 nt downstream of the end of mature 18S rRNA, to produce 18S-E pre-rRNA then exported in the cytoplasm to be cleaved at site 3 and generate the final 18S rRNA. In parallel, the 32S pre-rRNA is matured at site 3' in ITS2 to produce the 12S pre-rRNA and the 28S rRNA. The 12S is cut at site 4a into 7S and then at site 4' to generate the 5.8S rRNA. Two forms of 5.8S rRNA can be produced, short (S) or long (L), differing by the extension in the 5' extremity. Additional processing sites have been proposed but are not represented here to facilitate the lecture. Figure extracted from (114).

b. Transcription of 5S rRNA by RNA polymerase III and maturation

The last mature rRNA required for ribosomes formation is the 5S, encoded by a cluster of tandem repeats. In human, genes encoding 5S rRNA are mostly hosted on chromosome 1 (115), thus, not included in the NOR regions but closed to nucleolar periphery (116).

The 5S rRNA is transcribed by the RNA Polymerase III within nucleoplasm (117). Transcription of 5S rRNA starts after the recognition of the internal control region by the transcription factor IIIA (TFIIIA) allowing the formation of the pre-initiation complex (118). Then, the transcription factors TFIIIC2, TFIIIBb and TFIIIC1 join the pre-initiation complex and support TFIIIBb for the recruitment of the RNA Pol III initiating the transcription of 5S rRNA (119). Finally, clusters of thymidine signal the end of transcription (120).

After being synthesized, the 5S rRNA is transported in the cytoplasm with TFIIIA or RPL5 to complete its maturation (121). Then, mature 5S rRNA bound to RPL5 to shuttle back to the nucleus and being assembled in precursor ribosomes (122).

c. Ribosomes assembly, maturation and role in translation

The maturation of pre-ribosomal subunits and assembly of mature ribosomes are closely linked to each other and occurs concomitantly.

The assembly factors and ribosomal proteins transcribed by the RNA Pol II in the cytoplasm shuttled to the nucleolus to co-transcriptionally associate with the synthesized pre-rRNA. In the nucleolus, 18S rRNA assemble with 33 ribosomal proteins to give rise to the small 40S pre-ribosomal subunit, and the 28S, 5S and 5.8S rRNAs bound to other 47 ribosomal proteins to generate the large 60S pre-ribosomal subunit (97,102).

Maturation of the large and small pre-ribosomal subunits necessitate the intervention of more than hundred proteins involved in pre-rRNA folding and processing, rendering this process particularly complex to be entirely depicted and completely deciphered (97).

Besides the numerous actors involved in this process, it requires the shuttling of many of these proteins between the nucleus and the cytoplasm. For instance, the maturation of pre-ribosomal particles depends on the transport of ribosomal proteins produced in the cytoplasm to the nucleolus. Conversely, the pre-ribosomal subunits produced in the nucleolus need to make their way through the nucleus to reach the cytoplasm to complete their maturation (123).

Functional ribosomes are responsible for the association of amino acids one by one to synthesize a polypeptide chain that will be folded to produce a protein corresponding to the mRNA sequence decoded by ribosomes during the elongation phase of protein translation (94). To this end, the mRNA sequence is translated into series of three nucleotides named codon. As the elongation phase begins, P-site is occupied by a peptidyl-tRNA whereas aminoacyl and exit sites (A and E site) of the 80S ribosome are empty (Figure 11, step i). Then, the process is achieved in 3 steps:

- selection of an aminoacyl-tRNA (aa-tRNA) complementary to the mRNA codon in the A-site of the translating ribosome (Figure 11, step ii),
- establishment of a peptide bond between nascent protein and the aa-tRNA, transferring the peptide linked to tRNA in P-site to the aa-tRNA in the A-site. This leads to deacetylation of the tRNA in the P-site and to a new peptidyl-tRNA in the A-site (Figure 11, step iii).
- eEF2-supported translocation of the new peptidyl-tRNA to the P-site, and of the deacetylated-tRNA to the E-site (Figure 11, steps iv and v).

This process is repeated over and over while the ribosome scans the entire sequence of the mRNA and until it recognizes a stop codon.

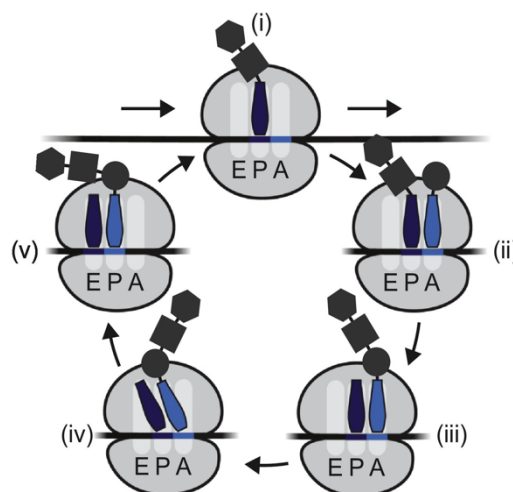


Figure 11: The elongation step of translation.

Elongation process is achieved in five steps: i) a peptidyl-tRNA is engaged in the P-site of the 80S ribosome, ii) then an aa-tRNA complementary to the mRNA sequence joined the A-site, iii) a peptide bound forms between the nascent polypeptide chain and the aa-tRNA resulting in a new peptidyl-tRNA in the A-site and a deacetylated-tRNA in P-site, iv) the new peptidyl-tRNA translocates from the A-site to the P-site whereas the deacetylated-tRNA translocates to the E-site, v) thus, a new cycle of elongation is ready to begin. Extracted from (94).

2) Consequences of the impairment of ribosome biogenesis and activity

a. The nucleolar stress

The nucleolar stress was originally defined as an impairment of ribosome biogenesis triggering the disruption of nucleolar homeostasis and the subsequent cellular stress response.

Yet, it has been widely accepted that the nucleolus is a central hub integrating various stress signals such as DNA damages, oxidative stress, hypoxia, nucleotides depletion or nutrient deprivation. Therefore, nowadays the nucleolar stress refers to all the stressful events leading to the perturbation of nucleolar morphology and function that induces the activation of a potentially lethal stress response.

In fact, two main categories of signals inducing a nucleolar stress can be defined: canonical factors as they directly impair ribosome biogenesis and non-canonical inducers disrupting the whole cell homeostasis (Table 2) (124).

Canonical (ribotoxic insults)	Non-canonical (wide range of cellular insults)
<ul style="list-style-type: none"><u>1. rDNA damage</u>1.1 UV, irradiation1.2 Act.D (high dose)<u>2. Impaired rRNA transcription</u>2.1 rRNA transcription inhibitor (Act.D (low dose) and other Pol I inhibitors)2.2 rRNA elongation inhibitor2.3 Transcription regulating protein defects<u>3. Impaired rRNA processing</u>3.1 Inhibitors3.2 Protein defects<u>4. Impaired ribosomal assembly</u><u>5. Impaired ribonucleoprotein import or ribosome export</u>	<ul style="list-style-type: none"><u>1. DNA damage:</u>1.1 UV, irradiation1.2 Genotoxic agents<u>2. Impaired RNA transcription:</u>RNA transcription inhibitor (Act.D (high dose) and other Pol II /III inhibitors)<u>3. Impaired protein translation</u>Inhibitors<u>4. Physiochemical perturbations</u>4.1 Hypoxia4.2 Oxidative stress4.3 Heat shock, cold shock4.4 Osmotic shock<u>5. Nutrient and serum starvation</u><u>6. Metabolic stress</u>

Table 2: Canonical and non-canonical inducers of nucleolar stress.

Two categories of nucleolar stressors: the direct inhibitors of ribosome biogenesis (canonical) and the different situations globally disrupting cell homeostasis and subsequently inducing nucleolar stress (non-canonical) (124).

It is of importance to notice that many pharmacological compounds disturb the nucleolar homeostasis. Historical antibacterial agents such as Doxorubicin or Actinomycin D impact the nucleolus, and of note, the latter is often employed *in vitro* as a positive control of nucleolar stress induction (125).

Moreover, several commonly used chemotherapies inhibit ribosome biogenesis at various levels and trigger a nucleolar stress that participate in the drug cytotoxicity (125–127). Among them, Oxaliplatin and 5-fluorouracil (5-FU) are two chemotherapies notably used for the treatment of colon adenocarcinomas and have been recognized as nucleolar stressors. For instance, 5-FU, usually considered as an antimetabolite, actually disrupts the nucleolus integrity through the impairment of pre-rRNA processing (127,128). Platinum-based compounds such as Oxaliplatin, but not Cisplatin, also induce a nucleolar stress but through the early inhibition of RNA Pol I (126,127,129), underlying its cytotoxic effect (126,130). Interestingly, Oxaliplatin presents a higher clinical activity in colon cancer cells in comparison with Cisplatin (131), suggesting that the impairment of ribosome biogenesis is critical for this particular histological subtype of cancer, associated with a strongly deregulated ribosome signature (130).

i. **Consequences of the nucleolar stress**

- **Impact on the nucleolar morphology**

The nucleolar stress is characterized by the alteration of nucleolar morphology that can notably be visualized through immunofluorescent staining of nucleolar proteins such as Fibrillarin or Nucleophosmin (NPM1) (126).

Indeed, the induction of nucleolar stress response, as a consequence of rRNA synthesis disturbance and collapsing of the nucleolus normal architecture, disrupt the assembly and shuttling of nucleolar proteins leading to an unusual arrangement of nucleolar markers. For instance, in physiological conditions, UBF is restricted to the fibrillary center, fibrillarin can be found in the dense fibrillary component, and finally NPM1 is mostly revealed in the granular component. The diffusion out of their defined nucleolar compartment as well as perturbations of the normal morphological patterns of these nucleolar markers is the reflect of a nucleolar stress.

To illustrate, treatment with the RNA Pol I inhibitor, Actinomycin D, or with the chemotherapy Oxaliplatin interfere with the nucleolus integrity and nucleolar proteins localization, such as NPM1 or fibrillarin. These proteins can spread out in the nucleoplasm or aggregate and lead to the formation of particular structures such as nucleolar caps (Figure 12).

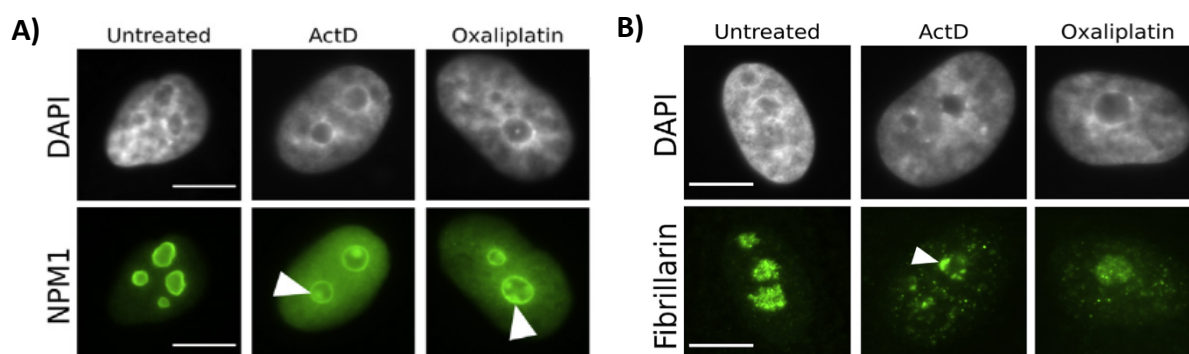


Figure 12: Delocalization of nucleolar markers upon nucleolar stress.

NPM1 and fibrillarin are two nucleolar proteins, thus their distribution is normally restricted to the nucleolus. Upon nucleolar stress induced by Actinomycin D (ActD) or Oxaliplatin treatments, their localization pattern is disrupted. NPM1 (A) and fibrillarin (B) diffuse in the nucleoplasm (DAPI staining) and aggregate at the periphery of the nucleolus in so-called nucleolar caps structures (arrows). Adapted from (126).

- **Activation of TP53 pathway**

The induction of nucleolar stress has been linked to the stabilization of so-called “guardian of the genome” TP53 and activation of its pathway, implicated in the regulation of several crucial cellular functions. Notably, the tumor suppressor TP53 can induce both cell cycle arrest or apoptosis and is also involved in many other important cellular processes such as DNA repair, induction of autophagy and differentiation.

Mechanistically, activation of the TP53 pathway relies either on: i) the direct stimulation of TP53 protein or ii) the disruption of its interaction with E3 ubiquitin ligase MDM2, the negative regulator of TP53 that promote its ubiquitination and degradation through the proteasome.

Indeed, the impairment of ribosome biogenesis through the repression of RNA Pol I transcription hinders the production of several rRNAs and ribosomes assembly, leading to free ribosomal proteins and 5S rRNA that cannot be incorporated. Notably, RPL5 and RPL11 associate to the 5S rRNA to form a 5S ribonucleoprotein particle (5S RNP). Yet, upon nucleolar stress, the 5S RNP cannot be included in the large ribosomal subunit due to a lack of other necessary rRNAs and thus, bind to MDM2, impairing its ubiquitin ligase activity and consequent degradation of TP53 (132,133). Of note, it has been demonstrated that the activation of the 5S RNP-MDM2-TP53 pathway requires both RPL5 and RPL11 proteins, highlighting their crucial role in the regulation of TP53 pathway in response to nucleolar stress (134).

Other factors have been implicated in the regulation of TP53 in response to nucleolar stress.

For instance, some nucleolar proteins can directly interact with TP53 upon stress. Of note, NPM1 translocation in the nucleoplasm allows its direct interaction with TP53 (135) and promotes also its association to MDM2 competing with binding of P53 (136), both enhancing the stabilization of TP53.

In addition, the tumor suppressor ARF sequesters MDM2 in the nucleolus, preventing its nucleoplasmic interaction with TP53 that lead to cell cycle arrest and apoptosis (137). Interestingly, ARF participates in the transcription of 47S pre-rRNA and processing in the nucleolus (138). This study highlights that the regulation of ribosome biogenesis is tightly linked to nucleolar integrity and control of the TP53 pathway and requires multiples layers of regulation, consistently with its crucial role in cell fate. Moreover, ARF-mediated stabilization of TP53 depends on the formation of the 5S RNP, further supporting the idea that each pathway concurring to the regulation of TP53 pathway are all intimately intricated (133). Hence, cellular outcome in response to nucleolar stress is the result of this interconnected regulation.

- **TP53-independent stress response**

Recently, studies reported that nucleolar stress can affect cells despite expressing a non-functional TP53 protein, suggesting that a TP53-independent stress response is concomitantly triggered.

To illustrate, in cell lines derived from osteosarcomas, colon cancer and breast tumors, repression of ribosome biogenesis and related nucleolar stress through the molecular interference with the catalytic subunit of the RNA Pol I promote the release of RPL11 that bind to MDM2 and impair its stabilization function toward the transcription factor E2F1 (139). Then, the downregulation of E2F1 was associated to an impairment of cell cycle progression, even in cells lacking TP53 protein.

In a similar manner, Lee et al also shown that ribosomal proteins participate in the regulation of c-Myc activity. Induction of nucleolar stress and increased in free RPL5 promote c-Myc degradation and, in turn, downregulates c-Myc-driven proliferation of tumor-derived cell lines, despite the absence of a functional TP53 (140). Consistently, RPL11 overexpression favors its association to c-Myc and impedes the c-Myc activity, resulting in a decreased proliferation of osteosarcoma and lung cancer cell lines as well as in mice and human fibroblasts (141).

Independently of the action of ribosomal proteins, a study reported that nucleolar stress-mediated downregulation of PIM1 kinase is sufficient to induce cell cycle arrest in hematopoietic cells through the increase of p27, independently of cells' TP53 status (142).

- **Impact of nucleolar stress on cell fate and outcome**

CELL CYCLE ARREST: The repression of cell division represents the first response to the nucleolar stress. This aims to prevent abnormal synthesis of ribosomal RNAs and the exhaustion of cellular energy and nutrient resources upon stress. Previous studies indeed highlighted that the cell cycle arrest caused by nucleolar stress occurs in a TP53-dependent (128,135,137,143–146) or independent manner (139–142). Impairment of cell cycle progression among ribosome biogenesis stress has been linked to both inhibition of G1/S and G2/M-phases cell-cycle checkpoints (147,148).

DIFFERENTIATION: As briefly mentioned previously, ribosome biogenesis is closely related to differentiation degree of the cells. This link has actually been demonstrated many years ago, with a reduction of rRNA production along the process of leukemia cell differentiation (149). Indeed, levels of rDNA transcription are dynamic in cells. Hematopoietic stem cells have moderate levels of Pol I transcription that increase progressively in progenitors, while mature hematopoietic cells are characterized by low levels of rDNA transcription, highlighting that the activity of RNA polymerases govern differentiation processes (150).

In embryonic stem cells, depletion of a nucleolar protein, the nucleolin, promotes the activation of P53 pathway and induces cell cycle arrest, apoptosis and differentiation of the cells (151). In the contrary, differentiated cells (i.e., fibroblasts) were less sensitive to downregulation of nucleolin, demonstrating that ribosome biogenesis and homeostasis of the nucleolus are particularly decisive for the maintenance of stemness features.

In a similar manner, the study of Watanabe-Susaki et al. reported an enrichment in another nucleolar protein, the fibrillarin, in stem cells (152), consistent with the involvement of fibrillarin in rRNA processing and ribosomes assembly (153). As a consequence, impairment of ribosomes synthesis and the related induction of nucleolar stress was sufficient to trigger differentiation of mouse-derived embryonic stem cells (152). In colorectal cancer samples as

well, Dr Battle's team intriguingly revealed enhanced rRNA and protein synthesis abilities in stem-like cells in comparison with differentiated cancer cells within the tumor (154).

APOPTOSIS: In many stresses' response, the molecular pathways stimulated by nucleolar stress participate in the accommodation to the stress. However, if the harmful situation cannot be relieved, this results in the activation of signals leading to apoptosis. To illustrate, the DNA damages induced by the inhibitor of topoisomerase I, camptothecin (155), eventually lead to the repression of rRNA synthesis and a lethal nucleolar stress in treated neural cells (156). In a similar manner, the genetic deletion of TIF-IA component of RNA Pol I in MEF resulted in cell cycle arrest and increased apoptosis (146). Indeed, the chemical inhibition of ribosome biogenesis increased cell death in several cancer cell lines, notably through the cleavage of pro-apoptotic proteins PARP and caspase-3 (98,140,157,158). Altogether, this demonstrates that the impairment of rRNA transcription can be deleterious for cells.

ii. Impact of the nutritional stress on the nucleolar homeostasis

Considering the determinant impact of the nucleolar stress on cell outcome, a fine regulation of the ribosome biogenesis is necessary to ensure nucleolus homeostasis and adaptation of the translation processes upon scarcity. Indeed, DNA transcription is the second largest energy consuming pathway, after protein translation (84,85). Ribosome biogenesis also requires nutrients supplies to produce the building blocks necessary for the synthesis of nucleotides, incorporated in rRNA transcription (96,98,148). Of note, in yeast cells, the integrality of rRNAs represents approximately 80% of total cellular nucleic acid, and almost 50% of the transcription mediated by the RNA Polymerase II is dedicated to ribosomal proteins genes (84,159). Yet, excessive consumption of cellular energy can be fatal when tumor cells are exposed to nutrient depletion.

Consequently, in such conditions, cells have to preserve its resources and downregulate these cellular processes with a high energy cost. Accordingly, tumor cells grown in conditions limiting the available pools of nucleotides (i.e., low glucose or low amino acids) display decreased transcription rates of rRNAs (100,160).

Indeed, the inhibition of pyrimidines synthesis in glioblastoma cells results in the downregulation of rRNA transcription, induction of the nucleolar stress described previously, and slower proliferation rates due to cell cycle arrest in S-phase (98). Furthermore, pharmacological inhibition of IMPDH, an enzyme responsible for the synthesis of guanosine monophosphate GMP, first impairs the ribosome biogenesis checkpoint and leads to a P21-mediated cell cycle arrest in G1-phase (148).

Lowering the rRNA transcription has been described as an efficient barrier against nucleotides exhaustion and induction of DNA damages. Indeed, impairing the nucleotide synthesis pathways fueling the DNA replication and repair is a therapeutic strategy for inducing cell toxicity. For instance, hydroxyurea treatment blocks the ribonucleotide reductase, an enzyme ensuring the conversion of ribonucleotides into deoxyribonucleotides. Hydroxyurea thus leads to the depletion of the pool of nucleotides dedicated to DNA replication and repair and cell cycle arrest in G1/S (161). However, upon prolonged decrease in nucleotides pools, P21 is degraded, allowing S-phase entry and exposing cells to replicative stress and potentially lethal accumulation of DNA damages (148).

Consequently, the cell has to adjust ribosome biogenesis in response to nucleotides scarcity that can be faced upon nutrients deprivation to avoid a nucleolar stress leading to cell death and rather induces cell cycle arrest. In line with this statement, the adaptive response to hydroxyurea in yeast implicates a decreased ribosome biogenesis, likely to preserve the available nucleotides for the DNA damage response pathway (162).

The molecular pathways allowing the modulation of rRNA transcription in condition of nutritional stress are described in the next chapter.

b. Impairment of ribosome function: ribosome stalling and collision

Impairment of the translational activity of ribosomes is relying on the dysregulation of the translation rates and translational efficiency leading to paused ribosomes, also called stalled ribosomes. Eventually, this event can result in the collision of two ribosomes, disturbing the translational processes.

Impact of nutritional stress on ribosomal stress

Upon nutrient starvation, the elongation phase of translation can be disrupted due to low energy resources and lack of amino acids. Low levels of amino acids available for tRNA synthetases results in a deficiency in charged tRNAs (aminoacyl-tRNAs), that impairs elongation and results in ribosome stalling and collision (163–165). This event is recognized as a translational aberration and need to be relieve to ensure cell survival. A long-lasting ribosome stalling will force cell to undergo apoptosis (166,167).

Hence, the translational activity of ribosomes as well needs to be modulated to slowdown protein synthesis in response to nutritional stress. This implies the activation of several signaling pathways, highly conserved throughout the evolution, aiming to promote cell adaptation or cell death if the stress cannot be alleviated (see next part III) (168).

III. NUCLEOLAR AND RIBOSOMAL STRESSES AND RELATED SIGNALING PATHWAYS

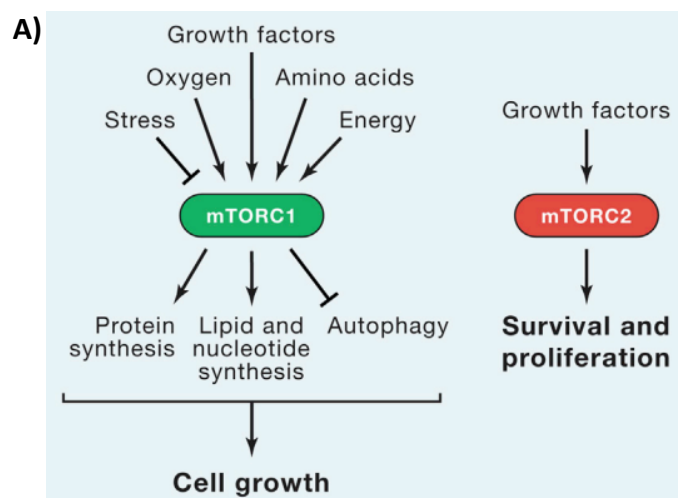
Multiple mechanisms adjust the ribosome biogenesis and related translational activity in response to nutrient availability, and among them nutrient sensing cellular pathways. The following chapter is focused on the description of the corresponding molecular stress sensors implicated in the adjustment of ribosome synthesis and function according the nutrient availability.

1) Modulation of RNA polymerases activity by mTORC1

Adjustment of the ribosome biogenesis is crucial for: i) stimulating the proliferation when nutrients are rich or ii) prevent a lethal nuclear stress upon depleted conditions. Hence, this pathway is tightly controlled by the availability of nutrients in the tumor cells' microenvironment.

The mTORC1 pathway is particularly important in the control of transcription rates of rRNA and ribosome synthesis in response to the nutritional context.

MTOR, for mechanistic (formerly “mammalian”) target of rapamycin, is a serine/threonine kinase of the phosphoinositide kinase-related family of protein kinases. This kinase is shared by two complexes in mammals, namely mTORC1 and mTORC2, controlling distinct cellular functions (Figure 13) (169).



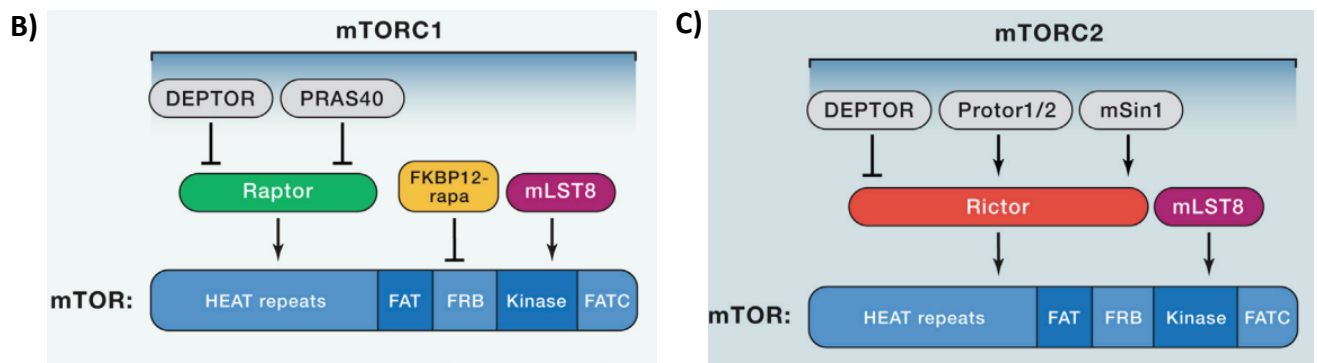


Figure 13: The signaling pathways of mTORC1 and mTORC1 complexes.

A) Schematic illustration of the mTORC1 and mTORC2 signaling pathways. **B)** mTORC1 subunits and binding site on mTOR. **C)** mTORC2 subunits and binding site on mTOR. Extracted from (169).

mTORC1 is constituted of three core components, namely mTOR, mLST8 (mammalian lethal with Sec13 protein 8) and Raptor (regulatory protein associated with mTOR). These three are associated to two inhibitory subunits, PRAS40 (proline-rich Akt substrate of 40 kDa) and DEPTOR (DEP domain containing mTOR interacting protein).

mTORC2 also contains mTOR and mLST8, in addition to mSIN1, Protor 1/2 and Rictor (rapamycin insensitive companion of mTOR).

Contrarily to mTORC2, mTORC1 is inhibited by rapamycin treatment (FKBP12-rapa complex) and is responding to nutrients variations.

Both complexes are implicated in the regulation of numerous cellular processes but the two complexes recognize different substrates. Basically, mTORC1 is responding to nutrients variations and is involved in the control of protein homeostasis, autophagy and metabolism, while mTORC2 is principally linked to cell survival and cytoskeleton organization (169). Altogether, the mTORC pathways are at the interface between extracellular (such as amino acid, oxygen and growth factors availability) and intracellular cues (such as energetic stress). The following paragraph focuses on the contribution of mTORC1 signaling into the regulation of the ribosome homeostasis.

mTORC1 is implicated in the control of protein synthesis rates by regulating the initiation and elongation steps (31,169). Nonetheless, this complex also contributes to the regulation of ribosome biogenesis, notably through the complex regulation of all three RNA polymerases activity (reviewed in (170)), among which the RNA Pol I.

Active mTORC1 is required to sustain S6K1-mediated phosphorylation of components of the RNA Pol I, UBF (171) and TIF-IA (172), fostering the production of rRNA.

The repression of mTORC1 signaling notably differentially regulates the activities of Cdk/cyclin complexes and PP2A phosphatases. Activity of mTORC1 is required to activate CDK2/cyclin E to phosphorylate TIF-IA on serine 44 and maintain RNA Pol I transcription. Yet, upon rapamycin treatment, downregulation of mTORC1 impairs CDK2/cyclin E activity and also derepresses PP2A phosphatase activity, leading to the fostered dephosphorylation of serine 44. The dephosphorylation of serine 44 impairs TIF-IA, in concert with the inhibitory phosphorylation of serine 199 by a still unknown kinase (172).

In addition, active S6K1 phosphorylates the S6 ribosomal protein, a component of the 40S small ribosomal subunit, that is required for the expression and translation of genes involved in ribosome biogenesis (173).

Interestingly, it has been demonstrated that the growth factors-induced stimulation of mTORC1 signaling in starved cells is not efficient to trigger the expected upregulation of rRNA transcription if autophagy and related amino acids salvage pathway are blocked (174). This suggests that activation of the signaling induced by amino acid scarcity is “prioritized” over growth factor signals to maintain ribosome biogenesis repression in this context of low nutrients. Hence, the nutrient availability is determinant in the adjustment of ribosome biogenesis rates.

Conversely, the RNA Pol I activity reciprocally controls mTORC1 activity. The repression of RNA Pol I transcription and decreased in 47S synthesis is sufficient to downregulate mTORC1. Ultimately, mTORC1 inhibition impairs the cell proliferation and promotes autophagy (133)(175–177). However, the precise underlying mechanism is not known.

2) The ribosomal-stress surveillance pathways

Ribosomes progression in the elongation phase of translation can also be impaired by the nutritional stress resulting in ribosome stalling (pausing of ribosomes) or ultimately collisions. This ribosomal dysfunction implies the activation of several signaling pathways, highly conserved throughout the evolution, aiming at promote cell adaptation or cell death if the stress cannot be alleviated.

Yet, only the GCN2-ISR axis will be extensively described in the following paragraph considering: i) its dual implication in ribosome stalling and nutrient sensing, and ii) that it represents the central subject of my research project.

a. The ribosome quality control

In eukaryotes, the ribosome quality control (RQC) constitutes a dedicated surveillance mechanism promoting the elimination of truncated polypeptides generated upon the stalling and collision of ribosomes that could lead to defects in proteostasis. This system ensures the degradation of non-functional proteins that can have deleterious effects on cells if accumulated (178). Stalling and collision of two ribosomes are sensed by the central player of the RQC pathway, RING E3 ubiquitin ligase zinc finger 598 (ZNF598) (179,180).

ZNF598 binds to the 40S ribosomal subunits of the collided ribosomes and induces the ubiquitination of specific ribosomal proteins (RPS3, RPS10, RPS20) of the small subunit of ribosomes (179–181). This promotes ribosomes splitting through the recruitment of RQC-trigger complex, constituted of several actors among with ASC-1 complex (ASCC1, ASCC2, ASCC3) and TRIP4. The latter TRIP4 is a nucleolar transcription factor, suspected to favor the binding of RQC-trigger complex to ribosomes through its zinc finger domain (182). ASCC2 and ASCC3 are respectively involved in the recognition of ubiquitinated proteins and in the dissociation of ribosomes (178,182).

In addition, the RQC signals for the detection of harmful situations such as nutrient deprivation, among other stresses toxic for ribosomes activity, and is intricately cooperating with two additional stress responses involved in the regulation of global translation and cell fate in response to ribosomes impairment: the ribotoxic stress response and the GCN2 pathway.

For an overview of the RQC pathway, refer to Figure 14.

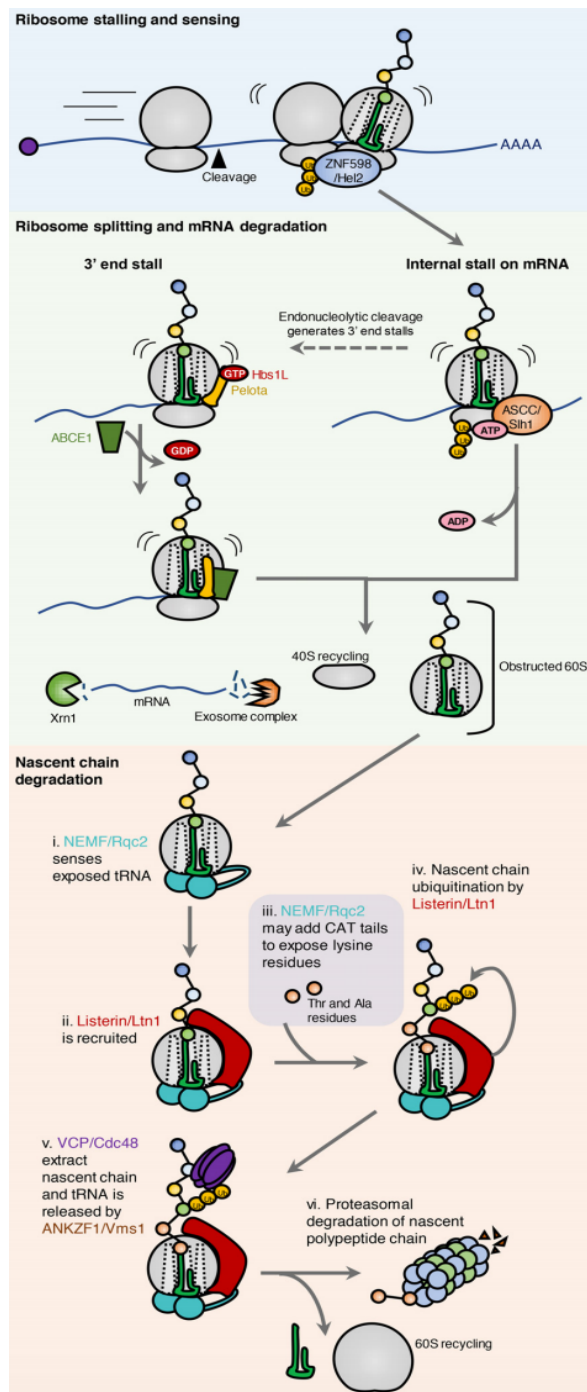


Figure 14: Overview of the Ribosome Quality Control pathway.

Stalling of elongating ribosomes can lead to the collision of ribosomes, recognized by the E3 ubiquitin ligase ZNF598. In turn, ZNF598 triggers the ubiquitination of the ribosomal proteins (RPS10, RPS10 and RPS20). The ASC complex (called Slh1 in yeast) detect the stalling on the mRNA and induce the dissociation of the leading ribosome, to release the trailing ribosome to continue translation. Upon specific circumstances, endonucleases cleave the mRNA in between two ribosomes, inducing ribosome stalling on the 3' end and its subsequent splitting by recycling factors among which Pelota, HBS1L and ABCE1 (Dom34, Hbs1 and Rli1 in yeast). The mRNA is then degraded by exoribonuclease Xrn1 and exosome complex to avoid the translation of an aberrant protein. Contrarily to the 40S subunit, the recycling of the 60S is hindered by a remaining peptidyl-tRNA. The occupied large subunit is thus recognized by the RQC component NEMF (Rqc2 in yeast) that enrolls the E3 ubiquitin ligase Listerin (Ltn1 in yeast) to the polypeptide chain. NEMF add CAT tails to expose lysine residues and promotes ubiquitination of the native chain by Listerin. This enables the recruitment of ATPase VCP (Cdc48 in yeast) to release the peptide and allow the removal of tRNA by ANKZF1 (Vms1 in yeast). Then, the polypeptide chain is degraded by the proteasome whereas tRNA and the large subunit of ribosome are recycled. Figure from (168).

b. Ribotoxic stress response (RSR)

Chemical agents and numerous stresses that restrain ribosomes activity are known as ribotoxic stressors. They share common features: i) interference with translational elongation through RNA damages or impairment of peptidyl transferase center leading to ribosomes collision and ii) the activation of stress kinases signaling called the ribotoxic stress response (RSR), requiring translationally active ribosomes (183,184).

The induction of the RSR pathway is mediated by the ribosome-associated leucine zipper and sterile-motif alpha longer isoform ZAK α and necessitates its binding to the 18S rRNA within the ribosomes (168). The activating autophosphorylation of ZAK α triggers the induction of MAPK pathways, leading to the phosphorylation and stimulation of p38 et c-Jun N-terminal kinase JNK (Figure 15) (168,183,185,186).

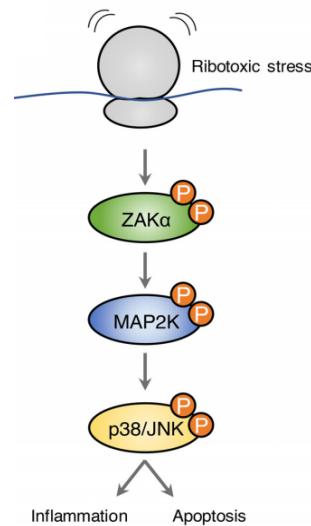


Figure 15: Schematic representation of the Ribotoxic Stress Response.

Ribosomes stalling activates the phosphorylation of ZAK α , triggering the induction of MAP2K to promote the activation of stress-associated protein kinases, p38 and JNK, leading to an inflammatory response or to apoptosis if the stress persists. Extracted from (168).

The induction of the RSR and MAPK have been related to induction of apoptosis in many studies (168,185,186). Moreover, it has been demonstrated that an off-target effect of the inhibitor of tyrosine kinases sorafenib leads to the inhibition of ZAK α , preventing its activation and RSR induction upon UV exposure. Consequently, JNK activation and related apoptosis were reduced in keratinocytes, suggesting that induction of ZAK in normal cells could play an anti-tumorigenic role (187). In the contrary, ZAK deletion leads to decreased lifespan in nematodes, highlighting that an impossibility to trigger RSR can be deleterious in simpler organisms (188). Altogether, these studies suggest that the intensity and duration of RSR induction probably modulates the balance between adaptation and survival or cell death in cells exposed to ribosomal stress.

c. The GCN2 pathway

First described in yeast (189), GCN2 (general control non derepressible 2) is a serine/threonine kinase responsible for: i) sensing the concentration of amino acids in the environment and, ii) adapting the cell's behavior and identity according to this availability (190). Despite low sequences homology between yeast and mammalian cells, the function of GCN2 is highly preserved in eukaryotes and strongly depends on the structure of the kinase (Figure 16) (190–193).

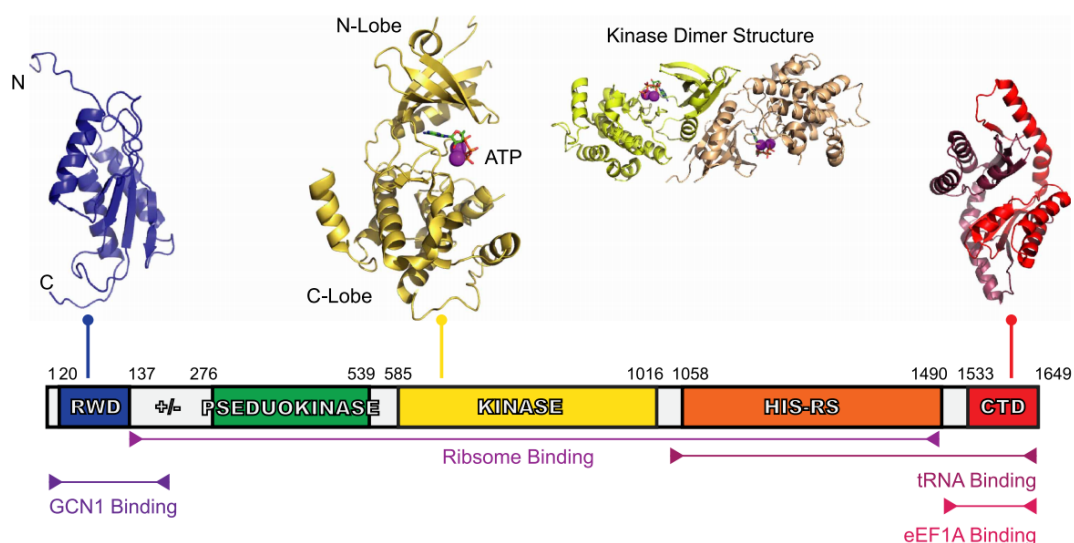


Figure 16: Structure of the human GCN2 protein kinase.

GCN2 is a 1649 amino acid protein constituted of five conserved domains: the RWD domain linked to pseudokinase domain by the charger linker (+/-) region rich in argine, lysine, glutamate and aspartate residues; the kinase domain; the histidyl tRNA-synthetase like (HisRS-Like) domain; and finally, the c-terminal domain CTD. Extracted from (190).

Originally, the canonical pathway of GCN2 has been characterized under conditions of nutritional stress. At first, GCN2 activation was thought to be depending on the accumulation of uncharged tRNAs due to low availability of amino acids to guarantee the appropriate aminoacylation of each tRNA by the tRNA synthetase enzymes. It was proposed that the uncharged tRNAs bind to GCN2 domain similar to histidyl-tRNA synthetase and induce conformational changes that trigger its autophosphorylation on Thr⁸⁸⁷ and Thr⁸⁸² that releases its kinase activity (164,165,194,195). Despite that the association of GCN2 with the ribosome has been highlighted long time ago (196,197), only recently this model has evolved. GCN2 is nowadays recognized as a sensor of ribosomal stress, compatible with others non-metabolic stresses activating GCN2 including UV exposure (186).

i. Modalities of activation of GCN2 signaling

Recent studies have shown that GCN2 can be activated through its direct binding to paused ribosomes in the context of translation disruption (166,190,198).

Specifically, GCN2 interacts with domain II of the uL10 protein (also called P0) of the ribosome P-stalk (198,199). The P-stalk is a protein complex consisting of a uL10 protein (P0) associated with 2 copies of P1 and P2 proteins (200,201). This complex forms a protuberance at the A site of the 60S large subunit of the ribosome (Figure 17) (199).

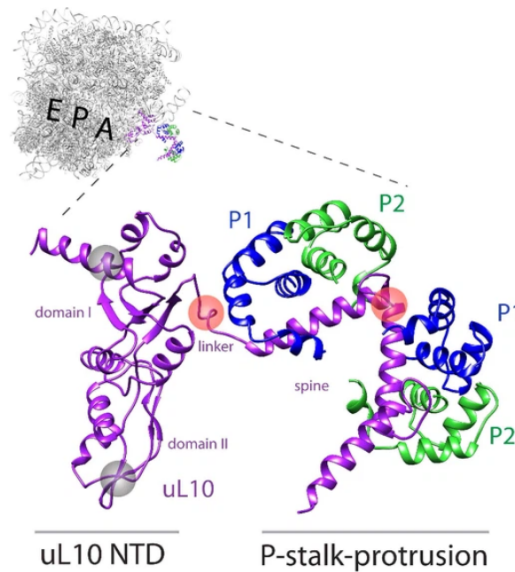


Figure 17: The P-stalk protrusion of ribosome.

Representation of the localization of P-stalk structure in the human ribosome compared to E, P and A sites for tRNAs. The N-terminal domain (NTD) of uL10 is associated to the ribosome and links with P1 and P2 protein of the P-stalk protrusion. Extracted from (199).

Briefly, the P-stalk is a dynamic complex of the ribosome, playing an important role in the control of translation fidelity through: i) the recognition of elongation factors, ii) the regulation of events requiring GTP hydrolysis during translation, and iii) through the modulation of GCN2 activity as recently reported (198,200,201). Harding and colleagues (199) proposed that in proliferative conditions, charged tRNAs and elongation factors eEF1A and eEF2 are recruited by the P-stalk during the elongation process, impairing its ability to activate GCN2 (Figure 18A). But upon amino acid starvation, the decrease in charged tRNAs disrupt this process, and GCN2 can be attracted to the P-stalk and activated (Figure 18B).

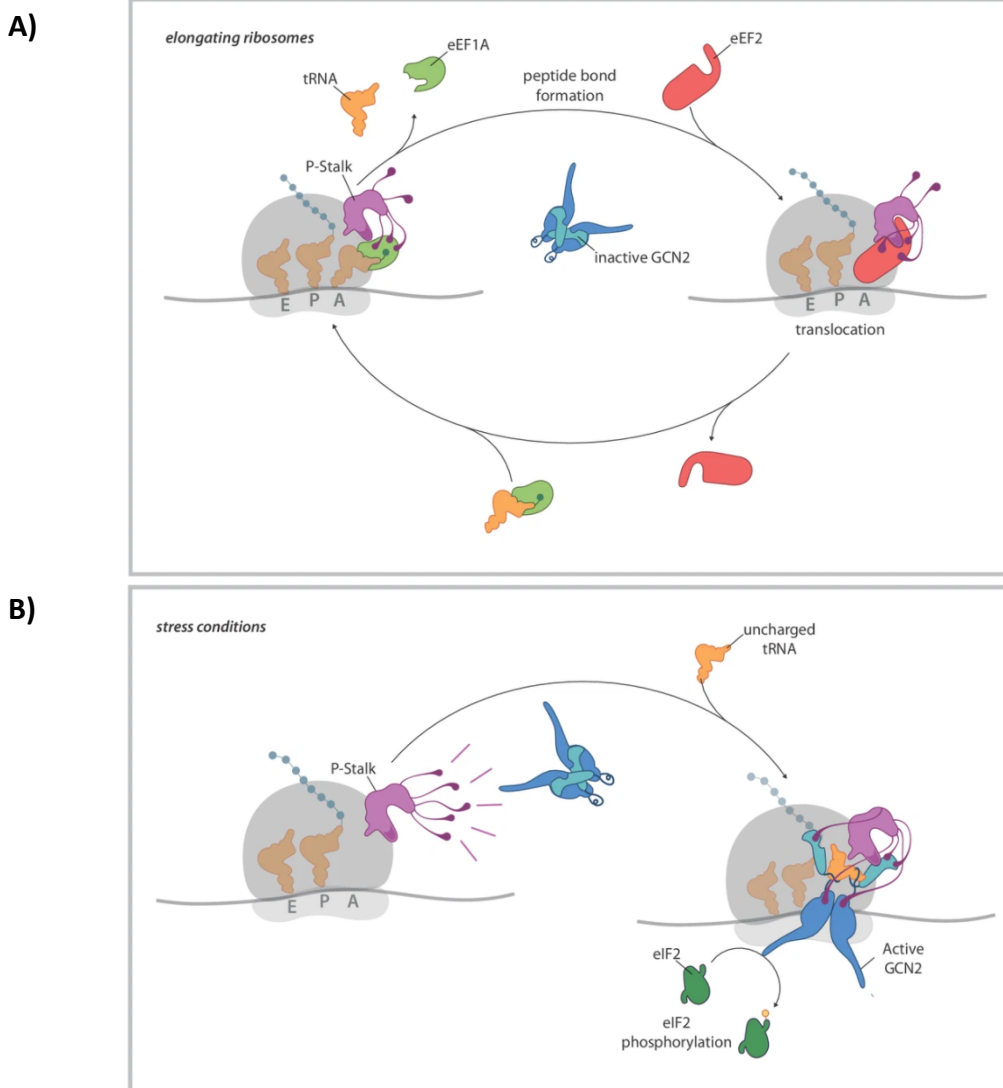


Figure 18: Proposed model for P-stalk mediated activation of GCN2 by Harding et al.

A) In conditions of full access to nutrients, ribosomes translational activity is enhanced by charged tRNAs and thus, elongation factors eEF1A and eEF2 cycle impairs the P-stalk mediated activation of GCN2. This repression relies on the competition for domain II of uL10 (a GCN2 binding site, in deep purple), engagement of the C-terminal tails of the pentameric P-stalk (represented as tentacle-like extensions) or a conformation not compatible with GCN2 activation, amongst other mechanisms.

B) Limited access to nutrients or impairment of tRNA synthetases decrease the pool of charged tRNAs, disrupts the cycling of eEF factors thus enabling the P-stalk to stimulate inactive dimers of GCN2 through its C-terminal tails. In addition, GCN2 dimers can also potentially be activated by uncharged tRNAs engaging in its HisRS domain (pale blue). Altogether, active GCN2 phosphorylates its substrate, eIF2a. Extracted from (199).

Yet, interestingly, the stimulation of GCN2 by ribosome arrest during translation is independent of an accumulation of deacetylated tRNA (166). Moreover, GCN2 affinity is even higher for ribosomes than for uncharged tRNAs (198). Recent investigation also demonstrated that the amplitude of ribosome stalling induced by amino acid limitations is linked to the activity of GCN2, the degree of GCN2 activation being proportional to the ribosome pausing (163).

In addition, the activation of GCN2 by UV exposure cannot be explained by an accumulation of uncharged tRNAs. In fact, similarly to the RSR, the activation of the GCN2 pathway following UV exposure relies on the ribosome stalling, independently of a decrease in nutrient availability (186). Consistently, interactome analyses performed in a context of ribosomal collision revealed that ZAKa, interacts with GCN1, a regulator of GCN2 activity, suggesting a cooperation between GCN2 signaling and the RSR upon ribosome dysfunctions (168,186)

Altogether, GCN2 is now considered as a sensor of broad ribosomal dysfunctions and mediates the induction its downstream axis, the integrated stress response (ISR) to repress translation rates and permit the resolution of the stressed situation (199–201).

ii. Activation of the ISR and consequences

The ISR is at the convergence of various cellular stresses pathways. Yet, in the context of ribosome dysfunctions, only active GCN2 can trigger this molecular axis (for review see (202)). Activation of the GCN2-ISR pathway concomitantly: i) represses the translation rates and ii) favors selective translation of mRNAs of protein involved in the response to stress, both concurring to the resolution of the cell homeostasis (Figure 19)(168).

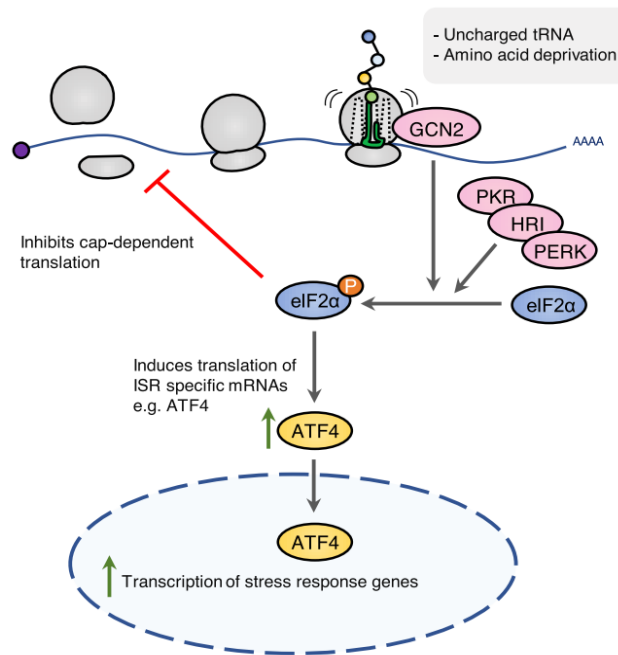


Figure 19: GCN2 triggers the ISR in response to ribosome stalling.

Four kinases triggering the ISR have been described: PKR, HRI, PERK and GCN2. Yet, only GCN2 is able to detect stalled ribosome and activate the ISR in response leading to: i) the phosphorylation of eIF2α to repress translation, and ii) the translation of specific mRNAs involved in stress response, globally concurring to the restoration of ribosome translational activity to alleviate the stress. Extracted from (168).

• TRANSLATION REPRESSION INDUCED BY THE ISR

The global repression of translation relies on the phosphorylation of alpha subunit of eIF2 on serine 51 mediated by GCN2 (203,204).

Indeed, to initiate translation, eIF2 must bound to a methionine-linked tRNA initiator and to a GTP molecule to generate a so-called ternary complex. Then, this ternary complex associates with a small 40S subunit of the ribosome to form the translation 43S pre-initiation complex, responsible for the recognition of the cap at the 5' end of mRNAs required for the start of corresponding protein synthesis (Figure 20) (205).

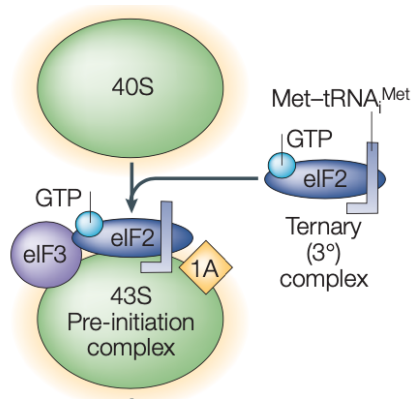


Figure 20: The pre-initiation complex formation.

Formation of the 43S pre-initiation complex requires the recruitment of the ternary complex, a methionyl-tRNA initiator (Met-tRNA_i) linked to eIF2 bounded to GTP, to associate with 40S ribosomal subunit and additional factors, eIF3 and eIF1A (1A). Extracted from (205).

The phosphorylation of the alpha subunit of eIF2 on Ser 51 prevents the exchange of GDP for GTP mediated by eIF2B (206). As a result, the eIF2-GTP pool is reduced, slowing down the pre-initiation complex formation and impairing cap recognition-dependent translation (Figure 21).

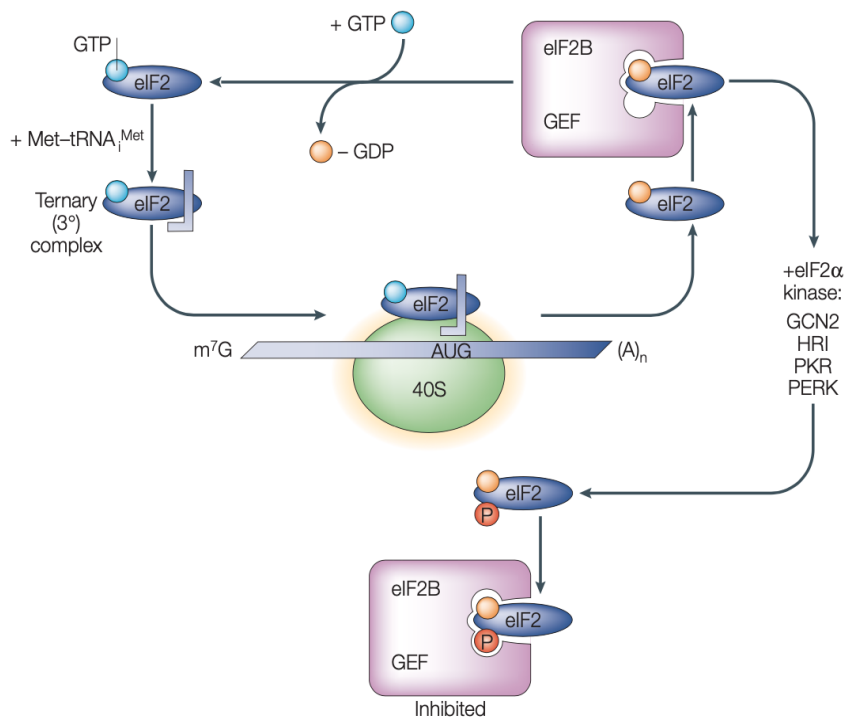


Figure 21: Regulation of pre-initiation complex formation by eIF2B and phosphorylation of eIF2 α .

Formation of the pre-initiation complex requires the recruitment of eIF2 bounded to GTP. However, in conditions where eIF2 α kinases are activated, the phosphorylation of alpha subunit of eIF2 is increased and impair eIF2B activity, resulting in low levels of eIF2-GTP required for pre-initiation formation and thus, global repression of translation initiation. Extracted from (205).

In situation of nutrient deprivation, the repression of the initiation step of protein synthesis allows the cell to: i) preserve energy and resources and, ii) reduce the translational demands in a situation of ribosomes dysfunctions. On the contrary, the incapacity to repress translation under stress conditions leads to cell death (86,91,207).

- **A SELECTIVE uORF-DEPENDENT TRANSLATION**

Besides the repression of global synthesis rate, specific mRNAs are translated in order to promote the adaptive response to cope with the stress (91,92). This selective translation program mostly relies notably on the presence of specific sequences in the 5'-untranslated region (5'UTR) of the mRNA called uORF (upstream open reading frame).

An uORF is a start codon (AUG) in the 5'UTR but out-of-frame with the main coding sequence (208). This sequence initiates the translation and leads to a non-functional peptide in proliferative conditions. The uORF thus prevents i) the binding of ribosomes to the downstream canonical ORF of the mRNA and ii) the translation of the coding sequence in basal conditions. This results in low amounts of the protein (208). But in conditions of nutrient deprivation, the phosphorylation of eIF2a affect the initiation of translation and so the formation of ribosomes ready to translate mRNA as well as described previously (205,206).

Since the ribosome turnover is low, the re-initiation of translation is impaired, leading to translation of proteins usually repressed in basal conditions. This cap-independent mechanism of translation relies on the presence of uORF within the 5'UTR of the mRNA sequence. The ATF4 mRNA is often used as study model for the uORF-dependent translation (Figure 22).

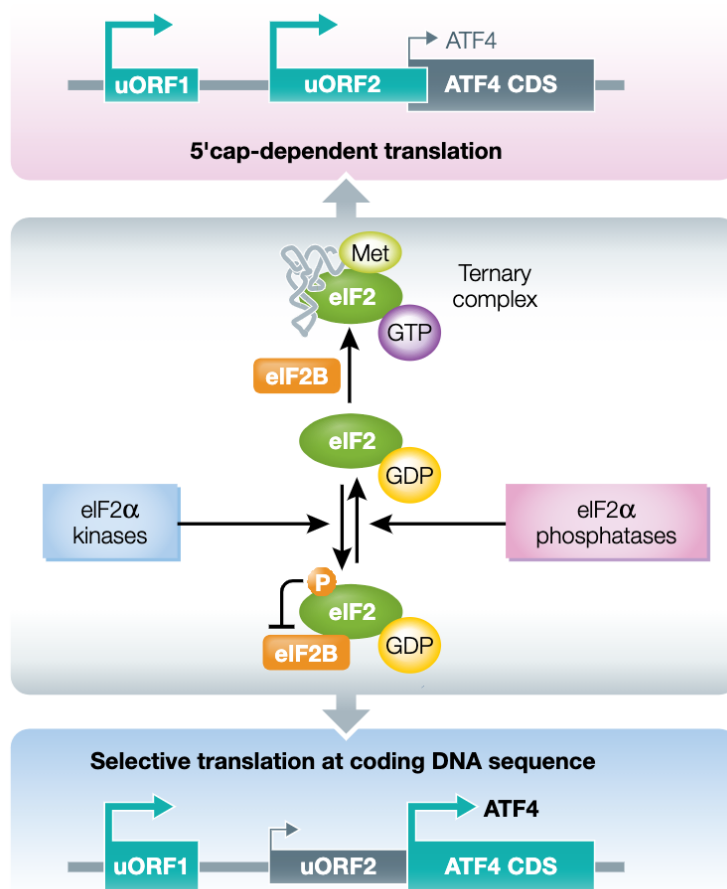


Figure 22: The role of eIF2 α in the control of selective translation.

Under normal conditions, eIF2 α is not phosphorylated, allowing the eIF2B-mediated exchange of GDP to GTP that is required for the initiation of translation. In conditions of stress, phosphorylation of eIF2 α inhibits eIF2B reducing eIF2 α -GTP and the ternary complex pools. The decrease in ternary complex available triggers longer ribosomal scanning and allows the reinitiation of translation at the coding sequence of mRNAs such as ATF4. Extracted from (202).

Upon stress, the low amount of ternary complex, caused by the phosphorylation of eIF2 α , drastically reduces the probability of the formation of a complete ribosome within the inhibitory uORF2. Hence, the ternary complex bypasses the inhibitory uORF and bind upstream of the main coding sequence of ATF4, enabling the translation and accumulation of the ATF4 protein. ATF4 is a transcription factor that then translocates into the nucleus to induce a transcriptional program supporting metabolic and proteostatic adaptation: amino acids synthesis and transport, autophagy, purine synthesis and transport, endoplasmic reticulum functioning, and redox balance among others (47,92,93,209,210).

This uORF-dependent translation, particularly in cancer cells upon glutamine starvation, is also determinant for the synthesis of proteins involved in: i) dedifferentiation, ii) migration, iii) inflammatory response (31,208).

iii. Other substrates of GCN2

Beside eIF2a, two other GCN2 substrates have been discovered. First, the integrase of retroviruses such as the human immunodeficiency virus (HIV). The HIV-1 integrase is phosphorylated on serine 255 by GCN2 that limits the virus replication and integration in the DNA (211).

Second, the methionyl tRNA-synthetase (MetRS), in charge of the transfer of methionyl to the tRNA initiator required for translation initiation, phosphorylated on serine 662 upon UV exposure (212). This phosphorylation induces structural modifications of the MetRS protein that decreases the affinity of MetRS for tRNAs. This reduces the charging of methionine of uncharged tRNAs and provokes the release of the ARS-interacting multifunctional proteins 3 (AIMP3). AIMP3 then translocates into the nucleus and activates the ATM/ATR-mediated DNA damage repair pathway. Furthermore, upon mitogenic signals, MetRS relocates into the nucleolus to enhance the 47S transcription and ribosome biogenesis (213). Consistently, accumulation of MetRS in human lung tumors is associated to high proliferation index and aggressiveness (214). The contribution of GCN2 in this protumorigenic role of MetRS is unknown.

The dogma according to which eIF2a is the only substrate of GCN2 raises questions about the role of the GCN2-MetRS axis in cancer progression.

iv. Towards a non-canonical GCN2 pathway and new functions in unstressed cell?

Because of its role as a sensor of amino acid availability, most of the studies concerning GCN2 have been performed under conditions of nutritional deficiency. Yet, as explained above, recent studies revealed that GCN2 may be involved in much broader cellular functions than the sole adaptation to nutritional deficiencies. Intriguingly, it has been shown that the loss of GCN2 leads to proliferation inhibition in leukemia cell lines and also in solid tumor derived cells, independently of any stress (215). This observation is corroborated by another study revealing that loss of GCN2 expression by RNA interference leads to reduced proliferation and loss of viability in papillary renal cancer cells, although not subjected to obvious nutrient deprivation (216).

These observations led us to question whether GCN2 could have a role in the regulation of the ribosome biogenesis both in starved and proliferative compartments of solid tumors.

OBJECTIVES & RESULTS OF THE STUDY

I. CONTEXT OF THE STUDY

The translational reprogramming underlying cell adaptation to nutritional stress is concomitant to the decrease in ribosomes production and activity. This step is crucial for cellular outcome to modulate high expenditure processes. Major efforts have been put on the characterization of the translational program and associated mechanisms underlying cell adaptation. However, the actors controlling the ribosome biogenesis and their role in cell survival remain poorly described. Their identification could lead to the discovery of new targetable proteins in order to impair the shift towards adaptation and rather force cancer cells to undergo apoptosis.

Active GCN2 is well-described for controlling the adjustment of translation and metabolism in response to nutritional stress, conferring a protective effect upon various ribotoxic stresses. However, recent studies suggest that GCN2 might be a molecular actor localized at the interface between ribosome homeostasis and the adjustment of translation. Indeed, deletion of GCN2 results in the induction of the P53 pathway and accumulation of 5S rRNA, suggesting that GCN2 might be involved in the maintenance of nucleolar integrity (217) However, cells were exposed to an unclear nutritional environment.

Yet, an increase in 5S rRNA associated to RPL5 and RPL11 in free 5S RNP is often considered as a consequence of a prior impairment of the 47S pre-rRNA metabolism and large ribosomal subunit assembly (133). Thus, these data suggest that: i) the deregulation of RNA Pol III activity upon loss of GCN2 could result of a prior impairment of RNA Pol I activity and ii) GCN2 is directly controlling the RNA Pol I activity, possibly independently of the nutritional context. The latter point is supported by recent set of clues, including data of our team, suggesting that GCN2 might promote cell proliferation in nutrient-rich condition.

In line with these observations, Ko et al shows that the methionyl tRNA synthetase (MetRS), an underestimated substrate of GCN2, stimulates ribosome biogenesis upon mitogenic signals (213). In these conditions, MetRS translocates into the nucleolus to support rRNA transcription by RNA Pol I, whereas blockade of ribosome biogenesis by actinomycin D results in MetRS

shuttling back to the cytoplasm. Whether this mechanism implicates GCN2 have not been investigated.

In summary, there are still many unknowns regarding the functions of GCN2 in the cell depending on the nutritional environment. Nonetheless, the known roles of two of its substrates, eIF2a and MetRS, indicate that GCN2 signaling might operate at multiple levels in the translation control and could be key in the global translational adaptation. Altogether, these recent studies suggest that GCN2 could be a central node in the coordination of ribosome biogenesis and translation adaptation according the nutritional context. Moreover, a whole field of studies is opening up to understand how GCN2 maintains cell proliferation and survival under basal conditions, far from its historical role as a sensor of nutrient deficiency.

Hypothesis: In regards to the data gathered by our team and in the literature, my research project aimed at investigating: i) whether GCN2 is implicated in the adaptation of ribosome biogenesis and maintenance of nucleolar homeostasis according the nutritional context and ii) define if this novel function would be of interest in the treatment of cancer, particularly in colon cancer therapeutic approach.

II. RESULTS

Targeting the cell and non-cell autonomous roles of GCN2 abrogates 47S rRNA synthesis and potentiates chemotherapy in colon cancer.

Piecyk, M.; Triki, M.; Laval, P.-A.; Duret, C.; Fauvre, J.; Cussonneau, L.; Manchon, C.; Guitton, J.; Rama, N.; Gibert, B.; Ichim, G.; Catez, F.; Bourdelais, F.; Durand, S ; Diaz, J.-J.; Coste, I.; Renno, T.; Manié, S.N.; Aznar, N.; Ansieau, S.; Ferraro-Peyret, C.; Chaveroux, C.

Submitted

To investigate the putative crosstalk between GCN2 and the ribosome biogenesis, I focused my project on colon adenocarcinoma, a type of cancer displaying marked dysregulation of genes involved i) in ribosome homeostasis, ii) response to amino acid deprivation and iii) ATF4 activity. Based on these correlative data, I used 3D models to mimic the heterogeneity of nutrient access in tumors and showed that GCN2 is essential for cell survival in deprived area. Analysis of the nucleolar integrity and RNA Pol I activity revealed that GCN2 contributes to the repression of ribosome biogenesis in stressed cells. At the contrary, inhibition of GCN2 in this context of nutrient scarcity triggers cell death through a lethal nucleolar stress that is dependent of TP53 activity.

Furthermore, I demonstrate that the impairment of GCN2 activity in cells that have no nutritional restrictions leads to a repression of mTORC1 pathway, associated to the induction of a protective autophagy and proliferation impairment. Mechanistically, my results show that this effect is independent of the canonical P-eIF2a-ATF4 branch. Originally, the GCN2-dependent role on cell proliferation rather implies the MetRS factor and its GCN2-dependent-translocation into the nucleus for promoting the RNA Pol I activity and the ribosome biogenesis.

Finally, I exploited these original mechanisms to show that targeting the GCN2-MetRS axis potentiates the cytotoxic effect of RNA Pol I inhibitors (Actinomycin D, Oxaliplatin) in colon cancer cells.

ARTICLE

Targeting the cell and non-cell autonomous regulation of 47S synthesis by GCN2 in colon cancer.

Marie Piecyk¹, Mouna Triki¹, Pierre-Alexandre Laval¹, Cedric Duret¹, Joelle Fauvre¹, Laura Cussonneau², Christelle Machon^{1,3}, Jérôme Guitton^{1,3}, Nicolas Rama¹, Benjamin Gibert¹, Gabriel Ichim¹, Frederic Catez¹, Fleur Bourdelais¹, Sebastien Durand¹, Jean-Jacques Diaz¹, Isabelle Coste¹, Toufic Renno¹, Serge N Manié¹, Nicolas Aznar¹, Stephane Ansieau¹, Carole Ferraro-Peyret^{1,4} and Cedric Chaveroux^{1*}

Affiliations :

¹ Centre de Recherche en Cancérologie de Lyon, INSERM U1052, CNRS 5286, Centre Léon Bérard, Université de Lyon, Université Claude Bernard Lyon 1, Lyon, France.

² Université Clermont Auvergne, INRAE, Unité de Nutrition Humaine, UMR1019, Clermont-Ferrand, France

³ Biochemistry and Pharmaco-toxicology laboratory, Lyon Sud Hospital, University Hospital of Lyon, Hospices Civils de Lyon Pierre-Bénite, France.

⁴ Hospices Civils de Lyon, Plateforme AURAGEN, Lyon, France.

Corresponding author:

*To whom correspondence should be addressed.

Email: cedric.chaveroux@lyon.unicancer.fr. Address: Cancer Research Center of Lyon, INSERM UMR 1052 CNRS 5286, Cheney D, floor 6, Centre Léon Bérard, 28 rue Laënnec, 69008 LYON, France. Tel: +33 (0)4 69 16 66 22

Abstract

Nutrient availability is a key determinant of tumor cell behavior. While nutrient-rich conditions favor proliferation and tumor growth, scarcity, and particularly glutamine starvation, promotes cell dedifferentiation and chemoresistance. Here, linking ribosome biogenesis plasticity with tumor cell fate, we uncover that the amino acid sensor GCN2 represses the expression of the precursor of ribosomal RNA, 47S, under metabolic stress. We show that blockade of GCN2 triggers cell death by an irremediable nucleolar stress and subsequent TP53-mediated apoptosis in patient-derived models of colon adenocarcinoma (COAD). In nutrient-rich conditions, GCN2 activity supports cell proliferation through the transcription stimulation of 47S rRNA, independently of the canonical ISR axis. However, impairment of GCN2 activity prevents nuclear translocation of the methionyl tRNA synthetase (MetRS) underlying the generation of a nucleolar stress, mTORC1 inhibition and autophagy induction. Inhibition of the GCN2-MetRS axis drastically improves the cytotoxicity of RNA pol I inhibitors, including the first-line chemotherapy oxaliplatin, on patient-derived COAD tumoroids. Our data thus reveal that GCN2 differentially controls the ribosome biogenesis according the nutritional context. Furthermore, pharmacological co-inhibition of the two GCN2 branches and the RNA pol I activity may represent a valuable strategy for elimination of proliferative and metabolically-stressed COAD cell.

Introduction

Cancer cell proliferation implicates a rewired metabolism to sustain the generation of biomass (Pavlova and Thompson, 2016). This cell growth is concomitantly supported by enhanced ribosome biogenesis (RiBi). However, in solid tumors, variation of nutrient availability determines protein homeostasis and the balance between proliferation capacity or quiescence. Hence, nutrient availability is often found in lower concentrations in various tumors, including colon adenocarcinoma (COAD), compared to the normal tissue or in tumor interstitial fluid compared to the plasma (Kamphorst et al., 2015; Sullivan et al., 2019). Fluctuations in amino acids availability also occur depending on the tumor region (Pan et al., 2016). Shifting cell fate from a proliferative to a quiescent state thus relies on the proteostatic flexibility, notably implicating a fine tuning of the RiBi. Nonetheless, the sensors and downstream mechanisms orchestrating the adaptation of RiBi according the nutritional context remain unclear.

RiBi depends on the production of ribosomal proteins (riboproteins) encoded by RNA polymerase II (pol II) and of the 5S ribosomal RNA (rRNA) encoded by RNA pol III. In addition, RNA pol I transcribes the 47S precursor rRNA (pre-rRNA), which will then be processed into final rRNA products, namely the 5.8S, 18S and 28S (Catez et al., 2019). The latter mechanism, occurring within the nucleolar sub-compartment, is sensitive to nutritional variations and is disrupted upon starvation, making the nucleolus a stress-integrator site (Clarke et al., 1996). Ultimately, defects in RiBi trigger nucleolar stress leading to cell cycle arrest and/or apoptosis (Russo and Russo, 2017).

Adjustment of the translation rate according the nutritional milieu implicates a tight reciprocal regulation between the ribosome biogenesis and nutrient sensor such as the mammalian target of rapamycin complex 1 (mTORC1). Active mTORC1 is commonly found in many types of cancers (Edinger and Thompson, 2002; Harachi et al., 2018; Saxton and Sabatini, 2017). In nutrient rich conditions, this complex supports protein synthesis and tumor progression notably by enabling RNA pol I and III transcription, rRNA processing and riboprotein translation (Guo et al., 2018; Sameer, 2013). However, in poorly-perfused areas, mTORC1 inactivation by the lack of nutrients contributes to RiBi repression. (Gomes et al., 2016; Riedl et al., 2017; Riffle and Hegde, 2017). Interestingly, the RNA pol I activity reciprocally controls the mTORC1 pathway. Indeed, decreased RNA pol I activity and impairment of 47S synthesis is sufficient to downregulate mTORC1 that in turns induces autophagy (Chen et al., 2016; Goudarzi et al., 2014; Li et al., 2016; Zajkovic et al., 2015). Inactive mTORC1 orchestrates a translational reprogramming alongside the phosphorylation of the eukaryotic initiation factor 2a (P-

eIF2a) on serine 51 (Jewer *et al.*, 2020). This latter triggers the integrated stress response (ISR) and has two major consequences: i) a repression of translation initiation and, ii) up-regulation of the translational of specific transcripts embedding open reading frames (uORFs) in their 5' untranslated region, including the activating transcription factor 4 (ATF4). ATF4 then orchestrates a transcriptional program to restore amino acids homeostasis, angiogenesis and antioxidant response to ultimately promote cell survival (Chaveroux *et al.*, 2016; Harding *et al.*, 2003; Sarcinelli *et al.*, 2020; Wang *et al.*, 2013). Following nutrient scarcity or proteotoxic stresses, GCN2 is the only eIF2a kinase activated by ribosome collision (Dong *et al.*, 2000; Harding *et al.*, 2019; Inglis *et al.*, 2019). Once activated, GCN2 participates to the adaptive translational and metabolic response by canonically inducing the ISR. However the contribution of GCN2 in the regulation of the ribosome biogenesis is poorly described. Cells silenced for GCN2 display an elevation of the RNA pol III activity and notably 5S rRNA (Nakamura and Kimura, 2017). Yet accumulation of 5S, in complex with RPL5 and RPL11, occurs subsequently to an impairment of the generation of 47S and related sub-products, suggesting that augmentation of the 5S content in GCN2-knockdown likely arise from a prior dysregulation of the 47S production and/or processing (Sloan *et al.*, 2013). Furthermore, the impact of the nutritional milieu on the GCN2-RiBi interplay was still unclear. Indeed, previous work by our group and others intriguingly suggested that GCN2 may also regulate cell viability and migration even when nutrients are abundant through an unknown mechanism (Chaveroux *et al.*, 2016; Ge *et al.*, 2018; Li *et al.*, 2022; Nakamura and Kimura, 2017).

Our present study is based on the hypothesis that GCN2 may differentially regulate the rate of protein synthesis in cancer cells through the modulation of 47S metabolism in quiescent and proliferative cells. Taking COAD as a paradigm of cancers displaying ribosomal dysfunctions associated to amino acid starvation, we show that, in a harsh nutritional context, GCN2 actively contributes to COAD cancer cell plasticity through the repression of 47S pre-rRNA synthesis, constituting a barrier against an irreversible nucleolar stress and ultimately cell death. Furthermore, in nutrient-abundant condition, we show that inhibition of GCN2 prevents the nuclear translocation of the methionyl tRNA synthetase (MetRS) and impairs the 47S pre-rRNA expression, further associated to mTORC1 repression and autophagy induction. This ribosomal vulnerability caused by GCN2 inhibition confers a higher sensitivity to RiBi stressors including the chemotherapeutic agent oxaliplatin. Our results unveil distinct cell-autonomous and non-autonomous functions for GCN2 according to the nutritional milieu both concurring to the maintenance of RiBi and COAD progression.

Results

I. Dysregulation of ribosomal function is associated with amino acid starvation and ATF4 activity in COAD.

To investigate the crosstalk between the altered nutritional microenvironment, activated GCN2 pathway and ribosomal stress, we first analyzed cancers that displayed clear proteostasis and/or ribosomal impairment. Comparison of normal and tumor samples from several cohorts in the TCGA database (figure supplement 1A) identified COAD as having highly dysregulated ribosome biogenesis (RiBi) and cell proliferation activities (Figure 1A). Defects in ribosome assembly in human tumors arise following impairment of rRNA production, or riboprotein (RP) processing and assembly (Albert et al., 2019; Kim et al., 2014). We then compiled a gene signature of RPs with a significantly dysregulated expression (negatively and positively) and confirmed enrichment of this signature in COAD compared to the normal tissue (table supplement 1) (Guimaraes and Zavolan, 2016). As expected, this signature was, validating its relevance for assessing ribosomal stress in this model (Figure 1B). To determine whether RP dysregulation was associated with metabolic stress, we compared enrichment of previously described signatures related to hypoxia or amino acid starvation in COAD based on two levels of RP dysregulation, low or high (Figure 1C, table supplement 1) (Dekervel et al., 2014; Krige et al., 2008). Interestingly, patients with a high RP dysregulation also displayed a significant enrichment in the amino acid starvation signature, albeit no difference was observed for the COAD-specific hypoxia signature between the two groups (figure supplement 1B), indicating that ribosomal stress may be strongly associated with a lack of amino acids. At the molecular level, amino acid deprivation and ribosomal stress are both strong inducers of the GCN2 kinase triggering the ISR-driven transcriptional program. We then assessed in the same subgroups of patients, a gene signature related to ATF4 transcriptional activity, the terminal factor of the GCN2-ISR pathway (table supplement 1). We first confirmed that the ATF4 signature was enriched in tumors compared to the normal tissue (Figure 1D). A correlation analysis then confirmed that this signature was linked to the amino acid deprivation signature (figure supplement 1C), and was higher in COAD tumors with a high RP dysregulation (Figure 1E). The data thus identified ATF4 as a major contributor to the stress response related to amino acid deprivation in COAD patients.

II. GCN2 represses 47S pre-RNA expression upon glutamine scarcity and prevents TP53-dependent apoptosis.

GCN2 takes part in survival upon ribotoxic stress. Here, we sought to decipher its role in maintaining cell viability and nucleolar integrity in those harsh conditions. We first confirmed the accumulation of GCN2 at the mRNA and protein levels, in a large group of patients and even at early stages of the pathology (figure supplement 2A-C, Figure 2A, B) (Marisa et al., 2013). Clinically, high levels of GCN2 expression in COAD patients were correlated with a lower disease-specific survival (figure supplement 2D). Considering the role of the ISR in cancer cell survival through cell plasticity in a nutrient-deprived microenvironment, we then set up *in vitro* conditions to assess whether GCN2 impacted COAD cell plasticity. HCT116 and LoVo COAD cells were grown as three dimensional (3D) models in order to mimic the complex metabolic heterogeneity and physiochemical gradients of solid tumors (Nath and Devi, 2016). Spheroids were then treated with a previously published GCN2 inhibitor, TAP20, hereafter referred to as GCN2i (Bröer et al., 2019). Prior validation in 2D culture confirmed the ability of GCN2i to abrogate the accumulation of ATF4 and related target genes (*CHOP*, *TRB3*, *GADD34*, *ASNS*, *SESN2*) upon leucine and glutamine (Gln) starvation (figure supplement 3A-C). In spheroids, viability assays following GCN2i treatment highlighted the presence of dead cells in the central region of spheroids confirming the protective role of GCN2 against an altered metabolic microenvironment and its implication in cell plasticity (Figure 2C, D). COAD patient-derived tumoroids were then grown as colospheres to reproduce the metabolic gradients (figure supplement 4) and our results were also confirmed by visualizing cell death in the compact core of the 3D models (Figure 2E). In contrast, the addition of the Rho-associated kinase (ROCK) inhibitor (Y-27632), a compound commonly present in tumoroids culture medium to inhibit cell death and enhance stem cell growth, abrogates the induction of cell death by the GCN2i (Kan et al., 2015; Ohata et al., 2012). Immunohistological analyses further confirmed the loss of cell viability and enhancement of apoptosis upon GCN2 inhibition in spheroids core, as attested by the measurement of cleaved PARP and cleaved caspase-3 staining (Figure 2F, G). Finally, the expression of two COAD stemness-related markers, *ALDH1A3* and *c-MYC* (Elbadawy et al., 2019; Gelardi et al., 2021), was reduced in spheroids treated with GCN2i, confirming that GCN2 is essential for the viability of c-Myc-expressing tumor cells and the elimination of quiescent tumor cells in the presence of the drug (Figure 2H).

Having validated that COAD represent a relevant context for studying the crosstalk between the GCN2 pathway and the RiBi. Then we determined whether this kinase is implicated in maintaining the nucleolar integrity under low amino acid conditions. Mechanistical investigations required to shift toward simpler

cellular models. In 2D culture, cells were exposed to low concentrations of asparagine or glutamine (Gln) similar to those found in poorly-perfused area of solid tumors. Cell death measurement revealed that GCN2i drastically killed the cells once associated to glutamine but not asparagine, (figure supplement 5A) (Pan et al., 2016). Combination with inhibitors of necroptosis (R3i, Nec1) or apoptosis (QVD, Z-VAD) confirmed that the loss of viability was caused by apoptosis when Gln starvation and GCN2i were combined (figure supplement 5B). Since the results obtained in 2D mirrored our observations in 3D, we hereafter applied the same Gln-deprived conditions to evaluate whether nucleolar integrity was impaired. A redistribution of fibrillarin, a canonical nucleolar marker, was observed in starved cells upon GCN2i indicating the induction of a nucleolar stress (Figure 3A) (Yuan et al., 2005). To document if this stress is a consequence of an impairment of the RNA pol I activity, northern blots were performed to assess 47S synthesis (Figure 3B). Gln-starved cells displayed a lower amount of 47S compared to the control, which is consistent with an inhibition of Pol I activity upon stress (Grummt et al., 1976). However, in presence of GCN2i, the level of 47S pre-rRNA increased again indicating the recovery of RNA pol I activity. To assess whether cell death caused by GCN2 inhibition upon low glutamine is a consequence of the nucleolar stress, the amount of TP53 was monitored in the same conditions. Indeed, TP53 is widely described as the molecular effector between nucleolar stress caused by RNA pol I repression and apoptosis (Fumagalli et al., 2012; James et al., 2014; Rubbi and Milner, 2003; Yang et al., 2018). Consistent with previous study, low glutamine alone did not change the level of TP53 during the starvation time (Lowman et al., 2019). However, cotreatment with GCN2i triggered an elevation of TP53 amounts and its target gene MDM2 (Figure 3C), two canonical markers of nucleolar stress (Morgado-Palacin et al., 2012). To functionally confirm whether GCN2i-induced cell death relies on TP53 upon, live-and-dead analyses were performed in spheroids made from COAD cell lines expressing a wild type (HCT116, LoVo) or mutant (HT29 and DLD-1) forms of TP53 (figure supplement 5C). Although a loss of cancer cell viability was obviously observed in the core area of LoVo and HCT116 spheroids upon GCN2i, the treatment did not lead to cell death in the spheroids mutated for TP53. To avoid a comparison bias related to the heterogenous capacities of the cell lines to form comparable spheroids, we shifted back to 2D cultures (figure supplement 5D). GCN2i treatment diminished cell viability of the TP53 WT cells upon low Gln whereas TP53 mutant cells were not affected by the blockade of GCN2 activity. Furthermore, toxicity assays performed on the isogenic HCT116 cell lines WT or knockout (KO) for TP53 confirmed, in 3D and 2D, that this latter is required for cell death

induction by the drug upon deprivation (Figure 3D, E). Of note, absence of TP53 did not impact the induction of ATF4 upon low Gln (figure supplement 5E). Altogether, these results demonstrate that GCN2 critically contributes to the RiBi repression upon amino acids scarcity thus preventing a TP53-mediated apoptosis.

III. GCN2, but not the ISR, sustains the mTORC1 signaling in proliferative condition.

Having shown the critical role of GCN2 in the maintenance of the RiBi pathway of COAD cells upon nutritional stress, we next investigated its role in nutrient-rich conditions. Indeed, data presented in figure 3E showed that GCN2 inhibition led to a decrease of HCT116 cell mass in nutrient-rich conditions, suggesting that GCN2 may support cell proliferation. To test this, we inhibited GCN2 in several cell lines, including HCT116, HT29, LoVo and DLD-1 grown under nutrient-balanced conditions (Figure 4A, figure supplement 6A). GCN2i treatment significantly reduced proliferation of HCT116, HT29 and LoVo cells, whereas DLD-1 cells were not affected. To ensure that this impaired proliferation was not due to medium exhaustion, similar experiments were conducted by refreshing the culture medium every day (Figure 4B). Western blot and qPCR analyses confirmed that cells grown in nutrient-rich conditions did not induce the ISR within 24 hours of culture (figure supplement 6B-D). Nonetheless, even in these controlled experimental conditions, we conserved a significant reduction of cell proliferation from 48 hours after GCN2i addition (Figure 4B). This reduction was further confirmed using an RNA interference approach and, pharmacologically, on patient primary COAD cells (Figure 4C, D). Intriguingly, treatment with a second GCN2 inhibitor, GCN2iB, did not impair cell proliferation, suggesting that the two compounds are distinctly modulating GCN2 activity (figure supplement 6E) (Nakamura et al., 2018). Furthermore, GCN2i also impaired spheroids formation indicating that proliferation promotion by this kinase is not restricted only to models in 2D (Figure 4E, figure supplement 6F). To evaluate if GCN2 supports cell proliferation in an ISR-dependent manner, HCT116 cells were treated with ISRIB, a chemical leading to the blockade of eIF2a phosphorylation, or transfected with a siRNA against ATF4 (Figure 4F-I) (Rabouw et al., 2019; Sidrauski et al., 2015). As expected, both treatments prevented the P-eIF2a-dependent elevation of ATF4 and its target gene CHOP in cells deprived for leucine, confirming that the pathway was impaired by the treatment. However, neither ISRIB treatment nor knocking-down ATF4 compromised cell proliferation after 48 hours of treatment. Altogether, these data demonstrate

that GCN2 promotes cell proliferation independently of its canonical pathway in abundant-nutrient condition.

To decipher the underlying mechanism by which GCN2 activity promotes cell proliferation, RNA sequencing was performed on HCT116 cells grown in 2D with daily media refreshment, silenced or not for GCN2 (Figure 5A). Gene set enrichment analysis revealed dysregulation of functions associated with protein homeostasis, particularly autophagy, and cell cycle checkpoint. Consistently, metabolomics experiments showed a perturbation in the intracellular content of several amino acids in cells silenced for GCN2 (Figure 5B) and a significant decrease in protein synthesis upon GCN2i (Figure 5C). Pharmacological inhibition of GCN2 increased the amount of the canonical autophagy markers LC3-I/II and P62 (Figure 5D). Based on the use of a molecular reporter, we confirmed the activation of an autophagic flux when the activity of GCN2 was blocked in HCT116 and HT-29 (Figure 5E, figure supplement 7A). Although treatment with a classical inhibitor of autophagy, namely chloroquine, did not affect significantly the cell mass (Figure 5F, figure supplement 7B), when both treatments were applied, chloroquine aggravated the reduction of cell mass caused by GCN2i, functionally demonstrating the protective role of the autophagic process.

We then investigated the molecular events underlying proteostasis defects when GCN2 is blocked. In complete media, mTORC1 maintains the autophagic flux at a low level and support protein translation. Additionally, previous studies report several molecular crosstalk linking mTORC1 repression to GCN2 induction or vice versa upon amino acid deprivation or rapamycin analog treatment (Averous et al., 2016; Wengrod et al., n.d.; Ye et al., 2015). Nonetheless, no evidence was reported regarding a GCN2-dependent upregulation of mTORC1 activity in proliferative state. We thus hypothesized that GCN2 inhibition could repress the mTORC1 pathway that, in turn, limits protein synthesis and induces autophagy. Activation degree of mTORC1 pathway was assessed through the amount of the phosphorylated forms of the S6 ribosomal protein, 4E-BP1 and ULK1 in COAD cells treated with GCN2i for 24 hours (Figure 5G, figure supplement 7C). The compound provoked a diminution of all tested canonical markers of mTORC1 activity, including phosphorylated ULK1 that is consistent with the autophagy activation (Kim et al., 2011). Inhibition of S6 phosphorylation by the GCN2i was also observed at the periphery of colon cancer spheroid indicating that mTORC1 pathway is also repressed in proliferating cells of 3D models and confirmed in GCN2 silenced cells (Figure 5H, figure supplement 7D). The relevance of this was then evaluated in patients using the COAD TCGA database. Our results

show that this connection is independent of the ISR but is highlighted by the lack of GCN2 expression. Thus, instead of discriminating tumors according an irrelevant stress-related gene signature, we compared the low-GCN2 expressing patients to the rest of the COAD cohort in the TCGA. Gene set enrichment analysis confirmed that a low or null expression of GCN2 was significantly associated with a downregulation of the AKT-mTORC1 pathway in COAD tumors (Figure 5I).

IV. Inhibition of GCN2 impairs MetRS translocation and 47S rRNA production

Then we sought to further define the mechanism by which lack of GCN2 activity impairs the mTORC1 signaling. RNA sequencing data indicated that a four-day GCN2 silencing triggered a dysregulation of RiBi as highlighted in figure 5A. Since RNA pol I inhibition is sufficient to repress mTORC1 and triggers subsequent autophagy, we explored whether repression of mTORC1 upon GCN2i might result from a prior defect in RiBi. This hypothesis was especially supported by the GCN2i-driven cell cycle arrest in G2/M phase that is consistent with pharmacological RNA pol I inhibition and the gene signature found in COAD patients associated to dysregulated ribosome biogenesis (Figures 1A and 6A) (Hald et al., 2019; Li et al., 2016; Ma and Pederson, 2013). Enlarged nucleoli associated with dispersion of fibrillarin were observed from 4 hours of treatment, confirming that GCN2 also controls nucleolus homeostasis in proliferative conditions (Figure 6B). Northern blot analysis revealed that GCN2 inhibition impaired 47S pre-rRNA generation (Figure 6C). However, no change in phosphorylation of S6 was observed at the same early time points, indicating that mTORC1 repression by GCN2i is rather a long-term consequence of RiBi defects upon treatment (figure supplement 8A). Then we investigated the molecular link between GCN2 and RNA pol I activity. As ISRIB treatment or ATF4 silencing did not mimic the proliferation arrest caused by the loss of GCN2 activity, a contribution of the ISR was thus excluded. However, we explored a role for the methionyl tRNA synthetase (MetRS), a second substrate of GCN2 (Kwon et al., 2011), for the two following reasons: i) MetRS has already been described to localize within the nucleolus to sustain rRNA synthesis and 47S products upon mitogenic signals although the contribution of GCN2 in this mechanism was not addressed (Ko et al., 2000) and ii) knockdown of MetRS leads to the downregulation of mTORC1 activity as well (Suh et al., 2020). Immunofluorescence assays confirmed that the colocalization of MetRS with the fibrillarin within the nucleus, in proliferative cells (figure supplement 8B). Similarly to GCN2 inhibition, MetRS silencing is sufficient to induce nucleolar stress as revealed by fibrillarin diffusion and impairs cell proliferation in nutrient-rich condition (Figure 6D, E, figure

supplement 8C). We then assessed whether the cytoplasmic/nuclear shuttling of MetRS was dependent of GCN2 (Figure 6F). Inhibiting GCN2 for 2 hours of GCN2i impaired MetRS translocation. Intriguingly the GCN2iB did not affect the MetRS shuttling between the two cellular compartment. Collectively these results demonstrate that lack of GCN2 activity impairs MetRS nuclear translocation provoking a downregulation of 47S synthesis and ultimately decreased mTORC1 signaling and protein synthesis.

V. Inhibition of the GCN2-MetRS axis potentiates COAD cell death upon RNA Polymerase I inhibitors in nutrient rich condition.

Finally, we investigated whether impairing the GCN2/MetRS axis might confer a ribosomal vulnerability to COAD cells. We hypothesized that further inhibition of 47S pre-RNA synthesis by combining GCN2i with drugs downregulating the RNA pol I might enhance the 47S/5S disequilibrium and cause cell death. To this end, COAD cells were co-treated with GCN2i and actinomycin D, a known inhibitor of RNA pol I activity (Figure 7A) (Catez et al., 2019). After 48 hours of treatment, GCN2i or actinomycin D alone triggered a slight but significant cell death in a similar manner and their co-treatment drastically increased cell death. We then explored whether this first proof-of-principle could be relevant for translational applications. Interestingly, the mode of action of oxaliplatin, a front-line chemotherapy used in COAD treatment, also relies on the repression of RNA Pol I and induction of an irremediable ribosomal stress (Bruno et al., 2017; Sutton and DeRose, 2021). Consistently, oxaliplatin cytotoxicity is higher when cells are in the G2/M phase of the cycle, corresponding to the peak of RNA pol I activity (Klein and Grummt, 1999; Narvi et al., 2018). To test whether GCN2 inhibition may also aggravate oxaliplatin-induced nucleolar stress, immunofluorescence against fibrillar in was first performed (Figure 7B). Early formation of cap-like structures, a mark of dramatic RNA Pol I inhibition and nucleolar stress, was observed within 4 hours of administration of the drug combination. Cytotoxicity assays confirmed that GCN2i drastically increased the cell death caused by oxaliplatin in nutrient-rich conditions (Figure 7C). However, ISRIB treatment did not change the efficacy of the chemotherapeutic drug (Figure 7D). A second approach by RNA interference confirmed that downregulation of GCN2 expression specifically sensitizes COAD cells to oxaliplatin and actinomycin D (figure supplement 8D, E). Furthermore, the cytotoxicity of oxaliplatin was significantly higher in cells silenced for MetRS, (figure supplement 8F). The improvement of oxaliplatin toxicity by the inhibition of the GCN2-MetRS axis was then validated in spheroids (figure supplement 8G and supplemental movie 1). Oxaliplatin or GCN2i alone led majorly to

growth impairment without clear impairment of the spheroid shape. The combination of the two compounds triggered a massive cell death at the periphery and resulted in complete unstructured spheroids. These observations were then confirmed with patient-derived colospheres in the presence or absence of the ROCK inhibitor (Figure 7F). Collectively, these results show that inhibition of the GCN2-MetRS axis drastically improves RNA pol I inhibitors-mediated COAD cell death in nutrient-rich conditions (figure supplement 8H).

Discussion

Cellular plasticity relies on the integration of intrinsic and extrinsic cues at the molecular level, notably contributing to the fine tuning of the translational program. In this context, the flexibility of RiBi represents a first and critical level of cell adaptation. In this study, we identify GCN2 as a novel and determinant regulator of RiBi and nucleolar homeostasis. Intriguingly, this kinase supports tumor-cell plasticity by repressing the 47S pre-rRNA transcription upon starvation, preventing the engagement of an irreversible nucleolar stress in dedifferentiated cells. Conversely, GCN2 sustains 47S pre-rRNA transcription in nutrient-rich conditions, and the combination of inhibitors of GCN2 and RNA Pol I allows a shift from cell cycle arrest towards apoptosis.

In harsh conditions, glutamine scarcity is a major driver of tumor cell dedifferentiation leading to the acquisition of a stem cell-like phenotype associated with chemoresistance (Pan et al., 2016). The underlying molecular program is evidently complex including at least an epigenetic and translational reprogramming supported by the concomitant phosphorylation of eIF2a and repression of mTORC1 (Jewer et al., 2020). Our results show that GCN2 also supports RiBi reprogramming. The adaptive cellular response to starvation implicates limitation of both RNA Pol I activity and rRNA processing (Pan et al., 2022). Our data supports a model in which GCN2 preserves the repression of 47S expression in amino acid-depleted conditions likely to sustain the translational dedifferentiation program. These observations are consistent with the previous work showing that, upon metabolic stress, restoration of 47S pre-RNA expression through the silencing of nucleomethylin (NML) triggers cell death, mimicking our results when GCN2 activity is blocked upon starvation (Murayama et al., 2008). Whether GCN2 might influence the NML function in stressed cells has so far not been reported. Furthermore, the ATF4-mediated augmentation of Sestrin-2 in starved cells might represent the molecular link between GCN2 and 47S synthesis inhibition (Ye et al., 2015). Indeed, elevation of Sestrin-2 maintains the repression of mTORC1 upon scarcity. Furthermore, abrogation of the GCN2 activity and absence of Sestrin-2 induction triggers the mTORC1 activity. Recovery of mTORC1 activity might explain the rescue of 47S transcription in starved-cells treated with GCN2i. Inhibition of GCN2 is sufficient to further alter RiBi and trigger cell death through the TP53-proapoptotic program. Although several studies support the use of GCN2 inhibitors in the clinic to eliminate adapted cells, the mechanisms related to cell death caused by GCN2 inhibition in starved cells remain unclear. Most often attributed to an impairment of the ISR and its related translational/metabolic adaptive response, our results demonstrate that the subsequent

apoptotic program likely results from the disruption of the nucleolar homeostasis. Cell death caused by the lack of GCN2 activity is accompanied by a decreased expression of c-Myc in a nutrient-scarce microenvironment. These results corroborate previous studies showing that cells overexpressing c-Myc are more sensitive to GCN2 inhibition (Schmidt et al., 2019; Tameire et al., 2019). Thus, one can postulate that increased c-Myc expression stimulates the glutaminolysis pathway and aggravates microenvironmental exhaustion of Gln. As a consequence of the c-Myc-driven nutritional stress, GCN2 activation and subsequent RiBi downregulation preserve the nucleolus homeostasis and optimize energy efficiency (Gao et al., 2009; Shore and Albert, 2022; Wise et al., 2008). Nonetheless, cell death caused by GCN2 inhibition is also effective in models expressing a wild type form of APC (e.g. HCT116), classically associated with a lower expression of c-Myc in COAD. These results suggest that, beyond the mutational status of APC previously proposed, the subset of tumors expressing a wild-type form of TP53 should be prioritized, considering that high levels of c-Myc might provide an optimal response to GCN2 inhibitors. Moreover, although GCN2 activity is required for repressing 47S expression upon low glutamine, whether the ISR axis plays a critical role in this mechanism requires further investigations. The Dr. Lyons' group recently showed that chemical stress (NaAsO₂), activating the HRI-p-eIF2a axis, limits the first step of rRNA processing. However, the authors demonstrated that this effect is independent of both HRI and eIF2a suggesting that, upon stress, an ISR-independent pathway controls the RiBi pathway (Szaflarski et al., 2022). Beside HRI, GCN2 is also activated in response to arsenate (Taniuchi et al., 2016). Thus we propose that, instead of HRI, GCN2 might be responsible of the modulation of the RiBi and determine the cell outcome upon NaAsO₂ (Taniuchi et al., 2016). Collectively, these results support the hypothesis that unknown substrates of GCN2 may be at the interface between external stresses and RiBi.

In addition to the canonical function of GCN2 in stressed cells, we found that this kinase also functions in nutrient-rich conditions. Our robust experimental set-up, distinguishing starved and non-starved conditions, revealed that inhibition of GCN2 represses proliferation and the mTORC1 pathway. This effect appeared to be cell type-dependent since proliferative DLD-1 or primary cells isolated from one COAD patient were insensitive to the loss of GCN2 activity. It is likely that mTORC1 repression is a consequence of RiBi impairment following GCN2 inhibition. Indeed, alteration of 47S synthesis is an early event in refreshed medium settings and is not associated, at these early time points with impaired phosphorylation of S6. These observations reinforce the notion that GCN2 also controls RiBi in the

absence of nutritional stress. The mechanism underlying this novel cell-autonomous function for GCN2 implicates its capacity to sustain MetRS translocation within the nucleus to ensure the stimulation of RNA Pol I and cell proliferation. How MetRS controls the 47S transcription and largely RiBi remains unknown. Yet, in line with our data, high expression of MetRS is of poor prognosis in several types of human tumors, including COAD, and consistently associated to enhanced mTORC1 activity and cancer cell proliferation confirming its role in promoting tumor growth (Jin et al., 2020; Kim et al., 2017; Kushner et al., 1976).

Finally, this work shows that GCN2 represents a novel regulator of the RiBi in deprived and non-deprived cells that can be therapeutically exploited in the clinic through the use of compounds targeting the kinase. Overall, the threshold of repression of the RNA Pol I activity is a key determinant in the induction of cell death. In this context, gastrointestinal cancers may constitute interesting types of cancer models since they are classically treated using FOLFOX or FOLFIRI, two chemotherapeutic regimens containing drugs targeting the ribosomal function. Indeed, oxaliplatin was reported to kill cells through the induction of a ribosomal stress and 5-fluorouracil was described to impair 47S processing and recently to be integrated in the ribosome and promoting profound translational reprogramming (Bruno et al., 2017; Burger et al., 2010; Ge et al., 2017; Sutton and DeRose, 2021; Therizols et al., 2022). Nonetheless, these compounds are mainly effective on proliferative cells since metabolic stress limits their efficacy (Xu et al., 2019). Moreover, glutamine starvation drives resistances to RNA Pol I inhibitors. Our results provide a solid basis for promoting the transfer of GCN2 inhibitors to the clinic as a promising approach and argue in favor of developing compounds inhibiting concomitantly the ISR and MetRS branches of the pathway and satisfying all the physicochemical requirements for in vivo applications. Such a strategy would allow: i) elimination of chemoresistance of TP53-WT quiescent tumor cells, and ii) sensitization of proliferative cells towards oxaliplatin or other RNA pol I inhibitors. The benefits of in such inhibitors would be of a greater translational value than ISR-centered compounds currently under development.

Figure 1

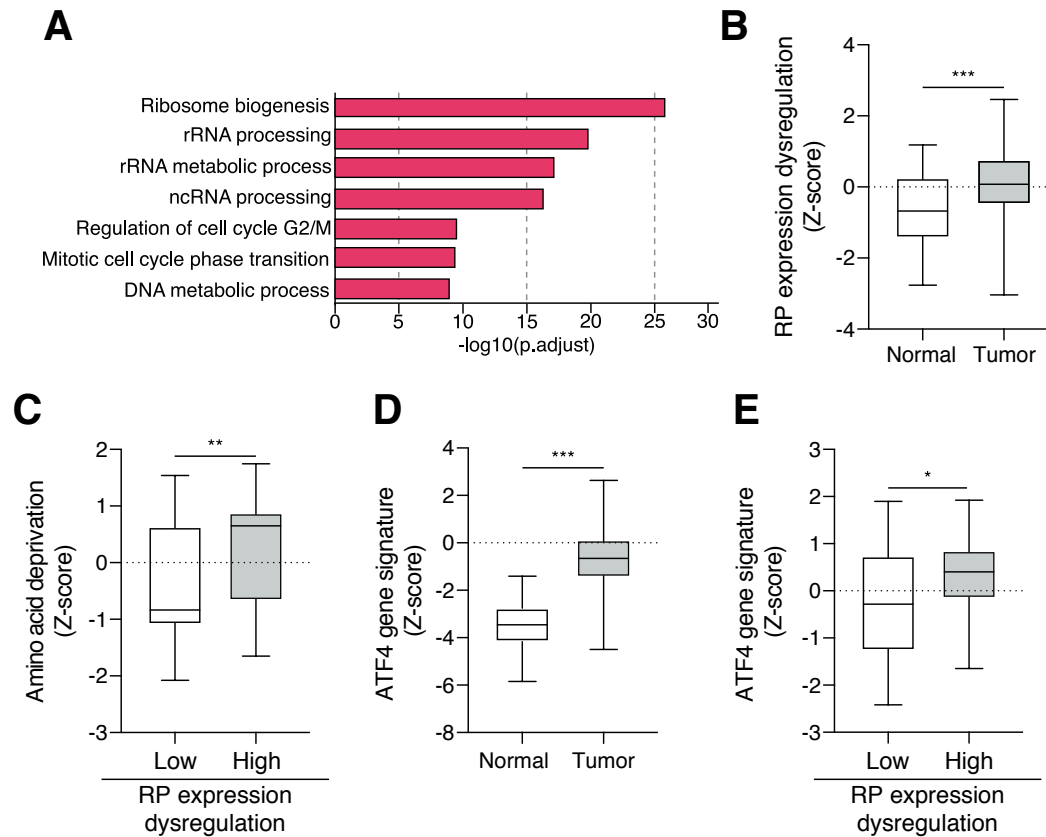


Fig. 1. Ribosomal dysfunction in colon adenocarcinoma (COAD) is correlated with the upregulation of ATF4 activity.

- A. Gene Ontology enrichment analysis on TCGA database highlights an upregulation of ribosomal biogenesis processes in COAD compared to normal tissue. Top enrichment GO terms in COAD tumors versus normal tissues are shown and significance is expressed as $-\log_{10}$ adjusted p-value.
- B. Dysregulated expression of riboproteins (RP) is higher in COAD compared to the normal tissue. TCGA COAD data, Mann-Whitney-test, (** $p < 0.001$)
- C. The amino acid deprivation gene signature is enriched in COAD tumors with high dysregulated RP expression. TCGA COAD data, Mann-Whitney-test, (** $p < 0.01$)
- D. ATF4 gene signature is higher in colon tumors compared to normal tissue. TCGA COAD data, Mann-Whitney-test, (** $p < 0.001$)
- E. ATF4 gene signature is enriched in COAD with high dysregulation of RP expression. TCGA COAD data, Mann-Whitney-test (* $p < 0.05$)

Figure 2

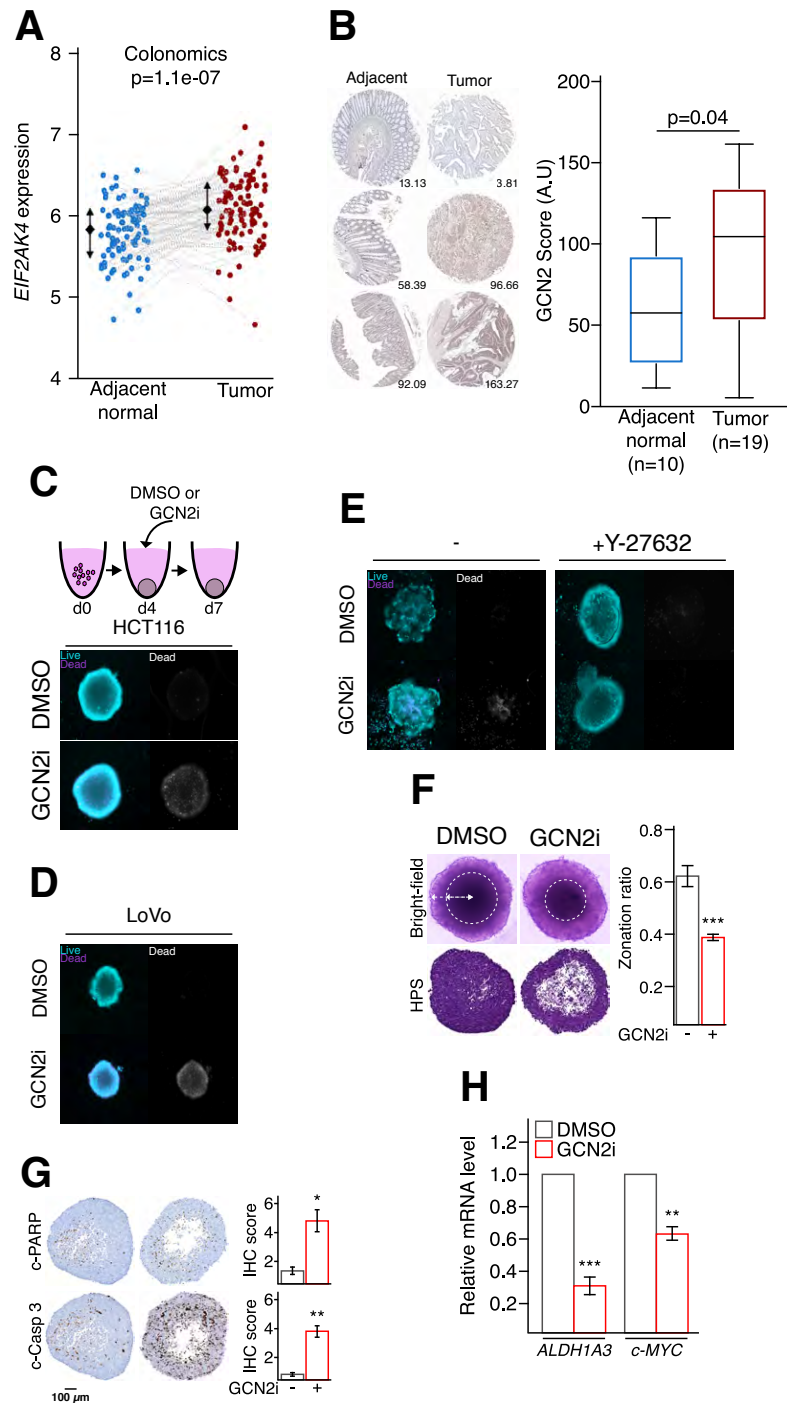


Fig. 2. GCN2 activity is critical to promote COAD cells plasticity.

- A. *GCN2* (gene name *EIF2AK4*) expression levels is higher in colon tumor tissues compared to the normal counterparts. Colonomics cohort, Unpaired t-test.
- B. Immunohistochemistry analysis confirmed that *GCN2* amount is augmented in human COAD tumors compared to adjacent normal tissues. Quantification is provided on the right panel. Unpaired t-test.

- C. Live-and-dead assay in HCT116 spheroids treated for 3 days with vehicle (DMSO) or GCN2i. To facilitate the observation of death induction, staining of non-viable cells is also represented in shades of grey (right panel).
- D. Live-and-dead assay in LoVo spheroids treated for 3 days with vehicle (DMSO) or GCN2i. To facilitate the observation of death induction, staining of non-viable cells is also represented in shades of grey (right panel).
- E. Live-and-dead assay in patient's derived colospheres, grown with or without the ROCK inhibitor (Y-27632), after 3 days of GCN2i treatment. To facilitate the visualization of cell death induction, staining of non-viable cells is also represented in shades of grey (right panel).
- F. Evaluation of cellular compaction in the core of HCT116 spheroids treated for 3 days with DMSO or GCN2i via bright-field microscopy and on hematoxylin-phloxine-saffron stained spheroid slices. Data are expressed as mean \pm s.e.m of independent experiments (n = 3), unpaired two-tailed t-test with the p-value (** p < 0.001).
- G. Measurements of immunohistochemical staining against cleaved PARP and cleaved caspase 3 on HCT116 spheroids treated with DMSO or with GCN2i for 3 days. Data are expressed as mean \pm s.e.m of independent experiments (n = 3), unpaired two-tailed t-test with the p-value (* p < 0.05, ** p < 0.01).
- H. RT-qPCR analysis of *ALDH1A3* and *c-MYC* mRNA levels in HCT116 spheroids treated for 48h with DMSO or GCN2i. Data are expressed as mean \pm s.e.m of independent experiments (n = 3), unpaired two-tailed t-test with the p-value (** p < 0.01, *** p < 0.001).

Figure 3

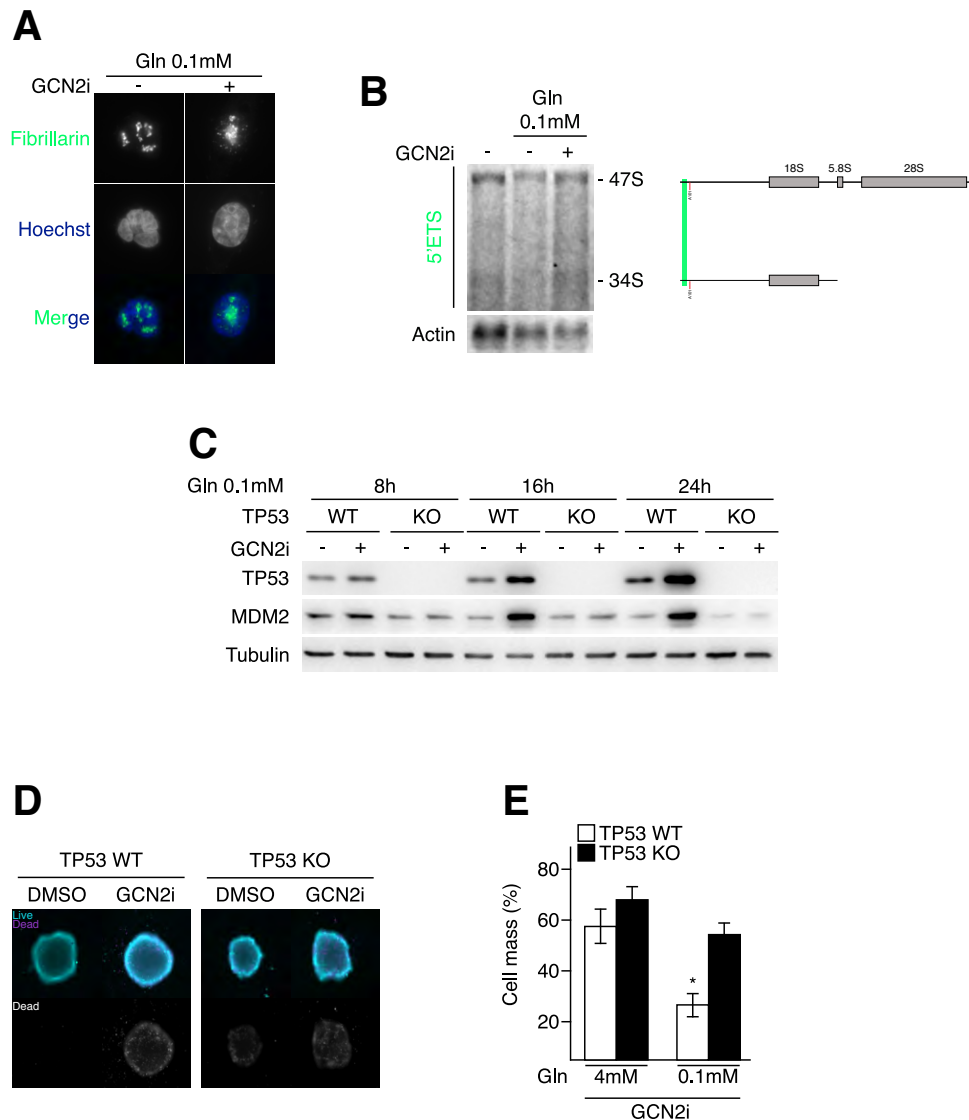


Fig. 3. GCN2 is required for repressing 47S transcription and preventing the TP53-proapoptotic program upon low glutamine.

- Fibrillarin localization assessed by immunofluorescence in glutamine-starved HCT116 cells treated with DMSO or GCN2i.
- Northern blotting of cellular rRNAs after indicated treatments. The position of the investigated probes on the 47S rRNA and sub-products are indicated according the corresponding colors.
- Western blot analysis of TP53 and MDM2 protein amounts in HCT116 TP53 WT and HCT116 TP53 KO treated with DMSO or GCN2i upon low glutamine condition (0.1 mM, -Gln) for the indicated period of time.
- Live-and-dead assay in HCT116 spheroids wild-type (WT) or knockout (KO) for TP53 treated for 3 days with vehicle (DMSO) or GCN2i. To facilitate the observation of death induction, staining of non-viable cells is also represented in shades of grey (right panel).
- Measurements of cell mass impairment in HCT116 TP53 WT and HCT116 TP53 KO treated with GCN2i for 48 h in medium containing 4 mM or 0.1 mM levels of glutamine. Data are expressed as mean +/- s.e.m of independent experiments (n = 5). Results of unpaired two-tailed t-test are indicated with the p-value (* p < 0.05).

Figure 4

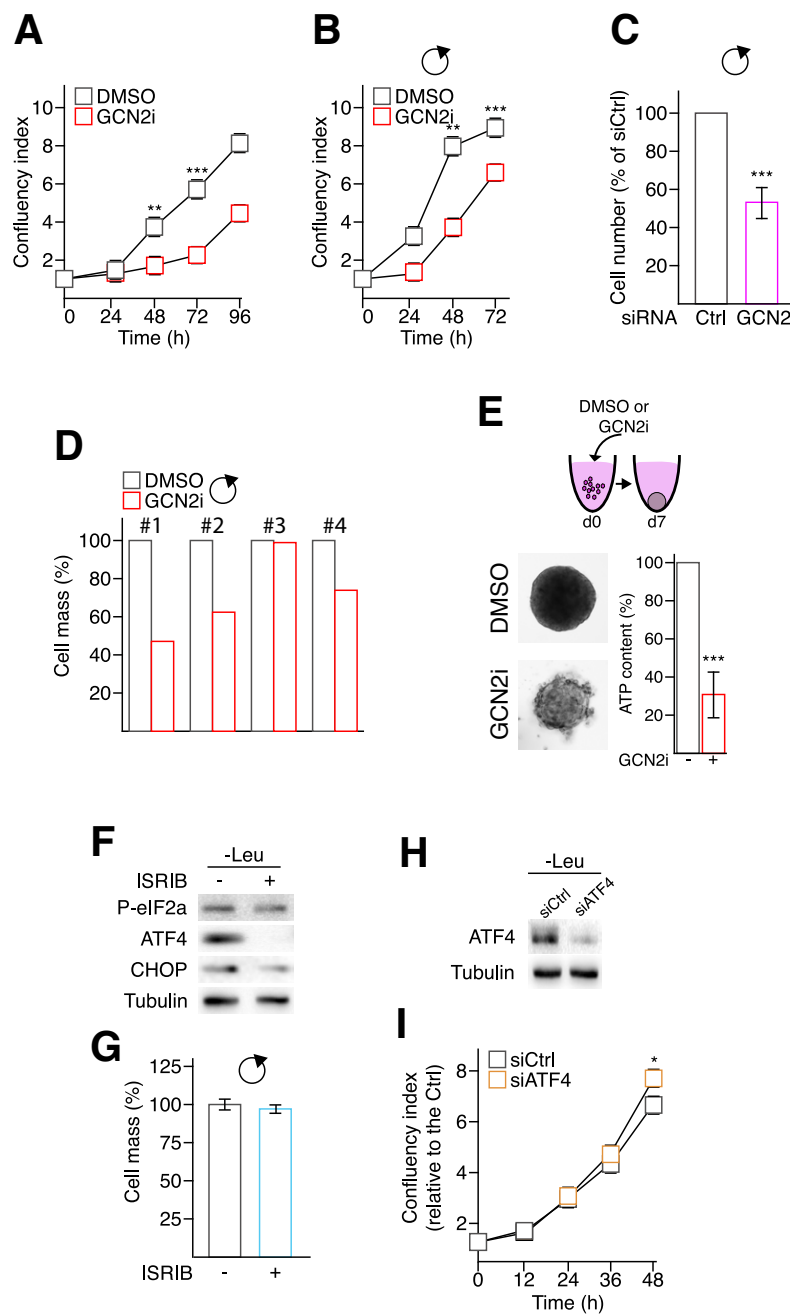


Fig. 4. GCN2 is necessary for COAD cancer cells proliferation independently of the ISR pathway.

- A. Cell proliferation assessed by the confluency index of HCT116 cells treated or not with GCN2i for 96 h. Data are expressed as mean \pm s.e.m of independent experiments (n = 3). Unpaired two-tailed t-test with p-value (** p < 0.01, *** p < 0.001).
- B. Cell mass was assessed every day over the indicated period of time in HCT116 cells treated or not with GCN2i by SRB assay. A daily refreshment of the medium (indicated by the black rounded arrow) was performed to ensure a full supply of nutrients over the time course of the experiment. Data are expressed as mean \pm s.e.m of independent experiments (n = 3). Unpaired two-tailed t-test with p-value (** p < 0.01).

- C. Relative number of HCT116 cells transfected either with a siRNA control (CTRL) or against GCN2 (GCN2) following 4 days of culture. Medium were daily refreshed (black rounded arrow) to prevent nutrients exhaustion. Data are expressed as mean +/- s.e.m of 3 independent experiments. Unpaired two-tailed t-test with p-value (** p < 0.01).
- D. Cell mass measurement of patient-derived primary cells cultured in 2D conditions and treated with DMSO or GCN2i for 48 h. Media were refreshed daily (black rounded arrow).
- E. Spheroid formation assays of HCT116 treated with DMSO or GCN2i. ATP content was measured after 7 days of treatment. Treatment was initiated concomitantly to plating. Data are expressed as mean +/- s.e.m of 3 independent experiments. Unpaired two-tailed t-test with p-value (** p < 0.01).
- F. Western blot analysis of P-eIF2a, ATF4 and CHOP protein amounts in HCT116 starved for leucine for 8h in the presence of ISRIB (200 nM) or not.
- G. Measurements of cell mass in HCT116 cells treated with ISRIB (200 nM) for 48 h. Medium were daily refreshed (black rounded arrow) to ensure complete nutrients supply. Data are expressed as mean +/- s.e.m of independent experiments (n = 5). Unpaired two-tailed t-test.
- H. Western blot analysis of ATF4 protein levels in HCT116 cells transfected either with a siRNA control (siCtrl) or against ATF4 (siATF4) following 2 days of culture with siCTRL and siATF4 upon 8 h of amino acid deprivation (leucine starvation).
- I. Cell proliferation assessed by the confluency index of HCT116 cells transfected with a siCtrl and siATF4 was monitored over 48 h. Data are expressed as mean +/- s.e.m of independent experiments (n = 3). Unpaired two-tailed t-test with p-value (* p < 0.05).

Figure 5

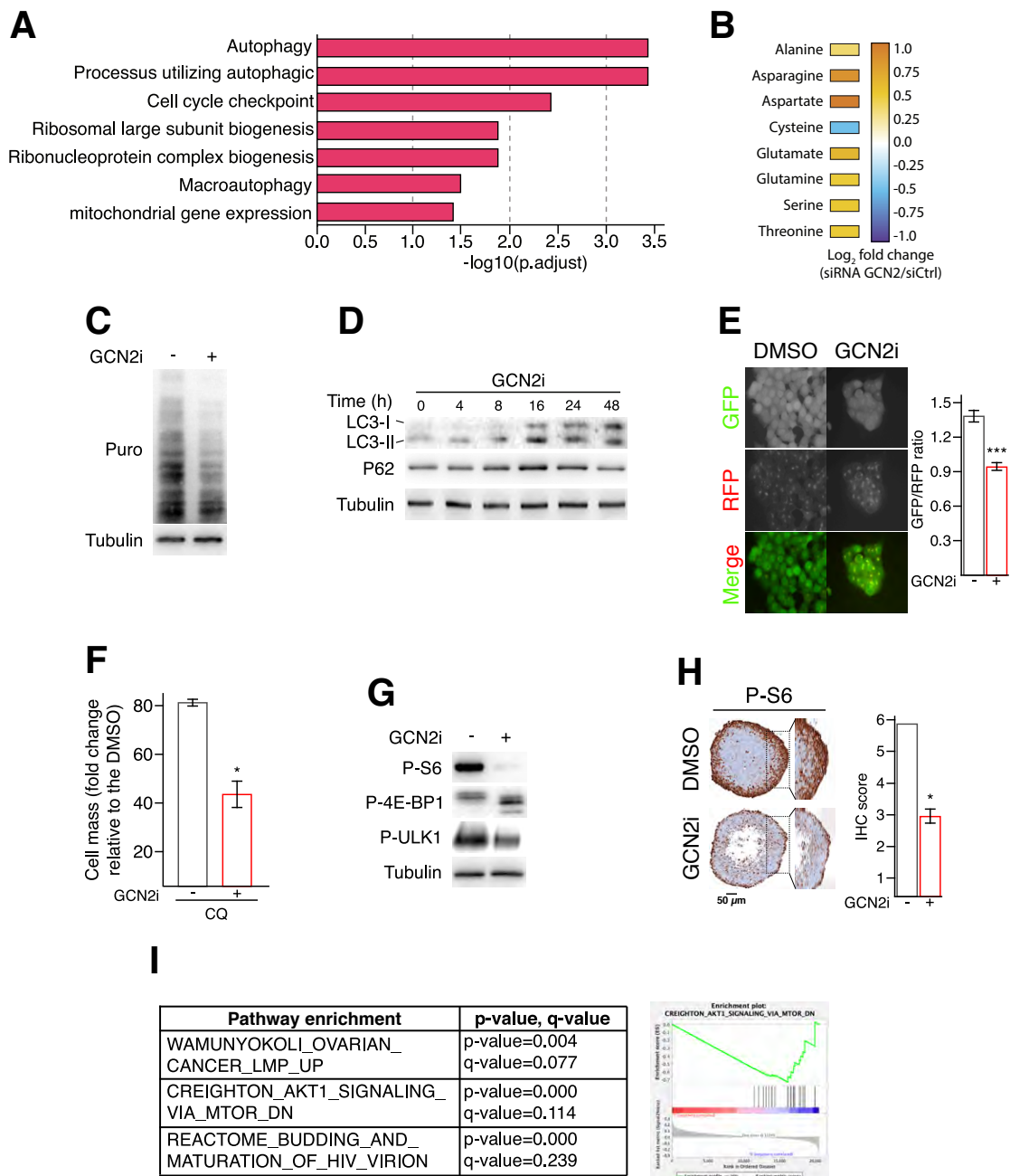


Fig. 5. GCN2 sustains the mTORC1 activity in proliferative colon cancer cells.

- Gene set enrichment analysis in HCT116 cells silenced for GCN2 compared to the control. Top enrichment GO terms in siGCN2 transfected cells versus siCtrl are shown and significance is expressed as $-\log_{10}$ adjusted p-value.
- Amino acid profiling of HCT116 cells transfected with a siRNA control or against GCN2.
- Assessment of protein synthesis rate in HCT116 cells treated for 24 h with GCN2i.
- Western blot analysis of autophagic markers, LC3-I, LC3-II and p62, in HCT116 cells treated with GCN2i for the indicated period of time.
- Autophagic flux analysis using HCT116 cells stably expressing the GFP-LC3-RFP-LC3 Δ G construct and treated with GCN2i for 48 h. Cleavage of GFP-LC3 by autophagy released the RFP-LC3 as an

internal control, thus reduction of the GFP/RFP ratio illustrates induction of the autophagy flux. Data are expressed as the mean of quantification \pm s.e.m. of independent experiments (n = 3). Unpaired two-tailed t test with p-value (* p < 0.05)

- F. Cell mass was measured in GCN2i-treated HCT116 cells after 48 h in combination with chloroquine. Data are expressed relative to the vehicle as mean \pm s.e.m of independent experiments (n = 7). Unpaired two-tailed t-test with p-value (***) p < 0.001).
- G. Western blot analysis of mTORC1 pathway markers (P-S6, P-4EBP1 and P-ULK1) amounts in HCT116 cells following 24 h of GCN2i treatment.
- H. Immunohistochemical staining against P-S6 in HCT116 spheroids treated for 3 days with DMSO or GCN2i. Quantification of the IHC staining is provided on the right panel. Data are expressed as mean \pm s.e.m of independent experiments (n = 3). Unpaired two-tailed t-test with p-value (* p < 0.05).
- I. Gene set enrichment analysis of COAD patients with low GCN2 expression (25%) compared to the rest of the COAD cohort (TCGA data).

Figure 6

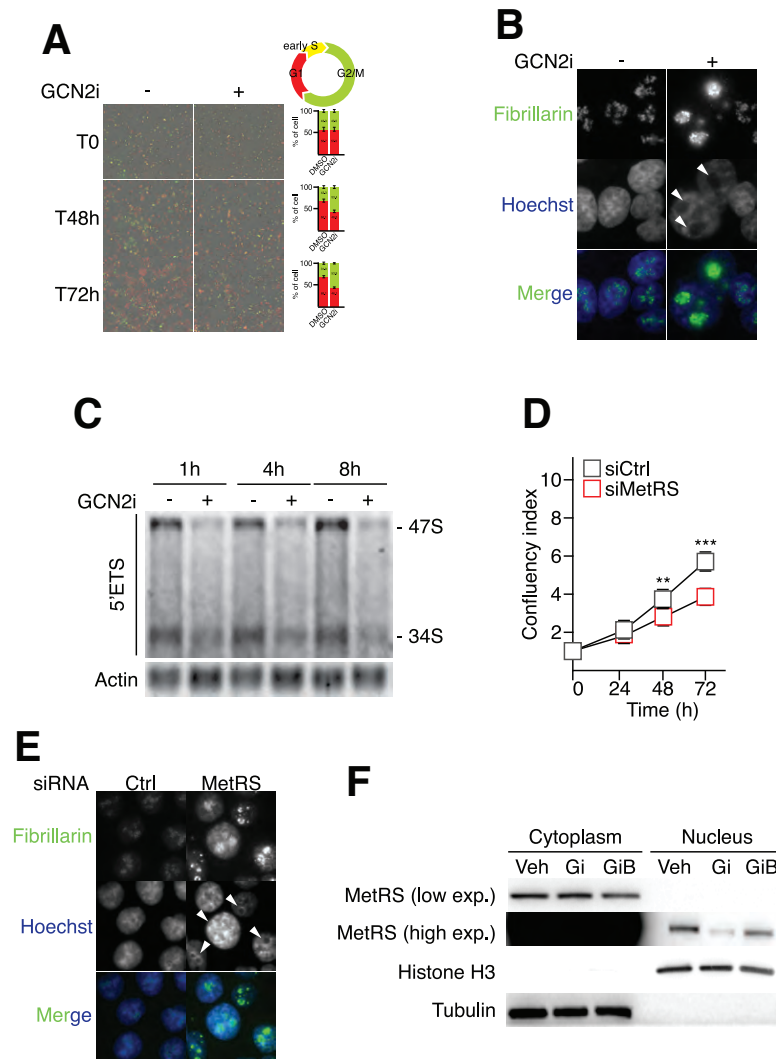


Fig. 6. GCN2 inhibition inhibits the MetRS translocation and RNA polymerase I activity.

- Time course analysis of cell cycle progression by monitoring HCT116 FUCCI cells upon DMSO or GCN2i. Data are expressed relative to the vehicle as mean +/- s.e.m of independent experiments (n = 3).
- Fibrillarin localization assessed by immunofluorescence in HCT116 cells treated with DMSO or GCN2i for 4 hours. Nuclei were stained by Hoechst solution.
- Time course analysis of cellular rRNAs by northern blotting following GCN2i treatment.
- Cell proliferation assessed by the confluency index of HCT116 cells treated or not with GCN2i for 72 h. Data are expressed as mean +/- s.e.m of independent experiments (n = 3). Unpaired two-tailed t-test with p-value (** p < 0.01, *** p < 0.001).
- Fibrillarin localization assessed by immunofluorescence in HCT116 cells, 48 hours after transfection with a siRNA control (Ctrl) or against MetRS. Nuclei were stained by Hoechst solution.
- Western blot analysis of MetRS amounts in the cytoplasmic or nuclear fractions upon 2 hours of GCN2i and GCNiB treatments. Histone H3 and tubulin are provided as loading controls for respectively nuclear and cytoplasmic samples.

Figure 7

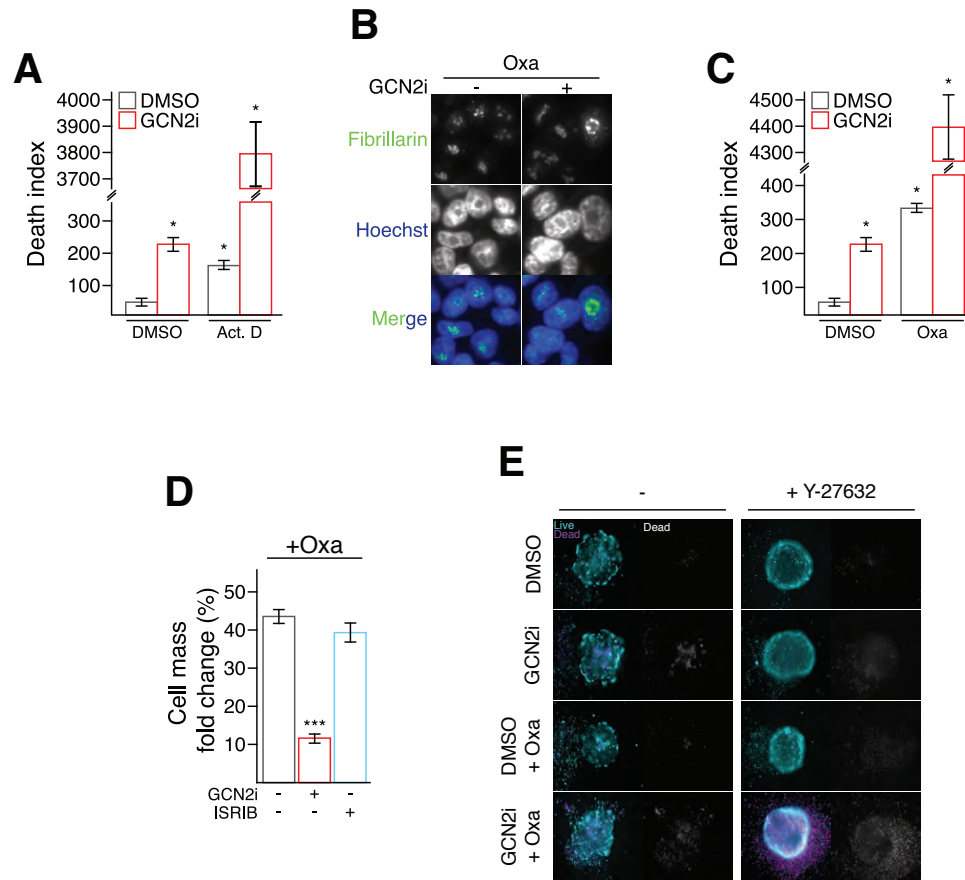


Fig. 7. GCN2 sensitizes COAD cancer cells to inhibitors of the RNA polymerase I activity.

- Cell death index of HCT116 treated or not with GCN2i combined to Actinomycin D (Act.D) or the vehicle (DMSO) for 48 h. Data are expressed relative to the vehicle as mean +/- s.e.m of independent experiments (n = 3). One-way ANOVA with Tukey's multiple comparisons test and p-value (* p < 0.05).
- Fibrillarin localization assessed by immunofluorescence in HCT116 cells treated with oxaliplatin (Oxa) in combination with DMSO or GCN2i for 4 hours. Nuclei were stained by Hoescht solution.
- Cell death index of HCT116 treated or not with GCN2i combined to Actinomycin D (Act.D) or the vehicle (DMSO) for 48 h. Data are expressed relative to the vehicle as mean +/- s.e.m of independent experiments (n = 3). One-way ANOVA with Tukey's multiple comparisons test and p-value (* p < 0.05).
- Cell mass measurement of HCT116 treated for 48 h with Oxa in combination with GCN2i or ISRIB. Data are expressed relative to the vehicle as mean +/- s.e.m of independent experiments (n ≥ 3). One-way ANOVA with Tukey's multiple comparisons test and p-value (***) p < 0.001).
- Live-and-dead assay in patient-derived colospheres, cultivated or not with ROCK inhibitor Y-27632, after 5 days of treatment with Oxa and/or GCN2i. To facilitate the observation of cell death induction, staining of non-viable cells is also represented in shades of grey.

Supplementary information for:

Targeting the cell and non-cell autonomous regulation of 47S synthesis by GCN2 in colon cancer.

Marie Piecyk¹, Mouna Triki¹, Pierre-Alexandre Laval¹, Cedric Duret¹, Joelle Favvre¹, Laura Cussonneau², Christelle Machon^{1,3}, Jérôme Guitton^{1,3}, Nicolas Rama¹, Benjamin Gibert¹, Gabriel Ichim¹, Frederic Catez¹, Fleur Bourdelais¹, Sebastien Durand¹, Jean-Jacques Diaz¹, Isabelle Coste¹, Toufic Renno¹, Serge N Manié¹, Nicolas Aznar¹, Stephane Ansieau¹, Carole Ferraro-Peyret^{1,4} and Cedric Chaveroux^{1*}

Affiliations:

¹ Centre de Recherche en Cancérologie de Lyon, INSERM U1052, CNRS 5286, Centre Léon Bérard, Université de Lyon, Université Claude Bernard Lyon 1, Lyon, France.

² Université Clermont Auvergne, INRAE, Unité de Nutrition Humaine, UMR1019, Clermont-Ferrand, France

³ Biochemistry and Pharmacology laboratory, Lyon Sud Hospital, University Hospital of Lyon, Pierre-Bénite, France.

⁴ Hospices Civils de Lyon, Plateforme AURAGEN, Lyon, France.

Corresponding author:

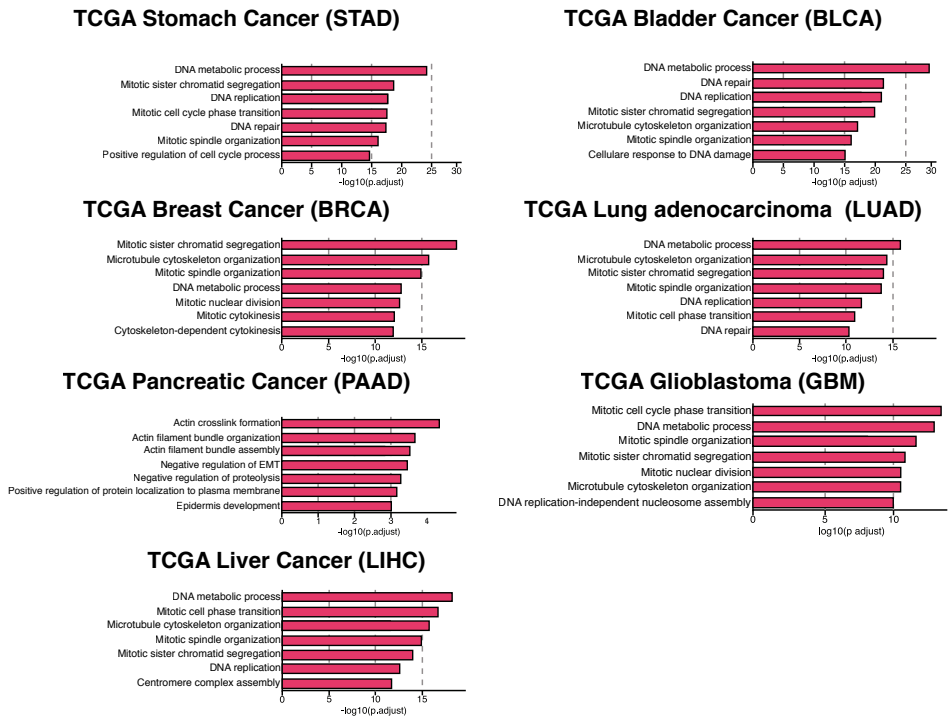
*To whom correspondence should be addressed.

Email: cedric.chaveroux@lyon.unicancer.fr. Address: Cancer Research Center of Lyon, Inserm UMR 1052 CNRS 5286, Cheney D, floor 6, Centre Léon Bérard, 28 rue Laënnec, 69008 LYON, France. Tel: +33 (0)4 69 16 66 22

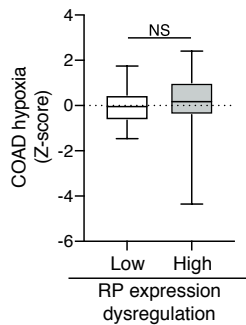
Supplementary information includes:

- Figure supplement S1-S8
- Supplementary tables 1-3
- Supplementary movie 1

A



B



C

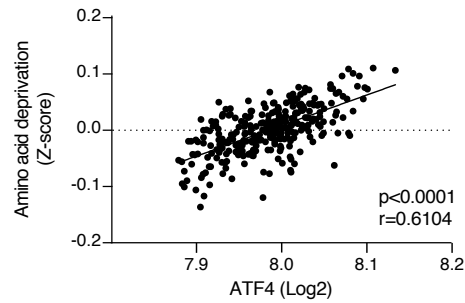


Figure supplement 1. Enrichment assessment of gene sets and signatures of interest in various types of cancers.

- Gene Ontology enrichment analysis on TCGA database of different cancers.
- Comparison of the COAD hypoxia gene signature in COAD cohorts with low and high levels of dysregulated riboproteins expression.
- Correlation between amino acid deprivation and ATF4 gene signatures.

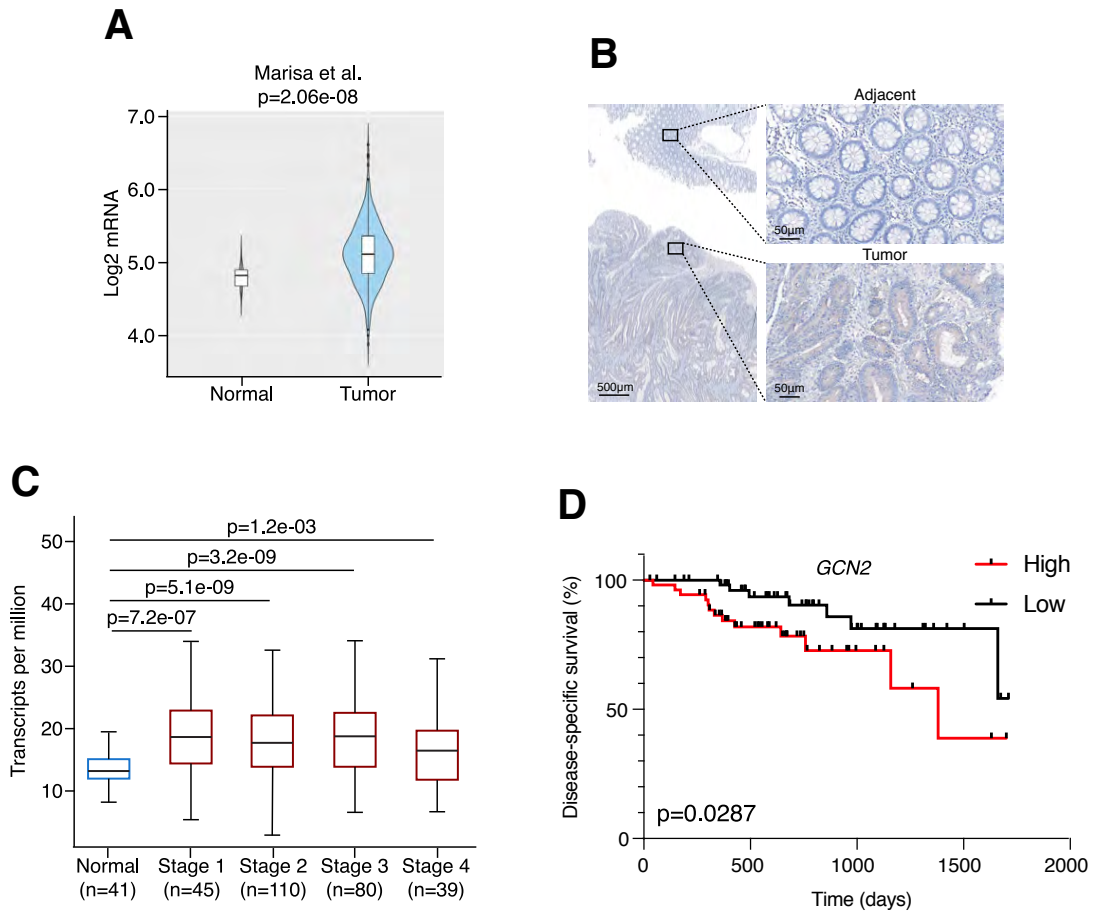
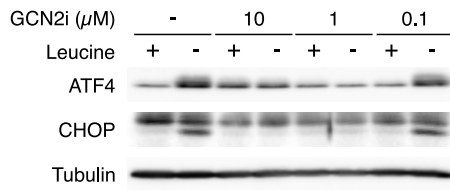
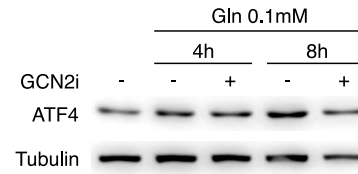
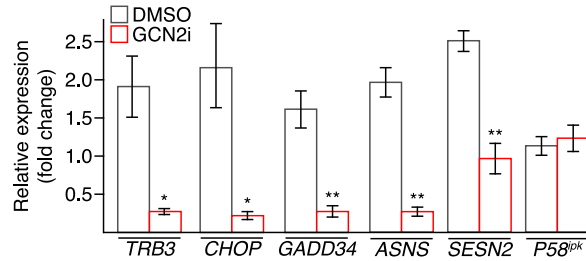


Figure supplement 2. GCN2 accumulation and prognostic value in human colon adenocarcinoma.

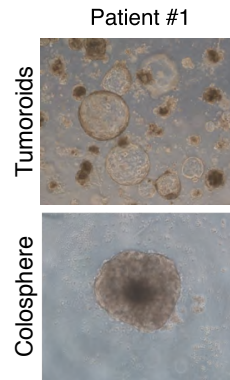
- A. GCN2 mRNA levels in normal tissue compared to tumoral tissue. (Marisa et al. cohort)
- B. Example of GCN2 amount accumulation in the tumor cells compared to the normal adjacent tissue.
- C. Analysis of GCN2 expression across normal tissue and the 4 stages of colon adenocarcinoma (TCGA database).
- D. Disease specific survival of COAD patients with high (red) or low (black) expression of GCN2 5 years after the diagnosis (TCGA data).

A**B****C****Figure supplement 3. Validation of the ISR impairment by the GCN2i.**

A. Western blot analysis of ISR markers induction (ATF4 and CHOP) after 8h of leucine starvation (0.45mM versus 0mM), a classical inducer of the GCN2 pathway, with or without GCN2i at the indicated concentrations. Tubulin served as a loading control.

B. Western blot analysis of ATF4 after 8h of glutamine deprivation (Gln 2mM versus 0.1mM) with or without GCN2i at the indicated time points. Tubulin served as a loading control.

C. RT-qPCR analysis of canonical ATF4 target genes (*TRB3*, *CHOP*, *GADD34*, *ASNS*, *SESN2*) upon low glutamine in combination with DMSO or GCN2i. *P58IPK* is given as a non-ATF4 target gene.

**Figure supplement 4. Illustration of patient-derived tumoroids grown in Matrigel® or as a colosphere in ultra-low attachment plate.**

Microscopy images of the morphology of patient's derived COAD cells grown as matrix-embedded cultures (tumoroids) or in ULA attachment plates (colospheres). Of note, primary cells grown as colosphere lead a visible compaction area.

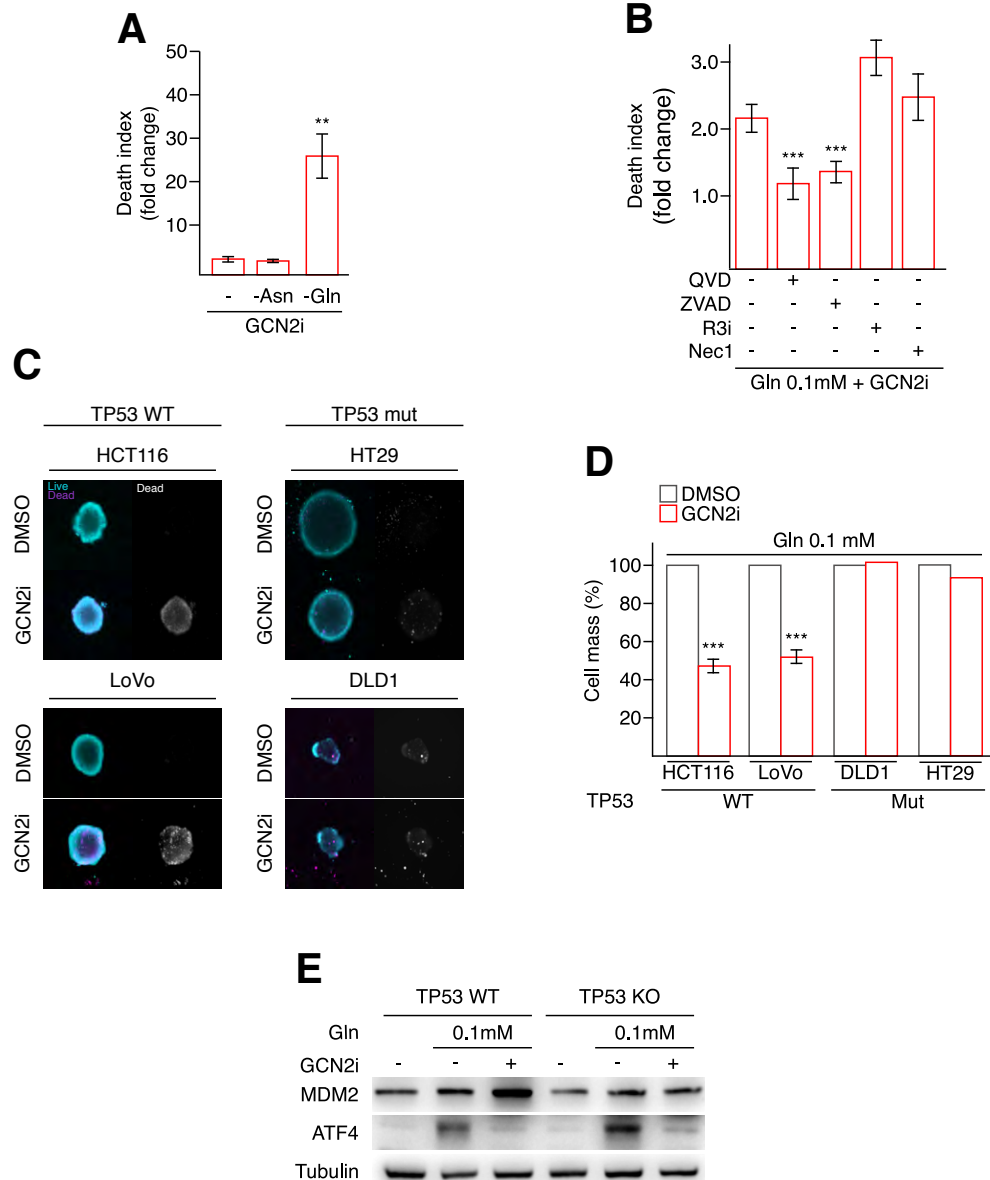


Figure supplement 5. Lack of GCN2 activity triggers a TP53-dependent cell death upon low glutamine.

A. HCT116 cell-death analysis following 4 days of GCN2i treatment in complete (-, 2mM Gln, 0.34mM Asn) or starved for glutamine (Gln, 0.1mM) or asparagine (Asn, 0.02mM) media.

B. Impact of inhibitors of necroptosis (Nec1, R3i) or apoptosis (z-VAD, QVD) on GCN2i-induced cell death following a 48h deprivation of glutamine (0.1 mM)

C. Live-and-dead assays in HCT116, LoVo, HT29 and DLD1 spheroids treated for 3 days with vehicle (DMSO) or GCN2i. Enlargement of the spheroids core is provided to visualize cell death.

D. Cell mass measurement of HCT116, LoVo, DLD-1 and HT-29 cells cultured in 2D conditions and treated with DMSO or GCN2i for 48 h. Media were refreshed daily (black rounded arrow).

E. Western blot analysis of ATF4 and MDM2 amounts after 8h of glutamine starvation with or without GCN2i, in HCT116 wild-type (WT) or knockout (KO) for TP53. Tubulin served as a loading control.

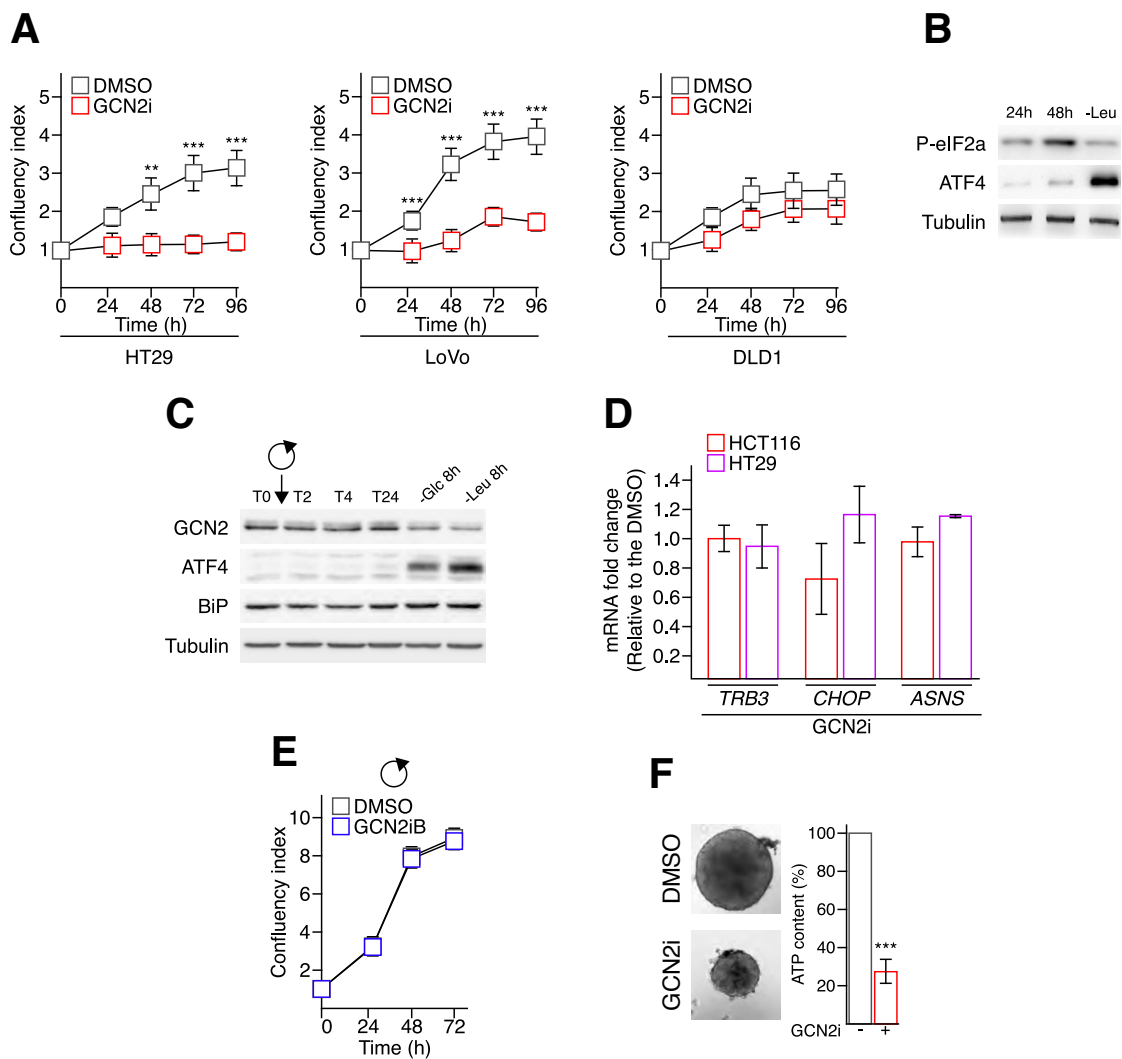


Figure supplement 6. Lack of GCN2 activity impairs cell proliferation and spheroid formation.

A. Cell proliferation assessed by the confluency index of HT29, LoVo and DLD1 cells treated or not with GCN2i for 96 hours.

B. Western blot analysis of P-eIF2a and ATF4 amounts after 24 and 48h of culture of HCT116 cells. HCT116 deprived for leucine (Leu) for 8h were used as positive control. Tubulin served as a loading control.

C. Time course analysis of GCN2, ATF4 and BiP amounts in HCT116 cells. HCT116 deprived for leucine (Leu) or glucose (Glc) for 8h were used as positive controls. Tubulin served as a loading control.

D. RT-qPCR analysis of ATF4 target genes (*TRB3*, *CHOP* and *ASNS*) in HCT116 cells grown in complete medium and treated with DMSO or GCN2i for 48h.

E. Cell proliferation measurement was assessed by the confluency index. HCT116 were treated or not with GCN2iB for 72 hours and media were refreshed every 24 hours.

F. Spheroid formation assays of HT29 treated with DMSO or GCN2i. ATP content was measured after 7 days of treatment. Treatment was initiated concomitantly to plating.

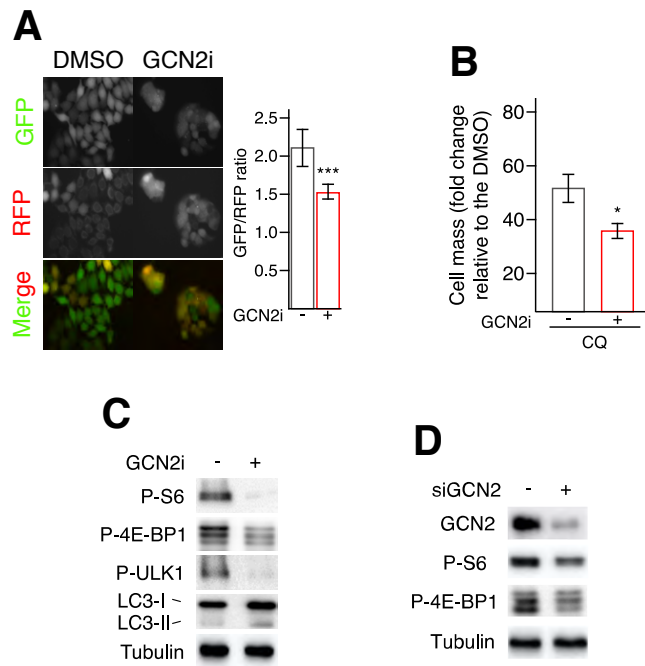


Figure supplement 7. Lack of GCN2 activity induces an autophagic flux and mTORC1 inhibition in HT29 cells grown in nutrient-rich conditions.

A. Autophagic flux analysis using HT29 cells stably expressing the GFP-LC3-RFP-LC3ΔG construct and treated with GCN2i for 48 h. Cleavage of GFP-LC3 by autophagy released the RFP-LC3 as an internal control, thus reduction of the GFP/RFP ratio illustrates induction of the autophagic flux.

B. Cell mass was measured in GCN2i-treated HT29 cells after 48 h in combination with chloroquine. Data are expressed relative to the vehicle.

C. Western blot analysis of mTORC1 and autophagy markers (P-S6, P-4E-BP1, P-ULK1, LC3-I/II) following GCN2i treatment for 24h. Tubulin served as a loading control.

D. Western blot analysis of mTORC1 markers (P-S6, P-4E-BP1) following GCN2 silencing for 96h. Tubulin served as a loading control.

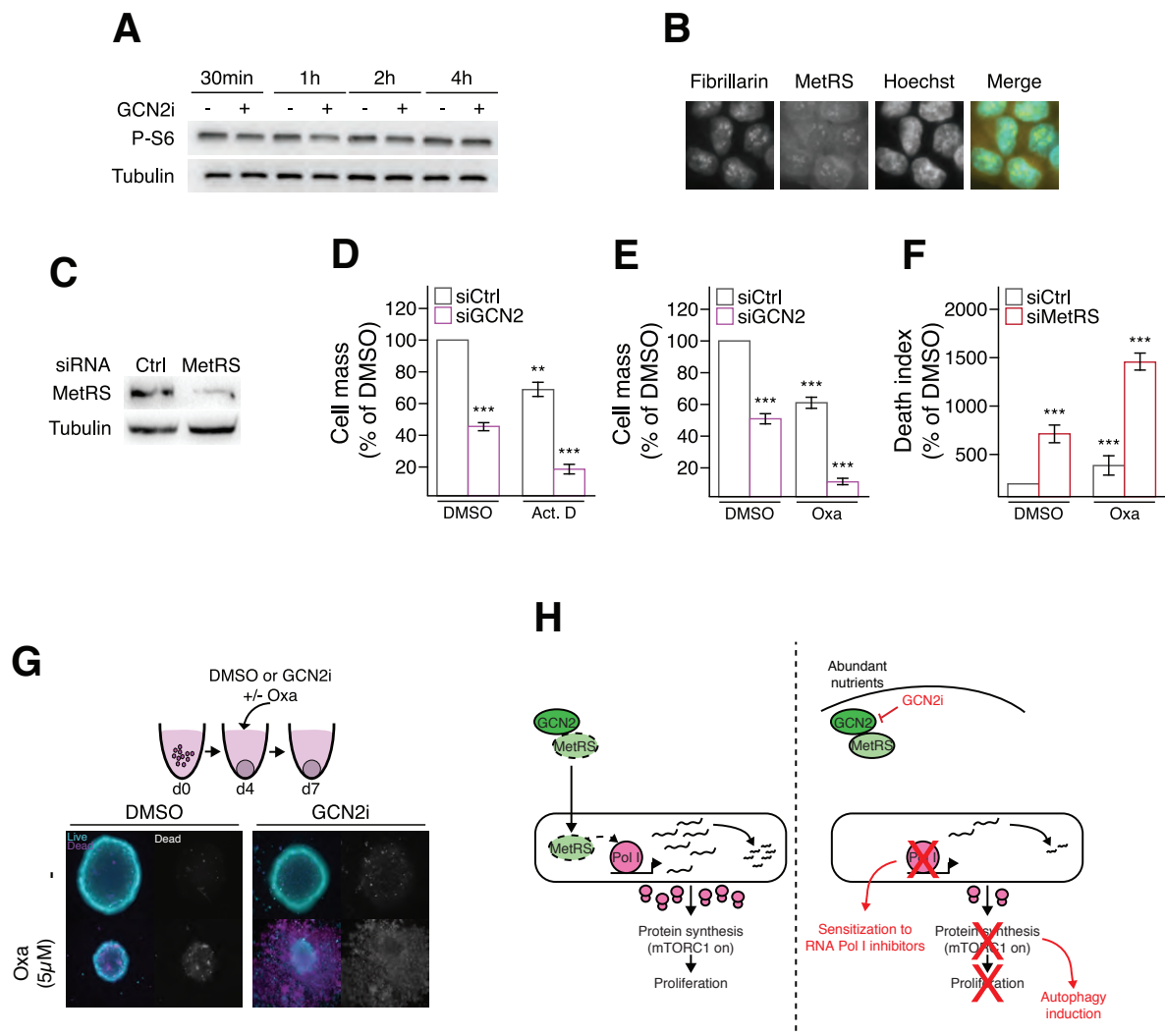


Figure supplement 8. Lack of GCN2 activity sensitizes COAD cells to oxaliplatin.

- A. Western blot analysis of P-S6 in HCT116 cells treated with or without GCN2i at the indicated time points.
- B. Immunocytofluorescence in HCT116 against fibrillarin and methionyl-tRNA synthetase (MetRS) associated to Hoechst coloration.
- C. Western blot analysis of MetRS amount in HCT116 cells transfected for 72h with a siRNA control (Ctrl) or against MetRS.
- D. Cell mass measurement of HCT116 silenced or not for GCN2 and treated for 48 h with actinomycin D (Act. D).
- E. Cell mass measurement of HCT116 silenced or not for GCN2 and treated for 48 h with oxaliplatin (Oxa).
- F. Cell death measurement of HCT116 silenced or not for MetRS and treated for 48 h with oxaliplatin (Oxa).
- G. Live-and-dead assays in HCT116 spheroids after 5 days of treatment with oxaliplatin (Oxa) and/or GCN2i. To facilitate the observation of cell death induction, staining of non-viable cells is also represented in shades of gray.
- H. Schematic model illustrating the role of GCN2 in the control of 47S synthesis in proliferative cells.

COAD ribosome dysfunction	Amino acid deprivation	COAD Hypoxia	ATF4
<i>Negatively-regulated genes</i> RPL34 RPL9 RPL21 RPS25 RPL3 RPL11 RPL26 RPL3L RPS4Y2 RPL15 RPL22 RPS4Y1 RPL10L RPS27L RPL36AL FAU RPS29 RPS26 RPL15 RPS12 RPL10A RPS27A RPS27 RPS13 RPS23 RPS3A RPL17 RPL39L	ASNS ASS1 ATF3 ATF5 CARS1 CBS CCNG2 CDKN1A CEBPB CHAC1 CLEC7A CTH CXCL8 DDIT3 DDIT4 FYN GADD45A MARS PPP1R15A PSAT1 RETN SARS SESN2 SLC38A2 SLC7A11 STC2 TRIB3 VEGFA WARS	BCCIP BNIP3L GADD45B INSIG2 MPHOSPH6 TP53	DDIT4 NARS1 PSAT1 SREBF1 IARS1 IARS2 MTHFD2 EIF2AK4 ATF3 GFPT1 WARS WARS2 NFE2L2 YARS YARS2
<i>Positively-regulated genes</i> RPL36A RPS2 RPL22L1 RPL8 RPL28 RPLP0 RPS19			

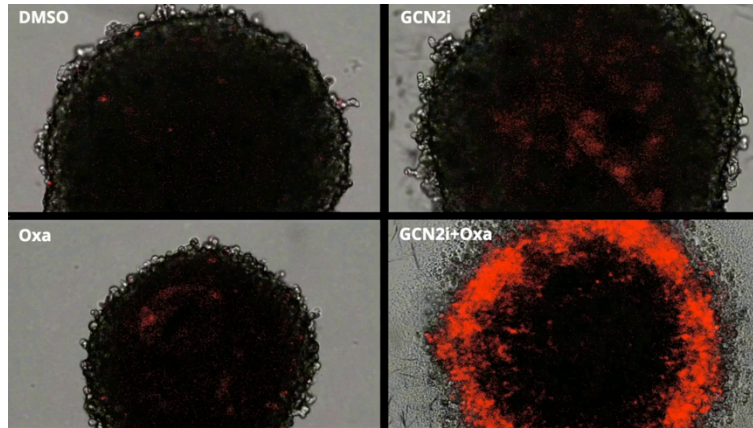
Supplementary table 1. List of gene signatures used in the present study.

<i>ALDH1A3</i>	Fw: CTGCTACAACGCCCTCTATGCA Rev: GTCGCCAAGTTTGATGGTGACAG
<i>c-MYC</i>	Fw: CCTGGTGCTCCATGAGGAGAC Rev: CAGACTCTGACCTTTTGCCAGG
<i>TRB3</i>	Fw: TGGTACCCAGCTCCTCTACG Rev: GACAAAGCGACACAGCTTGA
<i>ASNS</i>	Fw: CTGTGAAGAACAACCTCAGGATC Rev: AACAGAGTGGCAGCAACCAAGC
<i>P58IPK</i>	Fw: GCTGAATGTGGAGTAAATGCAG Rev: GTGCAGCTTTTGATTTGCC
<i>SESN2</i>	Fw: AGATGGAGAGCCGCTTTGAGCT Rev: CCGATGAAGTCCTCATATCCG
<i>CHOP</i>	Fw: GGTATGAGGACCTGCAAGAGGT Rev: CTTGTGACCTCTGCTGGTTCTG
<i>GADD34</i>	Fw: CTGTGATCGCTTCTGGCA Rev: GGAAGAAAGGGTGGGCATC
<i>47S</i>	Fw: GTGCGTGTCAGGCGTTC Rev: GGGAGAGGAGCAGACGAG
<i>RPS11</i>	Fw: TGACCTTGATTTATTTGCATACC Rev: CGAGCAAGACGTTTCAGTCCT

Supplementary table 2. List of human primers used for RT-qPCR experiments.

<i>Actin</i>	CGGTAGGACGCAGACCTGGACCGACCGGCCCTGG
<i>5'ETS</i>	CGACTGTGCGACAGGAGACCGCTGGACAGCAGCCTCTCCAACCCGGAGGC
<i>ITS2</i>	ACGCGCCGACCCCAAGGGAGCGTC

Supplementary table 3. List of human probes used for Northern blotting.



Supplemental movie 1. Live-imaging of cell death caused by the GCN2 inhibitor in combination with oxaliplatin. Cell death visualization by incorporation of propidium iodide in HCT116 spheroids treated with the vehicle (DMSO) or GCN2 inhibitor (GCN2i) in combination or not with oxaliplatin (time course of treatments: 120 hours).

Materials and methods

Cell culture

The following cell lines were obtained from ATCC: HCT116, HT29, DLD1 and LoVo. HCT116 TP53 WT and HCT116 TP53 KO were generated previously by Dr B. Vogelstein, Ludwig Center at Johns Hopkins, Baltimore (Bunz *et al*, 1998) and were kindly provided by Drs P. Mehlen and A. Paradisi at CRCL, Lyon. HCT116 FUCCI were obtained by transducing HCT116 with the Cdt1-mKO and Geminin-mAG constructs and FACS cell sorting. All cell lines were routinely cultured in McCoy medium (ref 16600082, GIBCO, Thermo Fisher Scientific, Whaltam, Massachussets, USA), except DLD1 cultured in RPMI medium (ref 21875034, GIBCO, Thermo Fisher Scientific, Whaltam, Massachussets, USA). Cell lines were tested for absence of mycoplasma after amplification. All media were supplemented with 10% fetal bovine serum (FBS) and 1% v/v penicillin/streptomycin (ref 15140122, GIBCO, Thermo Fisher Scientific, Whaltam, Massachussets, USA). Cells were maintained at 37°C in a 5% CO₂ incubator. For 2D experiments, treatment was initiated the day after plating with daily refreshment when indicated by a circular arrow. Glasstic slides (ref 87144, Kova International, Garden Grove, California, USA) were used for cell counting.

For patient-derived tissue culture, after tumor dissociation using a mix of DNase and collagenase, individualized tumor cells were embedded in Matrigel matrix (ref 354234, Corning, New York, USA) and cultivated as tumoroids using the Stemness system device and IntestiCult Organoid Growth Medium (ref 06010, Stemcell, Saint Égrève, France). The collection and use of all patient tissue specimens was carried out according to French laws and regulations in the frame of the ColonIM protocol (NCT03841799).

Nutritional manipulation and reagents

Leucine starvation experiments were performed using a DMEM medium devoid of leucine, lysine and arginine (ref 88425, GIBCO, Thermo Fisher Scientific, Whaltam, Massachussets, USA), in which lysine (final concentration 0.8 mM) (ref L8662, Sigma Aldrich, Saint Louis, Missouri, USA), arginine (final concentration 0.4 mM) (ref A6969, Sigma Aldrich, Saint Louis, Missouri, USA), non-essential amino acids (ref 11140050, GIBCO, Thermo Fisher Scientific, Whaltam, Massachussets, USA), 1% penicillin/streptomycin (ref 15140122, GIBCO, Thermo Fisher Scientific, Whaltam, Massachussets, USA) and 10% dialyzed serum were subsequently added. The control medium for

these experiments was supplemented with leucine (final concentration 0.45 mM) (ref L8912, Sigma Aldrich, Saint Louis, Missouri, USA)

To perform experiments in condition of low asparagine or low glutamine medium, we used Dulbecco's Modified Eagle Medium devoid of glucose and sodium pyruvate (ref A1443001, GIBCO, Thermo Fisher Scientific, Waltham, Massachusetts, USA), supplemented with 1% penicillin/streptomycin (ref 15140122, GIBCO, Thermo Fisher Scientific, Waltham, Massachusetts, USA), 1% sodium pyruvate (ref 11360070, GIBCO, Thermo Fisher Scientific, Waltham, Massachusetts, USA), and 10% dialyzed FBS. The concentrations mentioned in Tajan *et al.* (Tajan *et al.*, 2018) were used to supplement control medium with glucose (final concentration 16 mM) (ref A2494001, GIBCO, Thermo Fisher Scientific, Waltham, Massachusetts, USA) and the subsequent amino acids purchased as powders from Sigma Aldrich (Saint Louis, Missouri, USA) : L-proline (0.15 mM, ref P5607), L-alanine (0.15 mM, ref 05129), L-aspartic acid (0.15 mM, ref A8949), L-glutamic acid (0.03 mM, ref W328502), L-asparagine (0.34 mM, ref A4159) and L-glutamine (2 mM, ref G3126). For nutrient scarce medium, L-asparagine and L-glutamine were added respectively at the concentrations of 0.02 mM and 0.1 mM based on the work of Pan *et al.* (Pan *et al.*, 2016).

GCN2 inhibitor (GCN2i) used this study was previously described as TAP20 in (Dorsch *et al.*, 2014; Bröer *et al.*, 2019) and generously provided by Merck KGaA. The compound was resuspended in DMSO and, if not mentioned otherwise, used at a final concentration of 5 μ M. The GCN2iB was purchased from MedChemExpress (Monmouth Junction, NJ) and also used at final concentration of 5 μ M. Oxaliplatin was provided by the Centre Léon Bérard pharmacy, diluted in H₂O and used at a final concentration of 5 μ M. ISRIB (ref SML0843, Sigma Aldrich, Saint Louis, Missouri, USA) dissolved in DMSO was used at a final concentration of 200 nM. Chloroquine (ref C6628, Sigma Aldrich, Saint Louis, Missouri, USA) was prepared in PBS pH5 and used at a final concentration of 20 μ M. Rapamycin (ref T1537, Euromedex, Souffelweyersheim, France) dissolved in DMSO was used at a final concentration of 10 nM. Actinomycin D (ref A1410, Sigma Aldrich, Saint Louis, Missouri, USA) was diluted in DMSO and treatments were performed at a final concentration of 1 nM.

Regarding RNA interference experiments, HCT116 cells were seeded onto 6-well plates (2.5 \times 10⁵ cells per well) and concomitantly transfected with non-targeting siRNA (sc-37007) or human GCN2 siRNA (sc-45644) or human ATF4 siRNA (sc-35112) or human MetRS siRNA (sc-75775) (Santa Cruz Biotechnology, Dallas, Texas, USA). All siRNA transfections were performed using 50 nM siRNA and

HiPerFect reagent (ref 301704, Qiagen, Hilden, Germany), according to the manufacturer's traditional transfection protocol. Day after transfection, media were changed and treatments were performed 48 h later.

Cell cycle progression, Proliferation and Cytotoxicity assay in two-dimensional models

For cell cycle progression, HCT116 FUCCI cells were plated onto 6-well plate (2.50×10^5 cells per well). The green and red fluorescence of the FUCCI reporter, indicative of the cell cycle phase, was monitored and quantified over time using the Cellcyte X system (Cytex, Freiburg im Breisgau, Germany). Then, the percentages of green and red fluorescence were estimated in each studied condition to respectively evaluate the proportion of cells in G1 or G2/M phases of the cell cycle.

For proliferation and cell death assessment in 2D culture, colon cancer cells (1×10^5 cells/well) were seeded onto a 24-well plate and subjected 24h later to the indicated treatment. Propidium iodide was added in the media at 2.5 $\mu\text{g}/\text{mL}$ final for apoptosis assay. Inhibitors of apoptosis Q-VD-OPh (QVD 20 μM , ref 1170-3) and Z-VAD-FMK (ZVAD, 20 μM , ref A12373-5), and inhibitors of necroptosis necrostatin-1 (Nec1, 10 μM , ref A4213) and RIPK3 inhibitor (R3i, 5 μM , ref 2673-5) were all purchased from Clinisciences (Nanterre, France). Then, cell confluency and cell death were monitored over the indicated period of time with data collection every hour using the Cellcyte X system (Cytex, Freiburg im Breisgau, Germany). Death index was calculated using the formula "(PI Foci Number/Confluency) $\times 100$ ".

Cell mass was assessed by using the sulforhodamine B (SRB) assay. Cells were seeded onto 6-well plates (2.50×10^5 cells per well) and treated the day after plating for 24 to 96 h at 37°C, 5% CO₂ depending on the experiment. After removing the medium, wells were washed with PBS. Then, 1 mL of 10% trichloroacetic acid was added and after 1 h of incubation at 4°C, the plates were flicked and washed three times with tap water before being dried at room temperature for 1 h. The wells were then stained with 1.5 mL of SRB solution 0.057% in 1% acetic acid (ref 341738, Sigma Aldrich, Saint Louis, Missouri, USA) for 30 min at room temperature under gentle agitation. Plates were flicked and washed three times with 1% acetic acid and dried at 37°C for 1 h. Finally, 1.5 mL of 10 mM Tris base was added and shaken vigorously for 15 min. The absorbance was measured using Tecan Infinite M200 Pro (Tecan, Männedorf, Switzerland) at a wavelength of 510 nm.

Autophagic flux monitoring

To monitor autophagic flux, 293GP cells were transfected with a pMRX-IP-GFP-LC3-RFP-LC3ΔG construct described in Kaizuka et al (Kaizuka *et al*, 2016). Then, viral supernatant was collected to infect HCT116 and HT29 cells and generate stable cell lines carrying pMRX-IP-GFP-LC3-RFP-LC3ΔG plasmid, subsequently renamed HCT116 pLC3 and HT29 pLC3. Cells were then grown on glass coverslips with DMSO or GCN2i for 48h. After that, cells were fixed in 4% of paraformaldehyde in phosphate-buffered saline (PBS). Coverslips were mounted on microscope slides using the Fluoromount G mounting medium (ref 17984-25, EMS Diasum, Hatfield, Pennsylvania, USA). Nikon ECLIPSE NI-E microscope with a 100X immersion objective (Nikon, Tokyo, Japon) was used to acquire images. Final images were analyzed and cropped with the Fiji/ImageJ software (National Institutes of Health, Bethesda, Maryland, USA).

Spheroid and tumoroid assays

For spheroid formation assays, drops of 10μL containing 3 x 10³ cells were deposited on the lid of plastic dishes. The lid was inverted and placed over the dish containing 5mL of sterile PBS in the bottom. Treatment with GCN2i is concomitant to plating. Hanging drops were then maintained at 37°C in a 5% CO₂ incubator for 7 days.

For Live-and-Dead cell assays, 3 x 10³ cells from patient primary cells or indicated cell lines were plated per well in 96-wells ultra-low attachment plates (ref 650970, Greiner Bio-One, Les Ulis) 3 days before treatment. After 72 hours of treatment, viable and dead cells were stained using the Live/Dead cell imaging kit provided by Thermo Fisher (ref R37601, Thermo Fisher Scientific, Waltham, Massachusetts, USA) according to manufacturer's instructions. Fluorescence microscope was used to capture fluorescence signaling and then, pictures were colored and cropped with the Fiji/ImageJ software (National Institutes of Health, Bethesda, Maryland, USA).

Amino acid profiling

Before analysis, a mix of 24 internal standards was added to cell extracts. After homogenization and centrifugation, the supernatant was evaporated under nitrogen and the dry residue was resuspended in 200 μL mobile phase. Separation was performed by liquid chromatography on a Ultimate 3000 system (ThermoFisher Scientific™, Bremen, Germany), using a Synergi HydroRP column (250 x 2; 4 μm,

Phenomenex) and 0.1 % of formic acid in water and methanol as mobile phases. The detection was performed with a Q-Exactive Plus Orbitrap mass spectrometer (ThermoFisher Scientific™, Bremen, Germany) equipped with a heated electrospray ionization source which operated in positive and negative modes. Retention time, exact mass and isotopic pattern of the molecular ion, exact mass of the fragments and comparison of the fragmentation spectrum with a homemade database were used for identification of metabolites. The ratio (peak area of metabolites / peak area of internal standard) was used for quantification.

RNA extraction and RT-qPCR

Total cellular RNA was extracted after the indicated period of treatment using TRIzol Reagent (ref 15596026, Invitrogen, Carlsbad, California, USA) according to the manufacturer's protocol. For cDNA synthesis, 0.5 µg of RNA were reverse transcribed using Superscript II reverse transcriptase (ref 18064014, Invitrogen, Carlsbad, California, USA) with random primers (S0142, Thermo Fisher Scientific, Waltham, Massachusetts, USA), according to the manufacturer's instructions. cDNA was then amplified by qPCR using specific primers listed in supplementary Table 1 and the SYBR Green Master Mix (ref 1725274, Bio-Rad, Hercules, California, USA). qPCR was performed using the CFX connect real-time PCR system (Bio-Rad, Hercules, California, USA). Relative quantification was assessed using a standard curve-based method. Expression of target genes was normalized against RPS11 mRNA levels used as an internal control. qPCR experiments were repeated at least three times in duplicate.

Western blot analysis and SUNSET assays

To perform Western blot analysis, cells were seeded onto 100mm-diameter plates (1.50×10^6 cells per plate) and treated for the incubation period of corresponding figures. Whole cell extracts were prepared from cultured cells lysed at 4°C in RIPA protein buffer containing protease and phosphatase inhibitors (ref 11697498001, Roche, Bâle, Switzerland), and obtained by centrifugation at $13,000 \times g$ for 20 min at 4°C. Subcellular fractionation was performed as follows: cells were scratched on ice and collected in cold PBS before centrifugation at $3,000 \times g$ for 5 min at 4°C. The pellet was resuspended and lysed on ice in a hypotonic buffer (10 mM Hepes pH 7.5, 10 mM KCl, 0.1 mM EDTA, 1 mM DTT, 0.5% NP-40 and protease/phosphatases inhibitors) for 15 min. Centrifugation was performed at $12,000$

x g for 5 min at 4°C and the supernatant containing the cytoplasmic fraction was collected and an equal volume of Laemmli protein buffer 2X containing protease and phosphatase inhibitors was added. The pellet, representing the nuclear fraction, was dissolved in the hypotonic buffer and centrifuged again at 12,000 x g for 5 min at 4°C. The supernatant was removed and the pellet containing the nuclear fraction was resuspended in Laemmli protein buffer 1X supplemented with protease and phosphatase inhibitors. The nuclear fraction was obtained by centrifugation at 1500 x g for 30 minutes at 4°C. Tubulin and Histone H3 were used as loading control for purity of cytoplasmic and nuclear fractions, respectively.

Protein concentrations of the cellular extracts were determined using the DC Protein Assay (ref 5000112, Bio-Rad, Hercules, California, USA). Equal amounts of proteins (20 µg) were separated by SDS-PAGE and then transferred onto nitrocellulose membranes (ref 1704271, Bio-Rad, Hercules, California, USA). Membranes were incubated in blocking buffer, 5% milk or Bovine Serum Albumin (BSA) in Tris-Buffered Saline/Tween 20 (TBST), for 1 h at room temperature, then incubated overnight at 4°C with the appropriate primary antibodies diluted in TBST containing 5% milk or BSA. Membranes were washed three times with TBST, incubated for 1 h at room temperature with the appropriate secondary antibodies, diluted in TBST containing 5% milk, and again washed three times with TBST. Detection by enhanced chemiluminescence was performed using the Immobilon Forte HRP Western substrate (ref WBLUF0500, Merck Millipore, Darmstadt, Germany) or SuperSignal West Femto Maximum Sensitivity Substrate (ref 34096, Thermo Scientific, Thermo Fisher Scientific, Waltham, Massachusetts, USA). Tubulin was used as a loading control. The primary antibodies used were purchased either from Santa Cruz Biotechnology (Dallas, Texas, USA): TP53 (sc-47698) and CHOP (sc-7351); from Cell Signaling Technology (Danvers, Massachusetts, USA): Tubulin (2146), Histone H3 (4499), BiP (3177), P-eIF2a (3398), ATF4 (11815), LC3 (2775), P62 (5114), P-S6 (4858), P-4EBP1 (2855), P-Ulk1 (14202) and GCN2 (3302); from Merck Millipore (Darmstadt, Germany): Puromycin clone 12D10 (MABE343); from ABclonal Technology (Woburn, Massachusetts, USA): MetRS (A9938); or from Calbiochem (San Diego, California, USA): MDM2 clone 4B2C1.11 (OP145). The HRP-conjugated secondary antibodies (anti-rabbit and anti-mouse antibodies, respectively ref 7074 and 7076) were supplied by Cell Signaling Technologies (Danvers, Massachusetts, USA).

Rates of nascent protein synthesis were evaluated using the surface sensing of translation (SUnSET) method as previously described by Schmidt et al. (*Schmidt et al, 2009*). Cells were seeded onto 6-well plates (2.50×10^5 cells per well) and treated the day after plating with GCN2i for 48 h at

37°C, 5% CO₂. 15 min before being harvested and processed to prepare whole cell extracts in RIPA buffer, cells were incubated with 5 µg/mL of puromycin (ref P9620, Sigma Aldrich, Saint Louis, Missouri, USA) directly added into the medium. The amount of puromycin incorporated into nascent peptides was then evaluated by Western blot analysis on 20 µg of proteins using anti-puromycin antibody (ref MABE343) purchased from Merck Millipore (Darmstadt, Germany).

Immunohistochemistry and immunofluorescence staining

HCT116 cells were plated (3 x 10³ cells/well) and grown for 3 days in 96-wells ultra-low attachment plates (ref 650970, Greiner Bio-One, Les Ulis) before treatments. 72h after being treated, samples were formalin-fixed, embedded in paraffin and stained with antibodies purchased at Cell Signaling Technology (Danvers, Massachusetts, USA): cleaved caspase 3 (9664), cleaved PARP (5625), P-S6 (4858). Immunohistological analyses were performed at the Plateforme Anatomopathologie Recherche of the Centre de recherche en cancérologie de Lyon (CRCL).

Colon Disease spectrum tissue microarray (TMA) was obtained from US Biomax (ref BC5002b, Derwood, Maryland, USA) as fresh-cut slides. The tissue microarray containing Colon Malignant and Normal Adjacent Tissue cores was stained against GCN2 (Cell Signaling Technology, 3302) by immunohistochemistry. The analysis of the IHC-stained TMA slide was performed using QuPath0.3.2 software (Bankhead *et al*, 2017). Slides were scanned and imported into the program. Positive cells detection was performed following QuPath established method and then, rigorous quality control (QC) steps were taken to remove necrosis or keratin and tissue folds. IHC staining was scored for each TMA core using the built-in scoring tool. This analysis was double-checked by an anatomopathologist.

For immunofluorescence assays, cells were grown on glass coverslips, fixed in 4% of paraformaldehyde in phosphate-buffered saline (PBS) before permeabilization with 0.5% Triton X-100 in PBS. Fibrillarin were detected using the anti-FBL mouse polyclonal antibody (ref ab4566, Abcam, Cambridge, England) diluted at 1:500. Secondary Antibody Alexa Fluor 488 Goat anti-mouse IgG (ref A-11029, Life Technologies, Carlsbad, California, USA) was used at 1:800. Nucleus were stained for 5 min with Hoechst n°33342 (ref H3570, Invitrogen, Carlsbad, California, USA) at 1:2000. Coverslips were mounted using the Fluoromount G mounting medium (ref 17984-25, EMS Diasum, Hatfield, Pennsylvania, USA). Nikon ECLIPSE NI-E microscope with a 100X immersion objective (Nikon, Tokyo,

Japon) was used to acquire images. Final images were analyzed and cropped with the Fiji/ImageJ software (National Institutes of Health, Bethesda, Maryland, USA).

Northern blot analyses

For rRNA transcription/processing analysis, HCT116 cells were cultivated with treatments as previously described for the indicated period. Then, total RNA was extracted with TRIzol according to manufacturer's instruction as described before. Purified RNAs were resuspended in water and quantified by spectrophotometry. Briefly, 10 or 5 µg of total RNA was denatured in formamide loading buffer and electrophoresed in denaturing agarose gel. Then, separated RNAs were transferred and crosslinked on a nylon zeta-probe membrane before hybridization with 5'ETS probes coupled with infrared-emitting fluorophores (sequences provided in supplementary table 3). Blots were acquired using Chemidoc MP Imaging System and analyzed with ImageLab software.

RNA sequencing

For RNA sequencing, HCT116 cells were transfected with a control siRNA or human GCN2 siRNA as previously described. RNA was extracted 48h later using NucleoSpin RNA kit (ref 740955, Macherey-Nagel, Düren, Germany).

Library preparation and RNA sequencing were performed at the ProfileXpert platform (UCBL, Lyon). Quality of samples was checked by Bioanalyzer 2100 (Agilent technologies, Santa Clara, California, USA) and RNA was quantified by Quantifluor RNA kit (Promega, Madison, Wisconsin, USA). First, mRNA was enriched from 1 µg of total RNA, then library preparation was realized with the NextFlex Rapid Directional mRNA-Seq kit (Bio-Scientific, Perkin-Elmer, Waltham, Massachusetts, USA). Quality of libraries were checked by Fragment Analyzer (Agilent technologies, Santa Clara, California, USA) and quantified by qPCR. Samples were put on Flow Cell High Output. Amplification and sequencing were performed with Illumina NextSeq500: run Single Read 76 bp was performed. After demultiplexing of the data with Bcl2fastq v2.17.1.14, trimming was performed using cutadapt v1.9.1 software. Then the reads were mapped using Tophat2 v2.1.1 software with default parameters on the human genome GRCh38. The Fragments Per Kilobases of exon per Million mapped reads (FPKM) values were then computed for each gene using Cufflinks v2.1.1 software. Genes with a FPKM inferior to 0.01 were substituted by 0.01. Differential expression was estimated with a t-test with unequal

variance and p-value were corrected by Benjamini and Hochberg using the False Discovery Rate (FDR) controlling procedure. Genes were considered as differentially expressed if the absolute value was greater than or equal to 1.5 and p-value was less than 0.05. For each comparison, transcript was considered if the coverage was greater than or equal to 1 for all samples of at least one group. VolcanoR was used to perform the enrichment analysis (Naumov *et al*, 2017).

Patients' survival and expression data analyses.

Disease-specific survival were determined by using the Long-term Outcome and Gene Expression Profiling Database of pan-cancers (<http://bioinfo.henu.edu.cn/DatabaseList.jsp>) and the TCGA COAD cohort. GCN2 expression and respective statistical analyses were performed by using: the Cancertool interface (Cortazar *et al*, 2018) for Marisa *et al*. data (Marisa *et al*, 2013), UALCAN (Chandrashekar *et al*, 2017) for analyzing expression of GCN2 in COAD according to the stage of the disease (TCGA data), Colonomics (<https://www.colonomics.org/expression-browser>) for the paired samples comparison. USCS Xena Browser (Goldman *et al*, 2020) was used to perform Gene Ontology enrichment analysis on the TCGA database, comparison of genes expression and correlation between genes signatures. Enrichment of gene ontology analyses were performed by using the application Enrichr (Kuleshov *et al*, 2016).

Statistics

All of the statistical analyses were performed using GraphPad Prism version 6.0 (GraphPad Software, San Diego, CA, USA) by using unpaired t-test or one-way ANOVA. Survival analysis was performed by Kaplan–Meier and Log-rank test. p-values less than 0.05 were considered statistically significant.

Acknowledgements

We thank Drs. L. Le Cam and P. Fafournoux for their insightful comments sharing material and manuscript improvement, B. Manship for English editing, Y. Chaix for funding management. The authors are grateful to the members of the Anatomopathologie Recherche Lyon-Est, Imagerie Cellulaire, ProfileXpert and AniPath facilities for their collaborative work. This work was supported by the Cancéropôle CLARA (CVPPRCAN000174, CVPPRCAB000180 and CV-2021-039), Region Auvergne

Rhone-Alpes (19-010898-01), Projets Fondation and Aide doctorale (R16173CC, ARCMD-Doc22021020003295) from ARC, Ligue Nationale contre le Cancer (R17167CC, R19007CC), Institut Convergence François Rabelais (17IA66ANR-PLASCAN-MEHLEN), the Marie Sklodowska-Curie fellowship (n_839398), CNRS Prematuration (NA-7-07-20), and the IPR (Innovation Pharmaceutique et Recherche) program.

Competing interest statement: C.C. received financial supports from MERCK KGaA.

References

- Albert B, Kos-Braun IC, Henras AK, Dez C, Rueda MP, Zhang X, Gadal O, Kos M, Shore D. 2019. A ribosome assembly stress response regulates transcription to maintain proteome homeostasis. *eLife* **8**:e45002. doi:10.7554/eLife.45002
- Averous J, Lambert-Langlais S, Mesclon F, Carraro V, Parry L, Jousse C, Bruhat A, Maurin A-C, Pierre P, Proud CG, Fafournoux P. 2016. GCN2 contributes to mTORC1 inhibition by leucine deprivation through an ATF4 independent mechanism. *Sci Rep* **6**:27698. doi:10.1038/srep27698
- Bankhead P, Loughrey MB, Fernández JA, Dombrowski Y, McArt DG, Dunne PD, McQuaid S, Gray RT, Murray LJ, Coleman HG, James JA, Salto-Tellez M, Hamilton PW. 2017. QuPath: Open source software for digital pathology image analysis. *Sci Rep* **7**:16878. doi:10.1038/s41598-017-17204-5
- Bröer A, Gauthier-Coles G, Rahimi F, van Geldermalsen M, Dorsch D, Wegener A, Holst J, Bröer S. 2019. Ablation of the ASCT2 (SLC1A5) gene encoding a neutral amino acid transporter reveals transporter plasticity and redundancy in cancer cells. *J Biol Chem* **294**:4012–4026. doi:10.1074/jbc.RA118.006378
- Bruno PM, Liu Y, Park GY, Murai J, Koch CE, Eisen TJ, Pritchard JR, Pommier Y, Lippard SJ, Hemann MT. 2017. A subset of platinum-containing chemotherapeutic agents kills cells by inducing ribosome biogenesis stress. *Nat Med* **23**:461–471. doi:10.1038/nm.4291
- Bunz F, Dutriaux A, Lengauer C, Waldman T, Zhou S, Brown JP, Sedivy JM, Kinzler KW, Vogelstein B. 1998. Requirement for p53 and p21 to sustain G2 arrest after DNA damage. *Science* **282**:1497–1501. doi:10.1126/science.282.5393.1497
- Burger K, Mühl B, Harasim T, Rohrmoser M, Malamoussi A, Orban M, Kellner M, Gruber-Eber A, Kremmer E, Hölzel M, Eick D. 2010. Chemotherapeutic Drugs Inhibit Ribosome Biogenesis at Various Levels. *Journal of Biological Chemistry* **285**:12416–12425. doi:10.1074/jbc.M109.074211
- Catez F, Dalla Venezia N, Marcel V, Zorbas C, Lafontaine DLJ, Diaz J-J. 2019. Ribosome biogenesis: An emerging druggable pathway for cancer therapeutics. *Biochemical Pharmacology* **159**:74–81. doi:10.1016/j.bcp.2018.11.014
- Chandrashekar DS, Bachel B, Balasubramanya SAH, Creighton CJ, Ponce-Rodriguez I, Chakravarthi BVSK, Varambally S. 2017. UALCAN: A Portal for Facilitating Tumor Subgroup Gene Expression and Survival Analyses. *Neoplasia* **19**:649–658. doi:10.1016/j.neo.2017.05.002
- Chaveroux C, Sarcinelli C, Barbet V, Belfeki S, Barthelaix A, Ferraro-Peyret C, Lebecque S, Renno T, Bruhat A, Fafournoux P, Manie SN. 2016. Nutrient shortage triggers the hexosamine biosynthetic pathway via the GCN2-ATF4 signalling pathway. *Scientific reports* **6**:27278. doi:10.1038/srep27278
- Chen H, Duo Y, Hu B, Wang Z, Zhang F, Tsai H, Zhang J, Zhou L, Wang L, Wang X, Huang L. 2016. PICT-1 triggers a pro-death autophagy through inhibiting rRNA transcription and AKT/mTOR/p70S6K signaling pathway. *Oncotarget* **7**:78747–78763. doi:10.18632/oncotarget.12288
- Clarke EM, Peterson CL, Brainard AV, Riggs DL. 1996. Regulation of the RNA Polymerase I and III Transcription Systems in Response to Growth Conditions. *Journal of Biological Chemistry* **271**:22189–22195. doi:10.1074/jbc.271.36.22189
- Cortazar AR, Torrano V, Martín-Martín N, Caro-Maldonado A, Camacho L, Hermanova I, Guruceaga E, Lorenzo-Martín LF, Caloto R, Gomis RR, Apaolaza I, Quesada V, Trka J, Gomez-Muñoz A, Vincent S, Bustelo XR, Planes FJ, Aransay AM, Carracedo A. 2018. CANCERTOOL: A Visualization and Representation Interface to Exploit Cancer Datasets. *Cancer Research* **78**:6320–6328. doi:10.1158/0008-5472.CAN-18-1669
- Dekervel J, Hompes D, van Malenstein H, Popovic D, Sagaert X, De Moor B, Van Cutsem E, D'Hoore A, Verslype C, van Pelt J. 2014. Hypoxia-driven gene expression is an independent prognostic factor in stage II and III colon cancer patients. *Clin Cancer Res* **20**:2159–2168. doi:10.1158/1078-0432.CCR-13-2958
- Dong J, Qiu H, Garcia-Barrio M, Anderson J, Hinnebusch AG. 2000. Uncharged tRNA activates GCN2 by displacing the protein kinase moiety from a bipartite tRNA-binding domain. *Mol Cell* **6**:269–279. doi:10.1016/s1097-2765(00)00028-9
- Dorsch D, Hoelzemann G, Calderini M, Wegener A, Poeschke O. 2014. Triazolo[4,5-d]pyrimidine derivatives for the treatment of diseases such as cancer. WO2014135244A1.
- Edinger AL, Thompson CB. 2002. Akt maintains cell size and survival by increasing mTOR-dependent nutrient uptake. *Mol Biol Cell* **13**:2276–2288. doi:10.1091/mbc.01-12-0584
- Elbadawy M, Usui T, Yamawaki H, Sasaki K. 2019. Emerging Roles of C-Myc in Cancer Stem Cell-Related Signaling and Resistance to Cancer Chemotherapy: A Potential Therapeutic Target Against Colorectal Cancer. *IJMS* **20**:2340. doi:10.3390/ijms20092340
- Fumagalli S, Ivanenkov VV, Teng T, Thomas G. 2012. Supra-induction of p53 by disruption of 40S and

60S ribosome biogenesis leads to the activation of a novel G2/M checkpoint. *Genes Dev* **26**:1028–1040. doi:10.1101/gad.189951.112

Gao P, Tchernyshyov I, Chang T-C, Lee Y-S, Kita K, Ochi T, Zeller KI, De Marzo AM, Van Eyk JE, Mendell JT, Dang CV. 2009. c-Myc suppression of miR-23a/b enhances mitochondrial glutaminase expression and glutamine metabolism. *Nature* **458**:762–765. doi:10.1038/nature07823

Ge J, Karjilovich J, Zhai Y, Zheng J, Yu Y-T. 2017. 5-Fluorouracil Treatment Alters the Efficiency of Translational Recoding. *Genes* **8**:295. doi:10.3390/genes8110295

Ge L, Chen W, Cao W, Liu G, Zhang Q, Zhuang J, Zhang M, Yang J, Guo S, Zhao X, Guo H. 2018. GCN2 is a potential prognostic biomarker for human papillary renal cell carcinoma. *Cancer biomarkers : section A of Disease markers* **22**:395–403. doi:10.3233/CBM-170922

Gelardi ELM, Colombo G, Piccarazzi F, Ferraris DM, Mangione A, Petrarolo G, Aronica E, Rizzi M, Mori M, La Motta C, Garavaglia S. 2021. A Selective Competitive Inhibitor of Aldehyde Dehydrogenase 1A3 Hinders Cancer Cell Growth, Invasiveness and Stemness In Vitro. *Cancers* **13**:356. doi:10.3390/cancers13020356

Goldman MJ, Craft B, Hastie M, Repečka K, McDade F, Kamath A, Banerjee A, Luo Y, Rogers D, Brooks AN, Zhu J, Haussler D. 2020. Visualizing and interpreting cancer genomics data via the Xena platform. *Nat Biotechnol* **38**:675–678. doi:10.1038/s41587-020-0546-8

Gomes A, Guillaume L, Grimes DR, Fehrenbach J, Lobjois V, Ducommun B. 2016. Oxygen Partial Pressure Is a Rate-Limiting Parameter for Cell Proliferation in 3D Spheroids Grown in Physiologic Culture Condition. *PLoS ONE* **11**:e0161239. doi:10.1371/journal.pone.0161239

Goudarzi KM, Nistér M, Lindström MS. 2014. mTOR inhibitors blunt the p53 response to nucleolar stress by regulating RPL11 and MDM2 levels. *Cancer Biol Ther* **15**:1499–1514. doi:10.4161/15384047.2014.955743

Grummt I, Smith VA, Grummt F. 1976. Amino acid starvation affects the initiation frequency of nucleolar RNA polymerase. *Cell* **7**:439–445. doi:10.1016/0092-8674(76)90174-4

Guimaraes JC, Zavolan M. 2016. Patterns of ribosomal protein expression specify normal and malignant human cells. *Genome Biol* **17**:236. doi:10.1186/s13059-016-1104-z

Guo F, Gong H, Zhao H, Chen J, Zhang Y, Zhang L, Shi X, Zhang A, Jin H, Zhang J, He Y. 2018. Mutation status and prognostic values of KRAS, NRAS, BRAF and PIK3CA in 353 Chinese colorectal cancer patients. *Sci Rep* **8**:6076. doi:10.1038/s41598-018-24306-1

Hald ØH, Olsen L, Gallo-Oller G, Elfman LHM, Løkke C, Kogner P, Sveinbjörnsson B, Flægstad T, Johnsen JI, Einvik C. 2019. Inhibitors of ribosome biogenesis repress the growth of MYCN-amplified neuroblastoma. *Oncogene* **38**:2800–2813. doi:10.1038/s41388-018-0611-7

Harachi M, Masui K, Okamura Y, Tsukui R, Mischel P, Shibata N. 2018. mTOR Complexes as a Nutrient Sensor for Driving Cancer Progression. *IJMS* **19**:3267. doi:10.3390/ijms19103267

Harding HP, Ordonez A, Allen F, Parts L, Inglis AJ, Williams RL, Ron D. 2019. The ribosomal P-stalk couples amino acid starvation to GCN2 activation in mammalian cells. *Elife* **8**:e50149. doi:10.7554/eLife.50149

Harding HP, Zhang Y, Zeng H, Novoa I, Lu PD, Calton M, Sadri N, Yun C, Popko B, Paules R, Stojdl DF, Bell JC, Hettmann T, Leiden JM, Ron D. 2003. An integrated stress response regulates amino acid metabolism and resistance to oxidative stress. *Mol Cell* **11**:619–33.

Inglis AJ, Masson GR, Shao S, Perisic O, McLaughlin SH, Hegde RS, Williams RL. 2019. Activation of GCN2 by the ribosomal P-stalk. *Proc Natl Acad Sci U S A* **116**:4946–4954. doi:10.1073/pnas.1813352116

James A, Wang Y, Raje H, Rosby R, DiMario P. 2014. Nucleolar stress with and without p53. *Nucleus* **5**:402–426. doi:10.4161/nucl.32235

Jewer M, Lee L, Leibovitch M, Zhang G, Liu J, Findlay SD, Vincent KM, Tandoc K, Dieters-Castator D, Quail DF, Dutta I, Coatham M, Xu Z, Puri A, Guan B-J, Hatzoglou M, Brumwell A, Uniacke J, Patsis C, Koromilas A, Schueler J, Siegers GM, Topisirovic I, Postovit L-M. 2020. Translational control of breast cancer plasticity. *Nat Commun* **11**:2498. doi:10.1038/s41467-020-16352-z

Jin Q, Liu G, Wang B, Li S, Ni K, Wang C, Ren J, Zhang S, Dai Y. 2020. High methionyl-tRNA synthetase expression predicts poor prognosis in patients with breast cancer. *J Clin Pathol* **73**:803–812. doi:10.1136/jclinpath-2019-206175

Kaizuka T, Morishita H, Hama Y, Tsukamoto S, Matsui T, Toyota Y, Kodama A, Ishihara T, Mizushima T, Mizushima N. 2016. An Autophagic Flux Probe that Releases an Internal Control. *Mol Cell* **64**:835–849. doi:10.1016/j.molcel.2016.09.037

Kamphorst JJ, Nofal M, Comisso C, Hackett SR, Lu W, Grabocka E, Vander Heiden MG, Miller G, Drebin JA, Bar-Sagi D, Thompson CB, Rabinowitz JD. 2015. Human Pancreatic Cancer Tumors Are Nutrient Poor and Tumor Cells Actively Scavenge Extracellular Protein. *Cancer Research* **75**:544–553. doi:10.1158/0008-5472.CAN-14-2211

Kan L, Smith A, Chen M, Ledford BT, Fan H, Liu Z, He J-Q. 2015. Rho-Associated Kinase Inhibitor (Y-27632) Attenuates Doxorubicin-Induced Apoptosis of Human Cardiac Stem Cells. *PLoS One* **10**:e0144513. doi:10.1371/journal.pone.0144513

Kim EY, Jung JY, Kim A, Kim K, Chang YS. 2017. Methionyl-tRNA synthetase overexpression is associated with poor clinical outcomes in non-small cell lung cancer. *BMC Cancer* **17**:467. doi:10.1186/s12885-017-3452-9

Kim J, Kundu M, Viollet B, Guan KL. 2011. AMPK and mTOR regulate autophagy through direct phosphorylation of Ulk1. *Nature cell biology* **13**:132–41. doi:10.1038/ncb2152

Kim T-H, Leslie P, Zhang Y. 2014. Ribosomal proteins as unrevealed caretakers for cellular stress and genomic instability. *Oncotarget* **5**:860–871. doi:10.18632/oncotarget.1784

Klein J, Grummt I. 1999. Cell cycle-dependent regulation of RNA polymerase I transcription: the nucleolar transcription factor UBF is inactive in mitosis and early G1. *Proc Natl Acad Sci U S A* **96**:6096–6101. doi:10.1073/pnas.96.11.6096

Ko YG, Kang YS, Kim EK, Park SG, Kim S. 2000. Nucleolar localization of human methionyl-tRNA synthetase and its role in ribosomal RNA synthesis. *J Cell Biol* **149**:567–574. doi:10.1083/jcb.149.3.567

Krige D, Needham LA, Bawden LJ, Flores N, Farmer H, Miles LEC, Stone E, Callaghan J, Chandler S, Clark VL, Kirwin-Jones P, Legris V, Owen J, Patel T, Wood S, Box G, Laber D, Odedra R, Wright A, Wood LM, Eccles SA, Bone EA, Ayscough A, Drummond AH. 2008. CHR-2797: an antiproliferative aminopeptidase inhibitor that leads to amino acid deprivation in human leukemic cells. *Cancer Res* **68**:6669–6679. doi:10.1158/0008-5472.CAN-07-6627

Kuleshov MV, Jones MR, Rouillard AD, Fernandez NF, Duan Q, Wang Z, Koplev S, Jenkins SL, Jagodnik KM, Lachmann A, McDermott MG, Monteiro CD, Gundersen GW, Ma'ayan A. 2016. Enrichr: a comprehensive gene set enrichment analysis web server 2016 update. *Nucleic Acids Res* **44**:W90–97. doi:10.1093/nar/gkw377

Kushner JP, Boll D, Quagliana J, Dickman S. 1976. Elevated methionine-tRNA synthetase activity in human colon cancer. *Proc Soc Exp Biol Med* **153**:273–276. doi:10.3181/00379727-153-39526

Kwon NH, Kang T, Lee JY, Kim HH, Kim HR, Hong J, Oh YS, Han JM, Ku MJ, Lee SY, Kim S. 2011. Dual role of methionyl-tRNA synthetase in the regulation of translation and tumor suppressor activity of aminoacyl-tRNA synthetase-interacting multifunctional protein-3. *Proceedings of the National Academy of Sciences of the United States of America* **108**:19635–40. doi:10.1073/pnas.1103922108

Li C, Wu B, Li Y, Chen J, Ye Z, Tian X, Wang J, Xu X, Pan S, Zheng Y, Cai X, Jiang L, Zhao M. 2022. Amino acid catabolism regulates hematopoietic stem cell proteostasis via a GCN2-eIF2 α axis. *Cell Stem Cell* **29**:1119–1134.e7. doi:10.1016/j.stem.2022.06.004

Li L, Li Y, Zhao J, Fan S, Wang L, Li X. 2016. CX-5461 induces autophagy and inhibits tumor growth via mammalian target of rapamycin-related signaling pathways in osteosarcoma. *Onco Targets Ther* **9**:5985–5997. doi:10.2147/OTT.S104513

Lowman XH, Hanse EA, Yang Y, Ishak Gabra MB, Tran TQ, Li H, Kong M. 2019. p53 Promotes Cancer Cell Adaptation to Glutamine Deprivation by Upregulating Slc7a3 to Increase Arginine Uptake. *Cell Reports* **26**:3051–3060.e4. doi:10.1016/j.celrep.2019.02.037

Ma H, Pederson T. 2013. The nucleolus stress response is coupled to an ATR-Chk1-mediated G2 arrest. *Mol Biol Cell* **24**:1334–1342. doi:10.1091/mbc.E12-12-0881

Marisa L, de Reyniès A, Duval A, Selves J, Gaub MP, Vescovo L, Etienne-Grimaldi M-C, Schiappa R, Guenot D, Ayadi M, Kirzin S, Chazal M, Fléjou J-F, Benchimol D, Berger A, Lagarde A, Pencreach E, Piard F, Elias D, Parc Y, Olschwang S, Milano G, Laurent-Puig P, Boige V. 2013. Gene expression classification of colon cancer into molecular subtypes: characterization, validation, and prognostic value. *PLoS Med* **10**:e1001453. doi:10.1371/journal.pmed.1001453

Morgado-Palacin L, Llanos S, Serrano M. 2012. Ribosomal stress induces L11- and p53-dependent apoptosis in mouse pluripotent stem cells. *Cell Cycle* **11**:503–510. doi:10.4161/cc.11.3.19002

Murayama A, Ohmori K, Fujimura A, Minami H, Yasuzawa-Tanaka K, Kuroda T, Oie S, Daitoku H, Okuwaki M, Nagata K, Fukamizu A, Kimura K, Shimizu T, Yanagisawa J. 2008. Epigenetic control of rDNA loci in response to intracellular energy status. *Cell* **133**:627–639. doi:10.1016/j.cell.2008.03.030

Nakamura K, Kimura H. 2017. A new role of GCN2 in the nucleolus. *Biochemical and Biophysical Research Communications* **485**:484–491. doi:10.1016/j.bbrc.2017.02.038

Nakamura A, Nambu T, Ebara S, Hasegawa Y, Toyoshima K, Tsuchiya Y, Tomita D, Fujimoto J, Kurasawa O, Takahara C, Ando A, Nishigaki R, Satomi Y, Hata A, Hara T. 2018. Inhibition of GCN2 sensitizes ASNS-low cancer cells to asparaginase by disrupting the amino acid response. *Proc Natl Acad Sci USA* **115**:E7776–E7785. doi:10.1073/pnas.1805523115

Narvi E, Vaparanta K, Karrila A, Chakroborty D, Knuutila S, Pulliainen A, Sundvall M, Elenius K. 2018. Different responses of colorectal cancer cells to alternative sequences of cetuximab and oxaliplatin.

Sci Rep **8**:16579. doi:10.1038/s41598-018-34938-y

Nath S, Devi GR. 2016. Three-dimensional culture systems in cancer research: Focus on tumor spheroid model. *Pharmacol Ther* **163**:94–108. doi:10.1016/j.pharmthera.2016.03.013

Naumov V, Balashov I, Lagutin V, Borovikov P, Alexeev A. 2017. VolcanoR - web service to produce volcano plots and do basic enrichment analysis (preprint). *Bioinformatics*. doi:10.1101/165100

Ohata H, Ishiguro T, Aihara Y, Sato A, Sakai H, Sekine S, Taniguchi H, Akasu T, Fujita S, Nakagama H, Okamoto K. 2012. Induction of the stem-like cell regulator CD44 by Rho kinase inhibition contributes to the maintenance of colon cancer-initiating cells. *Cancer Res* **72**:5101–5110. doi:10.1158/0008-5472.CAN-11-3812

Pan M, Reid MA, Lowman XH, Kulkarni RP, Tran TQ, Liu X, Yang Y, Hernandez-Davies JE, Rosales KK, Li H, Hugo W, Song C, Xu X, Schones DE, Ann DK, Gradinaru V, Lo RS, Locasale JW, Kong M. 2016. Regional glutamine deficiency in tumours promotes dedifferentiation through inhibition of histone demethylation. *Nat Cell Biol* **18**:1090–1101. doi:10.1038/ncb3410

Pan M, Zorbas C, Sugaya M, Ishiguro K, Kato M, Nishida M, Zhang H-F, Candeias MM, Okamoto A, Ishikawa T, Soga T, Aburatani H, Sakai J, Matsumura Y, Suzuki T, Proud CG, Lafontaine DLJ, Osawa T. 2022. Glutamine deficiency in solid tumor cells confers resistance to ribosomal RNA synthesis inhibitors. *Nat Commun* **13**:3706. doi:10.1038/s41467-022-31418-w

Pavlova NN, Thompson CB. 2016. The Emerging Hallmarks of Cancer Metabolism. *Cell Metabolism* **23**:27–47. doi:10.1016/j.cmet.2015.12.006

Rabouw HH, Langereis MA, Anand AA, Visser LJ, de Groot RJ, Walter P, van Kuppeveld FJM. 2019. Small molecule ISRIB suppresses the integrated stress response within a defined window of activation. *Proc Natl Acad Sci USA* **116**:2097–2102. doi:10.1073/pnas.1815767116

Riedl A, Schleder M, Pudelko K, Stadler M, Walter S, Unterleuthner D, Unger C, Kramer N, Hengstschläger M, Kenner L, Pfeiffer D, Krupitza G, Dolznig H. 2017. Comparison of cancer cells in 2D vs 3D culture reveals differences in AKT–mTOR–S6K signaling and drug responses. *J Cell Sci* **130**:203–218. doi:10.1242/jcs.188102

Riffle S, Hegde RS. 2017. Modeling tumor cell adaptations to hypoxia in multicellular tumor spheroids. *J Exp Clin Cancer Res* **36**:102. doi:10.1186/s13046-017-0570-9

Rubbi CP, Milner J. 2003. Disruption of the nucleolus mediates stabilization of p53 in response to DNA damage and other stresses. *EMBO J* **22**:6068–6077. doi:10.1093/emboj/cdg579

Russo A, Russo G. 2017. Ribosomal Proteins Control or Bypass p53 during Nucleolar Stress. *Int J Mol Sci* **16**.

Sameer AS. 2013. Colorectal cancer: molecular mutations and polymorphisms. *Front Oncol* **3**:114. doi:10.3389/fonc.2013.00114

Sarcinelli C, Dragic H, Piecyk M, Barbet V, Duret C, Bartheleix A, Ferraro-Peyret C, Fauvre J, Renno T, Chaveroux C, Manié SN. 2020. ATF4-Dependent NRF2 Transcriptional Regulation Promotes Antioxidant Protection during Endoplasmic Reticulum Stress. *Cancers* **13**.

Saxton RA, Sabatini DM. 2017. mTOR Signaling in Growth, Metabolism, and Disease. *Cell* **168**:960–976. doi:10.1016/j.cell.2017.02.004

Schmidt EK, Clavarino G, Ceppi M, Pierre P. 2009. SUnSET, a nonradioactive method to monitor protein synthesis. *Nat Methods* **6**:275–277. doi:10.1038/nmeth.1314

Schmidt S, Gay D, Uthe FW, Denk S, Paaue M, Matthes N, Diefenbacher ME, Bryson S, Warrander FC, Erhard F, Ade CP, Baluapuri A, Walz S, Jackstadt R, Ford C, Vlachogiannis G, Valeri N, Otto C, Schüle-Völk C, Maurus K, Schmitz W, Knight JRP, Wolf E, Strathdee D, Schulze A, Germer C-T, Rosenwald A, Sansom OJ, Eilers M, Wiegering A. 2019. A MYC–GCN2–eIF2 α negative feedback loop limits protein synthesis to prevent MYC-dependent apoptosis in colorectal cancer. *Nat Cell Biol*. doi:10.1038/s41556-019-0408-0

Shore D, Albert B. 2022. Ribosome biogenesis and the cellular energy economy. *Curr Biol* **32**:R611–R617. doi:10.1016/j.cub.2022.04.083

Sidrauski C, Tsai JC, Kampmann M, Hearn BR, Vedantham P, Jaishankar P, Sokabe M, Mendez AS, Newton BW, Tang EL, Verschuere E, Johnson JR, Krogan NJ, Fraser CS, Weissman JS, Renslo AR, Walter P. 2015. Pharmacological dimerization and activation of the exchange factor eIF2B antagonizes the integrated stress response. *eLife* **4**:e07314. doi:10.7554/eLife.07314

Sloan KE, Bohnsack MT, Watkins NJ. 2013. The 5S RNP Couples p53 Homeostasis to Ribosome Biogenesis and Nucleolar Stress. *Cell Reports* **5**:237–247. doi:10.1016/j.celrep.2013.08.049

Suh YS, Yeom E, Nam J-W, Min K-J, Lee J, Yu K. 2020. Methionyl-tRNA Synthetase Regulates Lifespan in *Drosophila*. *Mol Cells* **43**:304–311. doi:10.14348/molcells.2019.0273

Sullivan MR, Danai LV, Lewis CA, Chan SH, Gui DY, Kunchok T, Dennstedt EA, Vander Heiden MG, Muir A. 2019. Quantification of microenvironmental metabolites in murine cancers reveals determinants of tumor nutrient availability. *eLife* **8**:e44235. doi:10.7554/eLife.44235

Sutton EC, DeRose VJ. 2021. Early nucleolar responses differentiate mechanisms of cell death induced by oxaliplatin and cisplatin. *Journal of Biological Chemistry* **296**:100633. doi:10.1016/j.jbc.2021.100633

Szafarski W, Leśniczak-Staszak M, Sowiński M, Ojha S, Aulas A, Dave D, Malla S, Anderson P, Ivanov P, Lyons SM. 2022. Early rRNA processing is a stress-dependent regulatory event whose inhibition maintains nucleolar integrity. *Nucleic Acids Research* **50**:1033–1051. doi:10.1093/nar/gkab1231

Tajan M, Hock AK, Blagih J, Robertson NA, Labuschagne CF, Kruijswijk F, Humpton TJ, Adams PD, Vousden KH. 2018. A Role for p53 in the Adaptation to Glutamine Starvation through the Expression of SLC1A3. *Cell Metab* **28**:721–736.e6. doi:10.1016/j.cmet.2018.07.005

Tameire F, Verginadis II, Leli NM, Polte C, Conn CS, Ojha R, Salas Salinas C, Chinga F, Monroy AlexandraM, Fu W, Wang P, Kossenkov A, Ye J, Amaravadi RK, Ignatova Z, Fuchs SY, Diehl JA, Ruggero D, Koumenis C. 2019. ATF4 couples MYC-dependent translational activity to bioenergetic demands during tumour progression. *Nat Cell Biol* **21**:889–899. doi:10.1038/s41556-019-0347-9

Taniuchi S, Miyake M, Tsugawa K, Oyadomari M, Oyadomari S. 2016. Integrated stress response of vertebrates is regulated by four eIF2 α kinases. *Scientific Reports* **6**. doi:10.1038/srep32886

Therizols G, Bash-Imam Z, Panthu B, Machon C, Vincent A, Ripoll J, Nait-Slimane S, Chalabi-Dchar M, Gaucherot A, Garcia M, Laforêts F, Marcel V, Boubaker-Vitre J, Monet M-A, Bouclier C, Vanbelle C, Souahlia G, Berthel E, Albaret MA, Mertani HC, Prudhomme M, Bertrand M, David A, Saurin J-C, Bouvet P, Rivals E, Ohlmann T, Guitton J, Dalla Venezia N, Pannequin J, Catez F, Diaz J-J. 2022. Alteration of ribosome function upon 5-fluorouracil treatment favors cancer cell drug-tolerance. *Nat Commun* **13**:173. doi:10.1038/s41467-021-27847-8

Wang Y, Ning Y, Alam GN, Jankowski BM, Dong Z, Nor JE, Polverini PJ. 2013. Amino acid deprivation promotes tumor angiogenesis through the GCN2/ATF4 pathway. *Neoplasia* **15**:989–97.

Wengrod J, Wang D, Weiss S, Zhong H, Osman I, Gardner LB. n.d. Phosphorylation of eIF2 α triggered by mTORC1 inhibition and PP6C activation is required for autophagy and is aberrant in PP6C-mutated melanoma 12.

Wise DR, DeBerardinis RJ, Mancuso A, Sayed N, Zhang X-Y, Pfeiffer HK, Nissim I, Daikhin E, Yudkoff M, McMahon SB, Thompson CB. 2008. Myc regulates a transcriptional program that stimulates mitochondrial glutaminolysis and leads to glutamine addiction. *Proc Natl Acad Sci U S A* **105**:18782–18787. doi:10.1073/pnas.0810199105

Xu K, Zhan Y, Yuan Z, Qiu Y, Wang H, Fan G, Wang J, Li W, Cao Y, Shen X, Zhang J, Liang X, Yin P. 2019. Hypoxia Induces Drug Resistance in Colorectal Cancer through the HIF-1 α /miR-338-5p/IL-6 Feedback Loop. *Molecular Therapy* **27**:1810–1824. doi:10.1016/j.ymthe.2019.05.017

Yang K, Yang J, Yi J. 2018. Nucleolar Stress: hallmarks, sensing mechanism and diseases. *Cell Stress* **2**:125–140. doi:10.15698/cst2018.06.139

Ye J, Palm W, Peng M, King B, Lindsten T, Li MO, Koumenis C, Thompson CB. 2015. GCN2 sustains mTORC1 suppression upon amino acid deprivation by inducing Sestrin2. *Genes Dev* **29**:2331–2336. doi:10.1101/gad.269324.115

Yuan X, Zhou Y, Casanova E, Chai M, Kiss E, Gröne H-J, Schütz G, Grummt I. 2005. Genetic Inactivation of the Transcription Factor TIF-IA Leads to Nucleolar Disruption, Cell Cycle Arrest, and p53-Mediated Apoptosis. *Molecular Cell* **19**:77–87. doi:10.1016/j.molcel.2005.05.023

Zajkowicz A, Gdowicz-Kłosok A, Krześniak M, Ściegłińska D, Rusin M. 2015. Actinomycin D and nutlin-3a synergistically promote phosphorylation of p53 on serine 46 in cancer cell lines of different origin. *Cell Signal* **27**:1677–1687. doi:10.1016/j.cellsig.2015.05.005

DISCUSSION & PERSPECTIVES

The main objective of this study was to investigate: i) the consequences of GCN2 loss on cellular outcome according to the nutritional context (nutrient deprived or rich conditions), ii) whether these functions rely on the regulation of ribosome biogenesis in colon cancer cells. This research project revealed that GCN2 ensures cellular plasticity, by maintaining nucleolar integrity through the regulation of ribosome biogenesis flexibility. These novel functions for GCN2 open a new avenue in the understanding of cancer progression, tumor cell plasticity and mechanisms underlying chemoresistance. It also questions about the transposition of these results in other pathophysiological contexts. In this section, I will discuss the integration of my results in the current challenges in cancer biology and beyond.

1. GCN2-MetRS at the interplay between ribosome biogenesis and DNA damages

Diverse RNA Pol I inhibitors have been developed and showed promising results in pre-clinical studies although they mainly impair cell proliferation (143,218–220). This effect is likely attributed to the need of biomass generation and subsequent translational upregulation. For instance, treatment with derivatives of rapamycin (rapalogs: everolimus and temsirolimus) that inhibit the RNA Pol I activity through mTORC1 repression, have moderate impacts on patients' solid tumors (169). Nonetheless, the RNA Pol I inhibitors currently under clinical trials still lead to cell death in preclinical settings. The mechanism by which these compounds kill the tumor cells might rather be attributed to their capabilities to induce DNA damages.

Indeed, pharmacological RNA Pol I inhibitors (actinomycin D, CX-5461, BMH-21) also associate to and stabilize particular structures in the DNA named G-quadruplex (G4) that accumulate in tumor cells (221–223). The non-resolution of G4 structures results in DNA replication stalling and DNA damages, promoting genome instability and tumorigenesis (223). Actually, the CX-5461 sensitizes tumor cells to radiations through its capacity to induce DNA damages, questioning the critical role of the RNA Pol I inhibition in the cell outcome (224). Similarly, oxaliplatin and glutamine deprivation trigger both RNA Pol I impairment and DNA damages (126,225).

If not associated to cytotoxicity, the repression of the ribosome biogenesis might act as an adjustment variable to divert the nucleotide pools into the DNA Damages Response (DDR) pathway rather than in rRNA transcription. In this case, the inhibition of the RNA Pol I as a protective response.

For instance, upon pharmacologically induced nucleotide depletion, impairment of ribosome biogenesis is the primary adaptive mechanism to trigger cell cycle arrest. This impaired ribosome biogenesis prevents the DNA replication and cell death caused by excessive DNA damages (148). Glutamine, and by extension, its conversion into nucleotides (Figure 23) represents one of the main substrates for the DNA repair machinery. Blocking this metabolic pathway thus represent an appealing approach for lowering the cellular ability to preserve the genomic integrity. In line with this hypothesis, the glutaminase inhibitor CB-839 blocks the conversion of glutamine into glutamate and thus the nitrogen supply, essential for nucleotides synthesis. Interestingly CB-839 potentiates the action of alkylating agents and irradiation (225,226).

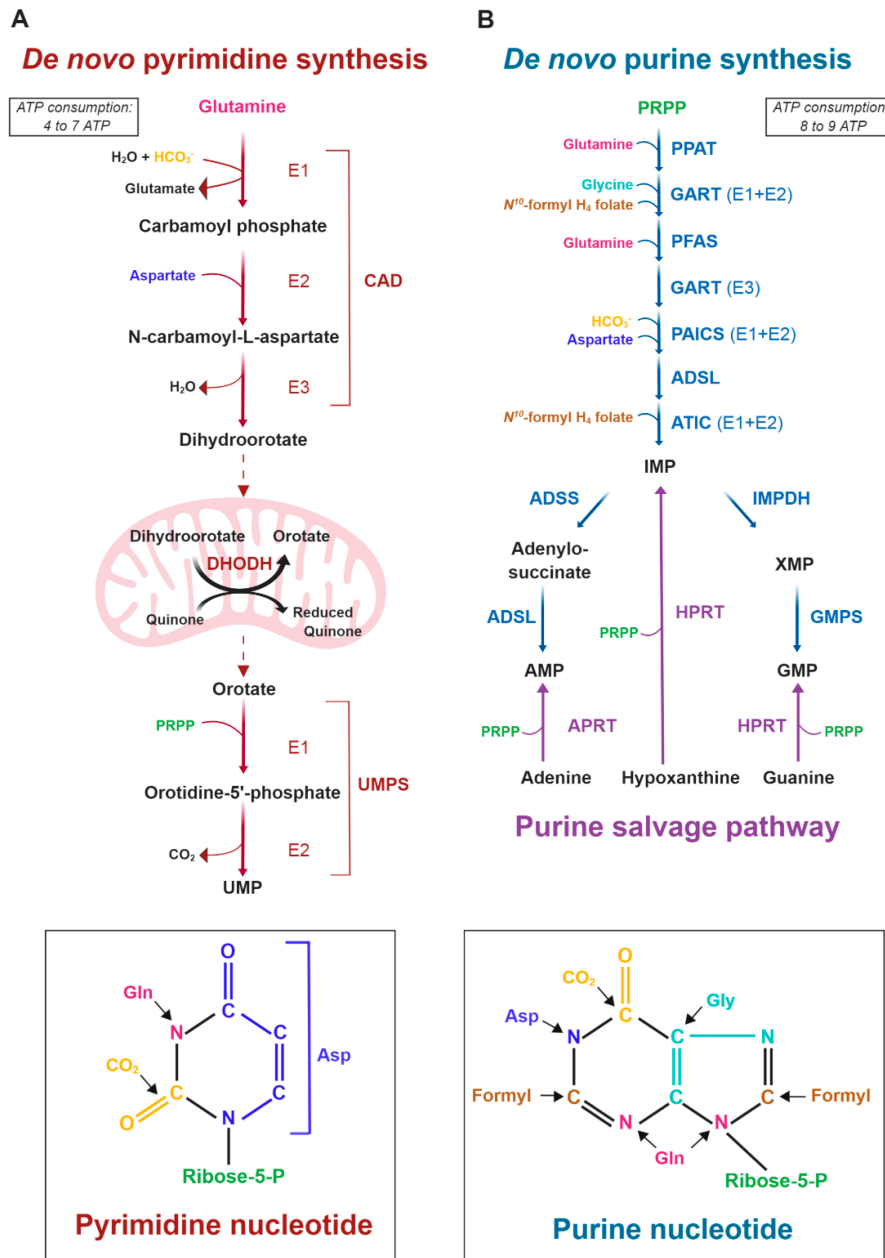


Figure 23: The pyrimidine and purine synthesis pathways.

A) Representation of the *de novo* pyrimidine synthesis pathway. Enzymes: CAD: Carbamoyl-Phosphate Synthetase 2, Aspartate Transcarbamylase, And Dihydroorotase; DHODH: Dihydroorotate Dehydrogenase; UMPS: Uridine Monophosphate Synthetase.

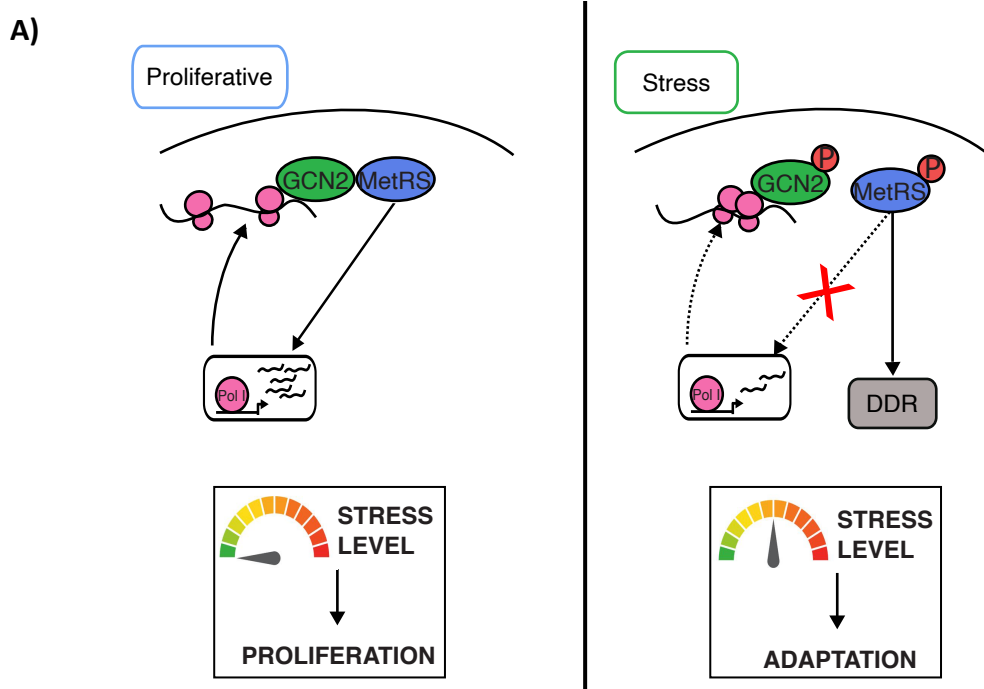
B) The *de novo* and purine salvage pathways. Enzymes: PPAT: phosphoribosyl pyrophosphate amidotransferase; GART: Glycinamide Ribonucleotide Transformylase; PFAS: Phosphoribosylformylglycinamide Synthase; PAICS: Phosphoribosylaminoimidazole Carboxylase And Phosphoribosylamino-imidazolesuccinocarboxamide Synthase; ADSL: Adenylosuccinate Lyase; ATIC: 5-Aminoimidazole-4-Carboxamide Ribonucleotide Formyltransferase; IMPDH: Inosine Monophosphate Dehydrogenase; GMPS: Guanine Monophosphate Synthase; ADSS: Adenylosuccinate Synthase; HPRT: hypoxanthine phosphoribosyltransferase; APRT: adenine phosphoribosyltransferase.

Extracted from (227).

Thus, nucleotide exhaustion is an efficient manner to greatly improve cell death upon DNA damaging conditions (metabolic stress or treatment). My results argue in favor of GCN2 inhibition as a relevant strategy to achieve nucleotides exhaustions and impairment of the DDR upon stress.

Indeed, at least upon chemotherapeutic stress, we demonstrate that the determinant protective effects of GCN2 is ensured by the MetRS branch rather than the canonical ISR axis. Existing data already established this connection upon UV treatment, MetRS phosphorylation by GCN2 promoting the nuclear translocation of AIMP3 to activate the ATM/ATR pathway (212). Moreover, activation of GCN2 upon UV requires the DNA-depend protein kinases DNA-PKcs, also involved in the DNA damages response, strengthening the link between the GCN2 and the DDR pathways (228).

The interest of this connection in clinics is still unknown. More intriguingly, the molecular coordination between repression of the ribosome biogenesis and induction of the DDR by the GCN2-MetRS axis is also undescribed. My results support the hypothesis that, in proliferating cells, GCN2-MetRS supports the ribosome biogenesis; but upon stress, a molecular shift, ensured by GCN2, prevents MetRS relocalization to the nucleolus to both: i) limit the RNA Pol I transcription and ii) promote the DDR pathway. At the contrary, cell death observed upon inhibition of GCN2 in stressed conditions might be explained by both: i) recovery of the RNA Pol I transcription and subsequent exhaustion of intracellular nucleotides pools and, ii) the molecular incapacity to trigger the DDR pathway (Figure 24).



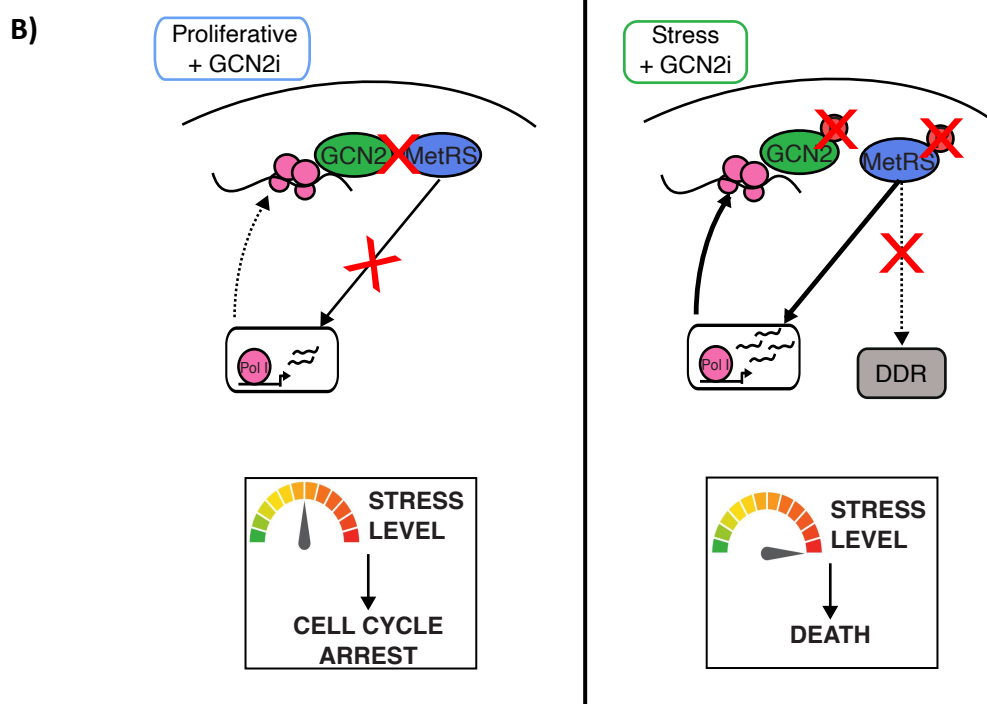


Figure 24: Hypothesis scheme for the pivotal role of the GCN2-MetRS axis in cancer cells.

A) GCN2 is constitutively bound to MetRS at translating ribosomes in proliferative cells, promoting ribosome biogenesis through an unknown mechanism (left panel). In condition of stress (i.e., RNA Pol I repression by chemical agents or nutritional stress), the ribosomal stress activates GCN2 that phosphorylates MetRS, allowing the repression of ribosome biogenesis and activation of the DDR pathway (right panel). **B)** In proliferative cells, loss of GCN2 prevents the relocalization of MetRS, impairing the ribosome biogenesis and leading to a cell cycle arrest (left panel). In condition of stress (i.e., RNA Pol I repression by chemical agents or nutritional stress), the impossibility for GCN2 to phosphorylate MetRS leads to a de-repression of the ribosome biogenesis and an incapacity to induce the DDR, resulting in cell death.

Further investigations are required for understanding i) how the GCN2-MetRS is activated in nutrient rich conditions and ii) the MetRS-dependent mechanism governing the coordinated shift towards DDR activation and concomitant RNA Pol I inhibition upon stress.

To this end, we are currently performing immunoprecipitations of the endogenous MetRS and GCN2 in HCT116 cells treated or not with the CX-5461, at different time points, in order to identify: i) the partner proteins for each factor and their dynamics along the stress, ii) the evolution of the GCN2-dependent phosphorylation of MetRS in the same conditions. The samples will then be analyzed by mass spectrometry. We expect to find novel partners within the GCN2 complex that will then be validated by biochemistry and functionally for their implication in stressed and non-stressed conditions.

2. The GCN2-MetRS axis as a new target in cancer

- *Relevance of targeting the DDR axis rather than the canonical ISR and revisiting the modalities of GCN2 activation.*

Regarding the translational aspect of this work, my results argue in favor of accelerating the transfer of GCN2 inhibitors to patients. To date, three GCN2 inhibitors are available for pre-clinical studies: GCN2iB provided by Takeda, A92 and GCN2iA (also called TAP20, used in my study) both synthesized by Merck.

However, our preliminary results show profound discrepancies in the mode of action of the three compounds. Although they all block the ISR induction upon amino acids restriction, only A92 and GCN2iA efficiently: i) impair cell proliferation and the induction of the ATM pathway upon glutamine starvation or BMH21/CX-5461 treatment, ii) induce cell death upon stress (Figure 25). In line with our observations, Dr Simons' team recently demonstrated that GCN2iB induces senescence, but not cell death, in hepatocarcinoma cells starved for arginine, another DNA-damaging stressor (229,230).

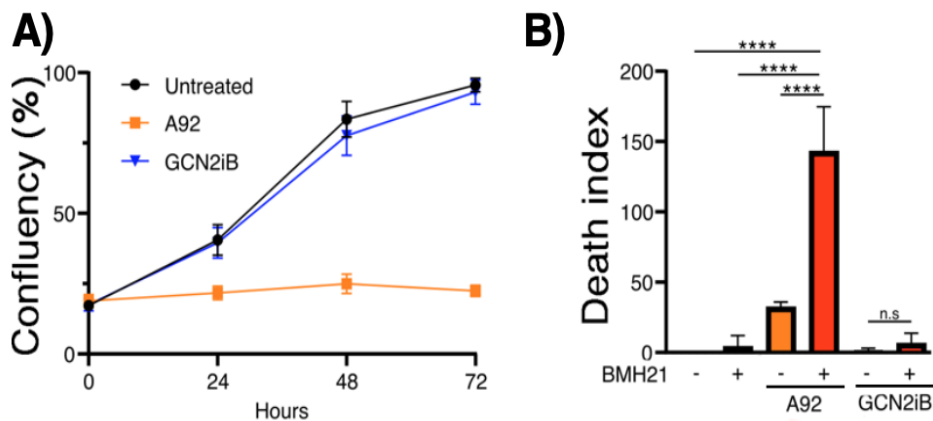


Figure 25: Discrepancies between different GCN2 inhibitors.

A) Impact of the different GCN2 inhibitors on cell proliferation. **B)** Cell death index upon RNA Pol I inhibitor (BMH21) combined to different GCN2 inhibitors (A92 and GCN2iB). Preliminary internal results.

The discrepancies observed between these inhibitors raise questions about the essentiality of the two axes triggered by GCN2 and thus, the relevance of their respective inhibition in cancer. Indeed, we did not detect any induction of cell death in spheroids upon ISRIB treatment, an inhibitor of P-eIF2a, suggesting that impairing the ISR is not sufficient to trigger apoptosis in a complex deprived metabolic environment as observed in tumors. In addition, if both axes are enabled by GCN2 upon metabolic stress, BMH-21 intriguingly activates only the GCN2-MetRS branch without triggering the ISR (Figure 26). Thus, the mechanisms of GCN2 activation differ according to the nature of the stress.

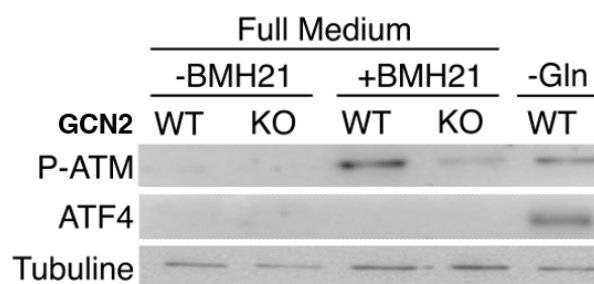


Figure 26: Activation of the DDR upon RNA Pol I inhibitor according to GCN2 status.

Upon RNA Pol I inhibitor (BMH-21), P-ATM is induced as a sign of DDR activation whereas the ISR marker ATF4 remains unchanged. Glutamine induction induces both the DDR and the ISR. Yet, activation of P-ATM is reduced in GCN2 ^{-/-} MEF cells. Preliminary internal results.

Despite the strong connection between stresses inducing eventually DNA damages, we do not think that GCN2 activation is directly caused by the DNA damages considering its predominant cytoplasmic localization. However, this assumption requires experimental validations.

GCN2 is indeed activated by a wide range of nutritional starvation (i.e.; leucine, glutamine, arginine) that are demonstrated for inducing DNA damages. Similarly, rapamycin treatment activates the DDR, however it does not induce DNA breaks (231–235). Yet, the contribution of GCN2 in the rapamycin-induced DDR has to be tested. Thus, we hypothesize that GCN2, in all stressed conditions, is rather activated by the ribotoxic stress caused by the ribosome biogenesis impairment.

Furthermore, the contribution of accumulated uncharged tRNAs (historical model of GCN2 activation) should be addressed in stresses upon ribosome biogenesis alteration. Previous studies suggest that ribosome stalling, caused by UV exposure activates GCN2 independently

of an impairment of tRNAs charging and leads to the dual activation of the DDR and the ISR axes (166,186). In our preliminary results as well, it is unlikely that BMH-21 treatment or other pharmacological stressors leads to uncharged tRNAs accumulation so rapidly (4h post treatment) in our experimental settings. I rather propose that the impairment of RNA Pol I transcription slows down translating ribosomes and consequently induces a low level of ribosomal stress sufficient to activate the DDR without DNA breaks, but not sufficient for triggering the ISR.

According to our model, impairment of the RNA Pol I by rapamycin or BMH-21 and activation of GCN2, through moderate ribosomal stress, is sufficient for activating the DDR without the ISR. Further mechanistical experiments are yet required to clarify the modalities underlying GCN2 pathways activation according the different stressors. Time-course analyses of the appearance of DNA damages and/or ribosomal stress upon the exposure to different stressors (RNA Pol I inhibitors, oxaliplatin, etoposide) will be performed and analyzed in regard of the activation of both GCN2 pathways.

To conclude on this part, the rationale behind the interest of blocking GCN2 activity has always been seen through the prism of the ISR downregulation. My results clearly question this dogma and rather argue in favor of the development of GCN2 inhibitors satisfying the physicochemical requirements for *in vivo* applications and targeting, at least, the GCN2-MetRS-DDR axis. Unfortunately, the GCN2iB, that is not targeting this branch, is the only inhibitor qualified for *in vivo* application. Current chemical optimization of the A92 to improve its physicochemical properties are under development in our lab for testing its impact on tumor growth *in vivo*.

- *Prognostic biomarkers for GCN2 inhibitors and patients' stratification*

Although the GCN2-MetRS can appear as a promising target in cancer, my results clearly demonstrate that tumors with specific biology and genetic alterations might be more sensitive to the inhibition of this axis. Thus, biomarkers allowing the identification of patients' subgroups susceptible to respond to this drug are required. For instance, as illustrated in my project, colon adenocarcinomas display a specific dysregulation of ribosome biogenesis, providing a rationale for investigating the function of GCN2 in this specific type of tumors. However, other types of molecular characteristics, and particularly genetic alterations, can be of interest for identifying the patients susceptible to respond the best to GCN2 inhibitors.

Considering that loss of GCN2-MetRS interaction impairs the DDR response, the genomic instability might be proposed as an interesting susceptibility biomarker for GCN2 inhibition. Basically, genomic instability arises from errors in the DNA leading to a replicative stress diverting DNA repair pathways to finally promote tumorigenesis.

Interestingly, the accumulation of DNA damages during replication stress mostly promotes chromosomal instability in mismatch repair (MMR) proficient cells (236,237). In the contrary, MMR-deficient cells suppress chromosomal instability and rather display an instability of specific repeated sequences along the genome, resulting in a molecular phenotype called microsatellite instability (MSI) (236–238). The mechanisms required to adapt and survive to genotoxic stress appear then to differ according to the abilities of the cell to repair DNA damages and result in different genomic instability patterns, rather promoting either chromosome or microsatellite instability (236).

MSI-high tumors are associated to poor sensitivity to 5-FU, low frequency of TP53 mutations, and strong immunogenicity sustained by the production of neoantigens recruiting T-cells (238–240). In our study, we demonstrated that MSI-high HCT116 cell line is sensitive to GCN2 targeting, independently of the ISR, particularly upon ribosome functions and situations challenging DNA damages repair (i.e., combination of GCN2i + oxaliplatin, glutamine deprivation, RNA Pol I inhibitors, or 5-FU).

This result supports that the GCN2-MetRS axis might be involved in the adaptation to the genotoxic stress displayed by MSI-high colon tumor cells. The high mutation burden in MSI-high tumor cells could be predictive of an enhanced cytotoxicity of GCN2 targeting because of their dependency towards the DDR. Consistently, MSI tumors in COAD display a higher enrichment for gene signature related to starvations, suggesting a high dependency for GCN2 in this specific subgroup (Figure 27).

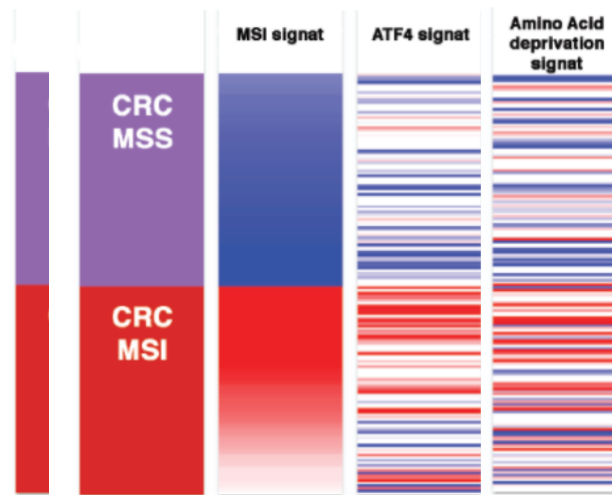


Figure 27: Association between amino acid deprivation signature and MSI status in colorectal cancer.

RNA-seq datasets from the TCGA database were analyzed to evaluate the association between GCN2 and amino acid deprivation gene signatures in MSI (n=82) vs MSS (n=81) colorectal cancers. Preliminary internal results.

To test this hypothesis, we propose to first validate the association between alterations of the metabolic microenvironment and higher dependency to the DNA response pathway, assessing markers nutritional stress (hypoxia CAIX, vascularization CD31, proteotoxic stress AGR2, aggresomes) and of the DDR pathway (P-ATM, γ H2Ax), including markers of the GCN2-MetRS pathway, previously identified by mass spectrometry in MSI tumors compared to MMR-proficient tumors samples. Then, a panel of MSS (such as HT29) or MSI (such as HCT116) cellular models will be subjected to nutritional stress *in vitro* in combination with A92 or GCN2IB to test their dependency towards the MetRS branch.

Cancer cells are exposed to a chronic replicative stress, consequently they face new genetic threat every day that enables the emergence of clonal population with mutations in TP53 with enhanced resistance abilities and higher probably to survive to the next stress (236,237). In our study as well, the survival of TP53-mutant cells exposed to stress conditions is not compromised by GCN2 inhibitor despite MSI high status for some of them (DLD1, SW480).

We still observed an antiproliferative effect and mTORC1 repression in TP53-mutant or null cell lines treated with GCN2i, suggesting that the impairment of ribosome biogenesis is effective in both genetic contexts. Yet, loss of GCN2 with or without additional stress (low glutamine or oxaliplatin) does not induce cell death in TP53-mutated cells, demonstrating that a functional TP53 pathway is required for fully inducing apoptosis. This is consistent with its function of guardian of the nucleus integrity and apoptosis inducer upon nucleolar stress (98).

Moreover, TP53-mutant tumor cells enhance autophagy and stemness features, favoring resistance to ribosome impairment such as upon asparaginase or oxaliplatin treatment (241,242). Similarly, in our study, GCN2i failed to induce cell death: i) in the core of TP53 mutant cell lines derived spheroids, a compartment associated with deprivation in oxygen and nutrients promoting stemness, and ii) in TP53-mutant proliferative cells, probably partly because of the enhanced capacities to induce protective autophagy compared to wild-type colon cancer cells, eventually contributing to restore pools of amino acids and resist. Hence, TP53 wild-type status is a relevant marker for the prediction of cells' response upon GCN2 inhibitors.

Investigating why the impairment of the GCN2-MetRS axis in TP53 mutant cells is not deleterious when exposed to ribosomal stress could: i) help deciphering molecular pathways diverted by the cell to cope with the situation and, ii) eventually lead to the identification of new targets to overcome the resistance.

Finally, our results show that a non-negligible proportion of COAD tumors were negative for GCN2. Similarly, in a lung adenocarcinoma (LUAD) TMA covering 152 tumors, we estimated at 20% the percentage of tumors without GCN2 expression (Figure 28). Consequently, these tumors cannot be targeted with GCN2 inhibitors. However, these observations question the specificity of this subgroup of tumors.

Although we were not able to find specific mutations within the GCN2 gene, intriguingly, we identified subgroups of tumors with one or two GCN2 alleles deleted. In these subgroups, loss of GCN2 was associated to the downregulation of DNA repair, an increased genome instability and perturbation of the nucleolar protein expression.

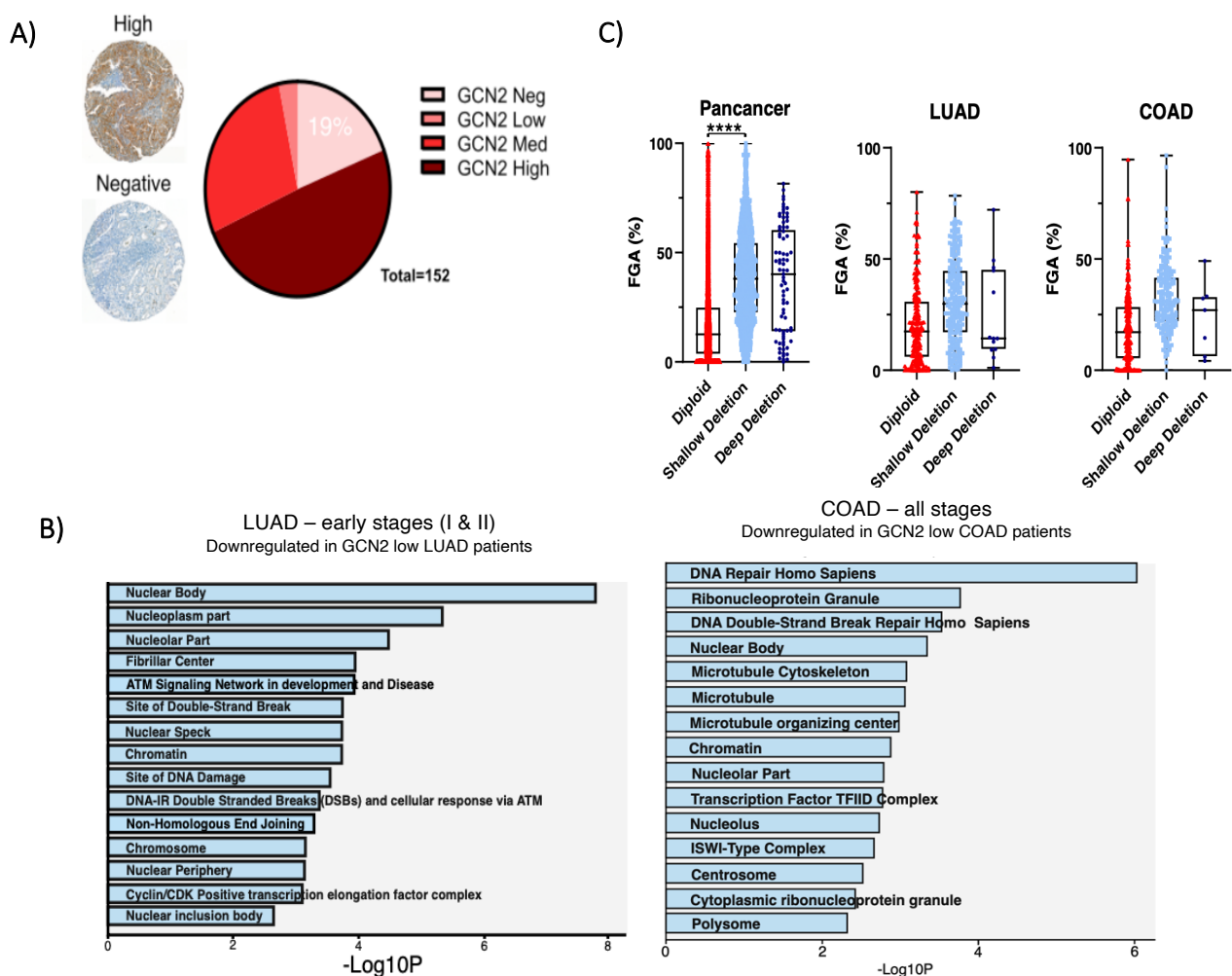


Figure 28: Genetic loss of GCN2 and genomic instability.

A) Analysis of GCN2 amounts in LUAD TMA. **B)** Low expression of GCN2 is associated to downregulation of nucleolar homeostasis and DNA damages response signature in LUAD and COAD tumor samples. **C)** Fraction Genome Altered (FGA) according to genetic deletion of GCN2 in all cancers, LUAD, or COAD. Preliminary internal results.

Interestingly, we observed a trend in the association of higher levels of TP53 mutation and low expression of GCN2 that could be associated to a drift towards chromosomal instability, such as it can be observed upon mutations in BRCA1 and BRCA2. Altogether, it suggests to investigate the suspected participation of the GCN2-MetRS pathway in the resolution of double-strand breaks during replication stress along tumorigenesis and the acquisition of either chromosomal aberrations or microsatellite mutations. Analyzing whether allelic loss of GCN2 is associated to: i) loss of the corresponding protein and ii) clinical outcome would be of interest. A PCR test is under development for assessing the genetic status of GCN2 in the LUAD tumors included in the presented TMA. The presence or absence of the GCN2 alleles will then be correlated to the status markers of the DDR (P-ATM, γ H2Ax) and clinical data.

Finally, considering that loss of GCN2 represents a vulnerability for both stressed and proliferative cells, the prognostic value of its allelic deletion should be examined as a biomarker of tumor sensitivity to drugs targeting concomitantly DNA repair and ribosome biogenesis (i.e., oxaliplatin, 5-FU...). Functionally, we have crossed the KRAS^{la2/+} the mice model developing spontaneously lung tumors with mice invalidated for GCN2. Although the tumor incidence is drastically reduced in the GCN2^{-/-} KRAS^{la2/+} compared to the wild-type, these mice still develop tumors. The characterization of the DDR in the WT and KO mice are currently under investigation and the effect of CX-5461 in the two models will be tested.

3. The GCN2-MetRS axis, a hidden partner-in-crime in inflammatory diseases?

Despite the strong recruitment of immune cells, about 30-50% of metastatic MSI colorectal tumors display innate or acquired resistance to immune checkpoints inhibitors (243). A strong inflammatory response underlies the decreased efficiency of immune checkpoints inhibitors unveiling questions regarding the mechanisms involved in this decreased sensitivity (244). Dysregulation in the GCN2 signaling should be investigated in such context considering its dual role in promoting DNA damages repair through MetRS and buffering proteotoxic stress through the ISR. I make the hypothesis that loss of GCN2 function or either independence from the GCN2 pathway could lead to an accumulation of DNA damages and chronic inflammation gradually promoting the instauration of an immunosuppressive environment, favoring resistance.

Consequently, I propose to investigate the potential dysregulations of the GCN2 signaling and eventual association with an inflammatory context in tumor tissues samples. Assessment of the different populations in the immune infiltrate, as well as markers of the inflammation (cytokines, NF- κ B, P38) and of the GCN2 pathway might provide first clues to support or not this hypothesis.

This under described function for GCN2 is not only critical for the understanding of the biology of cancer and predictions of sensitivity to agents targeting the ribosome biogenesis / DNA damages response control axis. The unclear non-canonical functions of GCN2 could also have implications for several other diseases. The most common risk factor for the development of diseases is aging, sharing many common features with cancer among which dysregulated nutrient sensing, proteostasis stress and genomic instability (245). Interestingly, dietary restriction is associated to increased lifespan and a protective role of GCN2 in the context of aging has been proposed in several studies (246–249). Yet, the contribution of the ISR in this process remains controversial and unclear. For instance, activation of GCN2 has been reported in old yeast compared to young ones, independently of a nutrient deprivation and of the expression of the ISR effector ATF4 (246).

Instability of genomic information encountered throughout life is setting up a favorable environment for the emergence of diseases associated with senescence and inflammation. Evidences in the literature suggest to investigate: i) the role of the GCN2-MetRS axis in the

protection against DNA damages cells have to face every day through the maintenance of the nucleolar integrity, and ii) implications of its dysfunction in the development of diseases.

Likewise, in patients with ulcerative colitis or Crohn's diseases, increased expression of GCN2 and other kinases of eIF2a (PERK and PKR) were observed compared to normal tissue. However, in a mice model of DSS-induced inflammation, the colitis was more severe and associated with high levels of oxidative stress in mice lacking GCN2 compared to mice lacking PERK or eIF2a phosphorylation (250). These observations argue in favor of the implication of the GCN2-MetRS axis in inflammatory diseases and aging likely to prevent genomic instability and ultimately the drift towards cancer.

The implication of the GCN2-MetRS axis should be also investigated in the development of the pulmonary veno-occlusive disease (PVOD), a rare form of pulmonary hypertension characterized by fibrosis and obliteration of small pulmonary vessels. Indeed, the biallelic mutations of the EIF2AK4 gene, leading to loss of function of GCN2 and development of the disease, suggests an implication of defective MetRS response that should be investigated in this inflammatory context (251,252). Exposition to chemotherapeutic agents such as mitomycin C can also induce PVOD, and is associated to a decrease in GCN2 protein levels. However, the phosphorylation of eIF2a was not affected (253), suggesting that loss of GCN2, through genetic deletions or enhanced degradation, favors inflammation and the PVOD onset independently of eIF2a signaling. Likewise, interestingly, young patients bearing a rare mutation in MARS gene (MetRS alias) display multi-organ dysfunctions among which interstitial lung disease, another pulmonary disease associated to fibrosis and inflammation (254,255).

Altogether, my findings underscore that there are open new avenues in evaluating the role of GCN2 in diseases, particularly related to inflammation, in which the genomic integrity is threatened.

ANNEXES

a. Article 2

CONTEXT OF THE STUDY

Translational reprogramming represents a crucial event underlying tumor cell adaptive response to extrinsic cues. It is now clearly demonstrated that some nutrient sensors controlling this reprogramming are also modulated by chemotherapeutic agents. Briefly, it was previously described that gemcitabine can increase the amounts of P-eIF2a (256), pemetrexed represses mTOR signaling (257), and doxorubicin disturb both of these two axes (258). This highlights that metabolic and therapeutic stresses, independently of the pharmacological class, share common molecular pathways involved in the regulation of proteostasis. Hence, both stresses contribute to the translational adaptation of cancer cells and so, to the acquisition of pro-survival features (256,258,259). Not surprisingly, resistance to therapies is associated with dysregulation of the molecular pathways controlling translational processes. For instance, hyperactivation of mTOR pathway (260,261) or increased phosphorylation of eIF2a (256,262) impairs treatments cytotoxicity.

However, most of the studies describing the influence of drugs on the activity of the nutritional sensing pathways do not take into consideration the deprived intratumoral microenvironment and are mainly performed on *in vitro* cellular models with aberrant proliferation rates. Thus, how this crosstalk between chemotherapeutic cues and metabolic stress can affect the regulation of protein synthesis in tumor cells exposed to low nutrients conditions remain unknown.

Lung adenocarcinoma (LUAD) is characterized by heterogenous perfusion rate (7) and chronic ER stress as illustrated by elevated amounts of P-eIF2a correlated with lower survival in patients (45). Thus, this type of cancer constitutes a paradigm of metabolic stress-driven tumorigenesis. In parallel, lung cancer cells are also exposed to therapeutic agents. Among them, pemetrexed is an antifolate treatment prescribed as a maintenance therapy for locally advanced and metastatic lung cancer (263). Its cytotoxic effect is based on its folate antagonist capacity,

resulting in the inhibition of several enzymes (thymidylate synthase, dihydrofolate reductase and glycinamide ribonucleotide formyltransferase) involved in folate metabolism and purine and pyrimidine synthesis (264). Consequently, pemetrexed results in the reduction of the pools of folates and nucleotides. Thus, we hypothesized that inhibiting the generation of precursors required for DNA replication and RNA synthesis might in turn also affect the protein synthesis pathway. Consistently, Reich et al. demonstrated that chemical induction of the UPR with thapsigargin or tunicamycin triggers PERK/eIF2a axis activation and its translational consequences results in resistance to antifolate treatment such as pemetrexed (265).

Hypothesis: considering eIF2a as a central integrator of microenvironmental cues and therapeutic stress, my work aimed at defining: i) whether this stress factor was localized at the crossroad of metabolic and therapeutic stresses and ii) its role on the proteosynthesis rewiring in proliferative or stressed cells.

RESULTS





“Pemetrexed Hinders Translation Inhibition upon Low Glucose in Non-Small Cell Lung Cancer Cells.”

Pieczyk M, Triki M, Laval PA, Dragic H, Cussonneau L, Fauvre J, Duret C, Aznar N, Renno T, Manié SN, Chaveroux C, Ferraro-Peyret C.

Metabolites **2021**, 11, 198. doi.org/10.3390/metabo11040198

Article

Pemetrexed Hinders Translation Inhibition upon Low Glucose in Non-Small Cell Lung Cancer Cells

Marie Piecyk^{1,2}, Mouna Triki¹, Pierre-Alexandre Laval¹, Helena Dragic¹, Laura Cussonneau³ , Joelle Favre¹, Cédric Duret¹ , Nicolas Aznar¹ , Toufic Renno¹, Serge N. Manié⁴, Cédric Chaveroux^{1,*}  and Carole Ferraro-Peyret^{1,2,*}

- ¹ Université Lyon, Cancer Research Centre of Lyon, INSERM 1052, CNRS 5286, F-69008 Lyon, France; marie.piecyk@chu-lyon.fr (M.P.); mouna.triki@lyon.unicancer.fr (M.T.); pierre-alexandre.laval@lyon.unicancer.fr (P.-A.L.); helena.dragic@lyon.unicancer.fr (H.D.); joelle.favre@inserm.fr (J.F.); cedric.duret@lyon.unicancer.fr (C.D.); nicolas.aznar@lyon.unicancer.fr (N.A.); toufic.renno@lyon.unicancer.fr (T.R.)
- ² Hospices Civils de Lyon, Biopathology of Tumours, CPE, GHE Hospital, F-69500 Bron, France
- ³ Université Clermont Auvergne, INRAE, Unité de Nutrition Humaine, UMR1019, 63122 Clermont-Ferrand, France; laura.cussonneau@inrae.fr
- ⁴ Inserm U1242, Université de Rennes, Centre de Lutte Contre le Cancer Eugène Marquis, 35042 Rennes, France; s.manie@rennes.unicancer.fr
- * Correspondence: cedric.chaveroux@lyon.unicancer.fr (C.C.); carole.ferraro-peyret@univ-lyon1.fr (C.F.-P.)



Citation: Piecyk, M.; Triki, M.; Laval, P.-A.; Dragic, H.; Cussonneau, L.; Favre, J.; Duret, C.; Aznar, N.; Renno, T.; Manié, S.N.; et al. Pemetrexed Hinders Translation Inhibition upon Low Glucose in Non-Small Cell Lung Cancer Cells. *Metabolites* **2021**, *11*, 198. <https://doi.org/10.3390/metabo11040198>

Academic Editors: Giuseppe Fiume, Camillo Palmieri, Maurizio Renna and Massimo D'Agostino

Received: 1 February 2021

Accepted: 24 March 2021

Published: 26 March 2021

Publisher's Note: MDPI stays neutral with regard to jurisdictional claims in published maps and institutional affiliations.



Copyright: © 2021 by the authors. Licensee MDPI, Basel, Switzerland. This article is an open access article distributed under the terms and conditions of the Creative Commons Attribution (CC BY) license (<https://creativecommons.org/licenses/by/4.0/>).

Abstract: Genetic alterations in non-small cell lung cancers (NSCLC) stimulate the generation of energy and biomass to promote tumor development. However, the efficacy of the translation process is finely regulated by stress sensors, themselves often controlled by nutrient availability and chemotoxic agents. Yet, the crosstalk between therapeutic treatment and glucose availability on cell mass generation remains understudied. Herein, we investigated the impact of pemetrexed (PEM) treatment, a first-line agent for NSCLC, on protein synthesis, depending on high or low glucose availability. PEM treatment drastically repressed cell mass and translation when glucose was abundant. Surprisingly, inhibition of protein synthesis caused by low glucose levels was partially dampened upon co-treatment with PEM. Moreover, PEM counteracted the elevation of the endoplasmic reticulum stress (ERS) signal produced upon low glucose availability, providing a molecular explanation for the differential impact of the drug on translation according to glucose levels. Collectively, these data indicate that the ERS constitutes a molecular crosstalk between microenvironmental stressors, contributing to translation reprogramming and proteostasis plasticity.

Keywords: protein synthesis; pemetrexed; glucose availability; ER stress signaling; NSCLC

1. Introduction

Non-small cell lung cancers (NSCLC), as many solid tumors, are characterized by genetic alterations causing metabolic rewiring [1]. A well-known example of this is that enhancement of glucose uptake and aerobic glycolysis favors the generation of energy and biomass, subsequently promoting tumor development [1–6]. However, poorly vascularized regions and the exacerbated metabolism of tumor cells can disrupt the nutritional homeostasis within the tumoral microenvironment, leading to decreased concentrations of several nutrients. Accordingly, glucose availability is often lower in different types of solid tumors [7–9]. Cell adaptation and tumor progression will thus depend on the cellular capacity to orchestrate a molecular and metabolic program to cope with such metabolic stress. One major key in this process relies on the level of activation of the nutrient sensors and their downstream molecular pathways that will modulate the cell response. The unfolded protein response (UPR) is one of those pathways. In response to glucose deprivation, UPR transiently inhibits protein synthesis and induces the production of chaperone molecules in order to restore endoplasmic reticulum (ER) homeostasis and

promote cell survival [10]. The failure of this rescue mechanism results in apoptotic cell death [11]. Three ER stress (ERS) transducers, controlling three distinct axes of the UPR, have been identified so far. Each branch is defined by a class of transmembrane ER-resident signaling components: IRE1 (inositol requiring enzyme 1), PERK (double-stranded RNA-activated protein kinase (PKR)-like ER kinase), and ATF6 (activating transcription factor 6) [12]. The activation of the PERK axis plays a pivotal role for pulmonary cell outcome upon metabolic stress, particularly the phosphorylation of its substrate, the translation initiation factor eIF2a (eukaryotic initiation factor 2a) [13–15]. Indeed, eIF2a phosphorylation provokes a cytoprotective repression of protein synthesis and cell cycle arrest [16,17]. Conversely, upon prolonged stress, recovery of protein synthesis mediated by dephosphorylation of eIF2a and mTORC1 (mechanistic target of rapamycin complex 1) activation triggers cell death [18,19].

In addition to intrinsic metabolic stress, NSCLC cells are subjected to chemotherapeutic cues. Interestingly, some of those are now described for modulating PERK signaling in non-limiting nutrient conditions. For instance, in lung cancer cells, cisplatin treatment induces a protective response mediated by ERS [20]. Therefore, eIF2a represents a common integrator of signals arising from microenvironmental and therapeutic stresses to control translation.

Pemetrexed (PEM) is one of the most-extensively prescribed antifolate chemotherapeutic drugs for maintenance therapy of patients with locally advanced or metastatic NSCLC [21,22]. This agent impedes the synthesis of the pool of folate and purine, which is crucial for the generation of nucleotides and cell replication. In addition, production impairment of the pool of purine by PEM leads to ATP depletion [23]. Although protein synthesis and biomass generation represent the most consuming energy pathway in the cell, the impact of PEM on translation remains unclear in nutrient rich conditions. Furthermore, chemical activation of the PERK-eIF2a-ATF4 axis protects tumor cells from antifolate treatment through the induction of carbon metabolism [24]. However, whether protein synthesis may be differently modulated by PEM when eIF2a is phosphorylated remains unknown.

In this study, we thus determined the consequences of PEM on biomass and translation in glucose-abundant or scarce conditions. We show that NSCLC cells, treated with PEM, are prone to a de-repression of the rate of protein synthesis under low glucose availability. Our molecular investigations revealed that this effect is associated with a down-regulation of the UPR level.

2. Results

2.1. Pemetrexed Partially Reverts Low Glucose Inhibition of Protein Synthesis

To evaluate the effect of PEM on protein synthesis when glucose availability is low, we first set up experimental conditions reflecting glucose availability in tumors *in vivo*. To this end, A549 NSCLC cells were cultivated in medium containing 10 mM or 1 mM of glucose. These concentrations are proportional to those measured respectively in the plasma and tumor interstitial fluids of mice bearing xenografts [9]. Cell mass monitoring revealed an impairment by low glucose at 72 h (Figure 1a). To avoid data misinterpretation between loss of viability and biomass, we performed our experiments at 72 h, prior to proliferation arrest or standard cell death. At this specific time point, cell counting revealed that the number of viable A549 cells in 1 mM of glucose was similar to that in the 10 mM condition, irrespective of the treatment administered (Figure 1b,c). Western blot analysis confirmed that a 72 h-glucose starvation did not lead to caspase 3 and PARP cleavage (Figure 1d) [25,26]. This result is in accordance with the previously published data indicating that NSCLC cells are resistant to glucose metabolism impairment [27]. However, upon PEM, the apoptotic activation process was lower in starved cells compared to the normal condition, suggesting a protective role for glucose deprivation at later time points.

Then cells were treated with PEM for 72 h, concomitantly to glucose starvation, and total protein mass was measured in each condition (Figure 2a). As previously observed, we found a significant loss of biomass when A549 cells were cultured in 1 mM of glucose compared to their counterparts cultivated in 10 mM. This demonstrates that low glucose alone reduces protein content by up to 43%. PEM treatment led to a 75% reduction in

protein mass in the 10 mM glucose condition. However, in low glucose medium, PEM caused a lower decrease (50%) in protein mass compared to the vehicle, suggesting that this drug dysregulated the effect of low glucose on protein homeostasis.

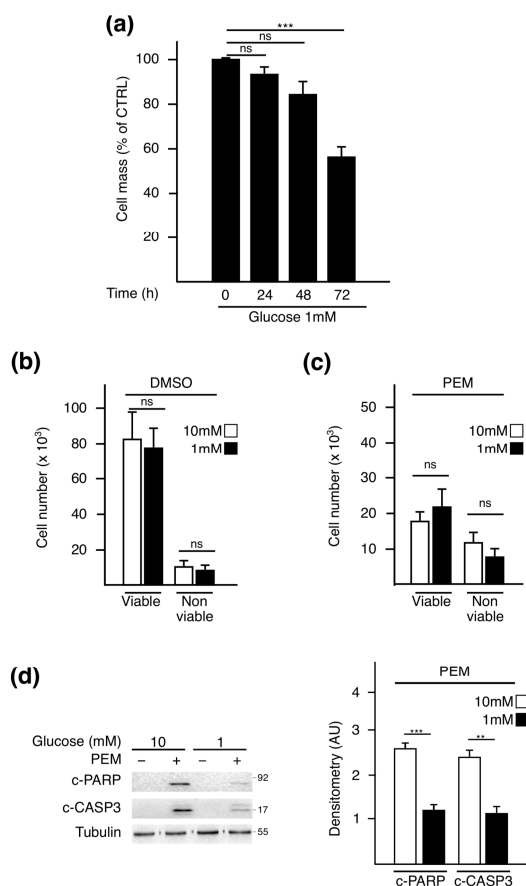


Figure 1. Experimental settings for assessing the impact of pemetrexed treatment on biomass independently of cytotoxicity. (a) Time course analysis of cell mass monitored by sulforhodamine B (SRB) assay performed on A549 cells cultured in 1 mM for the indicated time points. Control (CTRL) is referred to as the time point 0 h of deprivation. Data represent the mean of four independent experiments \pm SEM. Cell viability was assessed using trypan blue exclusion assay after 72 h of culture in medium containing 10 mM or 1 mM glucose and treated with (b) DMSO or (c) PEM (4 μ M). (d) Western blot analysis of apoptotic markers: cleaved forms of caspase 3 (c-CASP3) and PARP (c-PARP). For Western blotting, the most representative result from three independent experiments is displayed. Quantitative analysis was performed by comparing signals obtained in PEM-treated conditions normalized to tubulin using ImageJ software. ** $p < 0.01$, *** $p < 0.001$, ns: not significant.

To confirm that the PEM-mediated reduction in cell mass relied on an impaired translation, the rate of protein synthesis was assessed by using the SUnSET assay in the experimental conditions described above (Figure 2b). As expected, glucose deprivation provoked a dramatic (83%) decrease in puromycin incorporation. In non-limited glucose condition, PEM alone led to the repression (72%) of protein synthesis confirming that the

reduction in biomass in response to the drug could be attributed to the repression of protein translation. However, when PEM-treated cells were maintained in 1 mM glucose, the rate of protein synthesis was significantly higher than that in the glucose-starved condition alone. These results show that PEM treatment partially relieves translation inhibition caused by low glucose.

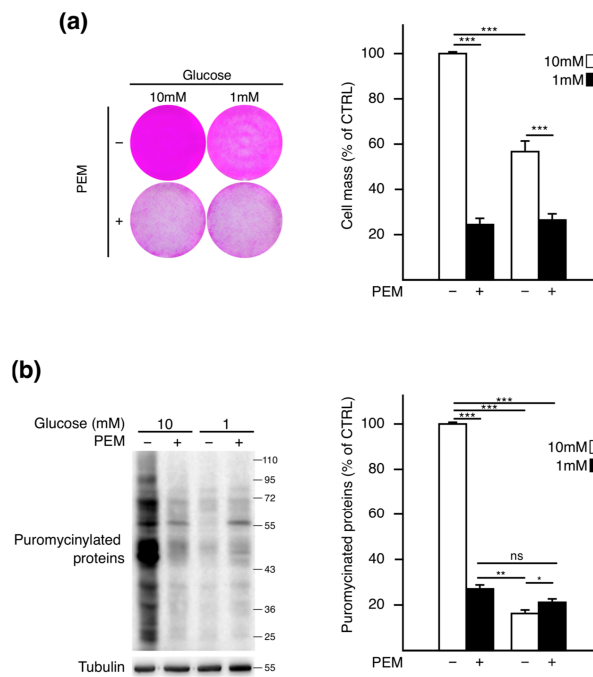


Figure 2. Protein synthesis is differently modulated according to glucose availability and pemetrexed treatment. **(a)** After 72 h, in 10 mM or 1 mM glucose-containing medium, A549 cells were treated or not with PEM (4 μ M), and protein mass was measured using a SRB assay. SRB staining was imaged before measuring the corresponding absorbance. Control (CTRL) is referred to as the 10 mM without PEM condition. Data represent the mean \pm SEM (n = 8). **(b)** The protein synthesis rate was assessed by SUnSET assay and quantified by measuring the ratio of puromycinylated proteins normalized against tubulin using the ImageJ software. Quantification data represent the mean \pm SEM (n = 3). * $p < 0.05$, ** $p < 0.01$, *** $p < 0.001$, ns: not significant.

Altogether, those data show that PEM differentially impacts the rate of protein synthesis according to the glucose availability.

2.2. Pemetrexed Treatment Alleviates UPR Induction in Low Glucose Condition

Next, we sought to determine the underlying mechanism by which PEM prevents low glucose-induced inhibition of protein synthesis. In glucose-starved cells, repression of protein synthesis is a consequence of various signaling pathways, including ERS signaling [28]. Particularly, activation of the PERK branch of the UPR leads to the inhibition of translation initiation and a selective elevation of the terminal transcription factor ATF4 (activation transcription factor 4). Thus, to investigate whether the UPR is affected in the different conditions, we first analyzed the degree of activation of ERS pathway at the studied time points (Figure 3a). We observed that ATF4 and ERS canonical target genes, CHOP (C/EBP homologous protein) and BiP (binding immunoglobulin protein), increased after 48 h of

glucose deprivation. Unlike CHOP, levels of ATF4 and BiP then decreased at 72 h, likely due to the action of molecular feedbacks on the UPR pathways [29,30], indicating that the peak of activation for ERS signaling occurs before 72 h of glucose starvation. Therefore, we then addressed whether induction of the UPR is impaired when glucose scarcity is associated with PEM at 48 h (Figure 3b). Glucose deprivation led to the activation of the ERS, as evidenced by a slower mobility of PERK, in addition to the accumulation of both ATF4 and CHOP and the canonical ATF6 marker BiP. PEM alone, compared to the vehicle, did not trigger ERS, as no change in these markers was observed. However, when glucose is low, PEM limits the increase in phosphorylated eIF2a, ATF4, CHOP, and BiP, further indicating that the weaker inducibility of the UPR by the agent is not restricted to the PERK axis. Expression analysis of canonical target genes of ATF4 (*ASNS* (asparagine synthetase), *TRB3* (tribble-3 related protein)) and ATF6 (*BIP*) confirmed the functional impairment of UPR signaling by PEM in deprived cells (Figure 3c). Indeed, although these three genes were upregulated upon low glucose, their inducibility was dramatically reduced when starvation was combined with PEM treatment.

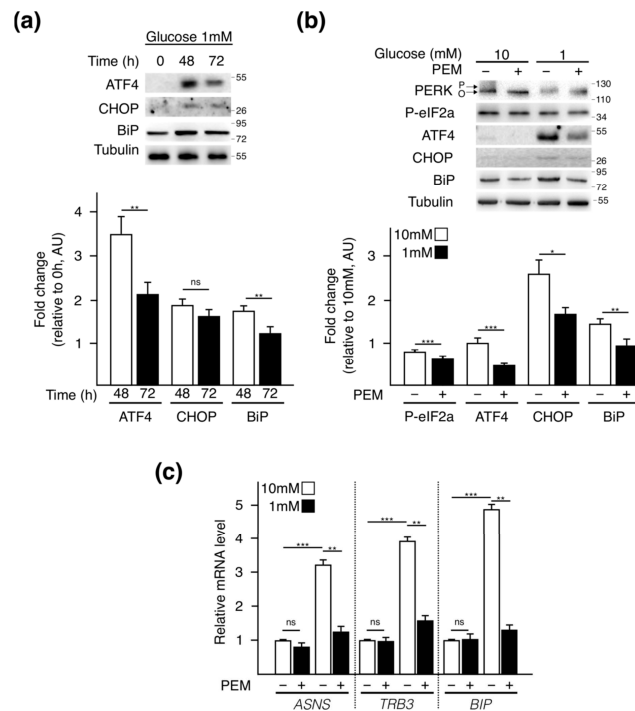


Figure 3. Pemetrexed constrains unfolded protein response (UPR) activation by glucose starvation. (a) Time course analysis of three ERS markers (ATF4, CHOP, BiP) at 48 h and 72 h following glucose deprivation. Quantification data represent the mean \pm SEM ($n = 3$). (b) A549 cells were grown for 48 h in 10 mM or 1 mM glucose-containing medium combined or not with PEM (4 μ M). Western blot analysis of UPR markers: PERK, phospho-eIF2a, ATF4, CHOP and BiP. O, inactivated and P, activated PERK. Quantification data represent the mean \pm SEM ($n = 3$). For all Western blotting, the most representative result from three independent experiments is displayed, quantification of each marker was performed using the Image J software, and data are represented as fold change relative to the indicated condition. (c) Expression measurements of canonical UPR-target genes *ASNS*, *TRB3*, and *BIP*. QPCR data represent mean \pm SEM ($n = 3$). * $p < 0.05$, ** $p < 0.01$, *** $p < 0.001$, ns: not significant.

Taken together, these results indicate that PEM limits UPR activation by low glucose levels, providing a mechanistic explanation as to the lower translation repression by the drug when glucose is scarce.

3. Discussion

This study aimed at determining whether PEM impairs protein homeostasis, and to unravel its crosstalk with glucose availability. Our data revealed that PEM treatment decreases translation activity in nutrient-rich conditions. However, in the context of repressed translation by glucose scarcity, PEM treatment dampened UPR activation and partially restored protein synthesis.

Our results provide a novel insight into the mode of action of PEM by showing that the drug counteracts protein biosynthesis when cells have a non-limited access to nutrients in a mechanism that is independent of the ERS signaling. In this context, the mode of action of PEM could implicate several molecular events converging to repressing protein synthesis. Knowing that PEM targets enzymes involved in decreasing nucleotide biosynthesis and pool, one could expect an alteration of mRNA synthesis [31–34]. However, this agent leads to an induction of PD-L1 expression in NSCLC cells, indicating that gene expression upon PEM is not totally repressed and might be selective [35]. As methotrexate, another antifolate compound, increases the AMP/ATP ratio, indicating that it depletes cells of ATP [23], PEM-induced reduction of the cellular pool of tetrahydrofolate likely diminishes the pool of ATP provoking a dysfunction of protein biosynthesis, one of the most consuming metabolic pathways [36]. Furthermore, alteration of energy metabolism represses the molecular axis that could contribute to translation inhibition. Indeed, several studies performed in complete medium reported that PEM inhibits mTORC1 signaling, a key regulator of cell growth, in an AMPK-dependent manner [37]. Repression of mTORC1 compromises the initiation and elongation stages through the dephosphorylation of 4EBP1 and S6K1/2 and by impairing ribosome biogenesis [38–40].

The nutritional context is emerging as a determinant of anticancer drug efficacy. Tumor cells evolving in nutrient-poor regions undergo dedifferentiation [41]. Acquisition of stemness features driven by metabolic stress including glucose starvation or hypoxia, triggers lower translation rates, particularly provoked by the repression of the mTOR pathway and phosphorylation of eIF2a [42,43]. Accordingly, rapamycin treatment, which mimics a starvation situation, antagonizes the cytotoxic effect in NSCLC cells [44,45]. The subsequent proliferation arrest and changes in tumor cell phenotype under stressed conditions might explain the resistance to PEM. Indeed, under severe hypoxia, expression of key enzymes and transporters in folate metabolism and nucleoside homeostasis is down-regulated [46]. Raz et al. showed that hypoxia in solid tumors, by inducing cell cycle arrest, prevents antifolates from inducing DNA damage and apoptosis [47]. Furthermore, a recent work by Postovit's group showed that the repression of mTOR caused by hypoxia or paclitaxel treatment promotes a 5'UTR selective translation of NANOG, SNAIL, and NODAL isoforms and the acquisition of stem-cell phenotypes and resistance to the drug [43]. Nonetheless, sensitivity to chemotherapy is restored upon ISRIB administration, a small molecule preventing eIF2a phosphorylation, by alleviating translation repression caused by stress [43].

Overall, further investigations are needed to comprehend whether the nutritional context impairs the efficacy of PEM treatment in clinics. In line with a previous study describing a protective role for the PERK pathway upon antimetabolites treatment [24], our results indicate that harsh nutritional microenvironment, reflecting the tumor glucose concentration, indeed protects against PEM in a lung cancer model mutated for KRAS. At the clinical level, these results propose the importance of assessing the stress degree in tumors for patient stratification and personalized adaptation of chemotherapeutic regimens. Recent data presented by the group of Dr. Koromilas confirm that increased phospho-eIF2a is associated with a poorer survival of patients [48]. Functionally, its pharmacological blockade by ISRIB prolonged survival of NSCLC mice models. These data, in conjunction

with our findings, provide strongly compelling evidence to assess phospho-eIF2a in NSCLC tumors as a prognostic and stratification marker for PEM eligibility. Furthermore, the moderate translation recovery in starved cells upon PEM treatment attributed to partial induction of phospho-eIF2a axis likely participate in PEM resistance. Complete abolition of this stress integrator by ISRIB might represent a therapeutic vulnerability to ameliorate PEM sensitivity to NSCLC cells.

4. Materials and Methods

4.1. Cell Culture and Treatments

A549 cells were purchased from the ATCC. They were routinely cultured in Dulbecco's Modified Eagle Medium DMEM high glucose (GIBCO) supplemented with 10% fetal bovine serum (FBS) and 1% *v/v* penicillin/streptomycin (GIBCO) and were maintained at 37 °C in a 5% CO₂ incubator. All of the treatments (chemotherapy and/or glucose deprivation) were performed the day after plating. Glucose deprivation was performed using Dulbecco's Modified Eagle Medium devoid of glucose and sodium pyruvate (GIBCO). One percent penicillin/streptomycin (GIBCO), 1% sodium pyruvate, and 10% dialyzed FBS were subsequently added. The respective control medium for these experiments were also supplemented with glucose 200 g/L (GIBCO) to reach a final concentration of 10 or 1 mM. When necessary, chemotherapeutic treatment was performed daily using Pemetrexed generously provided by the Centre Léon Bérard at a final concentration of 4 µM.

4.2. Cell Extracts and Western Blot Analysis

To perform Western blot analysis, A549 cells were seeded onto 6-well plates (2.50 × 10⁵ cells per well). Then, cells were treated with Pemetrexed and/or deprived of glucose for 72 h. Whole cell extracts were prepared from cultured cells lysed in RIPA protein buffer containing protease and phosphatase inhibitors (Roche) at 4 °C and obtained by centrifugation at 13,000 × *g* for 20 min at 4 °C. Protein concentrations of the cellular extracts were determined using the DC Protein Assay (Bio-Rad, Hercules, CA, USA). Equal amounts of proteins (40 µg) were separated by SDS-PAGE and then transferred onto nitrocellulose membranes (Bio-Rad). Membranes were incubated in blocking buffer, 5% milk or Bovine Serum Albumin (BSA) in Tris-Buffered Saline/Tween 20 (TBST), for 1 h at room temperature, then incubated overnight at 4 °C with the appropriate primary antibodies, diluted in TBST containing 5% milk or BSA. Membranes were washed three times with TBST, incubated for 1 h at room temperature with the appropriate secondary antibodies, diluted in TBST containing 5% milk, and again washed three times with TBST. Detection by enhanced chemiluminescence was performed using the Clarity Western ECL substrate (Bio-Rad). Tubulin was used as a loading control. The primary antibodies used were purchased with the indicated dilution either from BD Biosciences: BiP (1/1000, 610978); Santa Cruz Biotechnology: ATF4 (1/1000, sc-200 and sc-390063), CHOP (1/200, sc-7351) and α-Tubulin (1/1000, sc-23950); from Cell Signaling Technology: PERK (1/1000, 3192S), c-Caspase 3 (1/1000, 9664), c-PARP (1/1000, 5625S), phospho-eIF2a (1/1000, 3398S); or from Millipore: Puromycin clone 12D10 (1/10,000, MABE343). The HRP-conjugated secondary antibodies were supplied by Cell Signaling Technology (1/10,000, anti-rabbit and anti-mouse antibodies, respectively, 7074S and 7076S). Western blot images are representative of three independent experiments.

4.3. SUnSET Assay

Rates of protein synthesis were evaluated using the surface sensing of translation (SUnSET) method as previously described [49]. A549 cells were seeded onto 6-well plates (2.50 × 10⁵ cells per well) and treated with Pemetrexed and/or deprived of glucose for 72 h at 37 °C, 5% CO₂. Fifteen minutes before being harvested and processed to prepare whole cell extracts in RIPA buffer, cells were incubated with 5 µg/mL of puromycin (Sigma P9620), directly added into the medium. The amount of puromycin incorporated into nascent peptides was then evaluated by Western blot analysis on 15 µg of proteins using

anti-puromycin antibody purchased from Millipore (MABE343) and quantified with the ImageJ software (National Institutes of Health, Bethesda, MD, USA).

4.4. RNA Extraction and RT-qPCR

Total cellular RNA was extracted after 48 h of treatment using TRIzol Reagent (Life Technologies) according to the manufacturer's protocol. For cDNA synthesis, 0.5 µg of RNA were reverse transcribed using Superscript II reverse transcriptase (Invitrogen, ref: 18064014) with random primers (Invitrogen, ref: S0142), according to the manufacturer's instructions. cDNA was then amplified by qPCR using specific primers listed below and the SYBR Green Master Mix (Bio-Rad). qPCR was performed using the CFX connect real-time PCR system (Bio-Rad). Relative quantification was assessed using a standard curve-based method. Expression of target genes (*TRB3* Fw: TGGTACCCAGCTCCTCTACG Rev: GACAAAGCGACACAGCTTGA; *BIP* Fw: CTGTCCAGGCTGGTGTGCTCT Rev: CTGGTAGGCACCACTGTGTTC; *ASNS* Fw: CTGTGAAGAACAACCTCAGGATC; Rev: AACAGAGTGGCAGCAACCAAGC) was normalized against 3 endogenous mRNA levels (*18S* Fw: GAACGCCACTGTCCCTCTA Rev: GTTGGTGGAGCGATTGTCT, *Actin* Fw: TCCCTGGAGAAGAGCTACGA Rev: AGCACTGTGTGGCGTACAG, *HPRT* Fw: TGACCTTGATTATTTGCATACC Rev: CGAGCAAGACGTTTCAGTCT), used as internal controls. QPCR experiments were repeated at least three times in duplicate.

4.5. Cell Mass Assay

Cell mass biosynthesis was assessed by using the sulforhodamine B (SRB) assay. A549 cells were seeded onto 6-well plates (2.50×10^5 cells per well) and treated with Pemetrexed and/or deprived of glucose for 24 to 72 h at 37 °C, 5% CO₂. After removing the medium, wells were washed with PBS. Then, 1 mL of 10% trichloroacetic acid was added and after 1 h of incubation at 4 °C, the plates were flicked and washed three times with tap water before being dried at 37 °C for 1 h. The wells were then stained with 1.5 mL of SRB solution (0.057% in 1% acetic acid) for 30 min at room temperature under gentle agitation. Plates were flicked and washed three times with 1% acetic acid and air-dried for at least 1 h. Finally, 1.5 mL of 10mM Tris base was added and shaken vigorously for 15 min. The absorbance was measured using Tecan Infinite M200 Pro at a wavelength of 510 nm.

4.6. Cell Viability Assay

Cell viability was measured using the trypan blue dye exclusion assay. A549 cells were seeded onto 6-well plates (2.5×10^5 cells per well) and treated with Pemetrexed and/or deprived of glucose for 72 h at 37 °C, 5% CO₂. First, the medium was collected and centrifuged twice at $500 \times g$ for 5 min. Dead cells were then resuspended in 100 µL and counted. Second, adherent cells were washed with PBS and detached with 500 µL of accutase (ref 11-007, GE Life Sciences/PAA Laboratories) for 10–15 min at 37 °C. Detached cells were resuspended in trypan blue dye at a ratio of 1:1. After 5 min of incubation, viable (stainless) and non-viable (blue) cells were counted in all studied conditions using a Glasstic slide from Kova International (ref: 87144).

4.7. Statistical Analyses

Statistical analyses were performed using the SigmaPlot software (Systat Software, San Jose, CA, USA) via one-way ANOVA with Tukey's or Kruskal–Wallis multiple comparisons test. All data are expressed as means \pm SEM of the indicated number of experiments, * $p < 0.05$, ** $p < 0.01$, *** $p < 0.001$.

Author Contributions: Conceptualization, C.C. and C.F.-P.; funding acquisition, C.C., S.N.M., and C.F.-P.; data curation, M.P. and C.D.; investigation, M.P., H.D., L.C., J.F., C.D., M.T., C.F.-P., and C.C.; resources, P.-A.L., N.A., S.N.M., and T.R.; supervision, C.C. and C.F.-P.; writing, C.C. and C.F.-P. All authors have read and agreed to the published version of the manuscript.

Funding: This work was supported by the Cancéropôle Lyon Auvergne Rhône-Alpes (R19152CC, R19075CC), Region Auvergne Rhone-Alpes (19 010898 01—41024), Fondation ARC pour Recherche sur le Cancer (R16173CC), Ligue Nationale contre le Cancer (R17167CC, R19007CC), PLASCAN (BioMHet, MiStiM'Plast, 17IA66ANR-PLASCAN-MEHLEN), CNRS Prematuration program (NA-7-07-20) and Marie Skłodowska-Curie fellowship (grant agreement n°839398).

Institutional Review Board Statement: Not applicable.

Informed Consent Statement: Not applicable.

Acknowledgments: We thank Brigitte Manship for revisions and English editing of the manuscript, Yohann Chaix and the Lyon Ingénierie Projets for funding management and all our colleagues in the laboratory for technical support and helpful discussions.

Conflicts of Interest: The authors declare no conflict of interest.

References

- Vazquez, A.; Liu, J.; Zhou, Y.; Oltvai, Z.N. Catabolic Efficiency of Aerobic Glycolysis: The Warburg Effect Revisited. *BMC Syst. Biol.* **2010**, *4*, 58. [\[CrossRef\]](#) [\[PubMed\]](#)
- DeBerardinis, R.J.; Mancuso, A.; Daikhin, E.; Nissim, I.; Yudkoff, M.; Wehrli, S.; Thompson, C.B. Beyond Aerobic Glycolysis: Transformed Cells Can Engage in Glutamine Metabolism That Exceeds the Requirement for Protein and Nucleotide Synthesis. *Proc. Natl. Acad. Sci. USA* **2007**, *104*, 19345–19350. [\[CrossRef\]](#) [\[PubMed\]](#)
- Elstrom, R.L.; Bauer, D.E.; Buzzai, M.; Karnauskas, R.; Harris, M.H.; Plas, D.R.; Zhuang, H.; Cinalli, R.M.; Alavi, A.; Rudin, C.M.; et al. Akt Stimulates Aerobic Glycolysis in Cancer Cells. *Cancer Res.* **2004**, *64*, 3892–3899. [\[CrossRef\]](#)
- Flier, J.S.; Mueckler, M.M.; Usher, P.; Lodish, H.F. Elevated Levels of Glucose Transport and Transporter Messenger RNA Are Induced by Ras or Src Oncogenes. *Sci. New Ser.* **1987**, *235*, 1492–1495. [\[CrossRef\]](#) [\[PubMed\]](#)
- Shim, H.; Dolde, C.; Lewis, B.C.; Wu, C.-S.; Dang, G.; Jungmann, R.A.; Dalla-Favera, R.; Dang, C.V. C-Myc Transactivation of LDH-A: Implications for Tumor Metabolism and Growth. *Proc. Natl. Acad. Sci. USA* **1997**, *94*, 6658–6663. [\[CrossRef\]](#) [\[PubMed\]](#)
- Weinberg, F.; Hamanaka, R.; Wheaton, W.W.; Weinberg, S.; Joseph, J.; Lopez, M.; Kalyanaraman, B.; Mutlu, G.M.; Budinger, G.R.S.; Chandel, N.S. Mitochondrial Metabolism and ROS Generation Are Essential for Kras-Mediated Tumorigenicity. *Proc. Natl. Acad. Sci. USA* **2010**, *107*, 8788–8793. [\[CrossRef\]](#) [\[PubMed\]](#)
- Kamphorst, J.J.; Nofal, M.; Commisso, C.; Hackett, S.R.; Lu, W.; Grabocka, E.; Vander Heiden, M.G.; Miller, G.; Drebin, J.A.; Bar-Sagi, D.; et al. Human Pancreatic Cancer Tumors Are Nutrient Poor and Tumor Cells Actively Scavenge Extracellular Protein. *Cancer Res.* **2015**, *75*, 544–553. [\[CrossRef\]](#)
- Satoh, K.; Yachida, S.; Sugimoto, M.; Oshima, M.; Nakagawa, T.; Akamoto, S.; Tabata, S.; Saitoh, K.; Kato, K.; Sato, S.; et al. Global Metabolic Reprogramming of Colorectal Cancer Occurs at Adenoma Stage and Is Induced by MYC. *Proc. Natl. Acad. Sci. USA* **2017**, *114*, E7697–E7706. [\[CrossRef\]](#) [\[PubMed\]](#)
- Sullivan, M.R.; Danai, L.V.; Lewis, C.A.; Chan, S.H.; Gui, D.Y.; Kunchok, T.; Dennstedt, E.A.; Vander Heiden, M.G.; Muir, A. Quantification of Microenvironmental Metabolites in Murine Cancers Reveals Determinants of Tumor Nutrient Availability. *Elife* **2019**, *8*. [\[CrossRef\]](#)
- Ron, D.; Walter, P. Signal Integration in the Endoplasmic Reticulum Unfolded Protein Response. *Nat. Rev. Mol. Cell Biol.* **2007**, *8*, 519–529. [\[CrossRef\]](#)
- Tabas, I.; Ron, D. Integrating the Mechanisms of Apoptosis Induced by Endoplasmic Reticulum Stress. *Nat. Cell Biol.* **2011**, *13*, 184–190. [\[CrossRef\]](#)
- Urra, H.; Dufey, E.; Avril, T.; Chevet, E.; Hetz, C. Endoplasmic Reticulum Stress and the Hallmarks of Cancer. *Trends Cancer* **2016**, *2*, 252–262. [\[CrossRef\]](#) [\[PubMed\]](#)
- Pakos-Zebrucka, K.; Koryga, I.; Mnich, K.; Ljujic, M.; Samali, A.; Gorman, A.M. The Integrated Stress Response. *EMBO Rep.* **2016**, *17*, 1374–1395. [\[CrossRef\]](#)
- Huber, A.-L.; Lebeau, J.; Guillaumot, P.; Pétrilli, V.; Malek, M.; Chilloux, J.; Fauvet, F.; Payen, L.; Kfoury, A.; Renno, T.; et al. P58IPK-Mediated Attenuation of the Proapoptotic PERK-CHOP Pathway Allows Malignant Progression upon Low Glucose. *Mol. Cell* **2013**, *49*, 1049–1059. [\[CrossRef\]](#)
- Van 't Wout, E.F.A.; Hiemstra, P.S.; Marciniak, S.J. The Integrated Stress Response in Lung Disease. *Am. J. Respir. Cell Mol. Biol.* **2014**, *50*, 1005–1009. [\[CrossRef\]](#)
- Muaddi, H.; Majumder, M.; Peidis, P.; Papadakis, A.I.; Holcik, M.; Scheuner, D.; Kaufman, R.J.; Hatzoglou, M.; Koromilas, A.E. Phosphorylation of EIF2 α at Serine 51 Is an Important Determinant of Cell Survival and Adaptation to Glucose Deficiency. *Mol. Biol. Cell* **2010**, *21*, 3220–3231. [\[CrossRef\]](#)
- Hamanaka, R.B.; Bennett, B.S.; Cullinan, S.B.; Diehl, J.A. PERK and GCN2 Contribute to EIF2 α Phosphorylation and Cell Cycle Arrest after Activation of the Unfolded Protein Response Pathway. *Mol. Biol. Cell* **2005**, *16*, 5493–5501. [\[CrossRef\]](#) [\[PubMed\]](#)
- Guha, P.; Kaptan, E.; Gade, P.; Kalvakolanu, D.V.; Ahmed, H. Tunicamycin Induced Endoplasmic Reticulum Stress Promotes Apoptosis of Prostate Cancer Cells by Activating MTORC1. *Oncotarget* **2017**, *8*, 68191–68207. [\[CrossRef\]](#)

19. Han, J.; Back, S.H.; Hur, J.; Lin, Y.-H.; Gildersleeve, R.; Shan, J.; Yuan, C.L.; Krokowski, D.; Wang, S.; Hatzoglou, M.; et al. ER-Stress-Induced Transcriptional Regulation Increases Protein Synthesis Leading to Cell Death. *Nat. Cell Biol.* **2013**, *15*, 481–490. [[CrossRef](#)] [[PubMed](#)]
20. Shi, S.; Tan, P.; Yan, B.; Gao, R.; Zhao, J.; Wang, J.; Guo, J.; Li, N.; Ma, Z. ER Stress and Autophagy Are Involved in the Apoptosis Induced by Cisplatin in Human Lung Cancer Cells. *Oncol. Rep.* **2016**, *35*, 2606–2614. [[CrossRef](#)] [[PubMed](#)]
21. Cohen, M.H.; Justice, R.; Pazdur, R. Approval Summary: Pemetrexed in the Initial Treatment of Advanced/Metastatic Non-Small Cell Lung Cancer. *Oncologist* **2009**, *14*, 930–935. [[CrossRef](#)]
22. Cohen, M.H.; Cortazar, P.; Justice, R.; Pazdur, R. Approval Summary: Pemetrexed Maintenance Therapy of Advanced/Metastatic Nonsquamous, Non-Small Cell Lung Cancer (NSCLC). *Oncologist* **2010**, *15*, 1352–1358. [[CrossRef](#)]
23. Tedeschi, P.M.; Johnson-Farley, N.; Lin, H.; Shelton, L.M.; Ooga, T.; Mackay, G.; Van Den Broek, N.; Bertino, J.R.; Vazquez, A. Quantification of Folate Metabolism Using Transient Metabolic Flux Analysis. *Cancer Metab.* **2015**, *3*. [[CrossRef](#)] [[PubMed](#)]
24. Reich, S.; Nguyen, C.D.L.; Has, C.; Steltgens, S.; Soni, H.; Coman, C.; Freyberg, M.; Bichler, A.; Seifert, N.; Conrad, D.; et al. A Multi-Omics Analysis Reveals the Unfolded Protein Response Regulon and Stress-Induced Resistance to Folate-Based Antimetabolites. *Nat. Commun.* **2020**, *11*, 2936. [[CrossRef](#)]
25. Rasheva, V.I.; Domingos, P.M. Cellular Responses to Endoplasmic Reticulum Stress and Apoptosis. *Apoptosis* **2009**, *14*, 996–1007. [[CrossRef](#)] [[PubMed](#)]
26. Uppala, J.K.; Gani, A.R.; Ramaiah, K.V.A. Chemical Chaperone, TUDCA Unlike PBA, Mitigates Protein Aggregation Efficiently and Resists ER and Non-ER Stress Induced HepG2 Cell Death. *Sci. Rep.* **2017**, *7*. [[CrossRef](#)]
27. Goodwin, J.; Neugent, M.L.; Lee, S.Y.; Choe, J.H.; Choi, H.; Jenkins, D.M.R.; Ruthenborg, R.J.; Robinson, M.W.; Jeong, J.Y.; Wake, M.; et al. The Distinct Metabolic Phenotype of Lung Squamous Cell Carcinoma Defines Selective Vulnerability to Glycolytic Inhibition. *Nat. Commun.* **2017**, *8*, 15503. [[CrossRef](#)]
28. Almanza, A.; Carlesso, A.; Chintha, C.; Creedican, S.; Doultinos, D.; Leuzzi, B.; Luis, A.; McCarthy, N.; Montibeller, L.; More, S.; et al. Endoplasmic Reticulum Stress Signalling—From Basic Mechanisms to Clinical Applications. *FEBS J.* **2019**, *286*, 241–278. [[CrossRef](#)] [[PubMed](#)]
29. Brush, M.H.; Weiser, D.C.; Shenolikar, S. Growth Arrest and DNA Damage-Inducible Protein GADD34 Targets Protein Phosphatase 1 α to the Endoplasmic Reticulum and Promotes Dephosphorylation of the α Subunit of Eukaryotic Translation Initiation Factor 2. *Mol. Cell. Biol.* **2003**, *23*, 1292–1303. [[CrossRef](#)]
30. Yan, W.; Frank, C.L.; Korh, M.J.; Sopher, B.L.; Novoa, I.; Ron, D.; Katze, M.G. Control of PERK EIF2 α Kinase Activity by the Endoplasmic Reticulum Stress-Induced Molecular Chaperone P58IPK. *Proc. Natl. Acad. Sci. USA* **2002**, *99*, 15920–15925. [[CrossRef](#)] [[PubMed](#)]
31. Taylor, E.C.; Kuhnt, D.; Shih, C.; Rinzel, S.M.; Grindey, G.B.; Barredo, J.; Jannatipour, M.; Moran, R.G. A Dideazetetrahydrofolate Analog Lacking a Chiral Center at C-6: N-[4-[2-(2-Amino-3,4-Dihydro-4-Oxo-7H-Pyrrolo[2,3-d]Pyrimidin-5yl)Ethyl]Benzoyl]-L-Glutamic Acid Is an Inhibitor of Thymidylate Synthase. *J. Med. Chem.* **1992**, *35*, 4450–4454. [[CrossRef](#)]
32. Shih, C.; Chen, V.J.; Gossett, L.S.; Gates, S.B.; MacKellar, W.C.; Habeck, L.L.; Shackelford, K.A.; Mendelsohn, L.G.; Soose, D.J.; Patel, V.F.; et al. LY231514, a Pyrrolo[2,3-d]Pyrimidine-Based Antifolate That Inhibits Multiple Folate-Requiring Enzymes. *Cancer Res.* **1997**, *57*, 1116–1123. [[PubMed](#)]
33. Chen, V.J.; Bewley, J.R.; Andis, S.L.; Schultz, R.M.; Iversen, P.W.; Shih, C.; Mendelsohn, L.G.; Seitz, D.E.; Tonkinson, J.L. Preclinical Cellular Pharmacology of LY231514 (MTA): A Comparison with Methotrexate, LY309887 and Raltitrexed for Their Effects on Intracellular Folate and Nucleoside Triphosphate Pools in CCRF-CEM Cells. *Br. J. Cancer* **1998**, *78*, 27–34. [[CrossRef](#)]
34. Racanelli, A.C.; Rothbart, S.B.; Heyer, C.L.; Moran, R.G. Therapeutics by Cytotoxic Metabolite Accumulation: Pemetrexed Causes ZMP Accumulation, AMPK Activation, and MTOR Inhibition. *Cancer Res.* **2009**, *69*, 5467–5474. [[CrossRef](#)]
35. Lu, C.-S.; Lin, C.-W.; Chang, Y.-H.; Chen, H.-Y.; Chung, W.-C.; Lai, W.-Y.; Ho, C.-C.; Wang, T.-H.; Chen, C.-Y.; Yeh, C.-L.; et al. Antimetabolite Pemetrexed Primes a Favorable Tumor Microenvironment for Immune Checkpoint Blockade Therapy. *J. Immunother. Cancer* **2020**, *8*, e001392. [[CrossRef](#)]
36. Lindqvist, L.M.; Tandoc, K.; Topisirovic, I.; Furic, L. Cross-Talk between Protein Synthesis, Energy Metabolism and Autophagy in Cancer. *Curr. Opin. Genet. Dev.* **2018**, *48*, 104–111. [[CrossRef](#)] [[PubMed](#)]
37. Rothbart, S.B.; Racanelli, A.C.; Moran, R.G. Pemetrexed Indirectly Activates the Metabolic Kinase AMPK in Human Carcinomas. *Cancer Res.* **2010**, *70*, 10299–10309. [[CrossRef](#)] [[PubMed](#)]
38. Brunn, G.J.; Hudson, C.C.; Sekulić, A.; Williams, J.M.; Hosoi, H.; Houghton, P.J.; Lawrence, J.C.; Abraham, R.T. Phosphorylation of the Translational Repressor PHAS-I by the Mammalian Target of Rapamycin. *Science* **1997**, *277*, 99–101. [[CrossRef](#)] [[PubMed](#)]
39. Burnett, P.E.; Barrow, R.K.; Cohen, N.A.; Snyder, S.H.; Sabatini, D.M. RAFT1 Phosphorylation of the Translational Regulators P70 S6 Kinase and 4E-BP1. *Proc. Natl. Acad. Sci. USA* **1998**, *95*, 1432–1437. [[CrossRef](#)] [[PubMed](#)]
40. Holz, M.K.; Ballif, B.A.; Gygi, S.P.; Blenis, J. MTOR and S6K1 Mediate Assembly of the Translation Preinitiation Complex through Dynamic Protein Interchange and Ordered Phosphorylation Events. *Cell* **2005**, *123*, 569–580. [[CrossRef](#)] [[PubMed](#)]
41. Pan, M.; Reid, M.A.; Lowman, X.H.; Kulkarni, R.P.; Tran, T.Q.; Liu, X.; Yang, Y.; Hernandez-Davies, J.E.; Rosales, K.K.; Li, H.; et al. Regional Glutamine Deficiency in Tumours Promotes De-Differentiation through Inhibition of Histone Demethylation. *Nat. Cell Biol.* **2016**, *18*, 1090–1101. [[CrossRef](#)] [[PubMed](#)]

42. Brugarolas, J.; Lei, K.; Hurley, R.L.; Manning, B.D.; Reiling, J.H.; Hafen, E.; Witters, L.A.; Ellisen, L.W.; Kaelin, W.G. Regulation of MTOR Function in Response to Hypoxia by REDD1 and the TSC1/TSC2 Tumor Suppressor Complex. *Genes Dev.* **2004**, *18*, 2893–2904. [[CrossRef](#)] [[PubMed](#)]
43. Jewer, M.; Lee, L.; Leibovitch, M.; Zhang, G.; Liu, J.; Findlay, S.D.; Vincent, K.M.; Tandoc, K.; Dieters-Castator, D.; Quail, D.F.; et al. Translational Control of Breast Cancer Plasticity. *Nat. Commun.* **2020**, *11*. [[CrossRef](#)] [[PubMed](#)]
44. Markova, B.; Hähnel, P.S.; Kasper, S.; Herberitz, S.; Schuler, M.; Breitenbuecher, F. Pharmacologic Inhibition of MTOR Antagonizes the Cytotoxic Activity of Pemetrexed in Non-Small Cell Lung Cancer. *J. Cancer Res. Clin. Oncol.* **2012**, *138*, 545–554. [[CrossRef](#)] [[PubMed](#)]
45. Peng, T.; Golub, T.R.; Sabatini, D.M. The Immunosuppressant Rapamycin Mimics a Starvation-Like Signal Distinct from Amino Acid and Glucose Deprivation. *Mol. Cell. Biol.* **2002**, *22*, 5575–5584. [[CrossRef](#)] [[PubMed](#)]
46. Semenza, G.L. Hypoxia-inducible Factors: Coupling Glucose Metabolism and Redox Regulation with Induction of the Breast Cancer Stem Cell Phenotype. *EMBO J.* **2017**, *36*, 252–259. [[CrossRef](#)]
47. Raz, S.; Sheban, D.; Gonen, N.; Stark, M.; Berman, B.; Assaraf, Y.G. Severe Hypoxia Induces Complete Antifolate Resistance in Carcinoma Cells Due to Cell Cycle Arrest. *Cell Death Dis.* **2014**, *5*, e1067. [[CrossRef](#)] [[PubMed](#)]
48. Ghaddar, N.; Wang, S.; Woodvine, B.; Krishnamoorthy, J.; Darini, C.; Van Hoef, V.; Popper, H.; Topisirovic, I.; Larsson, O.; Le Quesne, J.; et al. The Integrated Stress Response Exposes a Therapeutic Vulnerability in KRAS Driven Lung Cancer. *Eur. J. Cancer* **2020**, *138*, S23. [[CrossRef](#)]
49. Schmidt, E.K.; Clavarino, G.; Ceppi, M.; Pierre, P. SUnSET, a Nonradioactive Method to Monitor Protein Synthesis. *Nat. Methods* **2009**, *6*, 275–277. [[CrossRef](#)]

b. Article 3

CONTEXT OF THE STUDY

Cells exposed to nutrient scarcity have to face endoplasmic reticulum stress and increased ROS. In this study, our group demonstrated that the stress response induced by the endoplasmic reticulum resident protein PERK contributes to the antioxidant response upon metabolic stress not only through the direct activation of NRF2, a major actor involved in the response to oxidative stress, but also by promoting NRF2 expression through the induction of the transcription factor ATF4.

RESULTS

"ATF4-Dependent NRF2 Transcriptional Regulation Promotes Antioxidant Protection during Endoplasmic Reticulum Stress.



Sarcinelli C, Dragic H, **Pieczyk M**, Barbet V, Duret C, Barthelaix A, Ferraro-Peyret C, Fauvre J, Renno T, Chaveroux C, Manié SN. *Cancers (Basel)*. 2020 Mar 1;12(3):569. doi: 10.3390/cancers12030569.

CONTRIBUTION

During the publication process of this study, I performed western blotting and RT-qPCR for the revised version of the article.

Article

ATF4-Dependent NRF2 Transcriptional Regulation Promotes Antioxidant Protection during Endoplasmic Reticulum Stress

Carmen Sarcinelli ¹, Helena Dragic ¹, Marie Piecyk ¹, Virginie Barbet ¹, Cédric Duret ¹, Audrey Barthelaix ², Carole Ferraro-Peyret ^{1,3}, Joelle Fauvre ¹, Toufic Renno ¹ , Cédric Chaveroux ^{1,*}  and Serge N. Manié ^{1,4,*}

¹ Centre de Recherche en Cancérologie de Lyon, INSERM U1052, CNRS 5286, Centre Léon Bérard, Univ Lyon, Université Claude Bernard Lyon 1, 69373 Lyon, France; carmen.sarcinelli@gmail.com (C.S.); Helena.DRAGIC@lyon.unicancer.fr (H.D.); Marie.PIECYK@lyon.unicancer.fr (M.P.); virg.fauvre@free.fr (V.B.); cedric.duret@lyon.unicancer.fr (C.D.); CAROLE.FERRARO-PEYRET@adm.univ-lyon1.fr (C.F.-P.); joelle.fauvre@inserm.fr (J.F.); toufic.renno@lyon.unicancer.fr (T.R.)

² Institute for Regenerative Medicine and Biotherapy, 34295 Montpellier, France; audrey.barthelaix@inserm.fr

³ Hospices Civils de Lyon, Centre de pathologie Est, 69500 Bron, France

⁴ Inserm U1242, Université de Rennes, Centre de Lutte Contre le Cancer Eugène Marquis, 35042 Rennes, France

* Correspondence: cedric.chaveroux@lyon.unicancer.fr (C.C.); s.manie@rennes.unicancer.fr (S.N.M.)

Received: 4 February 2020; Accepted: 27 February 2020; Published: 1 March 2020



Abstract: Endoplasmic reticulum (ER) stress generates reactive oxygen species (ROS) that induce apoptosis if left unabated. To limit oxidative insults, the ER stress PKR-like endoplasmic reticulum Kinase (PERK) has been reported to phosphorylate and activate nuclear factor erythroid 2-related factor 2 (NRF2). Here, we uncover an alternative mechanism for PERK-mediated NRF2 regulation in human cells that does not require direct phosphorylation. We show that the activation of the PERK pathway rapidly stimulates the expression of NRF2 through activating transcription factor 4 (ATF4). In addition, NRF2 activation is late and largely driven by reactive oxygen species (ROS) generated during late protein synthesis recovery, contributing to protecting against cell death. Thus, PERK-mediated NRF2 activation encompasses a PERK-ATF4-dependent control of NRF2 expression that contributes to the NRF2 protective response engaged during ER stress-induced ROS production.

Keywords: NRF2; ROS; ER stress; PERK; ATF4

1. Introduction

The endoplasmic reticulum (ER) orchestrates protein folding and export. This function is sensitive to cellular alterations in energy levels, redox status, or calcium homeostasis [1], resulting in accumulation of misfolded proteins in the ER lumen, a condition known as ER stress [2]. The detection and resolution of ER stress relies on three major ER-spanning transmembrane proteins, PERK, inositol requiring enzyme 1 (IRE1) and activating transcription factor 6 (ATF6), which trigger the unfolded protein response (UPR). The UPR induces global translational and transcriptional changes to improve the ER protein-folding capacity. However, if ER stress cannot be resolved, the UPR shifts from pro-survival to pro-apoptotic signaling pathways [2]. Several lines of evidence suggest a pivotal role for the PERK branch in the cellular outcome of ER stress [3]. Activated PERK phosphorylates the alpha subunit of eukaryotic translation initiation factor 2 (eIF2 α) that reduces protein synthesis but paradoxically increases the translation of mRNAs such as that of ATF4. ATF4 in turn initiates a transcriptional program including the up-regulation of the transcription factor C/EBP homologous protein (CHOP). ATF4 and CHOP cooperatively stimulate

the expression of genes encoding functions in protein synthesis, and the reactivated translation rate generates significant amounts of reactive oxygen species (ROS) that induce apoptosis [4,5]. As part of the mechanisms engaged to limit oxidative insults, PERK has been shown to directly phosphorylate the master regulator of the cellular antioxidant response nuclear factor erythroid 2-related factor 2 (NRF2), leading to NRF2/Kelch-like ECH-associated protein 1 (KEAP1) complex dissociation and NRF2 stabilization and activation [6]. In addition, IRE1 can also activate the NRF2 and the subsequent oxidative stress response [7], indicating that the molecular events governing NRF2 activity upon ER stress are multifaceted. Apart from the classical activation of NRF2 relying on the induced-dissociation of the NRF2/KEAP1 complex, evidence suggests that NRF2 regulation also occurs at the transcriptional level and that increased transcription promotes resistance to ROS [8–10]. Notably, chromatin immunoprecipitation (ChIP) sequencing data from human mammary cells have exposed the direct binding of ATF4 to the promoter of the *NRF2* gene (*NFE2L2*) upon ER stress [11], suggesting that PERK-mediated regulation of NRF2 might be more complex than previously anticipated.

Herein, we present an alternative mechanism to the direct phosphorylation by PERK that contributes to the protective NRF2-induced antioxidant response upon PERK activation.

2. Results

2.1. ER Stress-Independent PERK Activation Recapitulates ROS Production and NRF2 Activation

In order to investigate PERK-ATF4-dependent regulation of the NRF2 oxidative stress response, which can also be activated by IRE1 [7], we exclusively triggered the PERK pathway uncoupled from the other arms of the UPR to provide a simplified cellular context. To do so, the human cell line NCI-H358 was engineered to stably express the chimeric Fv2E-PERK protein in which the cytosolic PERK kinase domain is fused to a dimerization domain (Fv2E) with high affinity for the drug AP20187 (AP) [12]. This system allows the selective activation of the PERK signaling pathway uncoupled from the IRE1 and ATF6 arms of the UPR. Treatment of these modified NCI-H358 cells with AP resulted in an activation of the Fv2E-PERK construct, as revealed by a phosphorylation-induced shift in the migration of the protein, the phosphorylation of eIF2 α and the accumulation of ATF4 (Figure 1a). In contrast, the two other UPR markers p58IPK and BiP reflecting the activation of the IRE1 and ATF6 branches of ER stress, respectively [13], were not affected. Next, we used the surface sensing of translation (SUNSET) approach [14], to monitor the rate of protein synthesis following Fv2E-PERK activation. We observed the partial inhibition of protein translation between 3 and 6 h of AP treatment, and its recovery at 24 h (Figure 1b). In line with published results [4], the recovery phase was concomitant with an increase in intracellular ROS (Figure 1c). We then assessed NRF2 protein amounts. NRF2 abundance, which is maintained low in unstressed conditions through Kelch-like ECH-associated protein 1 (KEAP1)-mediated proteasomal degradation, increased as early as 6 h after Fv2E-PERK stimulation and peaked at 24 h (Figure 1d). Comparable results were obtained in response to classical ER stress inducers, namely tunicamycin and thapsigargin (Figure 1e,f). To assess if this increase in NRF2 proteins contributed to buffer AP-induced ROS, we silenced NRF2 expression using siRNA. While NRF2 knockdown did not affect intracellular ROS levels under basal growth conditions, loss of NRF2 consistently increased amounts of ROS following Fv2E-PERK activation (Figure 1g). Finally, Fv2E-PERK activation reduced cell viability, which was further increased upon NRF2 silencing, and these effects relied on ROS production, as they are alleviated by treatment with the ROS scavenger N-acetylcysteine (NAC) (Figure 1h).

Therefore, the activation of the artificial eIF2 α kinase recapitulates ROS production and NRF2 activation under conditions in which other ER stress-induced signaling pathways were not activated.

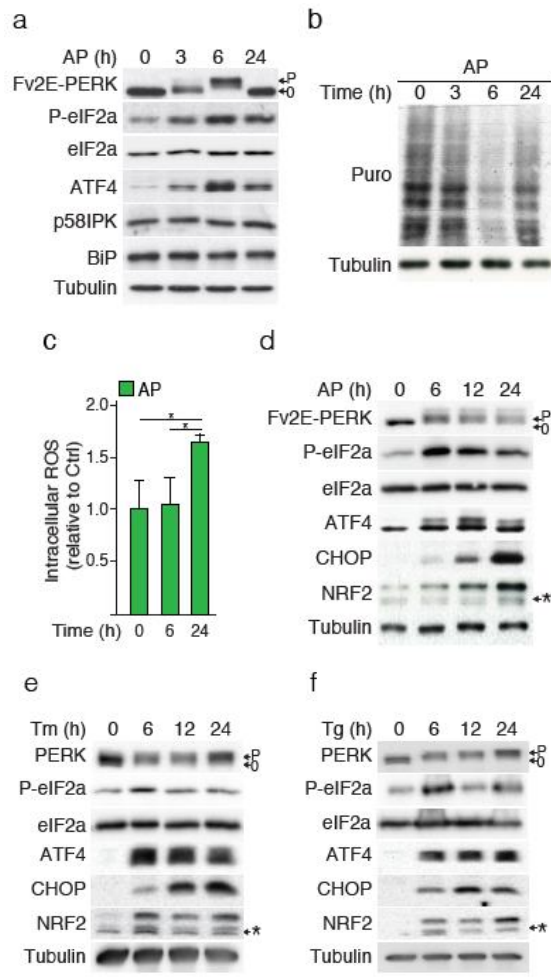


Figure 1. Cont.

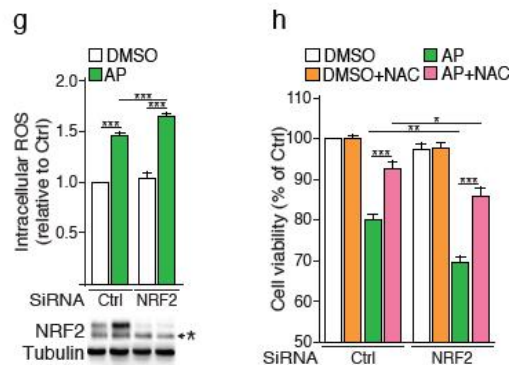


Figure 1. The sole activation of PERK recapitulates reactive oxygen species (ROS)-mediated cell death upon endoplasmic reticulum (ER) stress. (a) Time course analysis of Fv2E-PERK and unfolded protein response (UPR) markers following AP20187 (AP) treatment of NCI-H358 cells. Fv2E-PERK activation was assessed by monitoring changes in Fv2E-PERK band mobility upon AP treatment. P = phosphorylated and 0 = non-phosphorylated form of the protein. (b) Protein synthesis rate measurement by SUNSET assay. (c) Intracellular ROS measurement by fluorescence detection. Cells were treated with AP for 6 and 24 h. ROS fold increase per cell is reported. Time course analysis of Fv2E-PERK, P-eIF2 α , ATF4, CHOP and NRF2 following treatments with (d) AP, (e) tunicamycin or (f) thapsigargin. * = non-specific bands (g) Cell viability of NCI-H358 cells silenced for NRF2 upon PERK activation. NRF2 knockdown was confirmed by Western blot analysis. * = non-specific bands. (h) Cell viability of NCI-H358 cells silenced for NRF2 and treated with or without AP or N-Acetylcysteine (NAC). NAC was added to cell culture 1 h prior to adding AP for 24 h. Data are expressed as means \pm SEM of at least three independent experiments, * $p < 0.05$, ** $p < 0.01$, *** $p < 0.001$.

2.2. ROS Generated during Protein Synthesis Recovery Contribute to NRF2 Activation

We next investigated the mechanism(s) of NRF2 activation. Although accumulation of ATF4 and NRF2 occurred concomitantly upon AP treatment, induction of their respective transcriptional program was delayed. Indeed, ATF4-regulated genes such as *TRB3*, *GADD34*, *CHOP* were induced from 6 h of AP treatment onwards (Figure 2a), whereas induction of NRF2 canonical target genes such as *NQO1*, *HO1* and *GCLC*, was observed only at 24 h (Figure 2b). In this latter case, the slight but significant augmentation of HO1 expression observed at 6 h, is likely due to the rapid onset of ATF4 activity since this gene is also positively-regulated by ATF4 [15]. These results indicate that even though the amounts of both ATF4 and NRF2 proteins increase 6 h following PERK activation, detectable NRF2 activity is delayed by 24 h compared to that of ATF4.

To assess whether this increase in NRF2 is regulated by the canonical KEAP1 complex, we monitored NRF2/KEAP1 complex disruption using the Neh2-luc reporter. In this construct, the Neh2 domain of NRF2 responsible for its interaction with KEAP1, was fused to firefly luciferase and the protein stability of the reporter directly depends on its interaction with endogenous KEAP1 [16]. Figure 2c shows that the increase in Neh2-luc luminescence was not detectable at 6 h, but occurred after 24 h of AP stimulation. This result corroborates the measurement of NRF2 target gene expression presented above. Notably, PERK-mediated phosphorylation of NRF2 on threonine residues after 6 h of AP stimulation was not detected (Figure S1). Rather, NRF2 activation was correlated with protein synthesis recovery and ROS production. Indeed, the rise in Neh2-luciferase signal was alleviated by NAC treatment, indicating that oxidative stress is implicated in NRF2/KEAP1 dissociation (Figure 2c). Consistently, accumulation of activated NRF2 in the nucleus was mainly observed after 24 h of AP stimulation (Figure S2), and NAC reduced both NRF2 nuclear translocation (Figure 2d) and the induction of NRF2 canonical target genes (Figure 2e). In line with these results, leucine deprivation that

triggers the eIF2 α -ATF4 axis independently of PERK [17], also induced a concomitant ROS production and NRF2 nuclear translocation (Figure S3). Of note, protein kinase C-mediated phosphorylation of NRF2 Ser40 was decreased upon AP treatment (Figure 2d), suggesting that this mechanism for NRF2 activation is not engaged. To rule out the possibility that ROS-mediated NRF2 activation is specific to ER stress-independent PERK activation and/or to NCI-H358 cells, we used tunicamycin that activates PERK in a context of ER stress. Tunicamycin-induced NRF2 target genes were also strongly reduced by NAC in NCI-H358 cells (Figure 2f) or in HBEC-3KT cells (Figure S4).

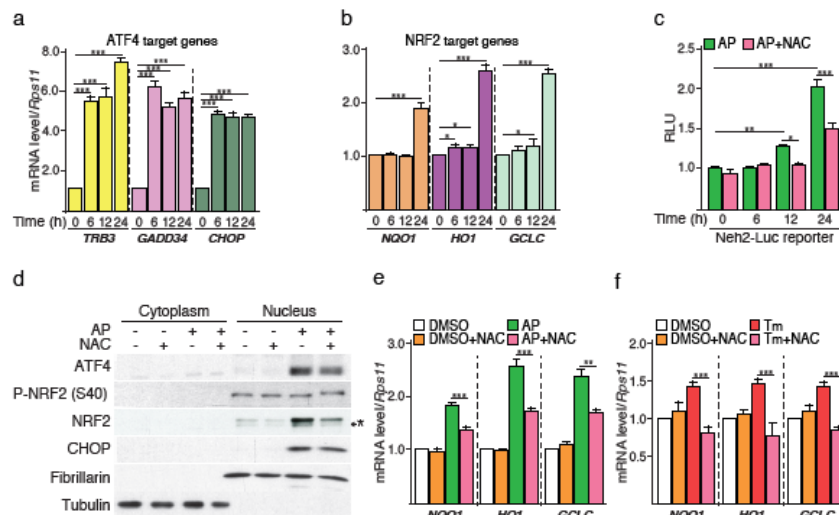


Figure 2. NRF2 activation by PERK partially relies on ROS generation during protein synthesis recovery. NCI-H358 cells were treated with AP over a time course of 24 h and RT-qPCR analysis were performed on canonical (a) ATF4-target genes (TRB3, GADD34, CHOP) or (b) NRF2-target genes (NQO1, HO1, GCLC). (c) Time course analysis of the KEAP1/NRF2 complex dissociation following AP treatment. CI-H358 cells were transiently co-transfected with the Neh2-Luc reporter and Renilla vectors and treated with NAC for 1 h prior to the addition of AP for the indicated periods of time. Data were normalized against the Renilla luciferase activity for each condition. Activity fold increase is reported. (d) Western blot analysis of ATF4, NRF2 and CHOP in cytoplasmic and nuclear fractions upon AP-mediated Fv2E-PERK activation with or without NAC. * = non-specific bands. (e) RT-qPCR analysis of NQO1, HO1 and GCLC expression levels. NCI-H358 cells were treated with or without NAC for 1 h prior to the addition of AP for 24 h. (f) RT-qPCR analysis of NQO1, HO1 and GCLC expression levels. NCI-H358 cells were treated with or without NAC for 1 h prior to the addition of tunicamycin for 24 h. Data are expressed as means \pm SEM of at least three independent experiments, * $p < 0.05$, ** $p < 0.01$, *** $p < 0.001$.

Collectively, these data demonstrate that following PERK activation, ROS generated during protein synthesis recovery contribute to activating NRF2. Therefore, NRF2 activation by the PERK pathway also relies on a complementary and/or alternative mechanism to its direct phosphorylation by PERK.

2.3. The PERK Pathway Induces a Rapid ATF4-Dependent NRF2 mRNA Increase

Given that ATF4 can bind to the promoter of the *NRF2* gene (*NFE2L2*) upon drug-induced ER stress [11], we next assessed whether the PERK pathway could also regulate NRF2 at the transcriptional level. We initially confirmed this hypothesis by showing that (i) tunicamycin induced a rapid increase

in *NRF2* mRNA, (ii) Fv2E-PERK activation and leucine deprivation, resulted in a similar induction (Figure 3a–c). These findings, in particular the latter also strongly suggested that the mechanism(s) controlling *NRF2* mRNA increase is independent of PERK-mediated phosphorylation of NRF2.

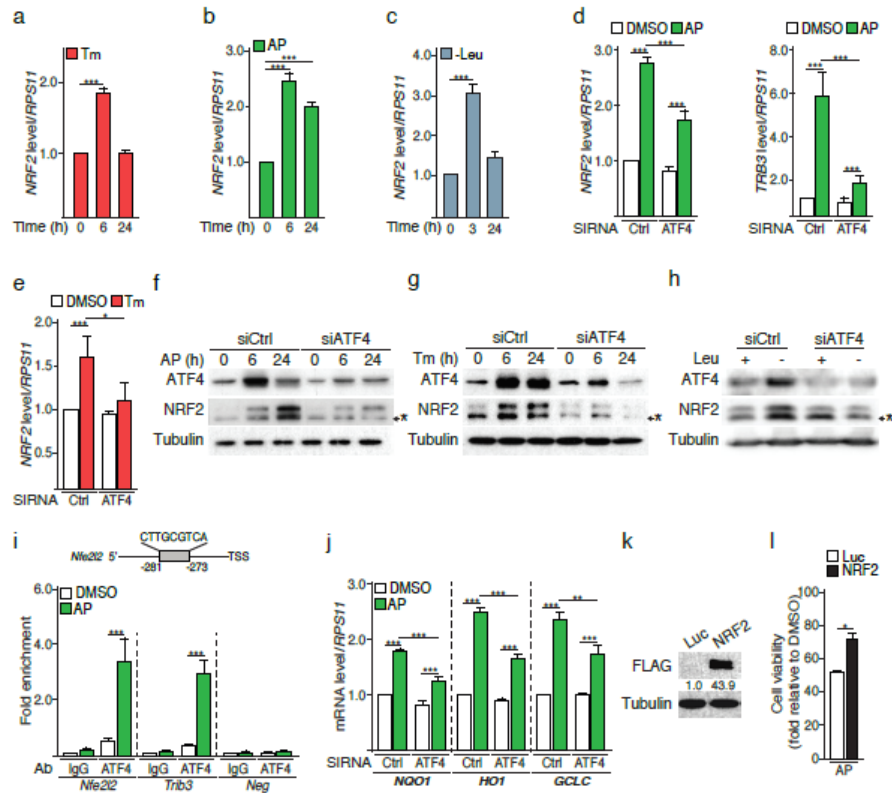


Figure 3. ATF4 directly controls NRF2 expression. Time course analysis of NRF2 mRNA levels in NCI-H358 cells upon (a) addition of tunicamycin (Tm), (b) AP treatment, or (c) leucine deprivation (-Leu). (d) NRF2 and TRB3 mRNA levels in NCI-H358 cells transfected with a siRNA Ctrl or directed against ATF4 and subjected to AP treatment for 6 h. (e) NRF2 mRNA levels in NCI-H358 cells transfected with a siRNA Ctrl or directed against ATF4 and subjected to tunicamycin treatment for 6 h. Kinetics analysis of ATF4 and NRF2 amount from NCI-H358 cells transfected with a siRNA Ctrl or directed against ATF4 and treated (f) with AP or (g) tunicamycin. * = non-specific bands. (h) Immunoblot analysis of ATF4 and NRF2 amounts from NCI-H358 cells transfected with a siRNA Ctrl or directed against ATF4 and leucine-starved for 6 h. (i) Chromatin immunoprecipitation (ChIP) analysis of ATF4 binding to a putative CARE located within the human Nfe2l2 promoter (-281bp upstream the TSS, negative sense). NCI-H358 cells were treated with AP for 6 h. Trib3 and Neg primers were used as positive and negative controls, respectively. (j) RT-qPCR analysis of NQO1, HO1 and GCLC mRNA levels, following a 24-h activation of FV2E-PERK in ATF4 silenced NCI-H358 cells. (k) Immunoblot analysis of the Flag tag from NCI-H358 cells transfected with a pcDNA encoding luciferase (Luc) or Flag-NRF2. (l) Cell viability measurement of NCI-H358 cells overexpressing Luc or NRF2 and treated with AP for 24 h. Data are expressed as means \pm SEM of at least three independent experiments, * $p < 0.05$, ** $p < 0.01$, *** $p < 0.001$.

We then tested whether ATF4 may control NRF2 mRNA up-regulation. ATF4 silencing strongly reduced NRF2 mRNA expression (Figure 3d, left panel) and protein amount (Figure 3f) as early as 6 h after Fv2E-PERK activation. Functionality of the ATF4 knockdown was confirmed by the reduction of the ATF4 target gene *TRB3* (Figure 3d, right panel) and of ATF4 protein surge (Figure 3f). The rapid ATF4-dependant NRF2 mRNA up-regulation was recapitulated upon tunicamycin treatment of H358, HBEC-3KT or A549 cells (Figure 3e and Figure S5). Consistently, ATF4 silencing decreased NRF2 protein abundance following global ER stress upon exposure to tunicamycin or leucine deprivation (Figure 3g,h). These results suggested that ATF4 may directly control *NRF2* mRNA. Indeed, we identified a putative C/EBP-ATF Response Element (CARE) in the human *NRF2* gene promoter through which ATF4 triggers transcription of a subset of target genes (Figure 3i). Chromatin immunoprecipitation (ChIP) assay following 6 h of AP treatment showed an enrichment in ATF4 binding to this CARE, comparable to that of the *Trib3* promoter region (Figure 3i). In addition, Figure 3j shows that the loss of ATF4 significantly decreased mRNAs level of NRF2 target genes upon AP stimulation, underlying the relevance of ATF4-dependent regulation of NRF2. Together, these data demonstrate that the PERK pathway engages a rapid ATF4-dependent up-regulation of *NRF2* mRNA expression.

Finally, to investigate the biological relevance of the increase in *NRF2* mRNA and protein amounts, we overexpressed NRF2 in Fv2E-PERK cells (Figure 3k) and triggered the PERK pathway activation using AP. Cells overexpressing NRF2 displayed an increased viability compared to the control counterparts (Luc) following PERK pathway activation (Figure 3l), indicating that higher basal levels of NRF2 render cells prone to respond to oxidative stress following activation of the PERK branch of the ER stress.

Therefore, in addition to the direct phosphorylation of NRF2, the PERK pathway can also control NRF2 amounts through an ATF4-dependent mechanism, which reinforces the cytoprotective effects of NRF2 against ROS (Figure 4).

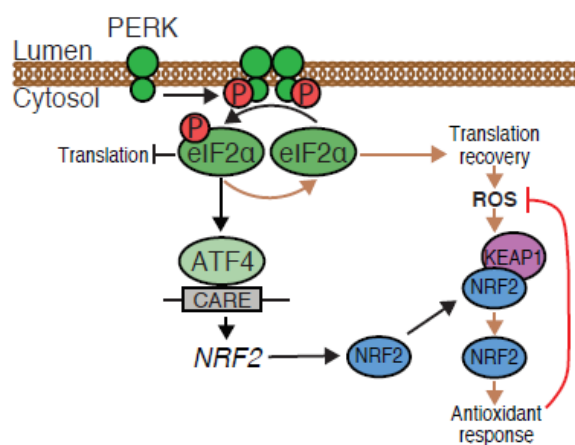


Figure 4. Schematic diagram of an alternative mechanism driving NRF2 activation upon PERK activation. In addition to the known NRF2 phosphorylation, activation of PERK triggers NRF2 transcription in an ATF4-dependent manner. During the protein synthesis recovery phase, subsequent generation of ROS induces the dissociation of the NRF2/KEAP1 complex, activation of the NRF2 antioxidant program and cell survival.

3. Discussion

ER stress-associated PERK activation has previously been reported to induce rapid and direct phosphorylation of NRF2 [6]. Although this mechanism results in a ROS-independent activation

of NRF2 during ER stress, we report that ROS generated during late stages of PERK-dependent protein synthesis recovery, also contribute to triggering the cytoprotective NRF2 antioxidant program. In addition, PERK activation triggers an ATF4-dependent control of *NRF2* mRNA abundance that reinforces the cytoprotective function of NRF2. These results show that the PERK pathway can engage different mechanisms to activate NRF2 during ER stress.

Lu and colleagues notably demonstrated that PERK-dependent changes in gene expression are mainly reliant on transcription factors downstream of eIF2 α phosphorylation [12], which has raised questions about the physiological importance of transcription activation by alternative PERK substrates such as NRF2 [2]. Our findings may reconcile these apparently discrepant results since the different mechanisms of NRF2 activation are theoretically not mutually exclusive but rather complementary or alternative.

The PERK pathway induced an ATF4-dependent *NRF2* mRNA increase and the binding of ATF4 to the CARE of *Nfe2l2* promoter region supporting a direct regulation of *NRF2* gene expression. Interestingly, no conserved CARE was found in the orthologous region of the murine *Nfe2l2* promoter and no ATF4 binding to this promoter has been described in mouse embryonic fibroblasts [4], suggesting a species-specific *NRF2* regulation by ATF4. Fv2E-PERK-mediated ATF4-dependent increase in *NRF2* protein amounts occurred relatively rapidly but did not readily translate into NRF2 activation. Considering that at steady-state, the abundance of NRF2 is maintained at a level significantly lower than that of KEAP1 [18], we hypothesize that a proportion of KEAP1 may act as a floodgate trapping the newly produced NRF2. Only when significant amounts of ROS are generated during protein synthesis recovery, is KEAP1 massively released from NRF2 leading to a strong NRF2 activation (Figure 4).

In the context of tumorigenesis, there has been a renewed interest in NRF2 as a driver of cancer progression and resistance to therapy, over the last years. Many cancer cells hijack ER stress signaling to promote progression [2], thus our findings suggest that ATF4-dependent NRF2 activation could be aiding in this process, therefore supporting the interest in targeting NRF2 in cancer treatment.

In summary, we show that in addition to the reported rapid and direct phosphorylation of NRF2 by PERK, the PERK-eIF2 α -ATF4 pathway controls NRF2 expression in human cells, which is at least in part activated by upcoming ER stress-associated oxidative stimuli. This work broadens our understanding of how cells cope with oxidative stress generated during ER stress.

4. Materials and Methods

4.1. Cell Culture and Treatments

NCI-H358 cells were grown in RPMI 1640 supplemented with 10% fetal bovine serum (FBS) and 1% *v/v* penicillin/streptomycin solution. Puromycin (2 μ g/mL) was used for the selection of Fv2E-PERK NCI-H358 cells, generated in-house. A549 cells were cultured in DMEM high glucose supplemented with 10% fetal bovine serum (FBS), glutamax and 1% *v/v* penicillin/streptomycin and HBEC-3KT were maintained in KSFM supplemented with bovine pituitary extract and recombinant human EGF. The cells were maintained at 37 °C in a 5% CO₂ incubator.

To induce ER stress, cells were treated with 0.5 μ g/mL tunicamycin (Sigma-Aldrich, ref: T7765, St Louis, MO, USA) or 30 nM thapsigargin (Sigma-Aldrich, ref: T9033, St Louis, MO, USA) added to the culture medium. To induce oxidative stress or NRF2-mediated response, cells were treated with 100 μ M H₂O₂ (Millipore, ref: 107209). To activate the Fv2E-PERK fusion protein cells were treated with 0.2 nM AP20187 (Clontech, ref: 635060, St Louis, MO, USA). An equivalent volume of DMSO was used for control experiments. Leucine starvation experiments were performed using a DMEM/Nutrient Mixture: F-12 (DMEM/F12) medium devoid of leucine, glutamine, lysine and methionine (Sigma-Aldrich, ref: D9785, St Louis, MO, USA), in which glutamine, lysine, methionine and 10% dialyzed serum were subsequently added. The control medium for these experiments was supplemented with leucine.

4.2. siRNA and Plasmid Transfections

NCI-H358 cells were transfected with ON-TARGETplus SMART pool human NFE2L2 siRNA (L-003755-00-0010), ON-TARGETplus non-targeting siRNA (D-001810-03-50) (Dharmacon, GE Healthcare) or human ATF4 siRNA (sc-35112) (Santa Cruz Biotechnology, Dallas, TX, USA). All siRNA transfections were performed using 50 nM siRNA and HiPerFect reagent (Qiagen, Venlo, Netherland), according to the manufacturer's traditional transfection protocol, for 72 h followed by treatments. Cells were seeded either onto 6-well plates (25×10^4 cells per well), onto 24-well plates (5×10^4 cells per well), or 96-well plates (2×10^4 cells per well).

For NRF2 overexpression experiments, cells seeded onto 6-well plates were transfected with a pcDNA3 vector encoding the Flag-NRF2 (addgene #36971) or luciferase by using the Attractene reagent (Qiagen), according to the manufacturer's transfection protocol.

4.3. Cell Extracts and Western Blot Analysis

Whole cell extracts were prepared from cultured cells lysed in the radioimmunoprecipitation assay (RIPA) protein buffer containing proteases and phosphatases inhibitors (Roche, Basel, Switzerland), and obtained by centrifugation at $16,000 \times g$ for 15 min at 4°C .

Subcellular fractionation was performed as follows: cells were detached by trypsin-EDTA and resuspended in 10 mM HEPES, pH 8.0, containing 10 mM KCl, 1.5 mM MgCl_2 , 0.5 mM DTT and protease and phosphatase inhibitors, incubated on ice for 10 min, to be then lysed by adding 0.1% NP-40. Cytoplasmic fraction was obtained by centrifugation at $1500 \times g$ for 10 min at 4°C . The pellet, representing the nuclear fraction, was dissolved in the RIPA protein buffer containing protease and phosphatase inhibitors, and incubated on ice for 30 min. The nuclear fraction was obtained by centrifugation at $1500 \times g$ for 30 min at 4°C . Tubulin and Fibrillarlin were used as loading control for purity of cytoplasmic and nuclear fractions, respectively.

Protein concentrations of the cellular extracts were determined using the DC Protein Assay (Bio-Rad). Equal amounts of proteins (20 μg) were separated by SDS-PAGE and then transferred onto nitrocellulose membranes (Biorad, Hercules, CA, USA). Membranes were incubated in the blocking buffer, 5% milk or Bovine Serum Albumin (BSA) in Tris-Buffered Saline/Tween 20 (TBST), for 1 h at room temperature, then incubated overnight at 4°C with the appropriate primary antibodies, diluted in TBST containing 5% milk or BSA. Membranes were washed three times with TBST, incubated for 1 h at room temperature with the appropriate secondary antibodies, diluted in TBST containing 5% milk, and again washed three times with TBST. Detection by enhanced chemiluminescence was performed using the Clarity western ECL substrate (Bio-Rad, Hercules, CA, USA).

For NRF2-flag immunoprecipitation, cells were transfected with the vector encoding the Flag-NRF2. 30 h later, cells were treated with PERK activators for 6 h. Then, cells were collected and lysed with the IP buffer (Tris-HCl 20mM pH 7.4, NaCl 300 mM, EDTA 1mM, NP40 0.5%, glycerol 10% complemented with proteases and phosphatases inhibitors). Supernatants were incubated with the Flag M2 beads (Sigma-Aldrich) overnight at 4°C . Then beads were washed three times with IP buffer and samples elution was performed in Laemmli buffer at 95°C for 5min.

The primary antibodies used were purchased either from Santa Cruz Biotechnology: ATF4 (sc-200 and sc-390063) and α -Tubulin (sc-23950); from Cell Signaling Technology: PERK (3192), eIF2 α (9722), P-eIF2 α (3398), CHOP (2895), P-Threonine (9381) and p58IPK (2940); from Abcam: NRF2 (ab62352), P-NRF2 Ser40 (ab76026) and Fibrillarlin (ab4566); from BD Biosciences: BiP (610978); from Enzo life sciences: FKBP12 (ALX-210-142); or from Millipore: Puromycin clone 12D10 (MABE343). The HRP-conjugated secondary antibodies were supplied by Jackson Laboratories (anti-rabbit and anti-mouse antibodies). Western blot images are representative of three independent experiments. Proteins bands quantification was performed using the ImageJ software (NIH, Bethesda, MD, USA).

4.4. SUnSET Assay

Rates of protein synthesis in NCI-H358 cultured cells were evaluated using the surface sensing of translation (SUnSET) method as previously described [14]. NCI-H358 cells were seeded onto 6-well plates (2×10^5 cells per well) and treated with 0.2 nM AP20187 for the indicated times. Cells were then incubated with 5 $\mu\text{g}/\text{mL}$ puromycin (Sigma-Aldrich P9620, St Louis, MO, USA), added directly into the medium for 15 min at 37 °C, 5% CO₂, prior to be harvested and processed to prepare whole cell extracts in the RIPA buffer. The amount of puromycin incorporated into nascent peptides was then evaluated by Western blot analysis by using anti-puromycin antibody.

4.5. Luciferase Assay

Luciferase assays were performed in NCI-H358 cells seeded onto 24 well-plates (12×10^4 cells per well), transiently co-transfected with Neh2-luc reporter plasmid [16] (0.4 μg for each sample) pRL-SV40 internal control vector (used at ratio of 10:1) and Attractene reagent (Qiagen), according to the manufacturer's transfection protocol. Cells were collected in 100 μL of passive lysis buffer and analyzed for Firefly and Renilla luciferase activities with the Dual-Luciferase Reporter Assay System (Promega, ref: E1910), according to the manufacturer's instructions. Luciferase activities were measured with a microplate reader (Tecan, Infinite M200 PRO, Life Science). The assays were repeated at least three times in triplicate.

4.6. Cell Viability Assay

Cell viability was determined using the CellTiter-Blue assay (Promega ref: G8081). NCI-H358 cells were plated onto 24-wells plate (5×10^4 cells per well) prior to the NRF2 knock-down and the appropriate treatment (5mM NAC treatment prior to AP). CellTiter-Blue reagent was added to each well (100 μL per well), to the replaced medium (500 μL) and the plates were incubated at for 1 h 37 °C, 5% CO₂. Fluorescence intensity (545 nm/600 nm excitation/emission) was measured using a microplate reader (Clariostar, BMG LABTECH). Cell viability is expressed as the mean percentage compared to the control. The assays were repeated at least three times in triplicate.

4.7. ROS Detection

Intracellular ROS measurement was performed using the fluorescent probe 5-(and-6)-chloromethyl-2',7'-dichlorodihydrofluorescein diacetate acetyl ester (CM-H₂DCFDA; C6827, Invitrogen Molecular Probes). Briefly, NCI-H358 cells were seeded onto 96-well plate (2×10^4 cells per well). Cells were pre-incubated with 10 μM CM-H₂DCFDA, diluted in PBS supplemented with 10% FBS, for 30 min at 37 °C, 5% CO₂. Following the treatment, fluorescence intensity (490 nm/530 nm excitation/emission) was measured using a microplate reader (Clariostar, BMG LABTECH). A sister plate for each experiment was used to determine the cell number by CellTiter-Blue assay, and a calibration curve was obtained by plating an increasing the number of cells per well ($2.5\text{--}40 \times 10^3$). The assays were repeated at least three times in triplicate. The results were presented as the fold increase in ROS per cell.

4.8. RNA Extraction and RT-qPCR

Total cellular RNA was extracted using the NucleoSpin RNA Kit (Macherey-Nagel), according to the manufacturer's protocol. For cDNA synthesis, 0.5 μg of RNA were reverse transcribed using Superscript II reverse transcriptase (Invitrogen, ref: 18064014, Carlsbad, CA, USA) with random primers (Invitrogen, ref: S0142, Carlsbad, CA, USA), according to the manufacturer's instructions. cDNA was then amplified by qPCR using specific primers listed in Supplementary Table S1 and the SYBR Green Master Mix (Biorad, Hercules, CA, USA). qPCR was performed using the CFX connect real-time PCR system (Biorad, Hercules, CA, USA). Expression of target genes was normalized against endogenous RPS11 mRNA levels, used as an internal control, and assessed using the comparative $\Delta\Delta\text{CT}$ method. qPCR experiments were repeated at least three times in triplicate. Primer

list: *NQO1* Fw: GAAGAGCACTGATCGTACTGG, Rev: GGATACTGAAAGTTCGCAGGG,
HO1 Fw: TCTTCGCCCCGTCTACTTC, Rev: CTTACATAGCGCTGCATGG, *GCLC*
 Fw: CCTGTCTGGGGAGAAAGTTC, Rev: ACTCGGACATTGTTCTCCG, *NRF2*
 Fw: ACATCGAGAGCCCAGTCTTC, Rev: AGCTCCTCCCAAAGTCTGCTC, *TRB3*
 Fw: TGGTACCCAGCTCCTCTACG, Rev: GACAAAGCGACACAGCTTGA, *RPS11*
 Fw: AGCAGCCGACCATCTTTC, Rev: ATAGCCTCCTGGGTGTCTTG, *GADD34*
 Fw: CTGTGATCGCTTCTGGCA Rev: GGAAGAAAGGGTGGGCATC and *CHOP* Fw:
 GGTATGAGGACCTGCAAGAGGT Rev: CTTGTGACCTCTGCTGGTCTG.

4.9. Chromatin Immunoprecipitation (ChIP) Assay

Chromatin immunoprecipitation (ChIP) was performed using the SimpleChIP Plus Enzymatic Chromatin IP Kit (Magnetic Beads) (9005; Cell Signalling Technology, Danvers, MA, USA, Country). Briefly, NCI-H358 cells were seeded in 150 mm in diameter dishes (4×10^6 cells per dish) and 3 dishes per treatment were used. Following the treatment with 0.2 nM AP20187 for 6 h, cells were washed with ice-cold PBS and cross-linked with 1% formaldehyde at room temperature for 10 min, to be then harvested in ice-cold PBS containing protease and phosphatase inhibitors. Chromatin was prepared and fragmented by partial digestion with Micrococcal Nuclease, followed by a mild sonication (Bioruptor Diagenode, Seraing, Belgium), according to the manufacturer's protocol. Chromatin immunoprecipitations were performed using the ATF4 mouse monoclonal antibody (11815, Cell Signalling Technology), normal rabbit IgG antibody and ChIP-Grade Protein G Magnetic Beads both supplied by the kit. After reversal of protein-DNA cross-links, DNA was purified using spin columns. DNA enrichment was analyzed by qPCR using 1 μ L of the template and the primers listed in Supplementary Table S1. The results were calculated as a signal relative to the total amount of input chromatin (Δ CT adjusted to % input), and fold-enrichment values are presented. Primer list: *Nfe2l2* Fw: GCTGAGCTCCGAAAATCCC, Rev: GGGAGCTAACGGAGACCTC, *Trib3* Fw: GCGGATGCAGAGGAGAGA, Rev: CACTTCCGCTGCGAGTCT, Negative region Fw: CCCATGTCCCAGGAAGAAG, Rev: AGTCCTGGAAGGGGTAGTGG.

4.10. Statistical Analyses

Statistical analyses were performed using the GraphPad Prism 6 software (GraphPad Software, La Jolla, CA, USA) via one-way ANOVA (with Holm-Sidak's post-test correction for multiple comparisons). All data are expressed as means \pm SEM of at least three independent experiments, * $p < 0.05$, ** $p < 0.01$, *** $p < 0.001$.

5. Conclusions

How cells cope with harmful oxidative stress generated during ER stress is still not fully understood. It has been previously reported that PERK, a signaling molecule of the UPR, directly phosphorylates and activates the master regulator of the cellular antioxidant response NRF2 to limit oxidative insults. In this study, we show the existence of an alternative pathway in which PERK is involved in the regulation of NRF2. Upon ER stress, the activation of the PERK pathway promoted a rapid ATF4-dependent up-regulation of *NRF2* mRNA in human cells that contributed to the protection from ROS-associated cell death. Notably, the NRF2/KEAP1 protein complex dissociation, leading to NRF2 activation, was delayed and largely induced by ROS produced during protein synthesis recovery in late phases of the UPR. These findings broaden our understanding of how ROS-mediated cell death is counterbalanced during ER stress.

Supplementary Materials: The following are available online at <http://www.mdpi.com/2072-6694/12/3/569/s1>, Figure S1: Analysis of phosphothreonine modification of NRF2 following PERK activation. Figure S2: Kinetic analysis of cytoplasmic and nuclear amount of NRF2 following PERK induction. Figure S3: (a) ROS generation following leucine deprivation. H358 cells were leucine-starved for 24 h. ROS fold increase per cell is reported. (b) Cytoplasmic and nuclear amount of NRF2 following leucine deprivation. Figure S4: Expression of canonical NRF2 target genes in cells treated with tunicamycin with or without NAC. Figure S5: NRF2 expression level in

cells silenced for ATF4 and subjected to tunicamycin treatment. Western blots quantifications of Figures 1–3; and uncropped blots.

Author Contributions: Conceptualization, C.C. and S.N.M.; data curation, C.S.; investigation, C.S., H.D., M.P., V.B., C.D., A.B., J.F. and C.C.; resources, C.F.-P. and T.R.; supervision, C.C. and S.M.; writing, S.N.M. All authors have read and agreed to the published version of the manuscript.

Funding: This research was funded by Fondation ARC pour Recherche sur le Cancer (R16173CC), Ligue Nationale contre le Cancer (R17167CC, R18159CC), and Institut National du Cancer (INCA_7981).

Acknowledgments: The authors are grateful to Ron (Institute of Metabolic Science, Cambridge, UK), Moon (University of Washington, Seattle, WA USA) and Gazarian (Burke Medical Research Institute) for sharing respectively the Fv2E-PERK, the Flag-NRF2 and the Neh2-luc reporter plasmids. We thank L. Du Fraysseix for technical assistance. The authors declare that they have no competing financial interests.

Conflicts of Interest: The authors declare no conflict of interest.

Abbreviation

ATF4	Activating transcription factor 4
ATF6	Activating transcription factor 6
BiP	Binding immunoglobulin protein
CARE	C/EBP-ATF Response Element
CHOP	C/EBP homologous protein
ChIP	Chromatin immunoprecipitation
eIF2a	Eukaryotic translation initiation factor 2A
ER	Endoplasmic reticulum
FKBP12	12-kDa FK506-binding protein
GADD34	Growth arrest and DNA damage-inducible protein 34
GCLC	Glutamate—cysteine ligase catalytic subunit
HO1	Heme oxygenase-1
IRE1	Inositol requiring enzyme 1
KEAP1	Kelch-like ECH-associated protein 1
NAC	N-Acetylcysteine
NQO1	NAD(P)H dehydrogenase [quinone] 1
NRF2	Nuclear factor (erythroid-derived 2)-like 2
P58IPK	DnaJ homolog subfamily C member 3
PERK	PKR-like endoplasmic reticulum kinase
RPS11	40S ribosomal protein S11
ROS	Reactive oxygen species
RT-qPCR	Reverse transcription quantitative polymerase chain reaction
SUnSET	Surface sensing of translation
Tg	Thapsigargin
Thr	Threonine
TRB3	Tribbles Pseudokinase 3
Tm	Tunicamycin
UPR	Unfolded protein response

References

1. Szegezdi, E.; Logue, S.E.; Gorman, A.M.; Samali, A. Mediators of endoplasmic reticulum stress-induced apoptosis. *Embo Rep.* **2006**, *7*, 880–885. [[CrossRef](#)] [[PubMed](#)]
2. Wang, M.; Kaufman, R.J. Protein misfolding in the endoplasmic reticulum as a conduit to human disease. *Nature* **2016**, *529*, 326–335. [[CrossRef](#)] [[PubMed](#)]
3. Wortel, I.M.N.; van der Meer, L.T.; Kilberg, M.S.; van Leeuwen, F.N. Surviving Stress: Modulation of ATF4-Mediated Stress Responses in Normal and Malignant Cells. *Trends Endocrinol. Metab. Tem.* **2017**, *28*, 794–806. [[CrossRef](#)] [[PubMed](#)]

4. Han, J.; Back, S.H.; Hur, J.; Lin, Y.H.; Gildersleeve, R.; Shan, J.; Yuan, C.L.; Krokowski, D.; Wang, S.; Hatzoglou, M.; et al. ER-stress-induced transcriptional regulation increases protein synthesis leading to cell death. *Nat. Cell Biol.* **2013**, *15*, 481–490. [[CrossRef](#)] [[PubMed](#)]
5. Marciniak, S.J.; Yun, C.Y.; Oyadomari, S.; Novoa, I.; Zhang, Y.; Jungreis, R.; Nagata, K.; Harding, H.P.; Ron, D. CHOP induces death by promoting protein synthesis and oxidation in the stressed endoplasmic reticulum. *Genes Dev.* **2004**, *18*, 3066–3077. [[CrossRef](#)] [[PubMed](#)]
6. Cullinan, S.B.; Zhang, D.; Hannink, M.; Arvisais, E.; Kaufman, R.J.; Diehl, J.A. Nrf2 is a direct PERK substrate and effector of PERK-dependent cell survival. *Mol. Cell. Biol.* **2003**, *23*, 7198–7209. [[CrossRef](#)] [[PubMed](#)]
7. Hourihan, J.M.; Moronetti Mazzeo, L.E.; Fernandez-Cardenas, L.P.; Blackwell, T.K. Cysteine Sulfenylation Directs IRE-1 to Activate the SKN-1/Nrf2 Antioxidant Response. *Mol. Cell* **2016**, *63*, 553–566. [[CrossRef](#)] [[PubMed](#)]
8. DeNicola, G.M.; Karreth, F.A.; Humpton, T.J.; Gopinathan, A.; Wei, C.; Frese, K.; Mangal, D.; Yu, K.H.; Yeo, C.J.; Calhoun, E.S.; et al. Oncogene-induced Nrf2 transcription promotes ROS detoxification and tumorigenesis. *Nature* **2011**, *475*, 106–109. [[CrossRef](#)] [[PubMed](#)]
9. Tao, S.; Wang, S.; Moghaddam, S.J.; Ooi, A.; Chapman, E.; Wong, P.K.; Zhang, D.D. Oncogenic KRAS confers chemoresistance by upregulating NRF2. *Cancer Res.* **2014**, *74*, 7430–7441. [[CrossRef](#)] [[PubMed](#)]
10. Tonelli, C.; Chio, I.I.C.; Tuveson, D.A. Transcriptional Regulation by Nrf2. *Antioxid. Redox Signal.* **2017**. [[CrossRef](#)] [[PubMed](#)]
11. Wang, S.; Chen, X.A.; Hu, J.; Jiang, J.K.; Li, Y.; Chan-Salis, K.Y.; Gu, Y.; Chen, G.; Thomas, C.; Pugh, B.F.; et al. ATF4 Gene Network Mediates Cellular Response to the Anticancer PAD Inhibitor YW3-56 in Triple-Negative Breast Cancer Cells. *Mol. Cancer* **2015**, *14*, 877–888. [[CrossRef](#)] [[PubMed](#)]
12. Lu, P.D.; Jousse, C.; Marciniak, S.J.; Zhang, Y.; Novoa, I.; Scheuner, D.; Kaufman, R.J.; Ron, D.; Harding, H.P. Cytoprotection by pre-emptive conditional phosphorylation of translation initiation factor 2. *Embo J.* **2004**, *23*, 169–179. [[CrossRef](#)] [[PubMed](#)]
13. Shoulders, M.D.; Ryno, L.M.; Genereux, J.C.; Moresco, J.J.; Tu, P.G.; Wu, C.; Yates, J.R., 3rd; Su, A.I.; Kelly, J.W.; Wiseman, R.L. Stress-independent activation of XBP1s and/or ATF6 reveals three functionally diverse ER proteostasis environments. *Cell Rep.* **2013**, *3*, 1279–1292. [[CrossRef](#)] [[PubMed](#)]
14. Schmidt, E.K.; Clavarino, G.; Ceppi, M.; Pierre, P. SUNSET, a nonradioactive method to monitor protein synthesis. *Nat. Methods* **2009**, *6*, 275–277. [[CrossRef](#)] [[PubMed](#)]
15. Dey, S.; Sayers, C.M.; Verginadis, I.I.; Lehman, S.L.; Cheng, Y.; Cerniglia, G.J.; Tuttle, S.W.; Feldman, M.D.; Zhang, P.J.; Fuchs, S.Y.; et al. ATF4-dependent induction of heme oxygenase 1 prevents anoikis and promotes metastasis. *J. Clin. Investig.* **2015**, *125*, 2592–2608. [[CrossRef](#)]
16. Smirnova, N.A.; Haskew-Layton, R.E.; Basso, M.; Hushpulia, D.M.; Payappilly, J.B.; Speer, R.E.; Ahn, Y.H.; Rakhman, I.; Cole, P.A.; Pinto, J.T.; et al. Development of Neh2-luciferase reporter and its application for high throughput screening and real-time monitoring of Nrf2 activators. *Chem. Biol.* **2011**, *18*, 752–765. [[CrossRef](#)]
17. Jousse, C.; Bruhat, A.; Harding, H.P.; Ferrara, M.; Ron, D.; Fournoux, P. Amino acid limitation regulates CHOP expression through a specific pathway independent of the unfolded protein response. *FEBS Lett.* **1999**, *448*, 211–216. [[CrossRef](#)]
18. Iso, T.; Suzuki, T.; Baird, L.; Yamamoto, M. Absolute Amounts and Status of the Nrf2-Keap1-Cul3 Complex within Cells. *Mol. Cell. Biol.* **2016**, *36*, 3100–3112. [[CrossRef](#)]



© 2020 by the authors. Licensee MDPI, Basel, Switzerland. This article is an open access article distributed under the terms and conditions of the Creative Commons Attribution (CC BY) license (<http://creativecommons.org/licenses/by/4.0/>).

BIBLIOGRAPHY

1. Hanahan D, Weinberg RA. Hallmarks of Cancer: The Next Generation. *Cell*. 4 mars 2011;144(5):646-74.
2. Nagy JA, Chang SH, Dvorak AM, Dvorak HF. Why are tumour blood vessels abnormal and why is it important to know? *Br J Cancer*. 24 mars 2009;100(6):865-9.
3. Fukumura D, Duda DG, Munn LL, Jain RK. Tumor Microvasculature and Microenvironment: Novel Insights Through Intravital Imaging in Pre-Clinical Models. *Microcirc N Y N* 1994. avr 2010;17(3):206-25.
4. Zaidi M, Fu F, Cojocari D, McKee TD, Wouters BG. Quantitative Visualization of Hypoxia and Proliferation Gradients Within Histological Tissue Sections. *Front Bioeng Biotechnol* [Internet]. 2019 [cité 15 janv 2023];7. Disponible sur: <https://www.frontiersin.org/articles/10.3389/fbioe.2019.00397>
5. Stylianopoulos T, Martin JD, Chauhan VP, Jain SR, Diop-Frimpong B, Bardeesy N, et al. Causes, consequences, and remedies for growth-induced solid stress in murine and human tumors. *Proc Natl Acad Sci U S A*. 18 sept 2012;109(38):15101-8.
6. Provenzano PP, Cuevas C, Chang AE, Goel VK, Von Hoff DD, Hingorani SR. Enzymatic targeting of the stroma ablates physical barriers to treatment of pancreatic ductal adenocarcinoma. *Cancer Cell*. 20 mars 2012;21(3):418-29.
7. Vaupel P. Physiological properties of malignant tumours. *NMR Biomed*. 1992;5(5):220-5.
8. Li J, Chekkoury A, Prakash J, Glasl S, Vetschera P, Koberstein-Schwarz B, et al. Spatial heterogeneity of oxygenation and haemodynamics in breast cancer resolved in vivo by conical multispectral optoacoustic mesoscopy. *Light Sci Appl*. 13 avr 2020;9:57.
9. DeBerardinis RJ, Chandel NS. Fundamentals of cancer metabolism. *Sci Adv*. 27 mai 2016;2(5):e1600200.
10. Hirayama A, Kami K, Sugimoto M, Sugawara M, Toki N, Onozuka H, et al. Quantitative Metabolome Profiling of Colon and Stomach Cancer Microenvironment by Capillary Electrophoresis Time-of-Flight Mass Spectrometry. *Cancer Res*. 1 juin 2009;69(11):4918-25.
11. Kamphorst JJ, Nofal M, Commisso C, Hackett SR, Lu W, Grabocka E, et al. Human pancreatic cancer tumors are nutrient poor and tumor cells actively scavenge extracellular protein. *Cancer Res*. 1 févr 2015;75(3):544-53.
12. Sullivan MR, Danai LV, Lewis CA, Chan SH, Gui DY, Kunchok T, et al. Quantification of microenvironmental metabolites in murine cancers reveals determinants of tumor nutrient availability. *eLife*. 8:e44235.
13. Pan M, Reid MA, Lowman XH, Kulkarni RP, Tran TQ, Liu X, et al. Regional Glutamine Deficiency in Tumours Promotes De-differentiation through Inhibition of Histone Demethylation. *Nat Cell Biol*. oct 2016;18(10):1090-101.
14. Wek RC, Jiang HY, Anthony TG. Coping with stress: eIF2 kinases and translational control. *Biochem Soc Trans*. 20 janv 2006;34(1):7-11.
15. Graham NA, Tahmasian M, Kohli B, Komisopoulou E, Zhu M, Vivanco I, et al. Glucose deprivation activates a metabolic and signaling amplification loop leading to cell death. *Mol Syst Biol*. 26 juin 2012;8:589.
16. Huber AL, Lebeau J, Guillaumot P, Pétrilli V, Malek M, Chilloux J, et al. p58IPK-Mediated Attenuation of the Proapoptotic PERK-CHOP Pathway Allows Malignant Progression upon Low Glucose. *Mol Cell*. 28 mars 2013;49(6):1049-59.
17. B'chir W, Chaveroux C, Carraro V, Averous J, Maurin AC, Jousse C, et al. Dual role for CHOP in the crosstalk between autophagy and apoptosis to determine cell fate in response to amino acid deprivation. *Cell Signal*. 1 juill 2014;26(7):1385-91.
18. Ohoka N, Yoshii S, Hattori T, Onozaki K, Hayashi H. TRB3, a novel ER stress-inducible gene, is induced via ATF4-CHOP pathway and is involved in cell death. *EMBO J*. 23 mars 2005;24(6):1243-55.
19. Puthalakath H, O'Reilly LA, Gunn P, Lee L, Kelly PN, Huntington ND, et al. ER Stress Triggers Apoptosis by Activating BH3-Only Protein Bim. *Cell*. 29 juin 2007;129(7):1337-49.
20. Galehdar Z, Swan P, Fuerth B, Callaghan SM, Park DS, Cregan SP. Neuronal Apoptosis Induced by Endoplasmic Reticulum Stress Is Regulated by ATF4-CHOP-Mediated Induction of the Bcl-2 Homology 3-Only Member PUMA. *J Neurosci*. 15 déc 2010;30(50):16938-48.
21. Inoki K, Zhu T, Guan KL. TSC2 Mediates Cellular Energy Response to Control Cell Growth and Survival. *Cell*. 26 nov 2003;115(5):577-90.
22. Barbet NC, Schneider U, Helliwell SB, Stansfield I, Tuite MF, Hall MN. TOR controls translation

- initiation and early G1 progression in yeast. *Mol Biol Cell*. janv 1996;7(1):25-42.
23. Yuan L, Sheng X, Willson AK, Roque DR, Stine JE, Guo H, et al. Glutamine promotes ovarian cancer cell proliferation through the mTOR/S6 pathway. *Endocr Relat Cancer*. août 2015;22(4):577-91.
24. Gaglio D, Soldati C, Vanoni M, Alberghina L, Chiaradonna F. Glutamine Deprivation Induces Abortive S-Phase Rescued by Deoxyribonucleotides in K-Ras Transformed Fibroblasts. *PLoS ONE*. 5 mars 2009;4(3):e4715.
25. Masuda F, Ishii M, Mori A, Uehara L, Yanagida M, Takeda K, et al. Glucose restriction induces transient G2 cell cycle arrest extending cellular chronological lifespan. *Sci Rep*. 25 janv 2016;6:19629.
26. Visagie MH, Mqoco TV, Liebenberg L, Mathews EH, Mathews GE, Joubert AM. Influence of partial and complete glutamine-and glucose deprivation of breast-and cervical tumorigenic cell lines. *Cell Biosci*. 8 juill 2015;5:37.
27. Saqcena M, Mukhopadhyay S, Hosny C, Alhamed A, Chatterjee A, Foster DA. Blocking anaplerotic entry of glutamine to TCA cycle sensitizes K-Ras mutant cancer cells to cytotoxic drugs. *Oncogene*. 14 mai 2015;34(20):2672-80.
28. Isono T, Chano T, Kitamura A, Yuasa T. Glucose Deprivation Induces G2/M Transition-Arrest and Cell Death in N-GlcNAc2-Modified Protein-Producing Renal Carcinoma Cells. *PLoS ONE*. 5 mai 2014;9(5):e96168.
29. Saqcena M, Menon D, Patel D, Mukhopadhyay S, Chow V, Foster DA. Amino Acids and mTOR Mediate Distinct Metabolic Checkpoints in Mammalian G1 Cell Cycle. *PLoS ONE*. 19 août 2013;8(8):e74157.
30. Yano S, Tazawa H, Kagawa S, Fujiwara T, Hoffman RM. FUCCI Real-Time Cell-Cycle Imaging as a Guide for Designing Improved Cancer Therapy: A Review of Innovative Strategies to Target Quiescent Chemo-Resistant Cancer Cells. *Cancers*. 17 sept 2020;12(9):2655.
31. Jewer M, Lee L, Leibovitch M, Zhang G, Liu J, Findlay SD, et al. Translational control of breast cancer plasticity. *Nat Commun*. 19 mai 2020;11:2498.
32. Kanska J, Aspúria PJP, Taylor-Harding B, Spurka L, Funari V, Orsulic S, et al. Glucose deprivation elicits phenotypic plasticity via ZEB1-mediated expression of NNMT. *Oncotarget*. 17 févr 2017;8(16):26200-20.
33. Valle S, Alcalá S, Martín-Hijano L, Cabezas-Sáinz P, Navarro D, Muñoz ER, et al. Exploiting oxidative phosphorylation to promote the stem and immunoevasive properties of pancreatic cancer stem cells. *Nat Commun*. 16 oct 2020;11:5265.
34. Kim H, Lin Q, Glazer PM, Yun Z. The hypoxic tumor microenvironment in vivo selects the cancer stem cell fate of breast cancer cells. *Breast Cancer Res BCR*. 2018;20:16.
35. Das B, Tsuchida R, Malkin D, Koren G, Baruchel S, Yeger H. Hypoxia Enhances Tumor Stemness by Increasing the Invasive and Tumorigenic Side Population Fraction. *Stem Cells*. 1 juill 2008;26(7):1818-30.
36. Zhang H, Chen P, Yan H, Fu G, Luo F, Zhang J, et al. Targeting mTORC2/HDAC3 Inhibits Stemness of Liver Cancer Cells Against Glutamine Starvation. *Adv Sci*. 20 févr 2022;9(20):2103887.
37. Tran TQ, Hanse EA, Habowski AN, Li H, Gabra MBI, Yang Y, et al. α -Ketoglutarate attenuates Wnt signaling and drives differentiation in colorectal cancer. *Nat Cancer*. mars 2020;1(3):345-58.
38. Prasad P, Ghosh S, Roy SS. Glutamine deficiency promotes stemness and chemoresistance in tumor cells through DRP1-induced mitochondrial fragmentation. *Cell Mol Life Sci*. 1 mai 2021;78(10):4821-45.
39. Shibue T, Weinberg RA. EMT, CSCs, and drug resistance: the mechanistic link and clinical implications. *Nat Rev Clin Oncol*. oct 2017;14(10):611-29.
40. Endo H, Owada S, Inagaki Y, Shida Y, Tatemichi M. Glucose starvation induces LKB1-AMPK-mediated MMP-9 expression in cancer cells. *Sci Rep*. 4 juill 2018;8:10122.
41. Jo H, Lee J, Jeon J, Kim S yoo, Chung J in, Ko H yong, et al. The critical role of glucose deprivation in epithelial-mesenchymal transition in hepatocellular carcinoma under hypoxia. *Sci Rep*. 30 janv 2020;10:1538.
42. Recouvreux MV, Moldenhauer MR, Galenkamp KMO, Jung M, James B, Zhang Y, et al. Glutamine depletion regulates Slug to promote EMT and metastasis in pancreatic cancer. *J Exp Med*. 7 sept 2020;217(9):e20200388.
43. Mi Y, Mu L, Huang K, Hu Y, Yan C, Zhao H, et al. Hypoxic colorectal cancer cells promote metastasis of normoxic cancer cells depending on IL-8/p65 signaling pathway. *Cell Death Dis*. 31 juill 2020;11(7):610.
44. Wei L, Lin Q, Lu Y, Li G, Huang L, Fu Z, et al. Cancer-associated fibroblasts-mediated ATF4 expression promotes malignancy and gemcitabine resistance in pancreatic cancer via the TGF- β 1/SMAD2/3 pathway and ABCC1 transactivation. *Cell Death Dis*. 29 mars 2021;12(4):334.

45. Ghaddar N, Wang S, Woodvine B, Krishnamoorthy J, van Hoef V, Darini C, et al. The integrated stress response is tumorigenic and constitutes a therapeutic liability in KRAS-driven lung cancer. *Nat Commun.* 30 juill 2021;12:4651.
46. Falletta P, Sanchez-del-Campo L, Chauhan J, Efferm M, Kenyon A, Kershaw CJ, et al. Translation reprogramming is an evolutionarily conserved driver of phenotypic plasticity and therapeutic resistance in melanoma. *Genes Dev.* 1 janv 2017;31(1):18-33.
47. Ye J, Kumanova M, Hart LS, Sloane K, Zhang H, De Panis DN, et al. The GCN2-ATF4 pathway is critical for tumour cell survival and proliferation in response to nutrient deprivation. *EMBO J.* 16 juin 2010;29(12):2082-96.
48. Wang M, Lu Y, Wang H, Wu Y, Xu X, Li Y. High ATF4 Expression Is Associated With Poor Prognosis, Amino Acid Metabolism, and Autophagy in Gastric Cancer. *Front Oncol.* 17 déc 2021;11:740120.
49. Thanki K, Nicholls ME, Gajjar A, Senagore AJ, Qiu S, Szabo C, et al. Consensus Molecular Subtypes of Colorectal Cancer and their Clinical Implications. *Int Biol Biomed J.* 2017;3(3):105-11.
50. Guinney J, Dienstmann R, Wang X, de Reyniès A, Schlicker A, Soneson C, et al. The Consensus Molecular Subtypes of Colorectal Cancer. *Nat Med.* nov 2015;21(11):1350-6.
51. Jongen JMJ, van der Waals LM, Trumpi K, Laoukili J, Peters NA, Schenning-van Schelven SJ, et al. Downregulation of DNA repair proteins and increased DNA damage in hypoxic colon cancer cells is a therapeutically exploitable vulnerability. *Oncotarget.* 17 oct 2017;8(49):86296-311.
52. Bristow RG, Hill RP. Hypoxia, DNA repair and genetic instability. *Nat Rev Cancer.* mars 2008;8(3):180-92.
53. Bindra RS, Schaffer PJ, Meng A, Woo J, Måseide K, Roth ME, et al. Down-Regulation of Rad51 and Decreased Homologous Recombination in Hypoxic Cancer Cells. *Mol Cell Biol.* oct 2004;24(19):8504.
54. Cohen SJ, Punt CJA, Iannotti N, Saidman BH, Sabbath KD, Gabrail NY, et al. Relationship of Circulating Tumor Cells to Tumor Response, Progression-Free Survival, and Overall Survival in Patients With Metastatic Colorectal Cancer. *J Clin Oncol* [Internet]. 21 sept 2016 [cité 15 janv 2023]; Disponible sur: <https://ascopubs.org/doi/pdf/10.1200/JCO.2007.15.8923?role=tab>
55. Su P, Lai W, Liu L, Zeng Y, Xu H, Lan Q, et al. Mesenchymal and Phosphatase of Regenerating Liver-3 Status in Circulating Tumor Cells May Serve as a Crucial Prognostic Marker for Assessing Relapse or Metastasis in Postoperative Patients With Colorectal Cancer. *Clin Transl Gastroenterol.* 15 déc 2020;11(12):e00265.
56. Li M, Zhang B, Zhang Z, Liu X, Qi X, Zhao J, et al. Stem Cell-Like Circulating Tumor Cells Indicate Poor Prognosis in Gastric Cancer. *BioMed Res Int.* 2014;2014:981261.
57. Strati A, Nikolaou M, Georgoulas V, Lianidou ES. Prognostic Significance of TWIST1, CD24, CD44, and ALDH1 Transcript Quantification in EpCAM-Positive Circulating Tumor Cells from Early Stage Breast Cancer Patients. *Cells.* 29 juin 2019;8(7):652.
58. Touil Y, Igoudjil W, Corvaisier M, Dessein AF, Vandomme J, Monté D, et al. Colon cancer cells escape 5FU chemotherapy-induced cell death by entering stemness and quiescence associated with the c-Yes/YAP axis. *Clin Cancer Res Off J Am Assoc Cancer Res.* 15 févr 2014;20(4):837-46.
59. Rodríguez-Fanjul V, Guerrero-López R, Fernández-Varas B, Perona R, Sastre-Perona A, Sastre L. Comparison of Colorectal Cancer Stem Cells and Oxaliplatin-Resistant Cells Unveils Functional Similarities. *Cells.* 1 févr 2022;11(3):511.
60. Denise C, Paoli P, Calvani M, Taddei ML, Giannoni E, Kopetz S, et al. 5-Fluorouracil resistant colon cancer cells are addicted to OXPHOS to survive and enhance stem-like traits. *Oncotarget.* 21 oct 2015;6(39):41706-21.
61. BERLE M, HESTETUN KE, VETHE H, CHERA S, PAULO JA, DAHL O, et al. Mapping Proteome Changes in Microsatellite Stable, Recurrent Colon Cancer Reveals a Significant Immune System Signature. *Cancer Genomics Proteomics.* 3 mars 2022;19(2):130-44.
62. Le DT, Uram JN, Wang H, Bartlett BR, Kemberling H, Eyring AD, et al. PD-1 Blockade in Tumors with Mismatch-Repair Deficiency. *N Engl J Med.* 25 juin 2015;372(26):2509-20.
63. Vasaikar S, Huang C, Wang X, Petyuk VA, Savage SR, Wen B, et al. Proteogenomic analysis of human colon cancer reveals new therapeutic opportunities. *Cell.* 2 mai 2019;177(4):1035-1049.e19.
64. Zandberg DP, Menk AV, Velez M, Normolle D, DePeaux K, Liu A, et al. Tumor hypoxia is associated with resistance to PD-1 blockade in squamous cell carcinoma of the head and neck. *J Immunother Cancer.* 13 mai 2021;9(5):e002088.
65. Lyssiotis CA, Kimmelman AC. Metabolic Interactions in the Tumor Microenvironment. *Trends Cell Biol.* nov 2017;27(11):863-75.

66. Estrella V, Chen T, Lloyd M, Wojtkowiak J, Cornell HH, Ibrahim-Hashim A, et al. Acidity generated by the tumor microenvironment drives local invasion. *Cancer Res.* 1 mars 2013;73(5):1524-35.
67. Newman AC, Falcone M, Huerta Uribe A, Zhang T, Athineos D, Pietzke M, et al. Immune-regulated IDO1-dependent tryptophan metabolism is source of one-carbon units for pancreatic cancer and stellate cells. *Mol Cell.* 3 juin 2021;81(11):2290-2302.e7.
68. Terness P, Bauer TM, Röse L, Dufter C, Watzlik A, Simon H, et al. Inhibition of Allogeneic T Cell Proliferation by Indoleamine 2,3-Dioxygenase-expressing Dendritic Cells. *J Exp Med.* 19 août 2002;196(4):447-57.
69. Morgan E, Arnold M, Gini A, Lorenzoni V, Cabasag CJ, Laversanne M, et al. Global burden of colorectal cancer in 2020 and 2040: incidence and mortality estimates from GLOBOCAN. *Gut.* févr 2023;72(2):338-44.
70. Alzahrani SM, Al Doghaither HA, Al-Ghafari AB. General insight into cancer: An overview of colorectal cancer (Review). *Mol Clin Oncol.* déc 2021;15(6):271.
71. Johnson CM, Wei C, Ensor JE, Smolenski DJ, Amos CI, Levin B, et al. Meta-analyses of Colorectal Cancer Risk Factors. *Cancer Causes Control CCC.* juin 2013;24(6):1207-22.
72. Greenstein AJ, Sachar DB, Smith H, Janowitz HD, Aufses Jr. AH. A comparison of cancer risk in crohn's disease and ulcerative colitis. *Cancer.* 1981;48(12):2742-5.
73. Rutter M, Saunders B, Wilkinson K, Rumbles S, Schofield G, Kamm M, et al. Severity of inflammation is a risk factor for colorectal neoplasia in ulcerative colitis. *Gastroenterology.* 1 févr 2004;126(2):451-9.
74. Schepers AG, Snippert HJ, Stange DE, van den Born M, van Es JH, van de Wetering M, et al. Lineage tracing reveals Lgr5+ stem cell activity in mouse intestinal adenomas. *Science.* 10 août 2012;337(6095):730-5.
75. Barker N, Ridgway RA, van Es JH, van de Wetering M, Begthel H, van den Born M, et al. Crypt stem cells as the cells-of-origin of intestinal cancer. *Nature.* janv 2009;457(7229):608-11.
76. Fre S, Pallavi SK, Huyghe M, Laé M, Janssen KP, Robine S, et al. Notch and Wnt signals cooperatively control cell proliferation and tumorigenesis in the intestine. *Proc Natl Acad Sci U S A.* 14 avr 2009;106(15):6309-14.
77. Fearon ER, Vogelstein B. A genetic model for colorectal tumorigenesis. *Cell.* 1 juin 1990;61(5):759-67.
78. Comprehensive molecular characterization of human colon and rectal cancer. *Nature.* 2012;487(7407):330-7.
79. Ullman TA, Itzkowitz SH. Intestinal Inflammation and Cancer. *Gastroenterology.* 1 mai 2011;140(6):1807-1816.e1.
80. Muller M, Hansmann F, Arnone D, Choukour M, Ndiaye NC, Kokten T, et al. Genomic and molecular alterations in human inflammatory bowel disease-associated colorectal cancer. *United Eur Gastroenterol J.* juill 2020;8(6):675-84.
81. Bronner CE, Baker SM, Morrison PT, Warren G, Smith LG, Lescoe MK, et al. Mutation in the DNA mismatch repair gene homologue hMLH1 is associated with hereditary non-polyposis colon cancer. *Nature.* mars 1994;368(6468):258-61.
82. Groden J, Thliveris A, Samowitz W, Carlson M, Gelbert L, Albertsen H, et al. Identification and characterization of the familial adenomatous polyposis coli gene. *Cell.* 9 août 1991;66(3):589-600.
83. Eshghifar N, Farrokhi N, Najj T, Zali M. Tumor suppressor genes in familial adenomatous polyposis. *Gastroenterol Hepatol Bed Bench.* 2017;10(1):3-13.
84. Warner JR. The economics of ribosome biosynthesis in yeast. *Trends Biochem Sci.* 1 nov 1999;24(11):437-40.
85. Buttgerit F, Brand MD. A hierarchy of ATP-consuming processes in mammalian cells. *Biochem J.* 15 nov 1995;312(Pt 1):163-7.
86. Muaddi H, Majumder M, Peidis P, Papadakis AI, Holcik M, Scheuner D, et al. Phosphorylation of eIF2 α at Serine 51 Is an Important Determinant of Cell Survival and Adaptation to Glucose Deficiency. *Mol Biol Cell.* 15 sept 2010;21(18):3220-31.
87. Koumenis C, Naczki C, Koritzinsky M, Rastani S, Diehl A, Sonenberg N, et al. Regulation of Protein Synthesis by Hypoxia via Activation of the Endoplasmic Reticulum Kinase PERK and Phosphorylation of the Translation Initiation Factor eIF2 α . *Mol Cell Biol.* nov 2002;22(21):7405-16.
88. Han J, Back SH, Hur J, Lin YH, Gildersleeve R, Shan J, et al. ER-stress-induced transcriptional regulation increases protein synthesis leading to cell death. *Nat Cell Biol.* mai 2013;15(5):481-90.
89. Kilberg MS, Shan J, Su N. ATF4-DEPENDENT TRANSCRIPTION MEDIATES SIGNALING OF AMINO ACID LIMITATION. *Trends Endocrinol Metab TEM.* nov 2009;20(9):436-43.
90. Gameiro PA, Struhl K. Nutrient Deprivation Elicits a Transcriptional and Translational Inflammatory

- Response Coupled to Decreased Protein Synthesis. *Cell Rep.* 7 août 2018;24(6):1415-24.
91. Leprivier G, Rotblat B, Khan D, Jan E, Sorensen PH. Stress-mediated translational control in cancer cells. *Biochim Biophys Acta BBA - Gene Regul Mech.* 1 juill 2015;1849(7):845-60.
 92. Harding HP, Zhang Y, Zeng H, Novoa I, Lu PD, Calfon M, et al. An integrated stress response regulates amino acid metabolism and resistance to oxidative stress. *Mol Cell.* mars 2003;11(3):619-33.
 93. Vattem KM, Wek RC. Reinitiation involving upstream ORFs regulates ATF4 mRNA translation in mammalian cells. *Proc Natl Acad Sci U S A.* 3 août 2004;101(31):11269-74.
 94. Sonneveld S, Verhagen BMP, Tanenbaum ME. Heterogeneity in mRNA Translation. *Trends Cell Biol.* 1 août 2020;30(8):606-18.
 95. Guerra-Moreno A, Isasa M, Bhanu MK, Waterman DP, Eapen VV, Gygi SP, et al. Proteomic Analysis Identifies Ribosome Reduction as an Effective Proteotoxic Stress Response. *J Biol Chem.* 11 déc 2015;290(50):29695-706.
 96. Pan M, Zorbas C, Sugaya M, Ishiguro K, Kato M, Nishida M, et al. Glutamine deficiency in solid tumor cells confers resistance to ribosomal RNA synthesis inhibitors. *Nat Commun.* 28 juin 2022;13:3706.
 97. Pelletier J, Thomas G, Volarević S. Ribosome biogenesis in cancer: new players and therapeutic avenues. *Nat Rev Cancer.* janv 2018;18(1):51-63.
 98. Lafita-Navarro MC, Venkateswaran N, Kilgore JA, Kanji S, Han J, Barnes S, et al. Inhibition of the de novo pyrimidine biosynthesis pathway limits ribosomal RNA transcription causing nucleolar stress in glioblastoma cells. *PLoS Genet.* 17 nov 2020;16(11):e1009117.
 99. Lane AN, Fan TWM. Regulation of mammalian nucleotide metabolism and biosynthesis. *Nucleic Acids Res.* 27 févr 2015;43(4):2466-85.
 100. Grummt I, Smith VA, Grummt F. Amino acid starvation affects the initiation frequency of nucleolar RNA polymerase. *Cell.* mars 1976;7(3):439-45.
 101. Zhang J, Pavlova NN, Thompson CB. Cancer cell metabolism: the essential role of the nonessential amino acid, glutamine. *EMBO J.* 15 mai 2017;36(10):1302-15.
 102. Goodfellow SJ, Zomerdijk JCBM. Basic mechanisms in RNA polymerase I transcription of the ribosomal RNA genes. *Subcell Biochem.* 2013;61:211-36.
 103. Raska I, Koberna K, Malínský J, Fidlerová H, Masata M. The nucleolus and transcription of ribosomal genes. *Biol Cell.* oct 2004;96(8):579-94.
 104. Brown DD, Gurdon JB. Absence of ribosomal rna synthesis in the anucleolate mutant of *xenopus laevis*. *Proc Natl Acad Sci.* janv 1964;51(1):139-46.
 105. Henderson AS, Warburton D, Atwood KC. Location of Ribosomal DNA in the Human Chromosome Complement. *Proc Natl Acad Sci U S A.* nov 1972;69(11):3394-8.
 106. Scheer U, Xia B, Merkert H, Weisenberger D. Looking at christmas trees in the nucleolus. *Chromosoma.* 1 juin 1997;105(7):470-80.
 107. Conconi A, Widmer RM, Koller T, Sogo JM. Two different chromatin structures coexist in ribosomal RNA genes throughout the cell cycle. *Cell.* 2 juin 1989;57(5):753-61.
 108. Panov KI, Friedrich JK, Russell J, Zomerdijk JCBM. UBF activates RNA polymerase I transcription by stimulating promoter escape. *EMBO J.* 26 juill 2006;25(14):3310-22.
 109. Panov KI, Friedrich JK, Zomerdijk JCBM. A Step Subsequent to Preinitiation Complex Assembly at the Ribosomal RNA Gene Promoter Is Rate Limiting for Human RNA Polymerase I-Dependent Transcription. *Mol Cell Biol.* avr 2001;21(8):2641-9.
 110. Bierhoff H, Dundr M, Michels AA, Grummt I. Phosphorylation by Casein Kinase 2 Facilitates rRNA Gene Transcription by Promoting Dissociation of TIF-IA from Elongating RNA Polymerase I. *Mol Cell Biol.* août 2008;28(16):4988-98.
 111. Hirschler-Laszkiwicz I, Cavanaugh AH, Mirza A, Lun M, Hu Q, Smink T, et al. Rrn3 Becomes Inactivated in the Process of Ribosomal DNA Transcription *. *J Biol Chem.* 23 mai 2003;278(21):18953-9.
 112. O'Sullivan AC, Sullivan GJ, McStay B. UBF Binding In Vivo Is Not Restricted to Regulatory Sequences within the Vertebrate Ribosomal DNA Repeat. *Mol Cell Biol.* janv 2002;22(2):657-68.
 113. Jansa P, Grummt I. Mechanism of transcription termination: PTRF interacts with the largest subunit of RNA polymerase I and dissociates paused transcription complexes from yeast and mouse. *Mol Gen Genet MGG.* 1 nov 1999;262(3):508-14.
 114. Mullineux ST, Lafontaine DLJ. Mapping the cleavage sites on mammalian pre-rRNAs: Where do we stand? *Biochimie.* 1 juill 2012;94(7):1521-32.
 115. Steffensen DM, Prenskey W, Mutton D, Hamerton JL. Mapping the human 5S RNA genes on chromosome 1 using translocations. *Birth Defects Orig Artic Ser.* 1975;11(3):264-8.
 116. Fedoriw AM, Starmer J, Yee D, Magnuson T. Nucleolar association and transcriptional inhibition

- through 5S rDNA in mammals. *PLoS Genet.* 1 janv 2012;8(1):e1002468.
117. Pombo A, Jackson DA, Hollinshead M, Wang Z, Roeder RG, Cook PR. Regional specialization in human nuclei: visualization of discrete sites of transcription by RNA polymerase III. *EMBO J.* 15 avr 1999;18(8):2241-53.
 118. Moorefield B, Roeder RG. Purification and characterization of human transcription factor IIIA. *J Biol Chem.* août 1994;269(33):20857-65.
 119. Weser S, Riemann J, Seifart KH, Meissner W. Assembly and isolation of intermediate steps of transcription complexes formed on the human 5S rRNA gene. *Nucleic Acids Res.* 1 mai 2003;31(9):2408-16.
 120. Cozzarelli NR, Gerrard SP, Schlissel M, Brown DD, Bogenhagen DF. Purified RNA polymerase III accurately and efficiently terminates transcription of 5s RNA genes. *Cell.* 1 oct 1983;34(3):829-35.
 121. Guddat Ulrich, Bakken AH, Pieler T. Protein-mediated nuclear export of RNA: 5S rRNA containing small RNPs in xenopus oocytes. *Cell.* 23 févr 1990;60(4):619-28.
 122. Rudt F, Pieler T. Cytoplasmic retention and nuclear import of 5S ribosomal RNA containing RNPs. *EMBO J.* 15 mars 1996;15(6):1383-91.
 123. Panse VG, Johnson AW. Maturation of Eukaryotic Ribosomes: Acquisition of Functionality. *Trends Biochem Sci.* mai 2010;35(5):260-6.
 124. Yang K, Yang J, Yi J. Nucleolar Stress: hallmarks, sensing mechanism and diseases. *Cell Stress.* 2(6):125-40.
 125. Burger K, Eick D. Functional ribosome biogenesis is a prerequisite for p53 destabilization: impact of chemotherapy on nucleolar functions and RNA metabolism. *Biol Chem.* 1 sept 2013;394(9):1133-43.
 126. Sutton EC, DeRose VJ. Early nucleolar responses differentiate mechanisms of cell death induced by oxaliplatin and cisplatin. *J Biol Chem.* 3 avr 2021;296:100633.
 127. Burger K, Mühl B, Harasim T, Rohrmoser M, Malamoussi A, Orban M, et al. Chemotherapeutic Drugs Inhibit Ribosome Biogenesis at Various Levels. *J Biol Chem.* 16 avr 2010;285(16):12416-25.
 128. Sun XX, Dai MS, Lu H. 5-Fluorouracil Activation of p53 Involves an MDM2-Ribosomal Protein Interaction *. *J Biol Chem.* 16 mars 2007;282(11):8052-9.
 129. Sutton EC, McDevitt CE, Prochnau JY, Yglesias MV, Mroz AM, Yang MC, et al. Nucleolar Stress Induction by Oxaliplatin and Derivatives. *J Am Chem Soc.* 1 nov 2019;141(46):18411-5.
 130. Bruno PM, Liu Y, Park GY, Murai J, Koch CE, Eisen TJ, et al. A subset of platinum-containing chemotherapeutic agents kill cells by inducing ribosome biogenesis stress rather than by engaging a DNA damage response. *Nat Med.* avr 2017;23(4):461-71.
 131. Legin AA, Schintlmeister A, Sommerfeld NS, Eckhard M, Theiner S, Reipert S, et al. Nano-scale imaging of dual stable isotope labeled oxaliplatin in human colon cancer cells reveals the nucleolus as a putative node for therapeutic effect. *Nanoscale Adv.* 3(1):249-62.
 132. Donati G, Peddigari S, Mercer CA, Thomas G. 5S Ribosomal RNA Is an Essential Component of a Nascent Ribosomal Precursor Complex that Regulates the Hdm2-p53 Checkpoint. *Cell Rep.* 11 juill 2013;4(1):87-98.
 133. Sloan KE, Bohnsack MT, Watkins NJ. The 5S RNP Couples p53 Homeostasis to Ribosome Biogenesis and Nucleolar Stress. *Cell Rep.* 17 oct 2013;5(1):237-47.
 134. Nicolas E, Parisot P, Pinto-Monteiro C, de Walque R, De Vleeschouwer C, Lafontaine DLJ. Involvement of human ribosomal proteins in nucleolar structure and p53-dependent nucleolar stress. *Nat Commun.* 1 juin 2016;7:11390.
 135. Colombo E, Marine JC, Danovi D, Falini B, Pelicci PG. Nucleophosmin regulates the stability and transcriptional activity of p53. *Nat Cell Biol.* juill 2002;4(7):529-33.
 136. Kurki S, Peltonen K, Latonen L, Kiviharju TM, Ojala PM, Meek D, et al. Nucleolar protein NPM interacts with HDM2 and protects tumor suppressor protein p53 from HDM2-mediated degradation. *Cancer Cell.* 1 mai 2004;5(5):465-75.
 137. Weber JD, Taylor LJ, Roussel MF, Sherr CJ, Bar-Sagi D. Nucleolar Arf sequesters Mdm2 and activates p53. *Nat Cell Biol.* mai 1999;1(1):20-6.
 138. Sugimoto M, Kuo ML, Roussel MF, Sherr CJ. Nucleolar Arf tumor suppressor inhibits ribosomal RNA processing. *Mol Cell.* 1 févr 2003;11(2):415-24.
 139. Donati G, Brighenti E, Vici M, Mazzini G, Treré D, Montanaro L, et al. Selective inhibition of rRNA transcription downregulates E2F-1: a new p53-independent mechanism linking cell growth to cell proliferation. *J Cell Sci.* 1 sept 2011;124(Pt 17):3017-28.
 140. Lee HC, Wang H, Baladandayuthapani V, Lin H, He J, Jones RJ, et al. RNA Polymerase I Inhibition with CX-5461 as a Novel Therapeutic Strategy to Target MYC in Multiple Myeloma. *Br J Haematol.* avr

2017;177(1):80-94.

141. Dai MS, Arnold H, Sun XX, Sears R, Lu H. Inhibition of c-Myc activity by ribosomal protein L11. *EMBO J.* 25 juill 2007;26(14):3332-45.

142. Iadevaia V, Caldarola S, Biondini L, Gismondi A, Karlsson S, Dianzani I, et al. PIM1 kinase is destabilized by ribosomal stress causing inhibition of cell cycle progression. *Oncogene.* oct 2010;29(40):5490-9.

143. Drygin D, Siddiqui-Jain A, O'Brien S, Schwaebe M, Lin A, Bliesath J, et al. Anticancer activity of CX-3543: a direct inhibitor of rRNA biogenesis. *Cancer Res.* 1 oct 2009;69(19):7653-61.

144. Rubbi CP, Milner J. Disruption of the nucleolus mediates stabilization of p53 in response to DNA damage and other stresses. *EMBO J.* 17 nov 2003;22(22):6068-77.

145. Ho JSL, Ma W, Mao DY, Benchimol S. p53-Dependent Transcriptional Repression of c-myc Is Required for G1 Cell Cycle Arrest. *Mol Cell Biol.* sept 2005;25(17):7423-31.

146. Yuan X, Zhou Y, Casanova E, Chai M, Kiss E, Gröne HJ, et al. Genetic Inactivation of the Transcription Factor TIF-IA Leads to Nucleolar Disruption, Cell Cycle Arrest, and p53-Mediated Apoptosis. *Mol Cell.* 1 juill 2005;19(1):77-87.

147. Fumagalli S, Ivanenkov VV, Teng T, Thomas G. Suprainduction of p53 by disruption of 40S and 60S ribosome biogenesis leads to the activation of a novel G2/M checkpoint. *Genes Dev.* 15 mai 2012;26(10):1028-40.

148. Pelletier J, Riaño-Canalias F, Almacellas E, Mauvezin C, Samino S, Feu S, et al. Nucleotide depletion reveals the impaired ribosome biogenesis checkpoint as a barrier against DNA damage. *EMBO J.* 1 juill 2020;39(13):e103838.

149. Schwartz EL, Nilson L. Multiple mechanisms for the inhibition of rRNA synthesis during HL-60 leukemia cell differentiation. *J Cell Physiol.* 1988;136(3):526-30.

150. Hayashi Y, Kuroda T, Kishimoto H, Wang C, Iwama A, Kimura K. Downregulation of rRNA Transcription Triggers Cell Differentiation. *PLoS ONE.* 30 mai 2014;9(5):e98586.

151. Yang A, Shi G, Zhou C, Lu R, Li H, Sun L, et al. Nucleolin maintains embryonic stem cell self-renewal by suppression of p53 protein-dependent pathway. *J Biol Chem.* 1 déc 2011;286(50):43370-82.

152. Watanabe-Susaki K, Takada H, Enomoto K, Miwata K, Ishimine H, Intoh A, et al. Biosynthesis of ribosomal RNA in nucleoli regulates pluripotency and differentiation ability of pluripotent stem cells. *Stem Cells Dayt Ohio.* déc 2014;32(12):3099-111.

153. Tollervey D, Lehtonen H, Jansen R, Kern H, Hurt EC. Temperature-sensitive mutations demonstrate roles for yeast fibrillarin in pre-rRNA processing, pre-rRNA methylation, and ribosome assembly. *Cell.* 12 févr 1993;72(3):443-57.

154. Morral C, Stanisavljevic J, Hernando-Momblona X, Mereu E, Álvarez-Varela A, Cortina C, et al. Zonation of Ribosomal DNA Transcription Defines a Stem Cell Hierarchy in Colorectal Cancer. *Cell Stem Cell.* 4 juin 2020;26(6):845-861.e12.

155. Wan S, Capasso H, Walworth NC. The topoisomerase I poison camptothecin generates a Chk1-dependent DNA damage checkpoint signal in fission yeast. *Yeast Chichester Engl.* juill 1999;15(10A):821-8.

156. Kalita K, Makonchuk D, Gomes C, Zheng JJ, Hetman M. Inhibition of nucleolar transcription as a trigger for neuronal apoptosis. *J Neurochem.* 1 juin 2008;105(6):2286-99.

157. Li L, Li Y, Zhao J, Fan S, Wang L, Li X. CX-5461 induces autophagy and inhibits tumor growth via mammalian target of rapamycin-related signaling pathways in osteosarcoma. *OncoTargets Ther.* 29 sept 2016;9:5985-97.

158. Pan M, Wright WC, Chapple RH, Zubair A, Sandhu M, Batchelder JE, et al. The chemotherapeutic CX-5461 primarily targets TOP2B and exhibits selective activity in high-risk neuroblastoma. *Nat Commun.* 9 nov 2021;12(1):6468.

159. Reeder RH. Regulation of RNA polymerase I transcription in yeast and vertebrates. *Prog Nucleic Acid Res Mol Biol.* 1999;62:293-327.

160. Hoppe S, Bierhoff H, Cado I, Weber A, Tiebe M, Grummt I, et al. AMP-activated protein kinase adapts rRNA synthesis to cellular energy supply. *Proc Natl Acad Sci U S A.* 20 oct 2009;106(42):17781-6.

161. Timson J. Hydroxyurea. *Mutat Res Genet Toxicol.* 1 janv 1975;32(2):115-31.

162. Charton R, Muguet A, Griesenbeck J, Smerdon MJ, Conconi A. In yeast cells arrested at the early S-phase by hydroxyurea, rRNA gene promoters and chromatin are poised for transcription while rRNA synthesis is compromised. *Mutat Res Mol Mech Mutagen.* 1 mai 2019;815:20-9.

163. Darnell AM, Subramaniam AR, O'Shea EK. Translational control through differential ribosome pausing during amino acid limitation in mammalian cells. *Mol Cell.* 19 juill 2018;71(2):229-243.e11.

164. Wek SA, Zhu S, Wek RC. The histidyl-tRNA synthetase-related sequence in the eIF-2 alpha protein kinase GCN2 interacts with tRNA and is required for activation in response to starvation for different amino acids. *Mol Cell Biol.* août 1995;15(8):4497-506.
165. Pavlova NN, King B, Josselson RH, Violante S, Macera VL, Vardhana SA, et al. Translation in amino-acid-poor environments is limited by tRNAGln charging. *eLife.* 9:e62307.
166. Ishimura R, Nagy G, Dotu I, Chuang JH, Ackerman SL. Activation of GCN2 kinase by ribosome stalling links translation elongation with translation initiation. *eLife.* 5:e14295.
167. Ishimura R, Nagy G, Dotu I, Zhou H, Yang XL, Schimmel P, et al. Ribosome stalling induced by mutation of a CNS-specific tRNA causes neurodegeneration. *Science.* 25 juill 2014;345(6195):455-9.
168. Vind AC, Genzor AV, Bekker-Jensen S. Ribosomal stress-surveillance: three pathways is a magic number. *Nucleic Acids Res.* 17 sept 2020;48(19):10648-61.
169. Saxton RA, Sabatini DM. mTOR Signaling in Growth, Metabolism, and Disease. *Cell.* 9 mars 2017;168(6):960-76.
170. Mayer C, Grummt I. Ribosome biogenesis and cell growth: mTOR coordinates transcription by all three classes of nuclear RNA polymerases. *Oncogene.* oct 2006;25(48):6384-91.
171. Hannan KM, Brandenburger Y, Jenkins A, Sharkey K, Cavanaugh A, Rothblum L, et al. mTOR-Dependent Regulation of Ribosomal Gene Transcription Requires S6K1 and Is Mediated by Phosphorylation of the Carboxy-Terminal Activation Domain of the Nucleolar Transcription Factor UBF†. *Mol Cell Biol.* déc 2003;23(23):8862-77.
172. Mayer C, Zhao J, Yuan X, Grummt I. mTOR-dependent activation of the transcription factor TIF-IA links rRNA synthesis to nutrient availability. *Genes Dev.* 15 févr 2004;18(4):423-34.
173. Chauvin C, Koka V, Nouschi A, Mieulet V, Hoareau-Aveilla C, Dreazen A, et al. Ribosomal protein S6 kinase activity controls the ribosome biogenesis transcriptional program. *Oncogene.* janv 2014;33(4):474-83.
174. James MJ, Zomerdijk JCBM. Phosphatidylinositol 3-Kinase and mTOR Signaling Pathways Regulate RNA Polymerase I Transcription in Response to IGF-1 and Nutrients *. *J Biol Chem.* 2 mars 2004;279(10):8911-8.
175. Goudarzi KM, Nistér M, Lindström MS. mTOR inhibitors blunt the p53 response to nucleolar stress by regulating RPL11 and MDM2 levels. *Cancer Biol Ther.* 29 oct 2014;15(11):1499-514.
176. Chen H, Duo Y, Hu B, Wang Z, Zhang F, Tsai H, et al. PICT-1 triggers a pro-death autophagy through inhibiting rRNA transcription and AKT/mTOR/p70S6K signaling pathway. *Oncotarget.* 27 sept 2016;7(48):78747-63.
177. Zajkowicz A, Gdowicz-Kłosok A, Krześniak M, Ściegłńska D, Rusin M. Actinomycin D and nutlin-3a synergistically promote phosphorylation of p53 on serine 46 in cancer cell lines of different origin. *Cell Signal.* 1 sept 2015;27(9):1677-87.
178. Juskiewicz S, Speldewinde SH, Wan L, Svejstrup JQ, Hegde RS. The ASC-1 Complex Disassembles Collided Ribosomes. *Mol Cell.* 20 août 2020;79(4):603-614.e8.
179. Matsuo Y, Ikeuchi K, Saeki Y, Iwasaki S, Schmidt C, Udagawa T, et al. Ubiquitination of stalled ribosome triggers ribosome-associated quality control. *Nat Commun.* 31 juill 2017;8:159.
180. Juskiewicz S, Chandrasekaran V, Lin Z, Kraatz S, Ramakrishnan V, Hegde RS. ZNF598 Is a Quality Control Sensor of Collided Ribosomes. *Mol Cell.* 1 nov 2018;72(3):469-481.e7.
181. Sundaramoorthy E, Leonard M, Mak R, Liao J, Fulzele A, Bennett EJ. ZNF598 and RACK1 Regulate Mammalian Ribosome-Associated Quality Control Function by Mediating Regulatory 40S Ribosomal Ubiquitylation. *Mol Cell.* 16 févr 2017;65(4):751-760.e4.
182. Hashimoto S, Sugiyama T, Yamazaki R, Nobuta R, Inada T. Identification of a novel trigger complex that facilitates ribosome-associated quality control in mammalian cells. *Sci Rep.* 1 févr 2020;10(1):3422.
183. Iordanov MS, Pribnow D, Magun JL, Dinh TH, Pearson JA, Magun BE. Ultraviolet Radiation Triggers the Ribotoxic Stress Response in Mammalian Cells *. *J Biol Chem.* 19 juin 1998;273(25):15794-803.
184. Iordanov MS, Pribnow D, Magun JL, Dinh TH, Pearson JA, Chen SL, et al. Ribotoxic stress response: activation of the stress-activated protein kinase JNK1 by inhibitors of the peptidyl transferase reaction and by sequence-specific RNA damage to the alpha-sarcin/ricin loop in the 28S rRNA. *Mol Cell Biol.* juin 1997;17(6):3373-81.
185. Wang X, Mader MM, Toth JE, Yu X, Jin N, Campbell RM, et al. Complete Inhibition of Anisomycin and UV Radiation but Not Cytokine Induced JNK and p38 Activation by an Aryl-substituted Dihydropyrrlopyrazole Quinoline and Mixed Lineage Kinase 7 Small Interfering RNA *. *J Biol Chem.* 13

mai 2005;280(19):19298-305.

186. Wu CCC, Peterson A, Zinshteyn B, Regot S, Green R. Ribosome collisions trigger general stress responses to regulate cell fate. *Cell*. 23 juill 2020;182(2):404-416.e14.
187. Vin H, Ching G, Ojeda SS, Adelman CH, Chitsazzadeh V, Dwyer DW, et al. Sorafenib suppresses JNK-dependent apoptosis through inhibition of ZAK. *Mol Cancer Ther*. 1 janv 2014;13(1):221-9.
188. Vind AC, Snieckute G, Blasius M, Tiedje C, Krogh N, Bekker-Jensen DB, et al. ZAK α Recognizes Stalled Ribosomes through Partially Redundant Sensor Domains. *Mol Cell*. 21 mai 2020;78(4):700-713.e7.
189. Hinnebusch AG. Evidence for translational regulation of the activator of general amino acid control in yeast. *Proc Natl Acad Sci U S A*. oct 1984;81(20):6442-6.
190. Masson GR. Towards a model of GCN2 activation. *Biochem Soc Trans*. 31 oct 2019;47(5):1481-8.
191. He H, Singh I, Wek SA, Dey S, Baird TD, Wek RC, et al. Crystal Structures of GCN2 Protein Kinase C-terminal Domains Suggest Regulatory Differences in Yeast and Mammals. *J Biol Chem*. 23 mai 2014;289(21):15023-34.
192. Berlanga JJ, Santoyo J, de Haro C. Characterization of a mammalian homolog of the GCN2 eukaryotic initiation factor 2 α kinase. *Eur J Biochem*. 1999;265(2):754-62.
193. Narasimhan J, Staschke KA, Wek RC. Dimerization Is Required for Activation of eIF2 Kinase Gcn2 in Response to Diverse Environmental Stress Conditions *. *J Biol Chem*. 1 mai 2004;279(22):22820-32.
194. Qiu H, Dong J, Hu C, Francklyn CS, Hinnebusch AG. The tRNA-binding moiety in GCN2 contains a dimerization domain that interacts with the kinase domain and is required for tRNA binding and kinase activation. *EMBO J*. 15 mars 2001;20(6):1425-38.
195. Dong J, Qiu H, Garcia-Barrio M, Anderson J, Hinnebusch AG. Uncharged tRNA Activates GCN2 by Displacing the Protein Kinase Moiety from a Bipartite tRNA-Binding Domain. *Mol Cell*. 1 août 2000;6(2):269-79.
196. Marton MJ, Vazquez de Aldana CR, Qiu H, Chakraborty K, Hinnebusch AG. Evidence that GCN1 and GCN20, translational regulators of GCN4, function on elongating ribosomes in activation of eIF2 α kinase GCN2. *Mol Cell Biol*. août 1997;17(8):4474-89.
197. Ramirez M, Wek RC, Hinnebusch AG. Ribosome association of GCN2 protein kinase, a translational activator of the GCN4 gene of *Saccharomyces cerevisiae*. *Mol Cell Biol*. juin 1991;11(6):3027-36.
198. Inglis AJ, Masson GR, Shao S, Perisic O, McLaughlin SH, Hegde RS, et al. Activation of GCN2 by the ribosomal P-stalk. *Proc Natl Acad Sci U S A*. 12 mars 2019;116(11):4946-54.
199. Harding HP, Ordonez A, Allen F, Parts L, Inglis AJ, Williams RL, et al. The ribosomal P-stalk couples amino acid starvation to GCN2 activation in mammalian cells. *eLife*. 8:e50149.
200. Jiménez-Díaz A, Remacha M, Ballesta JPG, Berlanga JJ. Phosphorylation of Initiation Factor eIF2 in Response to Stress Conditions Is Mediated by Acidic Ribosomal P1/P2 Proteins in *Saccharomyces cerevisiae*. *PLoS ONE*. 31 déc 2013;8(12):e84219.
201. Deryło K, Michalec-Wawiórka B, Krokowski D, Wawiórka L, Hatzoglou M, Tchórzewski M. The uL10 protein, a component of the ribosomal P-stalk, is released from the ribosome in nucleolar stress. *Biochim Biophys Acta BBA - Mol Cell Res*. 1 janv 2018;1865(1):34-47.
202. Pakos - Zebrucka K, Koryga I, Mnich K, Ljujic M, Samali A, Gorman AM. The integrated stress response. *EMBO Rep*. oct 2016;17(10):1374-95.
203. Scorsone KA, Panniers R, Rowlands AG, Henshaw EC. Phosphorylation of eukaryotic initiation factor 2 during physiological stresses which affect protein synthesis. *J Biol Chem*. oct 1987;262(30):14538-43.
204. Dever TE, Feng L, Wek RC, Cigan AM, Donahue TF, Hinnebusch AG. Phosphorylation of initiation factor 2 α by protein kinase GCN2 mediates gene-specific translational control of GCN4 in yeast. *Cell*. 7 févr 1992;68(3):585-96.
205. Klann E, Dever TE. Biochemical mechanisms for translational regulation in synaptic plasticity. *Nat Rev Neurosci*. déc 2004;5(12):931-42.
206. Krishnamoorthy T, Pavitt GD, Zhang F, Dever TE, Hinnebusch AG. Tight Binding of the Phosphorylated α Subunit of Initiation Factor 2 (eIF2 α) to the Regulatory Subunits of Guanine Nucleotide Exchange Factor eIF2B Is Required for Inhibition of Translation Initiation. *Mol Cell Biol*. août 2001;21(15):5018-30.
207. Yamaguchi S, Ishihara H, Yamada T, Tamura A, Usui M, Tominaga R, et al. ATF4-Mediated Induction of 4E-BP1 Contributes to Pancreatic β Cell Survival under Endoplasmic Reticulum Stress. *Cell Metab*. 5 mars 2008;7(3):269-76.
208. Gameiro PA, Struhl K. Nutrient Deprivation Elicits a Transcriptional and Translational

- Inflammatory Response Coupled to Decreased Protein Synthesis. *Cell Rep.* 7 août 2018;24(6):1415-24.
209. Chaveroux C, Sarcinelli C, Barbet V, Belféki S, Barthelaix A, Ferraro-Peyret C, et al. Nutrient shortage triggers the hexosamine biosynthetic pathway via the GCN2-ATF4 signalling pathway. *Sci Rep.* 3 juin 2016;6:27278.
210. Sarcinelli C, Dragic H, Piecyk M, Barbet V, Duret C, Barthelaix A, et al. ATF4-Dependent NRF2 Transcriptional Regulation Promotes Antioxidant Protection during Endoplasmic Reticulum Stress. *Cancers.* 1 mars 2020;12(3):569.
211. Jaspert A, Calmels C, Cosnefroy O, Bellecave P, Pinson P, Claverol S, et al. GCN2 phosphorylates HIV-1 integrase and decreases HIV-1 replication by limiting viral integration. *Sci Rep.* 23 mai 2017;7:2283.
212. Kwon NH, Kang T, Lee JY, Kim HH, Kim HR, Hong J, et al. Dual role of methionyl-tRNA synthetase in the regulation of translation and tumor suppressor activity of aminoacyl-tRNA synthetase-interacting multifunctional protein-3. *Proc Natl Acad Sci U S A.* 6 déc 2011;108(49):19635-40.
213. Ko YG, Kang YS, Kim EK, Park SG, Kim S. Nucleolar Localization of Human Methionyl-tRNA Synthetase and Its Role in Ribosomal RNA Synthesis. *J Cell Biol.* 1 mai 2000;149(3):567-74.
214. Kim EY, Jung JY, Kim A, Kim K, Chang YS. Methionyl-tRNA synthetase overexpression is associated with poor clinical outcomes in non-small cell lung cancer. *BMC Cancer.* 5 juill 2017;17:467.
215. Lough L, Sherman D, Becerra-Flores M, Vasudevan D, Lavinda O, Ni E, et al. Triazolo[4,5-d]pyrimidines as Validated General Control Nonderepressible 2 (GCN2) Protein Kinase Inhibitors Reduce Growth of Leukemia Cells. *Comput Struct Biotechnol J.* 28 sept 2018;16:350-60.
216. Ge L, Chen W, Cao W, Liu G, Zhang Q, Zhuang J, et al. GCN2 is a potential prognostic biomarker for human papillary renal cell carcinoma. *Cancer Biomark.* 1 janv 2018;22(3):395-403.
217. Nakamura A, Kimura H. A new role of GCN2 in the nucleolus. *Biochem Biophys Res Commun.* 1 avr 2017;485(2):484-91.
218. Peltonen K, Colis L, Liu H, Jäämaa S, Moore HM, Enbäck J, et al. Identification of Novel p53 Pathway Activating Small-Molecule Compounds Reveals Unexpected Similarities with Known Therapeutic Agents. *PLoS ONE.* 27 sept 2010;5(9):e12996.
219. Drygin D, Lin A, Bliesath J, Ho CB, O'Brien SE, Proffitt C, et al. Targeting RNA Polymerase I with an Oral Small Molecule CX-5461 Inhibits Ribosomal RNA Synthesis and Solid Tumor Growth. *Cancer Res.* 14 févr 2011;71(4):1418-30.
220. Ferreira R, Schneekloth JS, Panov KI, Hannan KM, Hannan RD. Targeting the RNA Polymerase I Transcription for Cancer Therapy Comes of Age. *Cells.* 21 janv 2020;9(2):266.
221. Chung SY, Chang YC, Hsu DSS, Hung YC, Lu ML, Hung YP, et al. A G-quadruplex stabilizer, CX-5461 combined with two immune checkpoint inhibitors enhances in vivo therapeutic efficacy by increasing PD-L1 expression in colorectal cancer. *Neoplasia N Y N.* 25 nov 2022;35:100856.
222. Hudson JS, Brooks SC, Graves DE. Interactions of actinomycin D with human telomeric G-quadruplex DNA. *Biochemistry.* 1 juin 2009;48(21):4440-7.
223. Kosiol N, Juranek S, Brossart P, Heine A, Paeschke K. G-quadruplexes: a promising target for cancer therapy. *Mol Cancer.* 25 févr 2021;20:40.
224. Lehman SL, Schwartz KR, Maheshwari S, Camphausen K, Tofilon PJ. CX-5461 induces radiosensitization through modification of the DNA damage response and not inhibition of RNA polymerase I. *Sci Rep.* 8 mars 2022;12(1):4059.
225. Tran TQ, Ishak Gabra MB, Lowman XH, Yang Y, Reid MA, Pan M, et al. Glutamine deficiency induces DNA alkylation damage and sensitizes cancer cells to alkylating agents through inhibition of ALKBH enzymes. *PLoS Biol.* nov 2017;15(11):e2002810.
226. Boysen G, Jamshidi-Parsian A, Davis MA, Siegel ER, Kore RA, Dings RPM, et al. Glutaminase Inhibitor CB-839 Increases Radiation Sensitivity of Lung Tumor Cells and Human Lung Tumor Xenografts in Mice. *Int J Radiat Biol.* avr 2019;95(4):436-42.
227. Villa E, Ali ES, Sahu U, Ben-Sahra I. Cancer Cells Tune the Signaling Pathways to Empower de Novo Synthesis of Nucleotides. *Cancers.* 17 mai 2019;11(5):688.
228. Powley IR, Kondrashov A, Young LA, Dobbyn HC, Hill K, Cannell IG, et al. Translational reprogramming following UVB irradiation is mediated by DNA-PKcs and allows selective recruitment to the polysomes of mRNAs encoding DNA repair enzymes. *Genes Dev.* 15 mai 2009;23(10):1207-20.
229. Hsu SC, Chen CL, Cheng ML, Chu CY, Changou CA, Yu YL, et al. Arginine starvation elicits chromatin leakage and cGAS-STING activation via epigenetic silencing of metabolic and DNA-repair genes. *Theranostics.* 4 juin 2021;11(15):7527-45.
230. Missiaen R, Anderson NM, Kim LC, Nance B, Burrows M, Skuli N, et al. GCN2 inhibition

- sensitizes arginine-deprived hepatocellular carcinoma cells to senolytic treatment. *Cell Metab.* 2 août 2022;34(8):1151-1167.e7.
231. Pospelova TV, Demidenko ZN, Bukreeva EI, Pospelov VA, Gudkov AV, Blagosklonny MV. Pseudo-DNA damage response in senescent cells. *Cell Cycle Georget Tex.* 15 déc 2009;8(24):4112-8.
232. Shen C, Houghton PJ. The mTOR pathway negatively controls ATM by up-regulating miRNAs. *Proc Natl Acad Sci U S A.* 16 juill 2013;110(29):11869-74.
233. Bandhakavi S, Kim YM, Ro SH, Xie H, Onsongo G, Jun CB, et al. Quantitative nuclear proteomics identifies mTOR regulation of DNA damage response. *Mol Cell Proteomics MCP.* févr 2010;9(2):403-14.
234. Chen H, Ma Z, Vanderwaal RP, Feng Z, Gonzalez-Suarez I, Wang S, et al. The mTOR inhibitor rapamycin suppresses DNA double-strand break repair. *Radiat Res.* févr 2011;175(2):214-24.
235. Osoegawa A, Gills JJ, Kawabata S, Dennis PA. Rapamycin sensitizes cancer cells to growth inhibition by the PARP inhibitor olaparib. *Oncotarget.* 20 oct 2017;8(50):87044-53.
236. Matsuno Y, Atsumi Y, Shimizu A, Katayama K, Fujimori H, Hyodo M, et al. Replication stress triggers microsatellite destabilization and hypermutation leading to clonal expansion in vitro. *Nat Commun.* 2 sept 2019;10(1):3925.
237. Lin X, Ramamurthi K, Mishima M, Kondo A, Howell SB. p53 interacts with the DNA mismatch repair system to modulate the cytotoxicity and mutagenicity of hydrogen peroxide. *Mol Pharmacol.* déc 2000;58(6):1222-9.
238. Svrcek M, Lascols O, Cohen R, Collura A, Jonchère V, Fléjou JF, et al. MSI/MMR-deficient tumor diagnosis: Which standard for screening and for diagnosis? Diagnostic modalities for the colon and other sites: Differences between tumors. *Bull Cancer (Paris).* févr 2019;106(2):119-28.
239. Zaanan A, Cuilliere-Dartigues P, Guilloux A, Parc Y, Louvet C, de Gramont A, et al. Impact of p53 expression and microsatellite instability on stage III colon cancer disease-free survival in patients treated by 5-fluorouracil and leucovorin with or without oxaliplatin. *Ann Oncol Off J Eur Soc Med Oncol.* avr 2010;21(4):772-80.
240. Colle R, Cohen R, Cochereau D, Duval A, Lascols O, Lopez-Trabada D, et al. Immunotherapy and patients treated for cancer with microsatellite instability. *Bull Cancer (Paris).* janv 2017;104(1):42-51.
241. Takahashi H, Inoue J, Sakaguchi K, Takagi M, Mizutani S, Inazawa J. Autophagy is required for cell survival under L-asparaginase-induced metabolic stress in acute lymphoblastic leukemia cells. *Oncogene.* 27 juill 2017;36(30):4267-76.
242. Therachiyil L, Haroon J, Sahir F, Siveen KS, Uddin S, Kulinski M, et al. Dysregulated Phosphorylation of p53, Autophagy and Stemness Attributes the Mutant p53 Harboring Colon Cancer Cells Impaired Sensitivity to Oxaliplatin. *Front Oncol.* 1 janv 2020;10:1744.
243. Sahin IH, Akce M, Alese O, Shaib W, Lesinski GB, El-Rayes B, et al. Immune checkpoint inhibitors for the treatment of MSI-H/MMR-D colorectal cancer and a perspective on resistance mechanisms. *Br J Cancer.* nov 2019;121(10):809-18.
244. Sui Q, Zhang X, Chen C, Tang J, Yu J, Li W, et al. Inflammation promotes resistance to immune checkpoint inhibitors in high microsatellite instability colorectal cancer. *Nat Commun.* 28 nov 2022;13(1):7316.
245. López-Otín C, Blasco MA, Partridge L, Serrano M, Kroemer G. The Hallmarks of Aging. *Cell.* 6 juin 2013;153(6):1194-217.
246. Hu Z, Xia B, Postnikoff SD, Shen ZJ, Tomoiaga AS, Harkness TA, et al. Ssd1 and Gcn2 suppress global translation efficiency in replicatively aged yeast while their activation extends lifespan. *eLife.* 17 août 2018;7:e35551.
247. Kang MJ, Vasudevan D, Kang K, Kim K, Park JE, Zhang N, et al. 4E-BP is a target of the GCN2-ATF4 pathway during *Drosophila* development and aging. *J Cell Biol.* 2 janv 2017;216(1):115-29.
248. Rousakis A, Vlassis A, Vlanti A, Patera S, Thireos G, Syntichaki P. The general control nonderepressible-2 kinase mediates stress response and longevity induced by target of rapamycin inactivation in *Caenorhabditis elegans*. *Aging Cell.* oct 2013;12(5):742-51.
249. Ferraz RC, Camara H, De-Souza EA, Pinto S, Pinca APF, Silva RC, et al. IMPACT is a GCN2 inhibitor that limits lifespan in *Caenorhabditis elegans*. *BMC Biol.* 7 oct 2016;14(1):87.
250. Ravindran R, Loebbermann J, Nakaya HI, Khan N, Ma H, Gama L, et al. The amino acid sensor GCN2 controls gut inflammation by inhibiting inflammasome activation. *Nature.* 24 mars 2016;531(7595):523-7.
251. Montani D, Lau EM, Dorfmueller P, Girerd B, Jaïs X, Savale L, et al. Pulmonary veno-occlusive disease. *Eur Respir J.* mai 2016;47(5):1518-34.
252. Eyries M, Montani D, Girerd B, Perret C, Leroy A, Lonjou C, et al. EIF2AK4 mutations cause

- pulmonary veno-occlusive disease, a recessive form of pulmonary hypertension. *Nat Genet.* janv 2014;46(1):65-9.
253. Manaud G, Nossent EJ, Lambert M, Ghigna MR, Boët A, Vinhas MC, et al. Comparison of Human and Experimental Pulmonary Venous Occlusive Disease. *Am J Respir Cell Mol Biol.* juill 2020;63(1):118-31.
254. Sun Y, Hu G, Luo J, Fang D, Yu Y, Wang X, et al. Mutations in methionyl-tRNA synthetase gene in a Chinese family with interstitial lung and liver disease, postnatal growth failure and anemia. *J Hum Genet.* juin 2017;62(6):647-51.
255. van Meel E, Wegner DJ, Cliften P, Willing MC, White FV, Kornfeld S, et al. Rare recessive loss-of-function methionyl-tRNA synthetase mutations presenting as a multi-organ phenotype. *BMC Med Genet.* 8 oct 2013;14:106.
256. Palam LR, Gore J, Craven KE, Wilson JL, Korc M. Integrated stress response is critical for gemcitabine resistance in pancreatic ductal adenocarcinoma. *Cell Death Dis.* oct 2015;6(10):e1913.
257. Rothbart SB, Racanelli AC, Moran RG. Pemetrexed indirectly activates the metabolic kinase AMPK in human carcinomas. *Cancer Res.* 15 déc 2010;70(24):10299-309.
258. Harvey RF, Pöyry TAA, Stoneley M, Willis AE. Signaling from mTOR to eIF2 α mediates cell migration in response to the chemotherapeutic doxorubicin. *Sci Signal.* 17 déc 2019;12(612):eaaw6763.
259. Bash-Imam Z, Thérizols G, Vincent A, Lafôrets F, Espinoza MP, Pion N, et al. Translational reprogramming of colorectal cancer cells induced by 5-fluorouracil through a miRNA-dependent mechanism. *Oncotarget.* 3 mai 2017;8(28):46219-33.
260. Deng J, Bai X, Feng X, Ni J, Beretov J, Graham P, et al. Inhibition of PI3K/Akt/mTOR signaling pathway alleviates ovarian cancer chemoresistance through reversing epithelial-mesenchymal transition and decreasing cancer stem cell marker expression. *BMC Cancer.* 24 juin 2019;19:618.
261. Liang SQ, Bühler ED, Berezowska S, Marti TM, Xu D, Froment L, et al. mTOR mediates a mechanism of resistance to chemotherapy and defines a rational combination strategy to treat KRAS-mutant lung cancer. *Oncogene.* janv 2019;38(5):622-36.
262. SHI S, TAN P, YAN B, GAO R, ZHAO J, WANG J, et al. ER stress and autophagy are involved in the apoptosis induced by cisplatin in human lung cancer cells. *Oncol Rep.* mai 2016;35(5):2606-14.
263. Cohen MH, Justice R, Pazdur R. Approval Summary: Pemetrexed in the Initial Treatment of Advanced/Metastatic Non-Small Cell Lung Cancer. *The Oncologist.* 2009;14(9):930-5.
264. Adjei AA. Pharmacology and Mechanism of Action of Pemetrexed. *Clin Lung Cancer.* 1 avr 2004;5:S51-5.
265. Reich S, Nguyen CDL, Has C, Steltgens S, Soni H, Coman C, et al. A multi-omics analysis reveals the unfolded protein response regulon and stress-induced resistance to folate-based antimetabolites. *Nat Commun.* 10 juin 2020;11(1):2936.

